End-Wall Flow of a Surface-Mounted Obstacle on a Convex Hump

by

Hamza Hafez Ahmed

A thesis submitted to the Graduate Faculty of
Auburn University
in partial fulfillment of the
requirements for the Degree of
Master of Science

Auburn, Alabama
December 18 2009

Approved by

Anwar Ahmed, Chair, Professor of Aerospace Engineering
Brian Thurow, Associate Professor of Aerospace Engineering
Jay Khodadadi, Professor of Mechanical Engineering

Abstract

A convex hump has been used to overcome the undesirable effects of the juncture vortex. The effects of a convex hump on the approach boundary layer and consequentially the end-wall flow were quantified. A convex geometry imposed a favorable pressure gradient on the boundary layer, reducing the turbulence intensities and the total kinetic energy of the flow. Increased radius of curvature resulted in a more favorable pressure gradient. A combination of these effects has been shown to delay flow separation and reduce the affected area of the juncture vortex on the surrounding flow.

Both laminar and turbulent flows were analyzed for four convex humps of different curvature. Particle Image Velocimetry (PIV) has been conducted in a water tunnel along with Planar Laser Induced Fluorescence (PLIF) to quantify the stream-wise two-dimensional properties of the system. Surface flow visualization and surface pressure measurements were conducted in the wind tunnel to define time-averaged turbulent surface effects.

As the pressure gradient became more favorable due to convex curvature, the primary singular point of separation formed closer to the leading edge of the obstacle. The vortices presented themselves in a more compact configuration as radius of curvature was increased. The increased streamline displacement associated with increasing radius of curvature, flattened the vortex increasing vorticity and strain in the juncture region. The bifurcation point moved downwards closer to the surface reducing the area of

influence of the system. Increased vortical activity was Reynolds number dependant, the physical location of singularities were dependent on curvature geometry.

Acknowledgments

The author would like to thank Dr. Anwar Ahmed along with the members of the advisory committee and Dr. Javed Khan for their guidance and support throughout this work. The author would also like to thank Mr. Bryan Recktenwald, Mr. Zachary Hall, and Mr. Samik Battacharya for their assistance. The author would especially like to thank his parents, sisters, and family and friends for their love and support.

Table of Contents

Abstract ii

Acknowledgments iv

Nomenclature ix

List of Figures xi

List of Tables xx

Introduction 1

1.1 Background 1

1.2 Previous Research 5

1.3 Objectives 12

Experimental Setup 13

2.1 Test Facilities 13

2.2 Coordinate System 13

2.3 Hump Geometry 14

2.4 Details of Obstacle Model 16

2.5 Water Tunnel Flow Visualization 16

2.6 Particle Image Velocimetry 18

2.7 Surface Pressure Measurements 19

2.8 Boundary Layer 20

2.9 Wind Tunnel Flow Visualization 20

Water Tunnel Results and Discussion 22

3.1 Boundary Layer and Integral Values 22
3.2 Range of Reynolds Number 30
3.3 Characteristic Frequency 33
3.4 Flow Visualization 35
3.5 Vorticity and Strain Contours 41
3.6 Okubo-Weiss Criterion 46
Wind Tunnel Results and Discussion 50
4.1 Boundary Layer and Integral Values 50
4.2 Surface Pressure Distribution on Hump 59
4.3 Flow Visualization 60
4.4 Surface Pressure Distribution on the Hump in the Presence of Obstacle 63
Conclusions 68
5.1 Conclusions 68
References 70
Water Tunnel Results 73
A.1 Vector Plots – Laminar Boundary Layer 73
A.2 Vector Plots – Tripped Boundary Layer 76
A.3 Streamlines – Laminar Boundary Layer 78
A.4 Streamlines – Tripped Boundary Layer 80
A.5 Bifurcation Streamline – Laminar Boundary Layer 82
A.6 Bifurcation Streamline – Tripped Boundary Layer 84
A.7 Vorticity – Laminar Boundary Layer 86
A.8 Vorticity – Tripped Boundary Layer 88

A.9 Strain – Laminar Boundary Layer 90
A.10 Strain – Tripped Boundary Layer 92
A.11 Vorticity and Strain Relation 94
A.12 Q Criterion – Laminar Boundary Layer 96
A.13 Q Criterion – Tripped Boundary Layer 98
Wind Tunnel Results 100
B.1 Boundary Layer and Integral Values 100
B.2 Surface Pressure Distribution, Hump Only 108
B.3 Surface Pressure Distribution, Juncture Vortex and Hump 112
B.4 Surface Pressure Distribution, Juncture Vortex 116
Water Tunnel Results 121
C.1 Laminar Boundary Layer 121
C.2 Tripped Boundary Layer 125
C.3 Defect Profile 129
Wind Tunnel Results 133
D.1 Integral Quantities 133
D.2 Laminar Boundary Layer 134
D.3 Tripped Boundary Layer 138
D.4 Defect Profile 142
D.5 Surface Pressure Distribution, Hump Only – Laminar Boundary Layer 146
D.6 Surface Pressure Distribution, Hump – Tripped Boundary Layer 158
D.7 Surface Pressure Distribution, Juncture Vortex and Hump – Laminar Boundary Layer 170

D.8 Surface Pressure Distribution, Juncture Vortex and Hump – Tripped Boundary Layer 182

Nomenclature

A – Planform area (m^2)

c – Chord length (cm)

C_f – Skin friction coefficient ($\frac{\tau_w}{\frac{1}{2}\rho U_\infty^2}$)

C_p – Pressure coefficient ($\frac{P - P_\infty}{\frac{1}{2}\rho U_\infty^2}$)

D – Cylinder diameter (m)

f – Frequency (Hz)

h – Apex height (cm)

L – Characteristic length (cm)

P – Total pressure (lb/ft^2)

P_∞ – Freestream pressure (lb/ft^2)

P_r – Total pressure in the potential core (lb/ft^2)

P_{sw} – Local wall static pressure (lb/ft^2)

R – Radius of curvature (cm)

Re – Reynolds number ($\frac{\rho DU}{\mu}$)

S – Arc length (cm)

t – Maximum thickness (cm)

u – Local velocity (*mm/s*)

U – Freestream velocity (*m/s*)

$U_{(n)}$ – Local velocity (*ft/s*)

U_p – Local potential velocity (*ft/s*)

U_{pw} – Potential core velocity (*ft/s*)

U_∞ – Freestream velocity (*mm/s*)

y – Vertical height (*mm*)

δ – Boundary layer thickness (*mm*)

δ^* – Displacement thickness (*mm*)

θ – Momentum thickness (*mm*)

μ – Dynamic viscosity (*kg/m•s*)

ρ – Density (kg/m^3)

τ_w – Wall shear stress ($\mu\left(\frac{\partial u}{\partial y}\right)_{y=0}$)

List of Figures

Figure 1.1 Evolution of the juncture flow (Ahmed and Khan 1995) 2

Figure 1.2 (a) 6 vortex system (b) 4 vortex system (c) 2 vortex system (Simpson 2001) .. 3

Figure 1.3 Regimes of juncture vortex (a) Regime 1 (b) Regime 2 (c) Regime 3 (d) Regime 4 (e) Regime 5 (R. Schwind 1962) 6

Figure 2.1 (a) Front view of coordinate system (b) Side view of coordinate system 13

Figure 2.2 Convex hump dimensions 14

Figure 2.3 Streamlined cylinder (dimensions in inches) 16

Figure 2.4 Water tunnel streamwise flow visualization setup 17

Figure 2.5 Cross section of wind tunnel surface pressure setup 19

Figure 3.1 Laminar boundary layer profile 26

Figure 3.2 Tripped boundary layer profile 26

Figure 3.3 Skin friction coefficient 27

Figure 3.4 Defect profile 27

Figure 3.5 Clauser shape factor 28

Figure 3.6 Boundary layer thickness 28

Figure 3.7 Displacement thickness 29

Figure 3.8 Momentum thickness 29

Figure 3.9 Shape factor 30

Figure 3.10 Range of ΔRe_t for h/t = 1.14 31

Figure 3.11 Range of ΔRe_t for h/t = 2.29 32

Figure 3.12 Range of ΔRe_t for h/t = 3.43 32

Figure 3.13 Characteristic frequency 34

Figure 3.14 Location of primary separation point 35

Figure 3.15 Vector plot for h/t = 3.43 – laminar boundary layer 36

Figure 3.16 Streamlines for h/t = 3.43 – laminar boundary layer 36

Figure 3.17 Vector plot for h/t = 3.43 – tripped boundary layer 37

Figure 3.18 Streamlines for h/t = 3.43 – tripped boundary layer 37

Figure 3.19 Location of primary vortex 38

Figure 3.20 Distance between vortex core and saddle point 39

Figure 3.21 Bifurcation streamline for h/t = 3.43 – laminar boundary layer 39

Figure 3.22 Bifurcation streamline for h/t = 3.43 – tripped boundary layer 40

Figure 3.23 Location of bifurcation streamline 41

Figure 3.24 Vorticity for h/t = 3.43 – laminar boundary layer 42

Figure 3.25 Vorticity for h/t = 3.43 – tripped boundary layer 42

Figure 3.26 Strain for h/t = 3.43 – laminar boundary layer 44

Figure 3.27 Strain for h/t = 3.43 – tripped boundary layer 44

Figure 3.28 Maximum positive and negative vorticity 45

Figure 3.29 Vorticity and strain relation for h/t = 3.43 45

Figure 3.30 Q criterion for h/t = 3.43 – laminar boundary layer 47

Figure 3.31 Q criterion for h/t = 3.43 – tripped boundary layer 48

Figure 3.32 Shape factor η 49

Figure 4.1 Laminar boundary layer profile, Re_t = 97,000 52

Figure 4.2 Tripped boundary layer profile, Re_t = 97,000 53

Figure 4.3 Skin friction coefficient, Re_t = 97,000 53

Figure 4.4 Defect profile, Re_t = 97,000 54

Figure 4.5 Clauser shape factor, Re_t = 97,000 54

Figure 4.6 Laminar boundary layer thickness, Re_t = 97,000 55

Figure 4.7 Tripped boundary layer thickness, Re_t = 97,000 55

Figure 4.8 Laminar displacement thickness, Re_t = 97,000 56

Figure 4.9 Tripped displacement thickness, Re_t = 97,000 56

Figure 4.10 Laminar momentum thickness, Re_t = 97,000 57

Figure 4.11 Tripped momentum thickness, Re_t = 97,000 57

Figure 4.12 Laminar shape factor, Re_t = 97,000 58

Figure 4.13 Tripped shape factor, Re_t = 97,000 58

Figure 4.14 Surface pressure distribution, hump only, Re_t = 97,000 – laminar boundary layer 59

Figure 4.15 Surface pressure distribution, hump only, Re_t = 97,000 – tripped boundary layer 60

Figure 4.16 Location of primary separation point 61

Figure 4.17 Distance from centerline to primary separation line at trailing edge 61

Figure 4.18 Location of primary separation point (a) h/t = 3.43 (b) h/t = 2.86 (c) h/t = 2.29 (d) h/t = 1.14 – laminar boundary layer 62

Figure 4.19 Location of primary separation point (a) h/t = 3.43 (b) h/t = 2.86 (c) h/t = 2.29 (d) h/t = 1.14 – tripped boundary layer 62

Figure 4.20 Surface pressure distribution, juncture vortex and hump, h/t = 3.43, Re_t = 97,000 64

Figure 4.21 Surface pressure distribution, juncture vortex and hump, h/t = 2.86, Re_t = 97,000 64

Figure 4.22 Surface pressure distribution, juncture vortex and hump, h/t = 2.29, Re_t = 97,000 65

Figure 4.23 Surface pressure distribution, juncture vortex and hump, h/t = 1.14, Re_t = 97,000 65

Figure 4.24 Surface pressure distribution, juncture vortex – laminar boundary layer 66

Figure 4.25 Surface pressure distribution, juncture vortex – tripped boundary layer 66

Figure 4.26 Pressure difference at location of primary vortex – tripped boundary layer . 67

Figure A.1 Vector plot for h/t = 2.86 – laminar boundary layer 73

Figure A.2 Vector plot for h/t = 2.29 – laminar boundary layer 74

Figure A.3 Vector plot for h/t = 1.14 – laminar boundary layer 74

Figure A.4 Vector plot for h/t = 0.00 – laminar boundary layer 75

Figure A.5 Vector plot for h/t = 2.86 – tripped boundary layer 76

Figure A.6 Vector plot for h/t = 2.29 – tripped boundary layer 76

Figure A.7 Vector plot for h/t = 1.14 – tripped boundary layer 77

Figure A.8 Vector plot for h/t = 0.00 – tripped boundary layer 77

Figure A.9 Streamlines for h/t = 2.86 – laminar boundary layer 78

Figure A.10 Streamlines for h/t = 2.29 – laminar boundary layer 78

Figure A.11 Streamlines for h/t = 1.14 – laminar boundary layer 79

Figure A.12 Streamlines for h/t = 0.00 – laminar boundary layer 79

Figure A.13 Streamlines for *h/t* = 2.86 – tripped boundary layer 80

Figure A.14 Streamlines for *h/t* = 2.29 – tripped boundary layer 80

Figure A.15 Streamlines for *h/t* = 1.14 – tripped boundary layer 81

Figure A.16 Streamlines for *h/t* = 0.00 – tripped boundary layer 81

Figure A.17 Bifurcation streamline for *h/t* = 2.86 – laminar boundary layer 82

Figure A.18 Bifurcation streamline for *h/t* = 2.29 – laminar boundary layer 82

Figure A.19 Bifurcation streamline for *h/t* = 1.14 – laminar boundary layer 83

Figure A.20 Bifurcation streamline for *h/t* = 0.00 – laminar boundary layer 83

Figure A.21 Bifurcation streamline for *h/t* = 2.86 – tripped boundary layer 84

Figure A.22 Bifurcation streamline for *h/t* = 2.29 – tripped boundary layer 84

Figure A.23 Bifurcation streamline for *h/t* = 1.14 – tripped boundary layer 85

Figure A.24 Bifurcation streamline for *h/t* = 0.00 – tripped boundary layer 85

Figure A.25 Vorticity for *h/t* = 2.86 – laminar boundary layer 86

Figure A.26 Vorticity for *h/t* = 2.29 – laminar boundary layer 86

Figure A.27 Vorticity for *h/t* = 1.14 – laminar boundary layer 87

Figure A.28 Vorticity for *h/t* = 0.00 – laminar boundary layer 87

Figure A.29 Vorticity for *h/t* = 2.86 – tripped boundary layer 88

Figure A.30 Vorticity for *h/t* = 2.29 – tripped boundary layer 88

Figure A.31 Vorticity for *h/t* = 1.14 – tripped boundary layer 89

Figure A.32 Vorticity for *h/t* = 0.00 – tripped boundary layer 89

Figure A.33 Strain for *h/t* = 2.86 – laminar boundary layer 90

Figure A.34 Strain for *h/t* = 2.29 – laminar boundary layer 90

Figure A.35 Strain for *h/t* = 1.14 – laminar boundary layer 91

Figure A.36 Strain for h/t = 0.00 – laminar boundary layer 91

Figure A.37 Strain for h/t = 2.86 – tripped boundary layer 92

Figure A.38 Strain for h/t = 2.29 – tripped boundary layer 92

Figure A.39 Strain for h/t = 1.14 – tripped boundary layer 93

Figure A.40 Strain for h/t = 0.00 – tripped boundary layer 93

Figure A.41 Vorticity and strain relation for h/t = 2.86 94

Figure A.42 Vorticity and strain relation for h/t = 2.29 94

Figure A.43 Vorticity and Strain relation for h/t = 1.14 95

Figure A.44 Vorticity and strain relation for h/t = 0.00 95

Figure A.45 Q criterion for h/t = 2.86 – laminar boundary layer 96

Figure A.46 Q criterion for h/t = 2.29 – laminar boundary layer 96

Figure A.47 Q criterion for h/t = 1.14 – laminar boundary layer 97

Figure A.48 Q criterion for h/t = 0.00 – laminar boundary layer 97

Figure A.49 Q criterion for h/t = 2.86 – tripped boundary layer 98

Figure A.50 Q criterion for h/t = 2.29 – tripped boundary layer 98

Figure A.51 Q criterion for h/t = 1.14 – tripped boundary layer 99

Figure A.52 Q criterion for h/t = 0.00 – tripped boundary layer 99

Figure B.1 Laminar boundary layer profile, Re_t = 47,000 100

Figure B.2 Laminar boundary layer profile, Re_t = 73,000 101

Figure B.3 Tripped boundary layer profile, Re_t = 47,000 101

Figure B.4 Tripped boundary layer profile, Re_t = 73,000 102

Figure B.5 Skin friction coefficient, Re_t = 47,000, 73,000 102

Figure B.6 Defect profile, Re_t = 47,000 103

Figure B.7 Defect profile, Re_t = 73,000 103

Figure B.8 Laminar boundary layer thickness, Re_t = 47,000, 73,000 104

Figure B.9 Tripped boundary layer thickness, Re_t = 47,000, 73,000 104

Figure B.10 Laminar displacement thickness, Re_t = 47,000, 73,000 105

Figure B.11 Tripped displacement thickness, Re_t = 47,000, 73,000 105

Figure B.12 Laminar momentum thickness, Re_t = 47,000, 73,000 106

Figure B.13 Tripped momentum thickness, Re_t = 47,000, 73,000 106

Figure B.14 Laminar shape factor, Re_t = 47,000, 73,000 107

Figure B.15 Tripped shape factor, Re_t = 47,000, 73,000 107

Figure B.16 Surface pressure distribution, hump only, Re_t = 47,000 – laminar boundary layer 108

Figure B.17 Surface pressure distribution, hump only, Re_t = 47,000 – tripped boundary layer 108

Figure B.18 Surface pressure distribution, hump only, Re_t = 73,000 – laminar boundary layer 109

Figure B.19 Surface pressure distribution, hump only, Re_t = 73,000 – tripped boundary layer 109

Figure B.20 Surface pressure distribution, hump only, h/t = 3.43 110

Figure B.21 Surface pressure distribution, hump only, h/t = 2.86 110

Figure B.22 Surface pressure distribution, hump only, h/t = 2.29 111

Figure B.23 Surface pressure distribution, hump only, h/t = 1.14 111

Figure B.24 Surface pressure distribution, juncture vortex and hump, h/t = 3.43, Re_t = 47,000 112

Figure B.25 Surface pressure distribution, juncture vortex and hump, h/t = 3.43 Re_t = 73,000 112
Figure B.26 Surface pressure distribution, juncture vortex and hump, h/t = 2.86 Re_t = 47,000 113
Figure B.27 Surface pressure distribution, juncture vortex and hump, h/t = 2.86 Re_t = 73,000 113
Figure B.28 Surface pressure distribution, juncture vortex and hump, h/t = 2.29 Re_t = 47,000 114
Figure B.29 Surface pressure distribution, juncture vortex and hump, h/t = 2.29 Re_t = 73,000 114
Figure B.30 Surface pressure distribution, juncture vortex and hump, h/t = 1.14 Re_t = 47,000 115
Figure B.31 Surface pressure distribution, juncture vortex and hump, h/t = 1.14 Re_t = 73,000 115
Figure B.32 Surface pressure distribution, juncture vortex, h/t = 3.43 116
Figure B.33 Surface pressure distribution, juncture vortex, h/t = 2.86 116
Figure B.34 Surface pressure distribution, juncture vortex, h/t = 2.29 117
Figure B.35 Surface pressure distribution, juncture vortex, h/t = 1.14 117
Figure B.36 Surface pressure distribution, juncture vortex, Re_t = 47,000 – laminar boundary layer 118
Figure B.37 Surface pressure distribution, juncture vortex, Re_t = 73,000 – laminar boundary layer 118

Figure B.38 Surface pressure distribution, juncture vortex, Re_t = 97,000 – laminar boundary layer 119

Figure B.39 Surface pressure distribution, juncture vortex, Re_t = 47,000 – tripped boundary layer 119

Figure B.40 Surface pressure distribution, juncture vortex, Re_t = 73,000 – tripped boundary layer 120

Figure B.41 Surface pressure distribution, juncture vortex, Re_t = 97,000 – tripped boundary layer 120

List of Tables

Table 2.1 Hump geometries 14

Table 2.2 Static pressure port locations from trailing to leading edge 15

Table 3.1 Integral quantities – laminar boundary layer 23

Table 3.2 Integral quantities – tripped boundary layer 23

Table 3.3 Range of ΔRe_t for h/t = 1.14, 2.29, 3.43 31

Table 4.1 Integral quantities, Re_t = 97,000 – laminar boundary layer 52

Table 4.2 Integral quantities, Re_t = 97,000 – tripped boundary layer 52

Table C.1 Laminar boundary layer data for h/t = 3.43, 2.86, 2.29 121

Table C.2 Laminar boundary layer data for h/t = 1.14, 0.00 123

Table C.3 Tripped boundary layer data for h/t = 3.43, 2.86, 2.29 125

Table C.4 Tripped boundary layer data for h/t = 1.14, 0.00 127

Table C.5 Defect profile for h/t = 3.43, 2.86, 2.29 129

Table C.6 Defect profile for h/t = 1.14, 0.00 131

Table D.1 Integral quantities - laminar boundary layer 133

Table D.2 Integral quantities – tripped boundary layer 133

Table D.3 Laminar boundary layer data for h/t = 3.43 134

Table D.4 Laminar boundary layer data for h/t = 2.86 135

Table D.5 Laminar boundary layer data for h/t = 2.29 136

Table D.6 Laminar boundary layer data for h/t = 1.14 137

Table D.7 Tripped boundary layer data for h/t = 3.43 138

Table D.8 Tripped boundary layer data for h/t = 2.86 139

Table D.9 Tripped boundary layer data for h/t = 2.29 140

Table D.10 Tripped boundary layer data for h/t = 1.14 141

Table D.11 Defect profile for h/t = 3.43 142

Table D.12 Defect profile for h/t = 2.86 143

Table D.13 Defect profile for h/t = 2.29 144

Table D.14 Defect profile for h/t = 1.14 145

Table D.15 Surface pressure distribution, hump only for h/t = 3.43, Re_t = 47,000 – laminar boundary layer 146

Table D.16 Surface pressure distribution, hump only for h/t = 3.43, Re_t = 73,000 – laminar boundary layer 147

Table D.17 Surface pressure distribution, hump only for h/t = 3.43, Re_t = 97,000 – laminar boundary layer 148

Table D.18 Surface pressure distribution, hump only for h/t = 2.86, Re_t = 47,000 – laminar boundary layer 149

Table D.19 Surface pressure distribution, hump only for h/t = 2.86, Re_t = 73,000 – laminar boundary layer 150

Table D.20 Surface pressure distribution, hump only for h/t = 2.86, Re_t = 97,000 – laminar boundary layer 151

Table D.21 Surface pressure distribution, hump only for h/t = 2.29, Re_t = 47,000 – laminar boundary layer 152

Table D.22 Surface pressure distribution, hump only for h/t = 2.29, Re_t = 73,000 – laminar boundary layer 153
Table D.23 Surface pressure distribution, hump only for h/t = 2.29, Re_t = 97,000 – laminar boundary layer 154
Table D.24 Surface pressure distribution, hump only for h/t = 1.14, Re_t = 47,000 – laminar boundary layer 155
Table D.25 Surface pressure distribution, hump only for h/t = 1.14, Re_t = 73,000 – laminar boundary layer 156
Table D.26 Surface pressure distribution, hump only for h/t = 1.14, Re_t = 97,000 – laminar boundary layer 157
Table D.27 Surface pressure distribution, hump only for h/t = 3.43, Re_t = 47,000 – tripped boundary layer 158
Table D.28 Surface pressure distribution, hump only for h/t = 3.43, Re_t = 73,000 – tripped boundary layer 159
Table D.29 Surface pressure distribution, hump only for h/t = 3.43, Re_t = 97,000 – tripped boundary layer 160
Table D.30 Surface pressure distribution, hump only for h/t = 2.86, Re_t = 47,000 – tripped boundary layer 161
Table D.31 Surface pressure distribution, hump only for h/t = 2.86, Re_t = 73,000 – tripped boundary layer 162
Table D.32 Surface pressure distribution, hump only for h/t = 2.86, Re_t = 97,000 – tripped boundary layer 163

Table D.33 Surface pressure distribution, hump only for h/t = 2.29, Re_t = 47,000 – tripped boundary layer 164
Table D.34 Surface pressure distribution, hump only for h/t = 2.29, Re_t = 73,000 – tripped boundary layer 165
Table D.35 Surface pressure distribution, hump only for h/t = 2.29, Re_t = 97,000 – tripped boundary layer 166
Table D.36 Surface pressure distribution, hump only for h/t = 1.14, Re_t = 47,000 – tripped boundary layer 167
Table D.37 Surface pressure distribution, hump only for h/t = 1.14, Re_t = 73,000 – tripped boundary layer 168
Table D.38 Surface pressure distribution, hump only for h/t = 1.14, Re_t = 97,000 – tripped boundary layer 169
Table D.39 Surface pressure distribution, juncture vortex and hump for h/t = 3.43, Re_t = 47,000 – laminar boundary layer 170
Table D.40 Surface pressure distribution, juncture vortex and hump for h/t = 3.43, Re_t = 73,000 – laminar boundary layer 171
Table D.41 Surface pressure distribution, juncture vortex and hump for h/t = 3.43, Re_t = 97,000 – laminar boundary layer 172
Table D.42 Surface pressure distribution, juncture vortex and hump for h/t = 2.86, Re_t = 47,000 – laminar boundary layer 173
Table D.43 Surface pressure distribution, juncture vortex and hump for h/t = 2.86, Re_t = 73,000 – laminar boundary layer 174

Table D.44 Surface pressure distribution, juncture vortex and hump for h/t = 2.86, Re_t = 97,000 – laminar boundary layer 175

Table D.45 Surface pressure distribution, juncture vortex and hump for h/t = 2.29, Re_t = 47,000 – laminar boundary layer 176

Table D.46 Surface pressure distribution, juncture vortex and hump for h/t = 2.29, Re_t = 73,000 – laminar boundary layer 177

Table D.47 Surface pressure distribution, juncture vortex and hump for h/t = 2.29, Re_t = 97,000 – laminar boundary layer 178

Table D.48 Surface pressure distribution, juncture vortex and hump for h/t = 1.14, Re_t = 47,000 – laminar boundary layer 179

Table D.49 Surface pressure distribution, juncture vortex and hump for h/t = 1.14, Re_t = 73,000 – laminar boundary layer 180

Table D.50 Surface pressure distribution, juncture vortex and hump for h/t = 1.14, Re_t = 97,000 – laminar boundary layer 181

Table D.51 Surface pressure distribution, juncture vortex and hump for h/t = 3.43, Re_t = 47,000 – tripped boundary layer 182

Table D.52 Surface pressure distribution, juncture vortex and hump for h/t = 3.43, Re_t = 73,000 – tripped boundary layer 183

Table D.53 Surface pressure distribution, juncture vortex and hump for h/t = 3.43, Re_t = 97,000 – tripped boundary layer 184

Table D.54 Surface pressure distribution, juncture vortex and hump for h/t = 2.86, Re_t = 47,000 – tripped boundary layer 185

Table D.55 Surface pressure distribution, juncture vortex and hump for h/t = 2.86, Re_t = 73,000 – tripped boundary layer 186

Table D.57 Surface pressure distribution, juncture vortex and hump for h/t = 2.29, Re_t = 47,000 – tripped boundary layer 188

Table D.58 Surface pressure distribution, juncture vortex and hump for h/t = 2.29, Re_t = 73,000 – tripped boundary layer 189

Table D.59 Surface pressure distribution, juncture vortex and hump for h/t = 2.29, Re_t = 97,000 – tripped boundary layer 190

Table D.60 Surface pressure distribution, juncture vortex and hump for h/t = 1.14, Re_t = 47,000 – tripped boundary layer 191

Table D.61 Surface pressure distribution, juncture vortex and hump for h/t = 1.14, Re_t = 73,000 – tripped boundary layer 192

Table D.62 Surface pressure distribution, juncture vortex and hump for h/t = 1.14, Re_t = 97,000 – tripped boundary layer 193

Chapter 1

Introduction

1.1 Background

The presence of an obstacle in a flow imposes an adverse pressure gradient on the oncoming boundary layer and as a result, the initially two-dimensional boundary layer undergoes two strains in the region where the obstacle meets the surface. Firstly, the adverse streamwise pressure gradient decelerates the incoming boundary layer, causing it to eventually separate. The vorticity in the separated boundary layer forms the system of vortices commonly known as the "juncture vortex system". Secondly, due to the cross-stream pressure gradient, the streamlines experience a skewing in the spanwise direction due to their low near-wall velocities while the outer layer remains unchanged. This results in an inflectional cross-flow boundary layer profile that is inherently unstable. Due to the presence of axial and cross-stream pressure gradients, a combination of singular points associated with separation and attachment lines appear in the plane of symmetry. The resulting streamlines formed around the obstacle resemble a horseshoe profile. Figure 1.1 shows the evolution of the juncture flow that is organized into four distinct regions (Khan and Ahmed 1994). Region (a) shows the skewed three-dimensional boundary layer upstream and around the obstacle. Region (b) encloses the junction flow upstream and the corner region where the turbulence-induced secondary flow dominates and the turbulence stress field is anisotropic. Region (c) and (d) are of the near wake

region where the split legs of the juncture vortex re-attach and form a fishtail pattern and far wake flow, respectively.

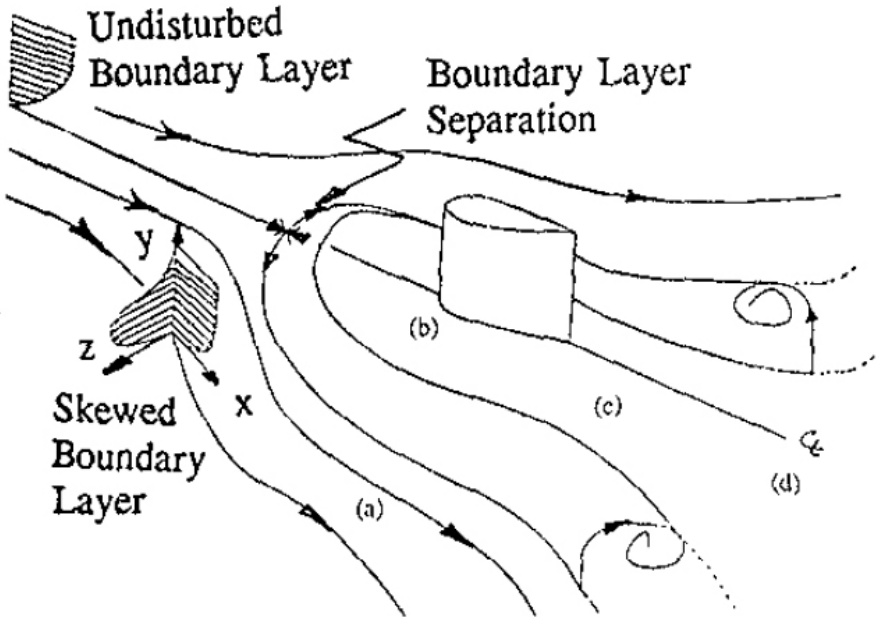

Figure 1.1 Evolution of the juncture flow (Khan and Ahmed 1994)

As streamlines begin and end at critical points and do not cross one another, their topological structure can be defined simply by the number, nature, and connection of singularities. Such streamline patterns in the plane of symmetry and shear-stress patterns on the surface are two-dimensional representations of the more complex three-dimensional systems. Dimensional analysis (Baker 1979) and available experimental evidence suggests that as the Reynolds number increases, the topology changes from a single steady primary vortex to multiple steady vortices. Baker suggested that above a critical vortex core Reynolds number the primary vortex becomes unstable, causing it to break-up and distribute its vorticity into smaller, more stable vortices having a lower core Reynolds number. Such a system is presented in Figure 1.2 (a-c). Figure 1.2 (a) is of a 6

vortex system with the primary singular point defined as *S*. Half saddles of separation and half nodes of attachment are represented as S_i and A_i.

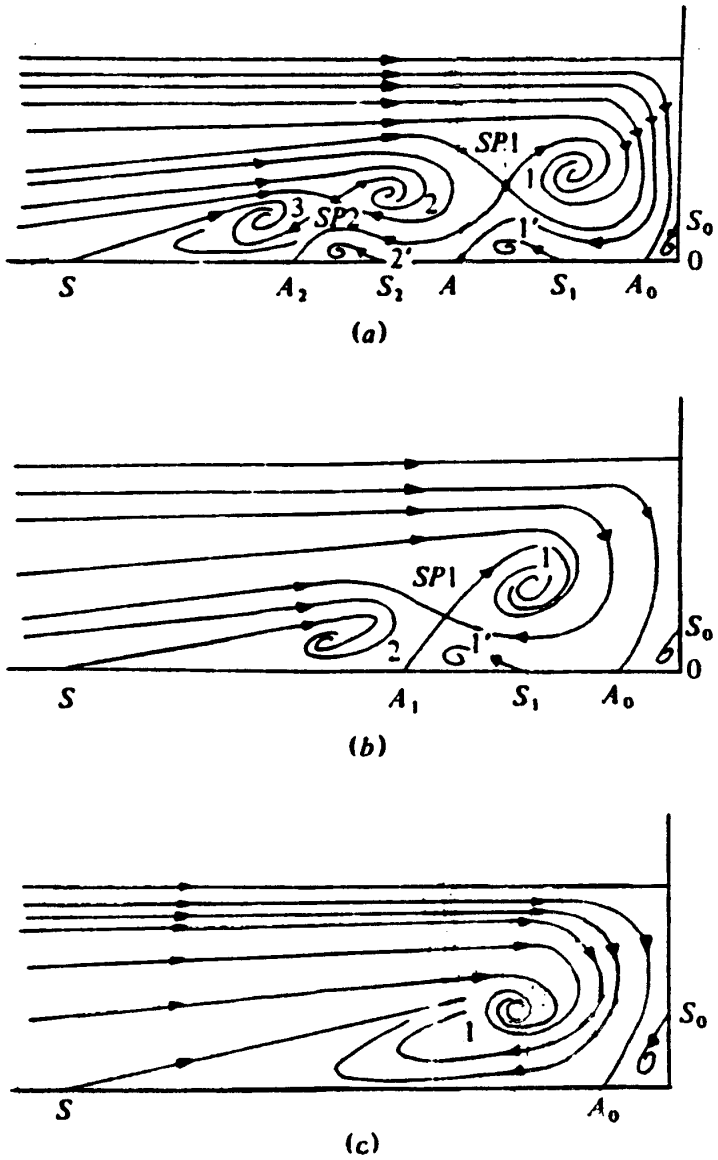

Figure 1.2 (a) 6 vortex system (b) 4 vortex system (c) 2 vortex system (Simpson 2001)

The span-wise vorticity of the incoming boundary layer is distributed among the 3 primary vortices (denoted as 1, 2, 3) separated by the internal saddle points *SP1* and *SP2* which are responsible for the growth of the vortices. The primary vortex is responsible for the high shear stresses in the wall region (Devenport and Simpson 1990). Secondary

vortices denoted as *1'* and *2'* separate from the bottom surface, concentrating the vorticity of the opposite sign generated by the reverse flow in the near-wall region. These secondary vortices are known as counter-rotating foci. The foci structures exist as a result of conservation of streamline topology (Simpson 2001) and backflow in the near-wall region.

Along the attachment line of the obstacle, a streamline commonly known as the bifurcation streamline, (denoted as the topmost streamline in Figure 1.2 (a-c)) divides the flow into an outward and an inward flow. The inward flow is further accelerated due to the primary vortex and continues upstream, affecting the location of the primary singular point. The entrainment of external fluid coupled with high backflow in the corner regions (Shabaka and Bradshaw 1981) and high turbulence near the center of the secondary flow (foci structure) increases the momentum transfer affecting pressure, heat, and mass transfer (Blair 1985) and energizing the mean flow close to the surface (Mehta 1984, Dickinson 1988). For applications involving thermal-fluids flow, the maximum heat flux occurs near the leading edge of the junction (Simpson 1996).

Juncture vortices can be found in the wing-body interface of an aircraft, the sail and fuselage interface of a submarine, support for piers and bridges as they meet the soil bed, masts, hulls, appendage protrusions such as antennae or sensors, and within a turbine blade passage to name a few examples. At low Reynolds numbers the juncture vortex can be characterized as either steady or having some periodic movement. As Reynolds number increases these vortices become highly unsteady resulting in aerodynamic and thermal loss, as well as contributing noise. In the case of a bridge or pier support the high shear stress in the junction erodes the soil, while in a turbine passage the vortices result in

hot spots (Aunapu et. al. 2000). As most of the practical occurrences of juncture flows occur at higher Reynolds number they are responsible for increased drag and heat transfer in the immediate region. An understanding of the various physical mechanisms underlying the evolution of juncture flows would help in controlling drag, noise, and other negative effects.

1.2 Previous Research

Much of past research has looked into model geometry, Reynolds number dependency and their impact on the vortex system. Circular cylinders, square prisms and pyramids and streamlined wings are but a few of the geometries tested as the adverse pressure gradient is directly related to the shape, size, and orientation of the obstacle.

Schwind (1962) defined a system of vortices consisting of five regimes for a 60° wedge. These regimes progressed for increasing Reynolds number. Regime one and two consisted of a single steady circular vortex and behind it, a counter-rotating focus. Further increase in the Reynolds number manifested the third regime as a second and a third pair of vortices and foci. The fourth and fifth regime saw oscillations of the primary vortex and merging with the second and third vortex respectively (Figure 1.3 (a-e)).

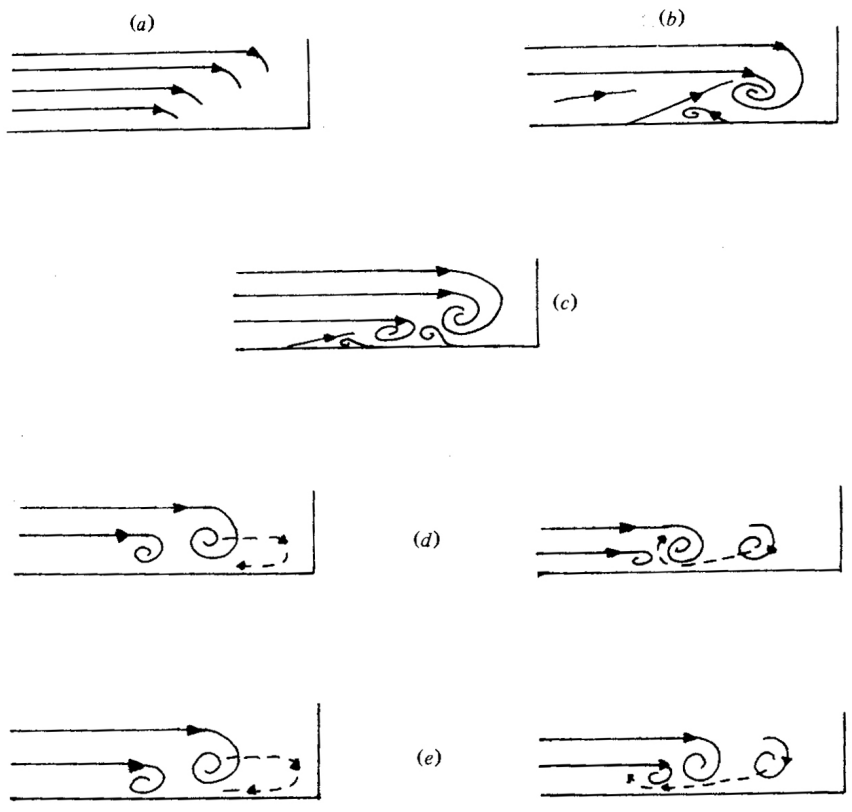

Figure 1.3 Regimes of juncture vortex (a) Regime 1 (b) Regime 2 (c) Regime 3 (d) Regime 4 (e) Regime 5 (Schwind 1962)

Baker (1979) simplified Schwind's five regime model to a three regime model. Baker investigated flow of a cylinder of diameter D and found a steady vortex system with an increasing number of vortices and corresponding counter-rotating foci, followed by an oscillating vortex system, and finally an irregular unsteady flow. As Re_D increased and D/δ^* decreased, the primary vortex moved closer to the leading edge of the obstacle. The primary separation point did follow this trend over the range of Re_D tested (2,000-16,000) suggesting that the position of the primary vortex did not solely depend on the position of the separation point. Analysis of the surface pressure distribution up to the leading edge revealed the presence of local minima, which was determined to be the location of the primary vortex. The absence of local minima was indicative of an

unsteady system. Baker (1980) also investigated the time-averaged effects of juncture flow produced by an incoming turbulent boundary layer. He found little variation in C_p over the range of Reynolds number tested, and reported the location of the primary vortex was mostly influenced by the obstacle's diameter. The vertical size of the primary vortex's influence in the plane of symmetry was dependent on the incoming δ^* (The leading edge C_p increased for larger D/δ. The system experienced a higher u/U_∞ at the leading edge of the obstacle). The primary separation point's location from the leading edge decreased for increasing D/δ^* and $Re_{\delta*}$. Baker (1980) also concluded for a turbulent juncture flow the length of the separated region scaled by diameter for a tall object and by height for a short object.

Kawamura et. al. (1984) investigated varying aspect ratio geometries on the juncture vortex and found von Karman shedding to be incited for aspect ratios greater than 4 along with an up-wash towards the tip of the cylinder. An additional pair of trailing vortices was observed at the tip of the cylinder due to flow separation at the front edge. Okamoto and Sunabashiri (1992) concluded that size of the juncture vortex reduced with an increase in aspect ratio. Khan and Ahmed (2002) investigated flow in the junction of a modified NACA 0015 airfoil for varying aspect ratios. An increase in aspect ratio was found to transition the system from a static to a dynamic system for lower Reynolds number. A reduction in aspect ratio was observed to cause the primary separation point to move closer towards the leading edge of the wing. The tip geometry was found to have little to no effect on the end wall flow. Rifki et. al. (2007) investigated the characteristics of end-wall flow of a surface mounted wing with aspect ratio varying from ½ to 8. As aspect ratio increased, the bifurcation point moved upwards increasing

the inflow and fluid entrained and subsequently the primary and secondary vortex moved downstream towards the leading edge. The system was less sensitive in regards to vortex location for the aspect ratio of four and the vorticity was least sensitive at an aspect ratio of six. The vorticity decreased due to a combination of vorticity diffusion and wall interaction as aspect ratio was further increased. This can be attributed to the higher inflow as the bifurcation point moved upwards.

Mehta (1984) and Rood (1984) have both shown that nose bluntness increased the vortex size and strength. Varying the angle of attack has the incoming flow encountering a more blunt geometry and a 16% decrease in section lift coefficient. The suction side experienced a stronger vortex (Wood and Westphal 1992). Igarashi (1984) varied the angle of attack of a square prism creating different streamwise projected areas for the incoming boundary layer. Very small angle of attacks exhibited perfect separation and symmetric flow while increased angle of attacks caused an imbalance in the flow-field with separation bubbles and re-attached flow to one side of the prism. The flow-field was similar to wedge flow for a 45° angle of attack.

Shizawa et. al. (1996) investigated corner flow where turbulent stresses increase for a constant-thickness cylindrical wing with a semicircular nose. As the angle of attack increased for up to 15°, the turbulent kinetic energy and shearing stresses increased on the suction side and on the pressure side, the downstream leg of the vortex moved away from the juncture. Rood and Anthony (1985) found that the shape of the wing's trailing edge had an effect on the juncture vortex. For a wing at a small angle of attack, a trailing edge geometry that produced greater an adverse pressure gradient increased the size of the vortex legs and the area over which their unsteadiness is felt.

Research by Herst and Gouldin (1997) on a pyramidal shape has shown that the apex angle (sweep) affected the re-attachment length and stabilized the instabilities in the obstacle's wake. Recent experiments for pyramidal structures by Abuomar and Martinuzzi (2000) over a range of vertical wall taper has been shown to modify the surface pressure distribution unlike a rectangular object. The local pressure and heat transfer were greatly affected by a pair of corner vortices that formed on the sides of the pyramid. The front projected area of the pyramid (and subsequently the angle of attack of the pyramid) is the natural scaling factor on which the separation point is dependant.

Khan and Ahmed (1995) reported for increasing back sweep the vortex and separation point travelled towards the leading edge. As forward sweep increased, an opposite effect on the vortex location was seen. The strength of the vortex followed similar trends as the reversed near-wall flow increased for up to -30° but decreased to nearly zero at a forward sweep of 45°.

More realistic wing-body geometries have been investigated by Maughmer et. al. (1989) and reported that the interference drag decreased by 2-3% through use of fairings in the juncture region. Smooth transitions decreased the adverse pressure gradient upstream of the leading edge. The increased area near the wing root helped to recover some of the lost lift and a sharp nose fairing performed better than a blunted geometry as the pressure distributions were less steep. The increase was more notable at lower Reynolds number as the vortex system was more stable in the presence of the thicker boundary layer.

The complexity of the juncture vortex system allows for a myriad of topological models. The system investigated herein is based on a model proposed by Khan et. al

(1995) and Khan and Ahmed (2005). Below Re_t of 2500, the system was shown to be steady and for increasing Reynolds number the system began to oscillate with characteristics dependant on Re_t. These vortex oscillations have been found to be periodic by Tobak and Peake (1979) and further defined by Baker (1991) in the case of a shed primary vortex to die as it travels downstream due to the diminishing supply of fluid from the upstream flow. This shed vortex splits at the leading edge and the two legs convect downstream of the obstacle to re-attach at the trailing edge.

At the lower end of the oscillatory Re_t range the primary vortex convects downstream before returning upstream to wedging between the vortices behind it. A new vortex then forms upstream and the primary vortex is absorbed by vortices 2 and 3. The new system travels downstream and the cycle repeats. As Re_t is increased the primary vortex travels further downstream and upon its return wraps around vortex 2 close to the leading edge instead of merging with vortex 2 and 3.

The third regime (Re_t = 3,900-6,000) is defined by an axial stretching and shedding of the primary vortex. The shed vortex travels downstream towards the leading edge where it is split due to viscous forces to re-connect behind the obstacle (Khan et. al. 1995).

Baker (1991) proposed two types of oscillations present in the case of unsteady convecting vortices; those caused by oscillations of the entire system upstream of the cylinder and those as a result of the oscillations of the vortex core of the primary vortex. Baker suggested at moderate to high values of t/δ^*, as Re_t increased, the secondary oscillations occurred first due to the instabilities in the vortex core at a frequency of $f\delta^*/U_\infty = 0.01$. These oscillations initiate the stronger primary oscillations for a frequency

of 0.08, beyond which the flow becomes fully turbulent. For low values of t/δ^*, because of the proximity in frequencies of primary and secondary oscillations, the main oscillations only occur at a single frequency.

Khan et. al. (1995) have investigated the interactions of the counter-rotating foci, and subsequently the interactions of separation and attachment lines. They have been shown to influence the oscillating regime as the foci interact. As the foci move towards one another the primary focus is flattened under the primary vortex. The primary focus then moves over focus 2 distributing its fluid amongst vortex 2, focus 2, and the near-wall flow, triggering the downstream movement of vortex 2 and the formation of a new focus 2 further upstream. As Re_t is increased the foci interaction rate increases, directly corresponding to higher oscillation of the vortices. However for the third regime, or mode 3, the primary vortex does not interact with the other vortices as neither does the primary focus. The shedding is instead caused as the primary focus reaches its full potential, the primary vortex's cross-section decreases in size increasing the vorticity gradients and thereby increasing viscous dissipation (Khan et. al. 1995). Similar to Thomas' report (1987) the split vortex of mode 3 travels downstream with their split ends at a higher velocity than their tails due to the higher local velocity in the corner region (Shabaka and Bradshaw 1979).

The stabilizing effects of convex curvature are well known, exhibiting a favorable pressure gradient and conferring a higher momentum to the flow. Explained by Von Karman, the angular momentum at any radius is conserved and the flow is maintained at the position by the pressure gradient. As the flow is disturbed and displaced outwards to a new radius where the velocities are greater, the higher radial pressure gradient forces the

fluid back to the lower radius. Consequently, radial and turbulence mixing is rapidly decreased in response to a sudden stabilizing streamwise curvature (Muck et. al. 1985, Baskaran et. al. 1987).

1.3 Objectives

Despite the extensive studies into the nature of juncture vortices, they have only been conducted in regards to varying the adverse pressure gradient of the obstacle. While some investigations delve into control of the vortices by methods of suction and blowing, the influence of the incoming boundary layer has been largely ignored. By introducing a favorable pressure gradient in the region with an adverse pressure gradient to an otherwise zero pressure gradient boundary layer, the goal was to suppress if not eliminate the effects of the juncture vortex upon the surrounding flow and obstacle.

The effects of mild to moderate convex curvature for an initial zero pressure gradient boundary layer were examined for both laminar and turbulent juncture flow of a streamlined cylinder. Physical quantities such as boundary layer integral quantities, location of singular points, periodic frequency, surface pressure, vorticity, and shear stress distribution, were determined as the curvature is varied in order to better understand the dynamics of the juncture vortex.

Chapter 2

Experimental Setup

2.1 Test Facilities

Tests were conducted in Auburn University's water tunnel and open circuit wind tunnel. The water tunnel has a 0.45m x 0.45m cross-section, 2m long transparent test section and is capable of a maximum speed of 1.1m/s with a peak free stream turbulence intensity of less than 1%. The low speed wind tunnel is of an open circuit design with a 0.61m x 0.61m test section capable of speeds of up to 50m/s.

2.2 Coordinate System

A curvilinear co-ordinate system was used for the present experiments (Figure 2.1). The *x* axis (streamwise direction) of a standard Cartesian coordinate was replaced by the *s* (arc length on the hump) axis, positive to the right. The *n* axis was normal to the surface and positive up.

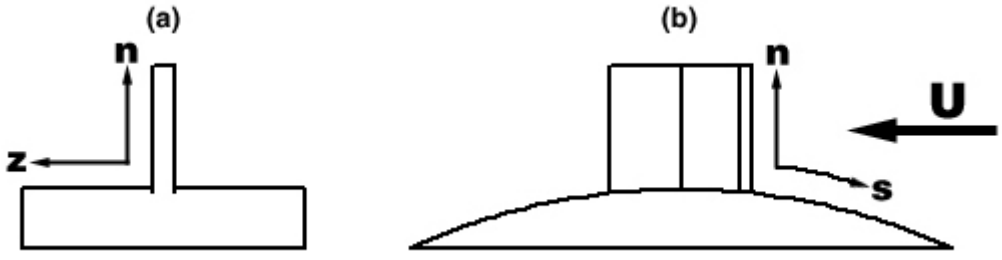

Figure 2.1 (a) Front view of coordinate system (b) Side view of coordinate system

2.3 Hump Geometry

Four different radii convex humps were constructed maintaining a constant arc length (*S*) of 122cm. The geometry of the convex hump is shown in Figure 2.2. Dimensions of four geometries tested are given in Table 2.1. The apex height is *h*, *c* is the chord and *R* represents the radius of curvature of each hump. The apex height *h* was non-dimensionalized by the streamlined cylinder's maximum thickness *t* to analyze hump results against results for a flat plate for which *h/t* = 0.00. A 6.35mm diameter rod placed 5.08cm from the leading edge of the curvature was used to trip the boundary layer for the turbulent boundary layer measurements.

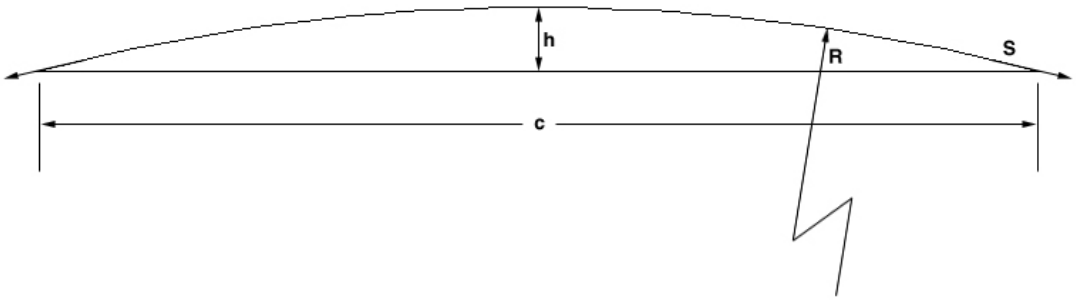

Figure 2.2 Convex hump dimensions

Table 2.1 Hump geometries

Apex h (cm)	h/t	c (cm)	R (cm)
5.08	1.14	121.36	365
10.16	2.29	119.63	181
12.70	2.86	118.32	144
15.24	3.43	116.68	119

Fifty-eight static pressure ports of 3.175mm diameter were drilled into each hump for surface pressure measurements. Forty-six ports were clustered close to the leading edge of the obstacle in an area were the juncture vortex was predicted to form. Twelve

additional pressure ports were drilled further upstream towards the trailing edge of the hump to capture the predicted favorable pressure gradient of the hump without the obstacle in place. The locations of all fifty-eight static pressure ports are presented in Table 2.2 where port 13 (s/t = 0.00) is the leading edge of the obstacle.

Table 2.2 Static pressure port locations from trailing to leading edge

Port No.	Location s/t	Port No.	Location s/t
1	-10.29	30	1.03
2	-9.43	31	1.10
3	-8.57	32	1.17
4	-7.71	33	1.24
5	-6.86	34	1.31
6	-6.00	35	1.38
7	-5.14	36	1.45
8	-4.29	37	1.52
9	-3.43	38	1.59
10	-2.57	39	1.67
11	-1.71	40	1.75
12	-0.86	41	1.83
13	0.00	42	1.92
14	0.06	43	2.00
15	0.11	44	2.07
16	0.17	45	2.16
17	0.23	46	2.24
18	0.29	47	2.33
19	0.34	48	2.43
20	0.40	49	2.52
21	0.46	50	2.62
22	0.52	51	2.71
23	0.59	52	2.81
24	0.65	53	2.92
25	0.71	54	3.03
26	0.78	55	3.15
27	0.84	56	3.26
28	0.91	57	3.38
29	0.97	58	3.52

2.4 Details of Obstacle Model

A streamlined cylinder geometry with a length of 30.48cm was made from black polyurethane. A tapered trailing edge eliminated the formation and shedding of the von Karman vortices in the wake (M. C. Smith 1968). Four base models (one for each hump) of 2.22cm height and diameter of 4.45cm were machined and then molded with epoxy to lie flush with the humps. A taller streamlined cylinder was then attached to the four individual models during testing to obtain an aspect ratio of 6 in order to negate any end-effects (Rifki 2006). The leading edge of the model was located at 45.72cm from the leading edge of each hump to ensure a consistent surface for the boundary layer to grow on. The midpoint of the models was located at the apex of each hump. A sectional view of the streamlined cylinder is represented in Figure 2.3.

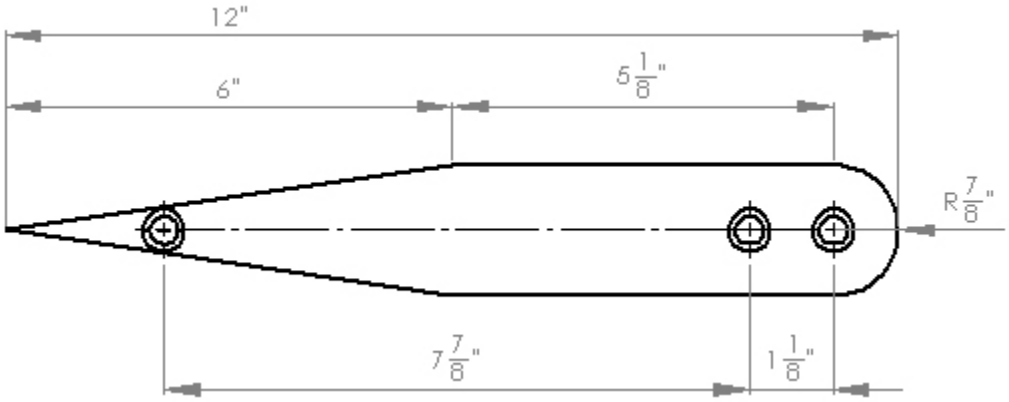

Figure 2.3 Streamlined cylinder (dimensions in inches)

2.5 Water Tunnel Flow Visualization

Preliminary flow visualization of the laminar juncture-vortex system in the streamwise plane was conducted through the use of hydrogen bubbles. The setup, shown in Figure 2.4 consisted of the model, a hydrogen bubble wire probe, an argon ion laser, and a camera for recording the images. The hydrogen bubbles produced from the bubble

wire were illuminated by the light sheet to visualize the juncture flow accurately for speeds above 0.03m/s. Both qualitative and quantitative data were obtained and used to define steady conditions for which PIV data was recorded.

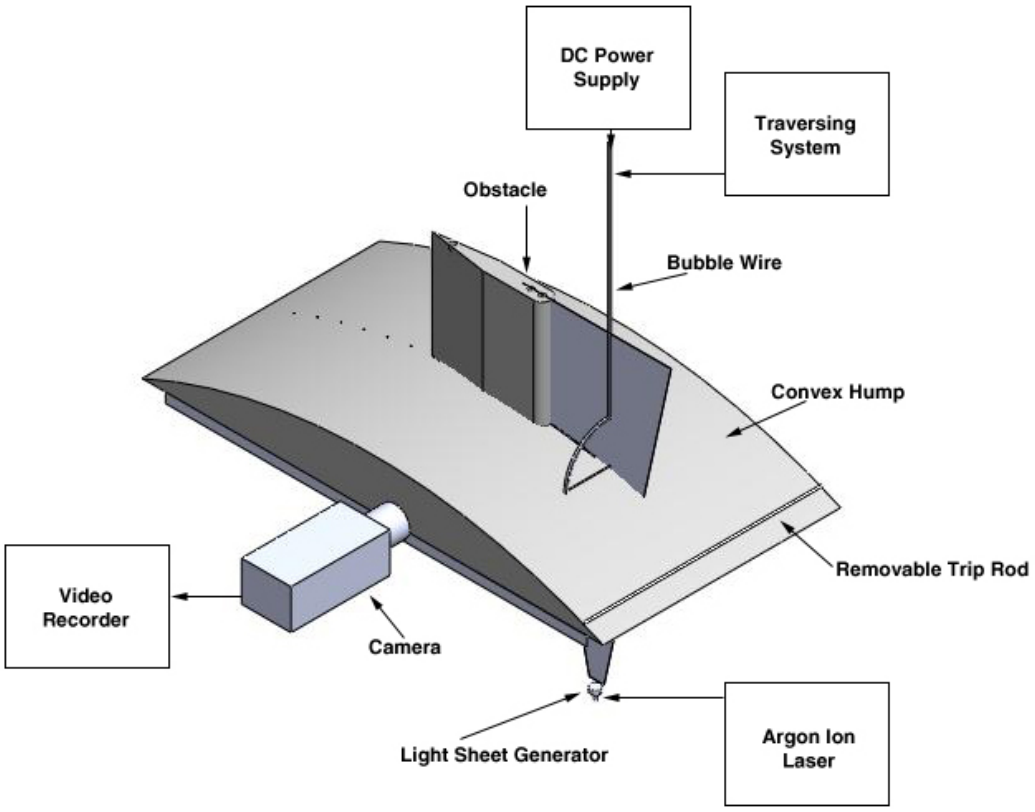

Figure 2.4 Water tunnel streamwise flow visualization setup

The hydrogen bubble probe had platinum wires of 32Swg spaced evenly on a flexible stainless steel bow. The wires were spaced accordingly in order to capture the inner and outer characteristics of the vortices. The probe was mounted on a two degree of freedom traversing system controlled by a Velmex Inc. VP9000 controller allowing for precision placement. Three DC power supplies were connected in series supplying 0-60 volts across the wires and a stainless steel anode submerged in the test section. Illumination was supplied from a 5 watt Argon Ion laser and an OZ optics fiber optic light sheet

generator. The flow was recorded onto S-VHS tape through a COHU solid state camera and a Kern 26mm f/1.1 macro lens at full aperture by a JVC BR-S622DXU video recorder. Selected images were then printed using a SONY thermal video graphic printer and further analyzed.

Surface visualization of the system was conducted for Re_t = 1,300, 2,000, and 3,200, corresponding to the vortex modes 1, 2, and 3 (respectively) (Khan et. al. 1995). Sodium fluorescein crystals were sprinkled onto the surface far upstream of the flow. The released dye traced the near-wall flow precisely. The argon ion laser sheet positioned tangent to the point of interest on the hump's surface and further thickened by passing it through a half-cylindrical lens in order to capture a larger area as the surface curved. A mirror was placed underneath the test section at 45° allowing for easy recording of the surface flow visualization.

2.6 Particle Image Velocimetry

Particle image velocimetry (PIV) measurements of the juncture-vortex system in the plane of symmetry were made with Dantec Dynamics FlowMap PIV system consisting of a 50 mJ double-pulsed Nd:YAG laser, a HiSense MKII PIV/PLIF 1,280 x 1,024 cross-correlation CCD camera with a Nikon 60mm f/2.8 at full aperture, and a PIV-2100 processor.

Silver coated hollow glass spheres of 20μm nominal diameter were used to seed the flow. The captured image pairs were 1,280px x 1,024px and processed using Dantec Dynamics FlowManager software with a 32px x 32px pixel interrogation area with 50% overlap. Sixty pairs of images were recorded for each juncture-vortex mode at Re_t =

1,300, 2,000, and 3,200. These were then adaptively correlated with a moving average. The uncertainty analysis yielded an error of 2.24% in mean velocities.

2.7 Surface Pressure Measurements

Surface pressure distributions were measured for Re_t = 47,000 73,000, and 97,000. A Scanivalve system passed through a calibrated signal conditioner and automated by LABVIEW 8.2 software was used to collect the pressure difference across each port. The surface pressure setup is represented in Figure 2.5. A splitter plate was constructed to negate any boundary layer growth on the sides of the wind tunnel. The two plates also added weight and stability to the convex hump, keeping any chance of the apparatus movement to a minimum. Measurements were also taken without the obstacle in place in order to obtain the pressure distribution over just the convex hump.

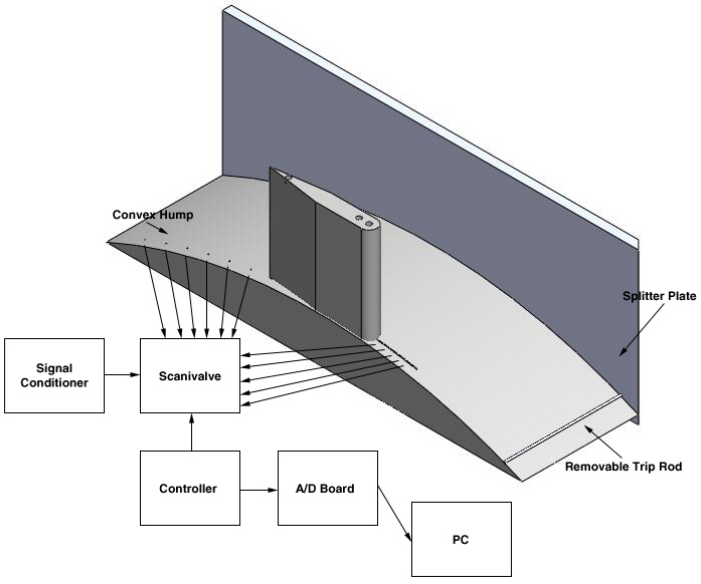

Figure 2.5 Cross section of wind tunnel surface pressure setup

2.8 Boundary Layer

Laminar and turbulent boundary layer data were taken normal to the hump at the location where the leading edge of the obstacle was positioned. A pitot probe of 0.3175mm diameter was attached to a two degree of freedom traversing system controlled by a Velmex Inc. VP9000 controller. LABVIEW 8.2 and a digital acquisition board were used to obtain data. The central Scanivalve port was connected to the local static pressure port directly underneath the boundary layer port. Dynamic pressure was calculated following the technique outlined by Gillis and Johnston (1983) for curved surfaces (Eq. 2.1-2.3) where P_t, P_r, and P_{sw}, are the total pressure, total pressure in the potential core, and local wall static pressure, respectively. U_p is the local potential velocity, U_{pw} is the potential core velocity (defined as the free-stream velocity), and $U_{(n)}$ is the local velocity.

$$P_r - P_{sw} = \frac{1}{2}\rho U_{pw}^2 \tag{2.1}$$

$$U_p = U_{pw}\frac{R}{R+n} \tag{2.2}$$

$$U_{(n)} = \left[\frac{2}{\rho}\left\{\left(P_t - P_{sw}\right) - \left(P_r - P_{sw}\right)\left(1 - \frac{1}{\left(1+\frac{n}{R}\right)^2}\right)\right\}\right]^{\frac{1}{2}} \tag{2.3}$$

2.9 Wind Tunnel Flow Visualization

To understand the complex nature of the flow, surface flow visualization was accomplished using a combination of kerosene and tempera powder. Vellum sheets covered the surface of the convex humps to ensure a uniform, smooth surface for the flow

to establish and to provide contrast against the black tempera powder. Areas near the leading edge, trailing edge, and sides of the streamlined cylinder were painted with the mixture to capture the juncture flow in its entirety. As the kerosene evaporated, the powder traced the limiting streamline patterns of a time averaged vortex system for Re_t = 97,000. Once the pattern was established, photographic records were made. Photographs were taken for both laminar and turbulent approach boundary layers.

Chapter 3

Water Tunnel Results and Discussion

3.1 Boundary Layer and Integral Values

Boundary layer data was extracted from a 1,280px x 1,024px PIV image map in the water tunnel for Re_t = 1,300. The window gave a 2D flow field of 79 x 63 velocity vectors. Resultant velocity vectors at each point *(i, j)* normal to the surface were calculated (Eq. 3.1) 46cm from the leading edge of the hump without the surface obstacle in place. For turbulent boundary layer a 6.35mm diameter rod placed at 5.08cm from the leading edge of the hump to trip the boundary layer. Turbulent boundary layer data was obtained for Re_t = 1,800. These values of Re_t were chosen to correspond with the mode 1 (Khan et. al. 1995) steady vortex system.

$$\sqrt{U^2 + V^2} \tag{3.1}$$

The boundary layer height δ is defined as the height where the local velocity is 99% of the free-stream velocity (Eq. 3.2).

$$u(y) = 0.99U_\infty \tag{3.2}$$

Displacement and momentum thickness is defined in Eq. 3.3, 3.4

$$\delta^* = \int_0^\delta \left(1 - \frac{u}{U_\infty}\right) dy \tag{3.3}$$

$$\theta = \int_0^1 \frac{u}{U_\infty}\left(1 - \frac{u}{U_\infty}\right)dy \tag{3.4}$$

The corresponding shape factor was calculated using

$$H = \frac{\delta^*}{\theta} \tag{3.5}$$

For laminar boundary layers H is around 2.5 whereas turbulent boundary layers exhibit H ~ 1.6. Tables 3.1, 3.2 contain laminar and tripped boundary layer data for the four humps and their corresponding Reynolds numbers based on displacement thickness and momentum thickness. PIV data was also collected a flat plate configuration for comparison purposes.

Table 3.1 Integral quantities – laminar boundary layer

h/t	δ (mm)	δ* (mm)	θ (mm)	H	Re_{δ^*}	Re_θ
3.43	9.17	2.34	1.28	1.82	107.73	59.09
2.86	10.18	2.45	1.27	1.93	108.72	56.30
2.29	14.39	4.36	2.39	1.82	179.44	98.44
1.14	17.45	4.81	2.16	2.23	174.26	78.28
0.00	20.76	6.10	2.83	2.15	205.48	95.36

Table 3.2 Integral quantities – tripped boundary layer

h/t	δ (mm)	δ* (mm)	θ (mm)	H	Re_{δ^*}	Re_θ
3.43	9.07	2.06	1.20	1.71	135.16	78.84
2.86	10.73	2.64	1.49	1.77	160.12	90.58
2.29	11.25	2.73	1.37	1.99	157.97	79.36
1.14	22.80	4.48	2.47	1.82	223.11	122.76
0.00	25.97	4.81	2.96	1.63	220.22	135.46

Simpson (2001) defined the laminar and turbulent juncture flow regimes based on Re_{δ^*}. He reported that for Re_{δ^*} below 1,000, the vortex system remains laminar. For the

present tests $Re_{\delta*}$ was well below 1,000 for all cases and was the flow was confirmed to be steady and laminar as observed in the flow visualization tests.

The laminar boundary layer profiles collapse well in similarity coordinates (Figure 3.1). The tripped boundary layer profiles were fitted to the law (Eq. 3.6) of the wall through an iterative procedure for the correct value of C_f.

$$u^+ = 5.6\ln(y^+) + 4.9 \tag{3.6}$$

$$u^* = U_\infty \sqrt{\frac{C_f}{2}} \tag{3.7}$$

$$u^+ = \frac{u}{u^*} \tag{3.8}$$

$$y^+ = \frac{yu^*}{\nu} \tag{3.9}$$

The profiles are presented in Figure 3.2. The viscous sub-layer and logarithmic layer is clearly visible however the wake dips below due to a very thin boundary layer on the convex surface (Bandyopadhyay and Ahmed 1993). The skin friction coefficients show little variance up till $h/t = 2.29$ but steadily decrease with increasing h/t.

The velocity defect profiles are presented in (Figure 3.4). The profiles collapsed to one curve, however do not exactly match that of a turbulent boundary layer. It was concluded that the boundary layer was at best transitional due to low Reynolds number and shorter length than needed for establishment of a fully grown turbulent boundary layer.

To determine the influence of a favorable pressure gradient due to a convex surface, the Clauser shape factor G was calculated using Eq. 3.10, 3.11 and is presented in Figure 3.5.

$$\Delta = \int_0^\infty \frac{U_\infty - \bar{u}}{u^*} dy \tag{3.10}$$

$$G = \frac{1}{\Delta} \int_0^\infty \left(\frac{U_\infty - \bar{u}}{u^*} \right)^2 dy \tag{3.11}$$

The value of G for an equilibrium boundary layer is 6 to 7. As convex curvature is introduced through an increase in h/t, the system progressed towards equilibrium due to the favorable pressure gradient.

A decreasing boundary layer thickness with increasing h/t for the same freestream Reynolds number indicates the effects of increasing local velocity as the flow encounters a steeper hump (Figure 3.6). Integral quantities are plotted in Figure 3.7-3.9 for varying h/t with h/t = 0.00 corresponding to the flat plate and h/t = 3.43 corresponding to the steepest hump. It was observed that the growth of the tripped boundary layer decreased with increasing curvature. The shape factors for both the laminar and tripped boundary layers on a flat plat plate are comparable to the generally accepted values found in the literature. As evident in Figure 3.10, the shape factor, after an initial increase, continues to decrease and with increasing h/t.

Previous experiments on the juncture vortex have been conducted for a fully developed boundary layer with a zero pressure gradient. It was concluded that for the water tunnel experiments, the total length of 46cm measured from the leading edge of the obstacle was not enough to develop an equilibrium boundary layer. A possible explanation is that the tripped boundary layer re-laminarized due to curvature induced favorable pressure gradient.

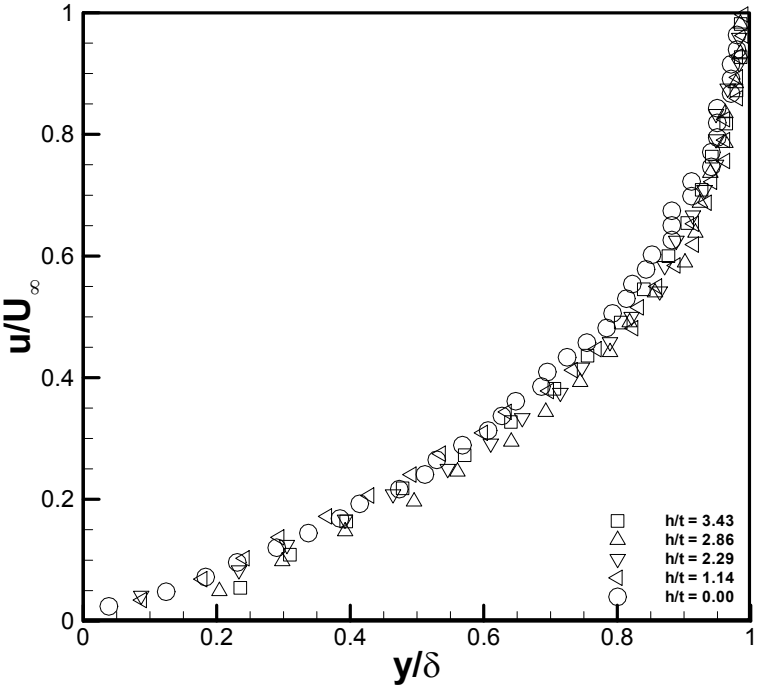

Figure 3.1 Laminar boundary layer profile

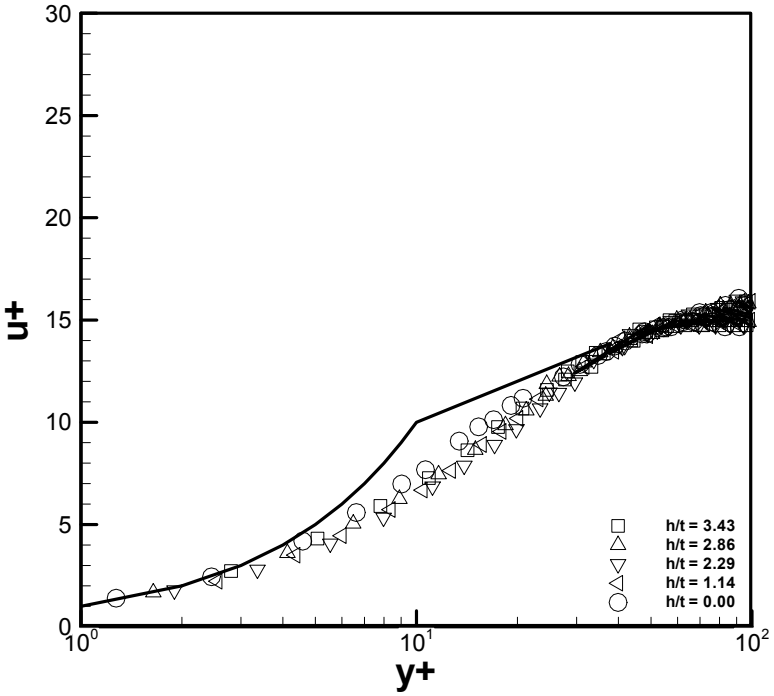

Figure 3.2 Tripped boundary layer profile

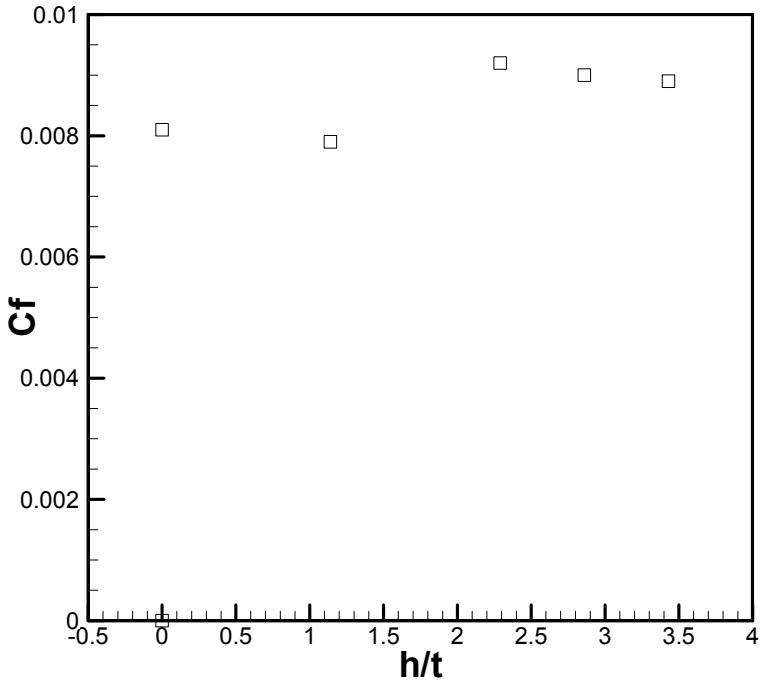

Figure 3.3 Skin friction coefficient – tripped boundary layer

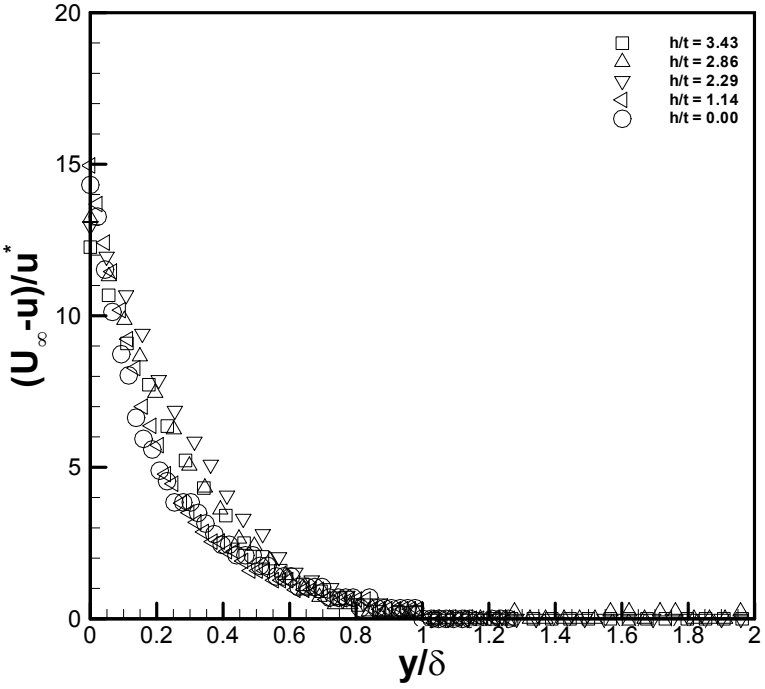

Figure 3.4 Defect profile – tripped boundary layer

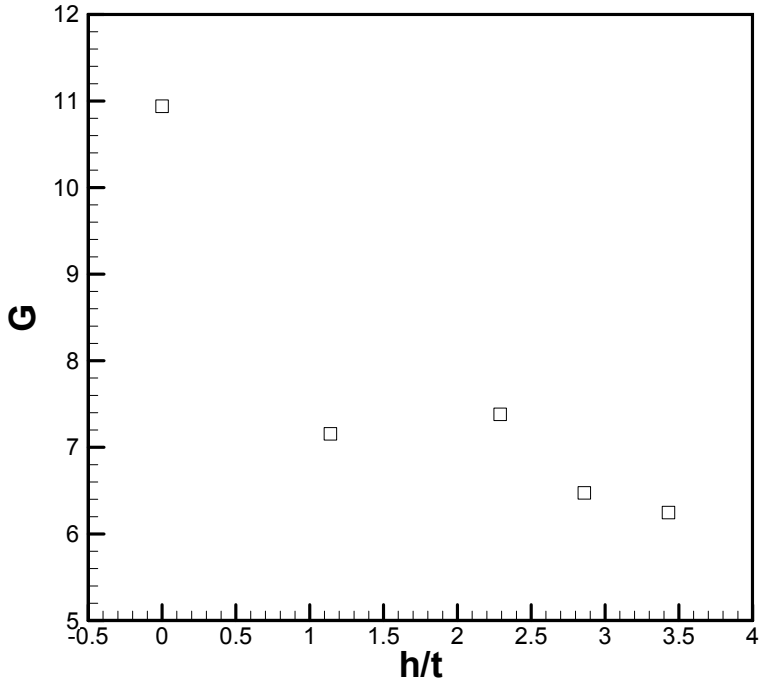

Figure 3.5 Clauser shape factor – tripped boundary layer

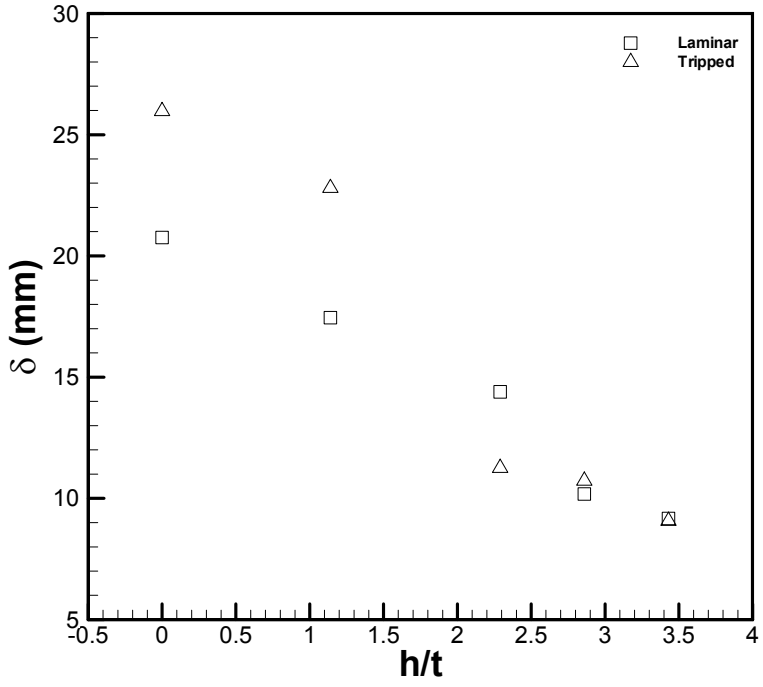

Figure 3.6 Boundary layer thickness

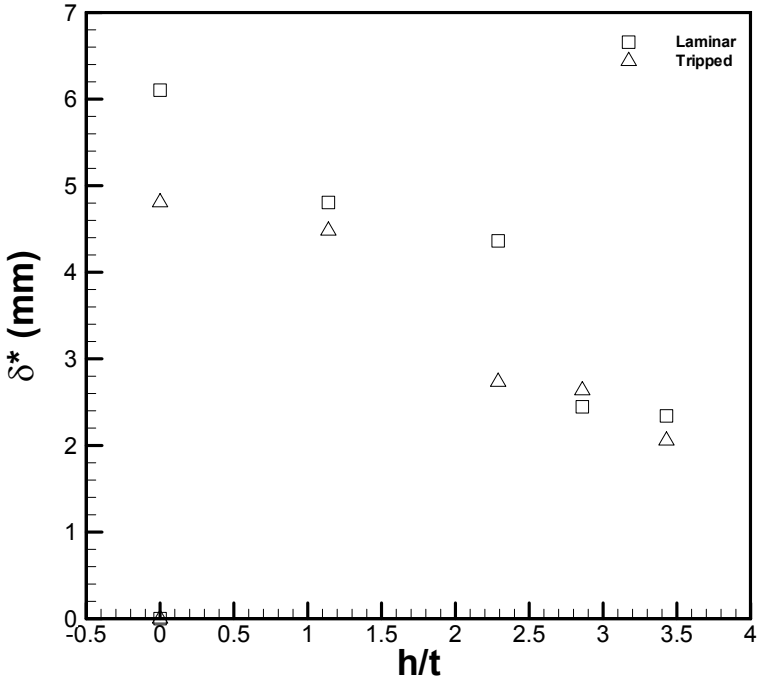

Figure 3.7 Displacement thickness

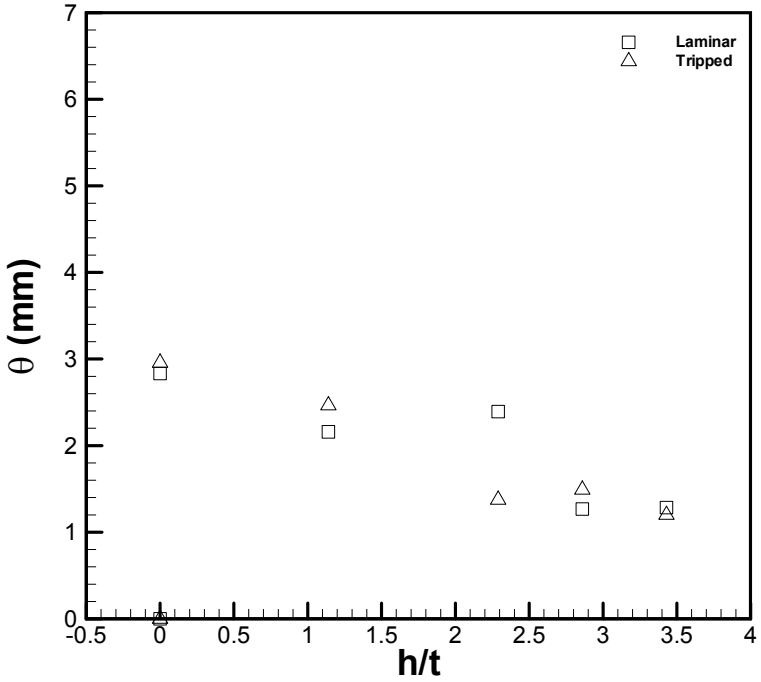

Figure 3.8 Momentum thickness

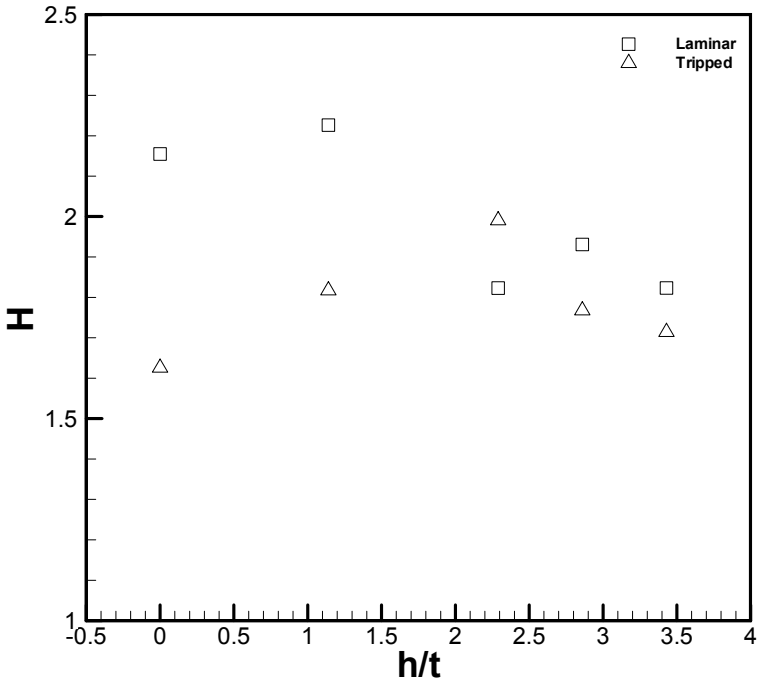

Figure 3.9 Shape factor

3.2 Range of Reynolds Number

Khan et. al. (1995) defined a range of Reynolds number, based on maximum thickness, for which the three modes of the vortex system in the juncture region manifested. Mode 1 was defined below Re_t = 2,500, mode 2 was observed between Re_t = 2,500-3,500, and mode 3 was between Re_t = 3,900 and 6,000. Detailed observations on the behavior of the juncture flow for changes in ΔRe_t = 72 were made using flow visualization of hydrogen bubbles in the plane of symmetry. Ranges over which the three modes manifested are documented (Table 3.3, Figure 3.10-3.12) for h/t = 1.14, 2.29, 3.43.

Table 3.3 Range of ΔRe_t for h/t = 1.14, 2.29, 3.43

	Mode	Start (Re_t)	End (Re_t)	Range (ΔRe_t)
h/t = 1.14	1	1,081	2,229	1,148
	2	2,301	3,090	789
	3	3,161	5,026	1,865
h/t = 2.29	1	1,081	1,870	789
	2	1,942	2,803	861
	3	2,874	5,169	2,295
h/t = 3.43	1	1,081	1,799	717
	2	1,870	2,516	646
	3	2,587	4,739	2,152

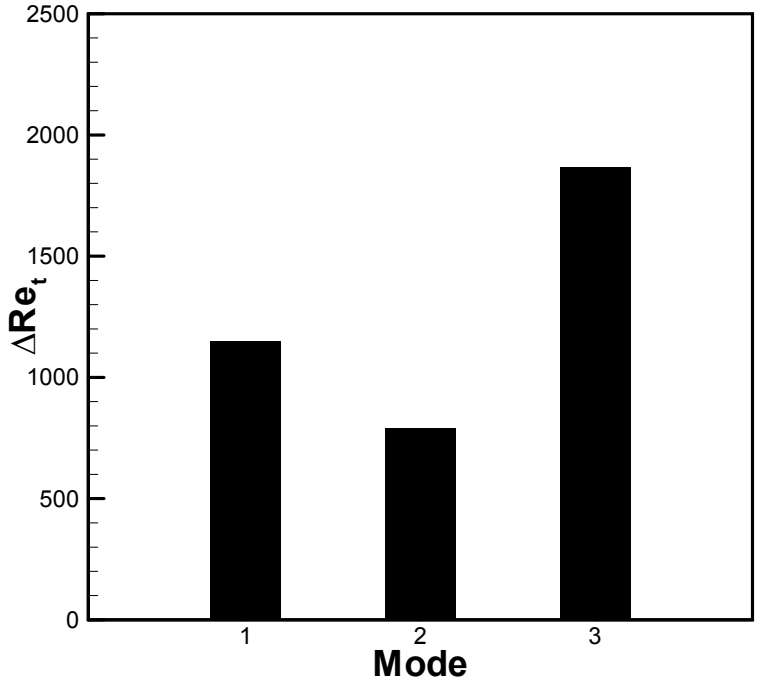

Figure 3.10 Range of ΔRe_t for h/t = 1.14

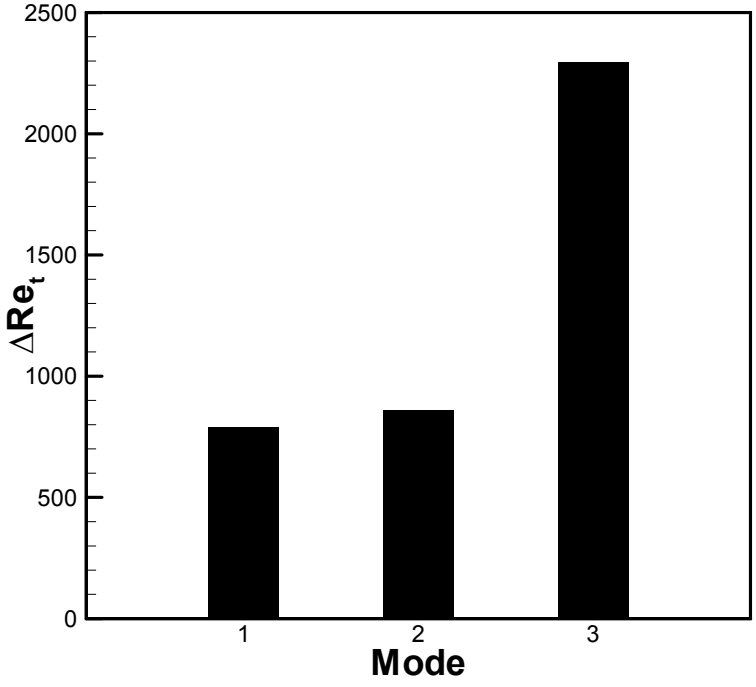

Figure 3.11 Range of ΔRe_t for $h/t = 2.29$

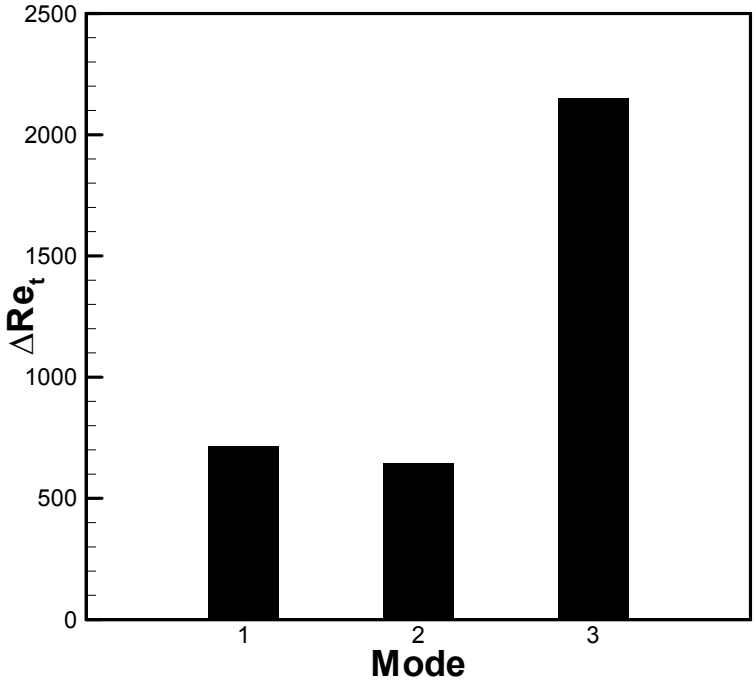

Figure 3.12 Range of ΔRe_t for $h/t = 3.43$

From the preceding table and Figure it is evident that mode 2 is the shortest lived regime; its range shortened as *h/t* increased. Mode 1 also transitioned earlier as *h/t* increased. Though not observed, it can be speculated that for even steeper humps for which the flow remains attached, the range of Reynolds number for mode 2 will decrease further; the oscillations of mode 2 occurring at higher frequencies till the system transitions from a steady mode 1 to a shedding and splitting mode 3.

The decrease in range of Reynolds number over all humps can be attributed to the increased local velocity. Whereas the mode 2 and 3 range is lower than reported by Khan et. al. (1995), the range of existence for mode 3 is similar to earlier reports. The stabilizing effects of convex curvature delayed transition of the juncture vortex to a turbulent system.

3.3 Characteristic Frequency

The non-dimensionalized frequency of the oscillations of the vortex system was calculated as the Strouhal number

$$St = \frac{fL}{U_\infty} \tag{3.12}$$

f is the frequency of oscillation, L is the characteristic length (maximum thickness t of the streamlined cylinder), and U_∞ is the free-stream velocity. The Strouhal number varied linearly for modes 2 and 3; the mode 2 slope increased while the mode 3 slope decreased with increasing *h/t*.

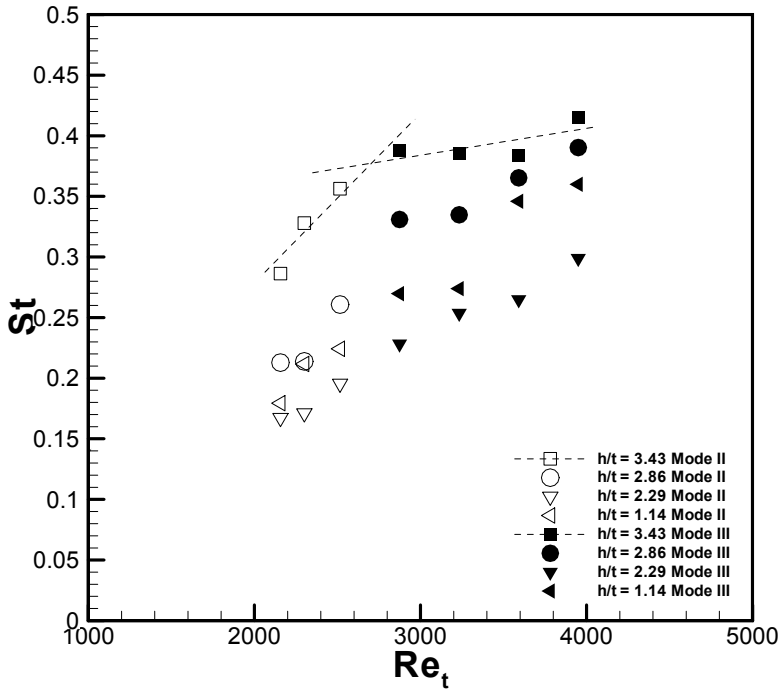

Figure 3.13 Characteristic frequency

The steepest hump (*h/t* = 3.43) displayed the steepest variation in the oscillations of the primary vortex as a function of Reynolds number indicating the short longevity of mode 2 in conjunction with Table 3.3. Mode 3 was the most persistent; a fully turbulent system delayed due to its near flat variance with Reynolds number. The vortices progressed slower towards an unsteady system as Reynolds number is increased. For *h/t* = 1.14, the characteristic frequency lies within that reported by Khan et. al. (1995), as the curvature is increased the reported values are upwards of 1.5 times those previously observed indicating faster shedding of the primary vortex. Again this can be attributed to the increased local velocity in the juncture region increasing the local Reynolds number.

3.4 Flow Visualization

Flow visualization of the streamwise and spanwise vortex system confirmed the presence of a two vortex system with one foci structure. The system behaves accordingly to the model proposed by Khan and Ahmed (2005). Planar measurements allowed the location of the primary separation point to be accurately measured from the leading edge of the obstacle (Figure 3.14).

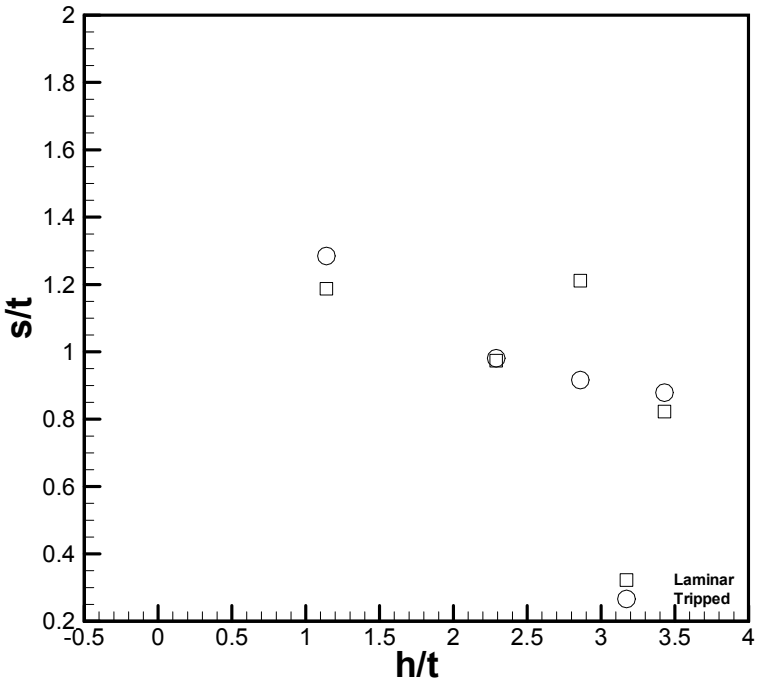

Figure 3.14 Location of primary separation point

The laminar system showed little difference till h/t = 3.43. The tripped boundary layer shows a more consistent trend. The increased favorable pressure gradient as h/t is increased delayed separation and as a result, the vortex system formed closer to the leading edge of the object.

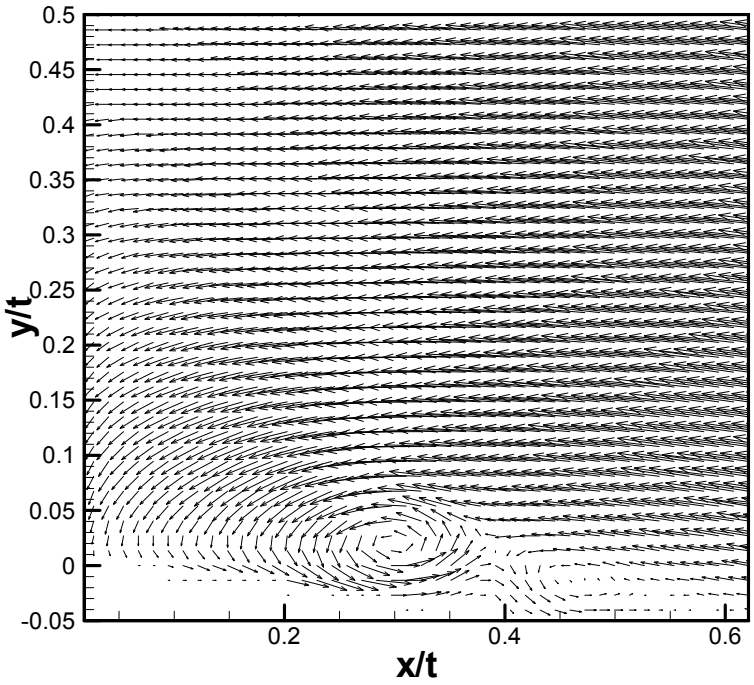

Figure 3.15 Vector plot for $h/t = 3.43$ – laminar boundary layer

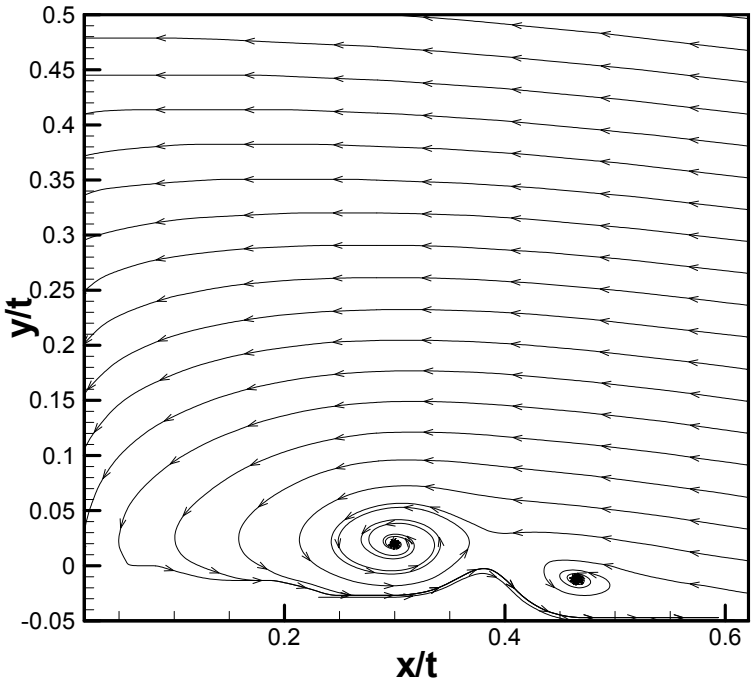

Figure 3.16 Streamlines for $h/t = 3.43$ – laminar boundary layer

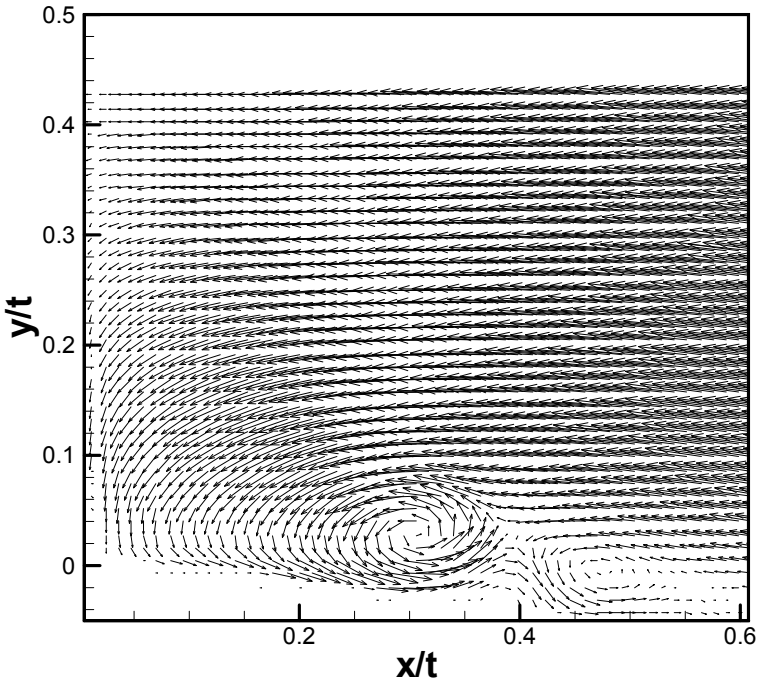

Figure 3.17 Vector plot for h/t = 3.43 – tripped boundary layer

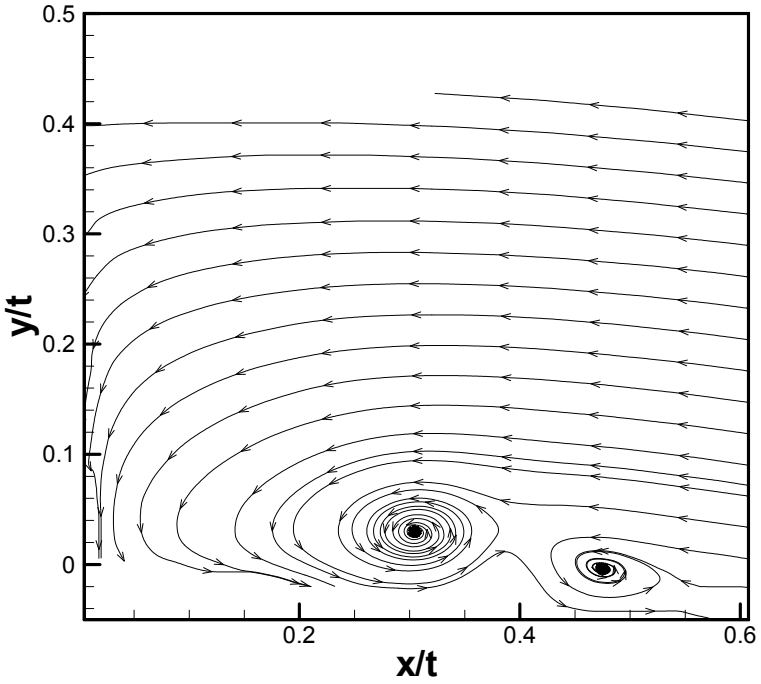

Figure 3.18 Streamlines for h/t = 3.43 – tripped boundary layer

PIV was used for the determination of the location of the primary vortex and the primary saddle point. The saddle point exhibits high shear and is responsible for the growth of the primary vortex. Figure 3.15-3.18 is of the resultant velocity vectors and resulting streamlines of the vortex system for $h/t = 3.43$. For both the laminar and tripped boundary layer the primary vortex moved closer towards the object as h/t was increased (Figure 3.19).

Figure 3.20 shows the distance between the vortex core and primary saddle point. The flat plate ($h/t = 0.00$) shows a large gap between the two, but the distance decreases as h/t is increased. The convex curvatures show little difference between laminar and tripped boundary layers whereas the trip rod greatly impacts the distance between the vortex core and saddle point for the flat plate.

The displacement of the bifurcation point was determined from velocity vectors (Figure 3.21-3.22) along with interpolation of the location of zero y velocity as the vector plots have a finite difference between data points.

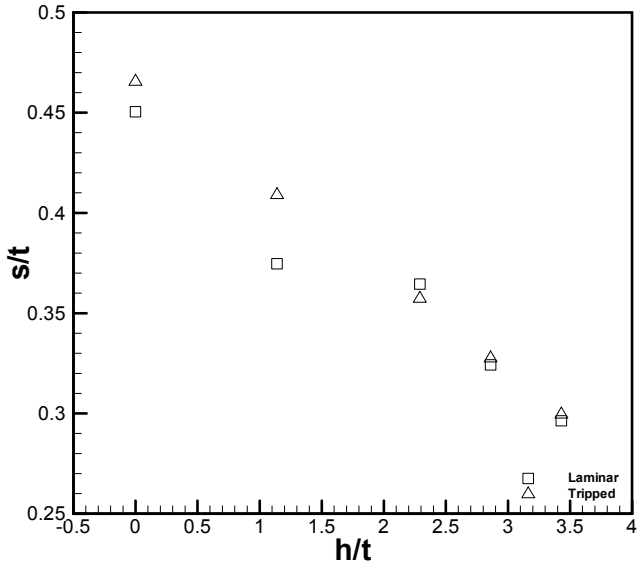

Figure 3.19 Location of primary vortex

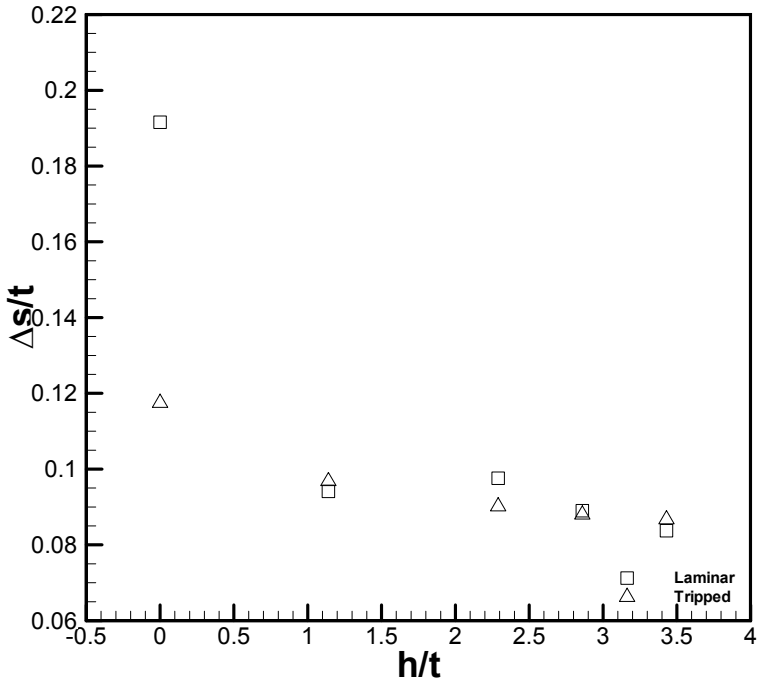

Figure 3.20 Distance between vortex core and saddle point

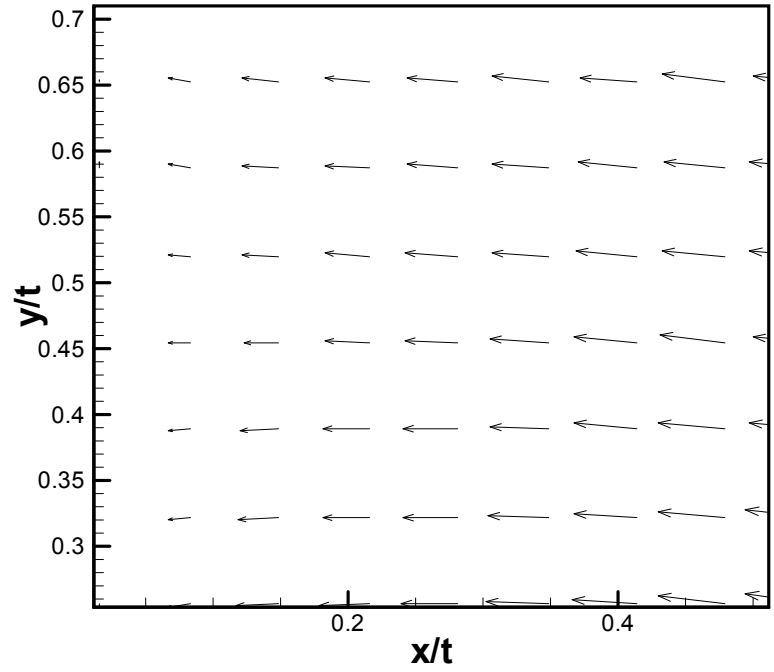

Figure 3.21 Bifurcation streamline for $h/t = 3.43$ – laminar boundary layer

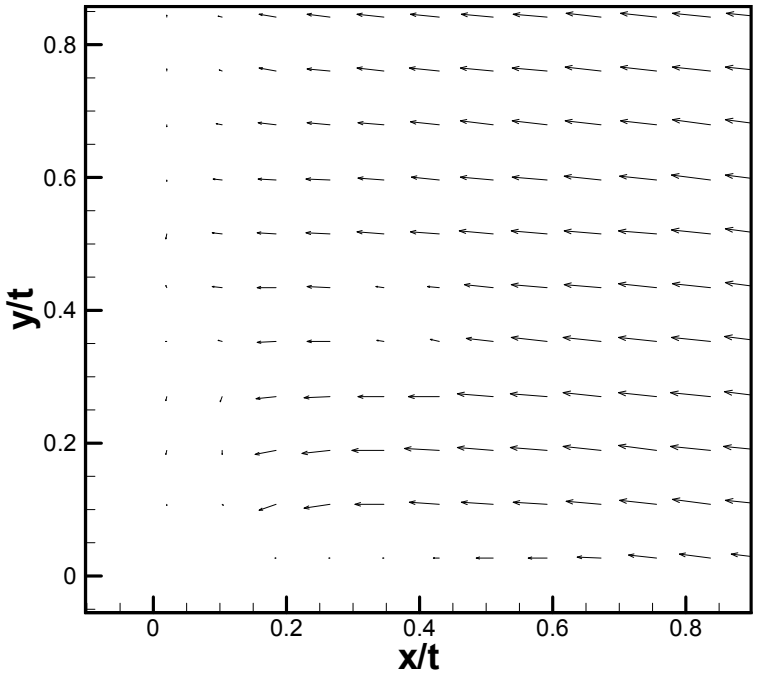

Figure 3.22 Bifurcation streamline for h/t = 3.43 – tripped boundary layer

The bifurcation point is the vertical location of the streamline along the attachment line of the obstacle. The flow is divided into the inflow and the outflow, partially defining the amount of fluid entrained within the vortex system. As h/t is increased, the bifurcation point moves downwards (Figure 3.23) decreasing the fluid entrained within the vortex system. Combined with delayed separation, a more compact vortex system is formed. The influence of the juncture vortex on the face of the obstacle is greatly diminished. The tripped boundary layer shows less sensitivity to the effects of the convex curvature in regards to the vertical location of the bifurcation point.

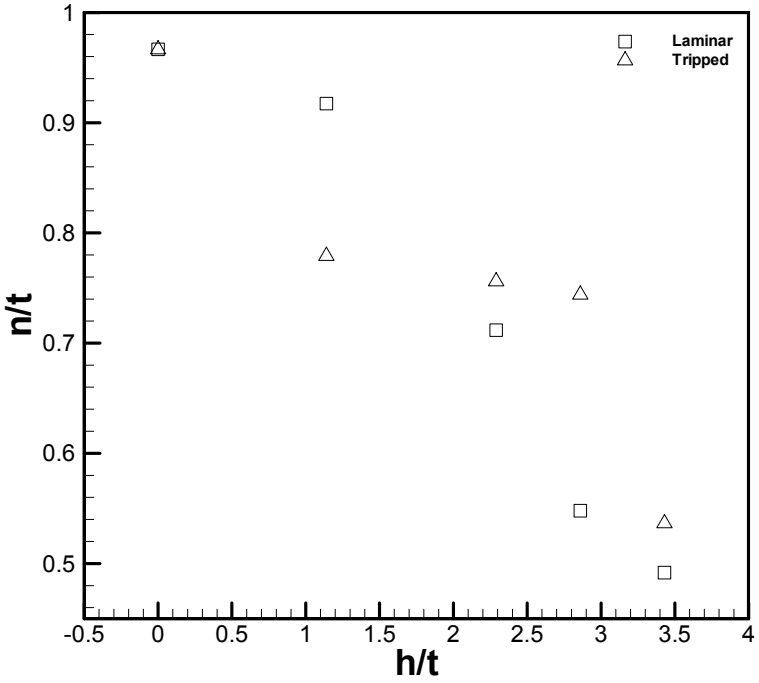

Figure 3.23 Location of bifurcation streamline

3.5 Vorticity and Strain Contours

Since PIV gave a two-dimensional vector field for the juncture vortex, it is possible to calculate quantities such as vorticity and strain (Eq. 3.13, 3.14 respectively)

$$\omega = \left(\frac{dv}{dx} - \frac{du}{dy} \right) \tag{3.13}$$

$$S = \left(\frac{dv}{dx} + \frac{du}{dy} \right) \tag{3.14}$$

these quantities were matched with vector maps to further analyze the vortex structures. The maximum positive vorticity can be seen to correspond with the location of the primary vortex while the maximum positive strain corresponds with the location directly beneath the primary vortex (Figure 3.24, 3.25).

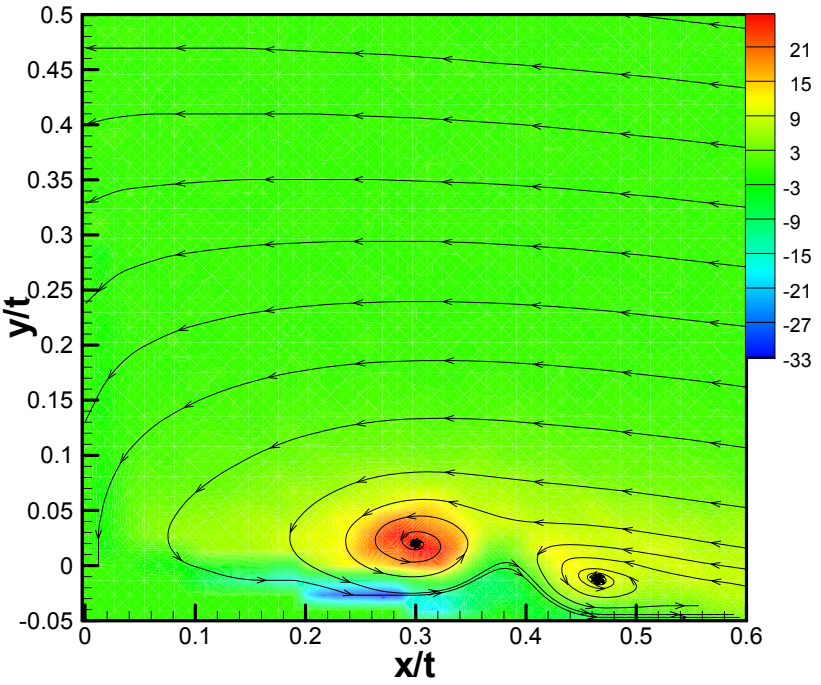

Figure 3.24 Vorticity for $h/t = 3.43$ – laminar boundary layer

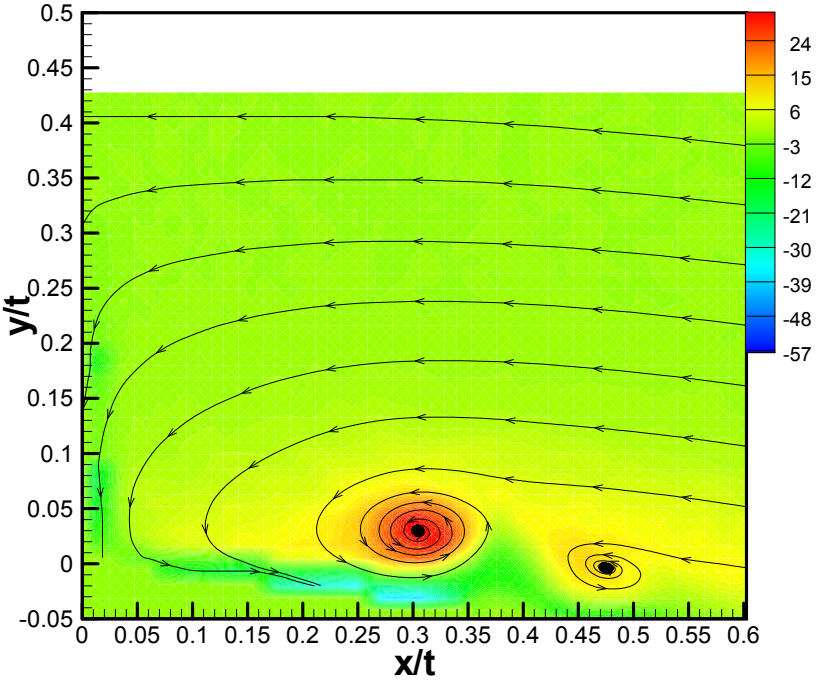

Figure 3.25 Vorticity for $h/t = 3.43$ – tripped boundary layer

This near-wall area is a region of the most intense backflow of the entire flow-field, further accelerated by the circulation of the primary vortex.

Also discernable is the primary saddle point and its association with high negative strain along with the high shear experienced on the face of the obstacle as the fluid is entrained in the vortex (Figure 3.26, 3.27). Simpson (2001) and Baker (1979) have reported the formation of a counter-rotating corner vortex on the face of the obstacle in the near-wall region. While the vector and streamline plots show no such formation, the vorticity and strain plots show a slight signature of such a vortex. As the juncture vortex is compacted with increasing *h/t*, presence of this vortex is greatly diminished.

As *h/t* is increased, both the maximum positive (corresponding with the primary vortex) and the maximum negative (corresponding with the focus) vorticity increased (Figure 3.28). The decreased location (*n/t*) of the bifurcation point and increased local velocity of the steeper humps lead to an increased axial stretching of the primary vortex and increased circulation. The case of the incoming boundary layer tripped by the rod displays larger values for both positive and negative vorticity leading to further proof for the re-laminarization of an initially turbulent boundary layer. The relation between vorticity and strain were analyzed for varying distances along *n* from the surface of the hump. In the near-wall region there is near one to one inverse relationship between vorticity and strain as the backflow feeds the focus. Further up from the surface there is more scatter among the data and a relation is difficult to obtain. A point of interest is the somewhat reverse *y* shape the data presents. It is assumed the upper right arm (Figure 3.29) of the structure to be representative of the location above the vortex core (*n*) in an area where the strain is positive and vorticity is near zero.

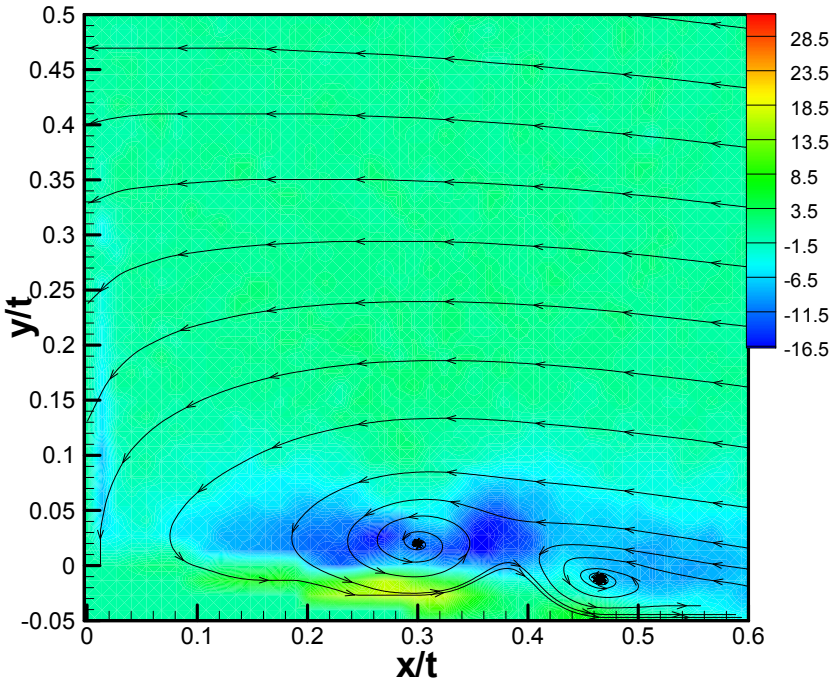

Figure 3.26 Strain for *h/t* = 3.43 – laminar boundary layer

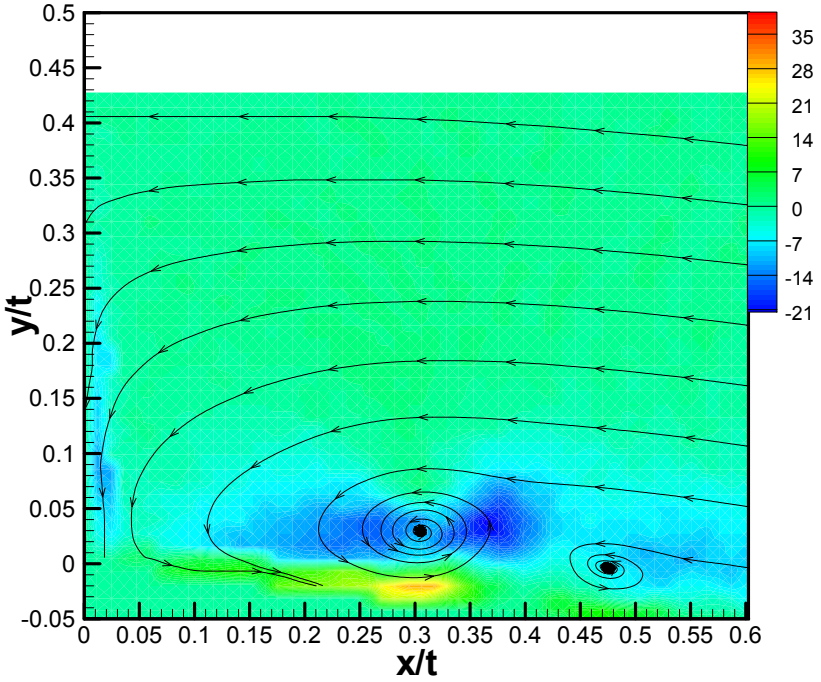

Figure 3.27 Strain for *h/t* = 3.43 – tripped boundary layer

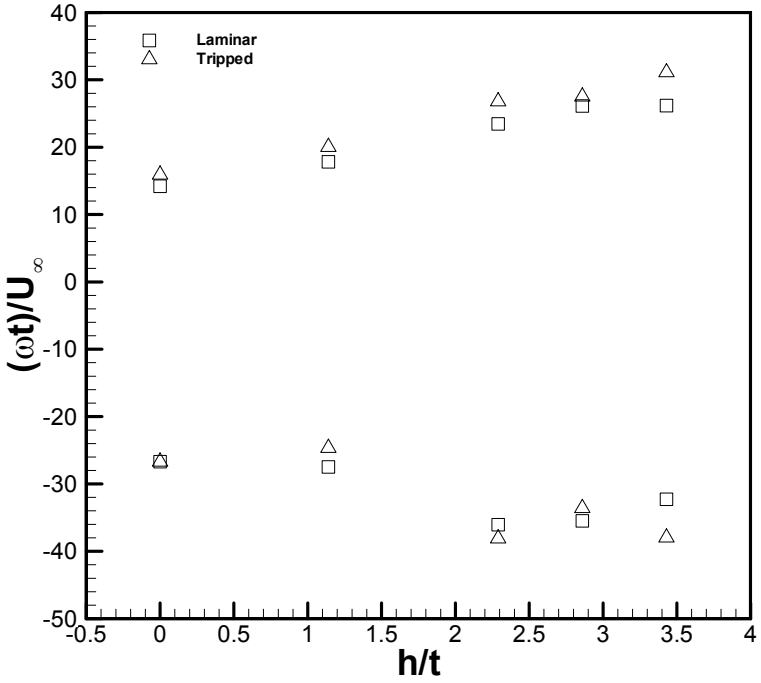

Figure 3.28 Maximum positive and negative vorticity

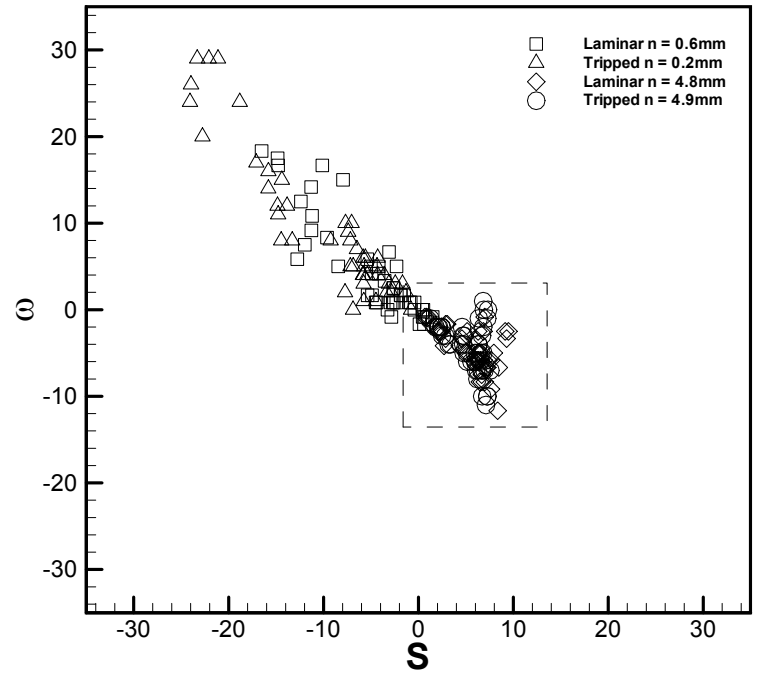

Figure 3.29 Vorticity and strain relation for $h/t = 3.43$

The upper left arm is close to the saddle point in an area of mostly negative shear. This trend is less pronounced as *h/t* is decreased. The appearance of this trend suggests a compact juncture vortex system where consisting of distinct regions of strain and vorticity due to axial stretching of the vortex, the delayed separation, and the downward movement of the bifurcation streamline.

3.6 Okubo-Weiss Criterion

The definition of what constitutes a vortex core and its outer bounds have been subject to numerous interpretations. McWilliams (1990) proposed a two-dimensional vortex as a region of fluid bounded where vorticity is 20% of the local extreme. As the juncture vortex flow is dominated by regions of high axial strain as well as vorticity, the areas of interest can be investigated by different mathematical mapping techniques. The Okubo-Weiss criterion (or Q criterion) is a physical interpretation of the flow-field and is defined as half the norm of the angular velocity squared minus the norm of the strain squared (Eq. 3.15). Unlike some methods where only vorticity is defined, the Q criterion allows for strain to be identified. When Q is positive, the field is dominated by the vorticity magnitude. While Q is negative, strain dominates.

$$Q := \frac{1}{2}\left(\|\Omega\|^2 - \|S\|^2\right) = \|\omega\|^2 - \frac{1}{2}\|S\|^2 \qquad 3.15$$

It is therefore possible to concretely define areas where vortices are present. Previously such observations were made on basis of circulation, velocity vectors, streamlines and subject to much ambiguity. Likewise, topographical singular points such as saddle points and nodes can also be determined as saddle points lay in regions of high strain and nodes lie in regions of intense vorticity

Where previously the primary vortex would have to be deduced from the vector field and vorticity contour, a clearer image can be seen where Q > 0. The intensity decreases as the curvature is flattened and the diffusivity is increased indicating a larger vortex with lower circulation. Figure 3.30, 3.31 of the laminar and tripped boundary layer vortex for h/t = 3.43 shows features that otherwise were not observable. Of note is the focus between the primary and secondary vortex, the backflow and saddle points denoted by intense strain. Investigating the Q criterion for the entirety of the DPIV flow field shows the juncture vortex for all six configurations to be dominated by strain as is expected. The adverse pressure gradient of the obstacle caused the near-wall flow to slow down and roll under the faster outer wall flow creating strain on the surface.

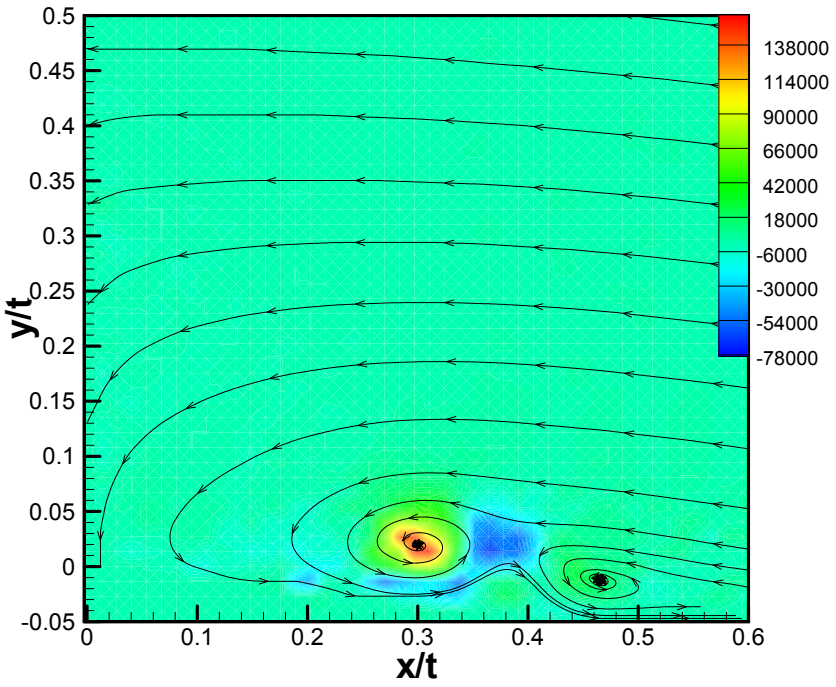

Figure 3.30 Q criterion for h/t = 3.43 – laminar boundary layer

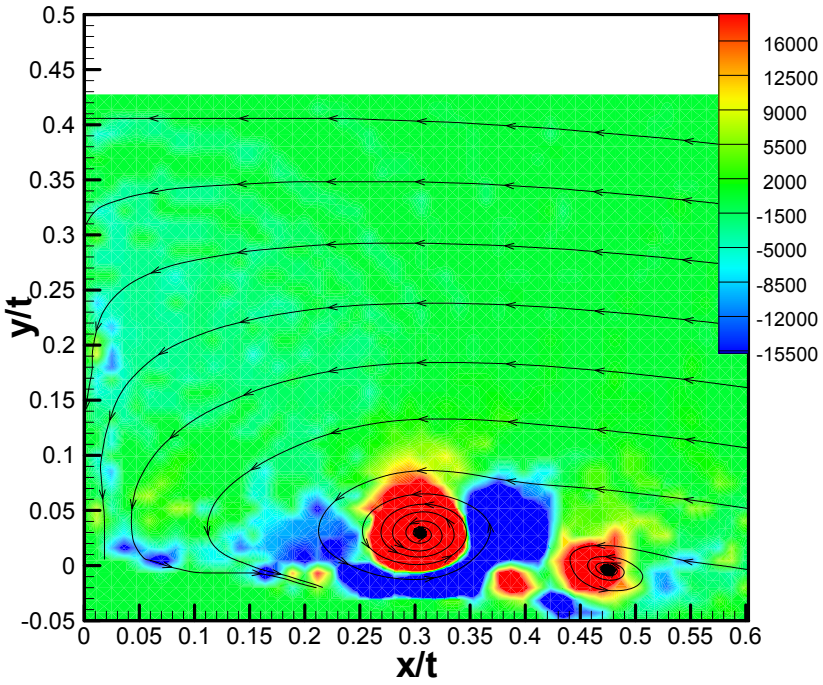

Figure 3.31 Q criterion for h/t = 3.43 – tripped boundary layer

To further analyze the effects of strain on the end wall flow, a shape parameter η was defined as the number of points *(i, j)* where dominated by strain relative to the number of points *(i, j)* dominated by vorticity non-dimensionalized by the base results for the flat plate. Values greater than one indicate the flow field to be dominated by strain. As h/t is increased (leading to a steeper curvature) there are more strain dominated regions (Figure 3.32).

$$\eta = \frac{\sum Q_{i,j} < 0}{\sum Q_{i,j} > 0} \qquad 3.16$$

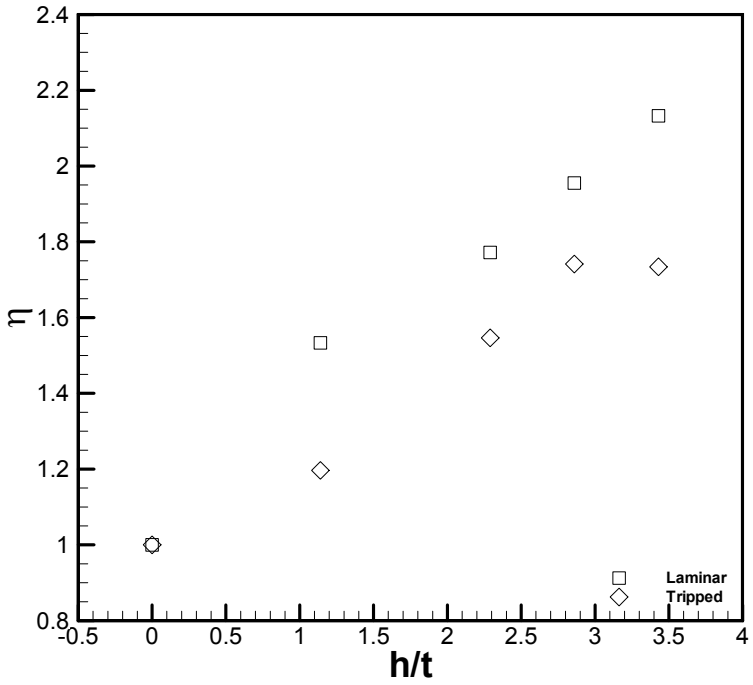

Figure 3.32 Shape factor η

Chapter 4

Wind Tunnel Results and Discussion

4.1 Boundary Layer and Integral Values

Boundary layer data was taken for both laminar and tripped flow for Re_t of 47,000, 73,000, and 97,000 corresponding to velocities of 17m/s, 26m/s, and 34m/s (or wind tunnel frequency controller of 20Hz, 30Hz, and 40Hz) respectively for a broad range of Reynolds number. Data was obtained with the help of a pitot probe of diameter 0.0635cm for varying step sizes. Integral values and local Reynolds numbers are presented in Table 4.1, 4.2. The $Re_{\delta*}$ values correspond with turbulent juncture flows (Simpson 2001) as $Re_{\delta*} > 1{,}000$.

The laminar boundary layer profiles (Figure 4.1) collapse to two different profiles, however for increasing Re_t, due to the curvature effects, a transitional profile is observed for the steeper humps. Tripped boundary layer profiles (Figure 4.2) are presented in wall coordinates and match the law of the wall well in the logarithmic region. Increasing h/t shows a more pronounced dip beneath the logarithmic region before the wake region is established. This is contrary to the boundary layer that convex surfaces exhibit (Gillis and Johnston 1983). In the wake region a positive Δu^+ is established for turbulent boundary layers.

The skin friction coefficient (Figure 4.3) for the most part was less sensitive to changes in h/t but decreased as Re_t increased. Defect profiles for the tripped boundary

layer (Figure 4.4) show the presence of a favorable pressure gradient and fit a similar curve for all Re_t tested. The Clauser shape factor G increases (still below 6 for a favorable pressure gradient) as h/t is increased suggesting for a tripped boundary layer, the curvature effects dominate the favorable pressure gradient effects, especially past h/t = 2.29 (Figure 4.5). The boundary layer, displacement, and momentum thickness (Figure 4.6-4.11) also decrease for increasing h/t indicating an increased local velocity. The tripped boundary layer shows a more consistent trend however the values for h/t = 3.43 are larger than expected. The steep curvature of h/t = 3.43 is assumed to have tripped the boundary layer earlier than expected leading to a laminar and tripped boundary layer where the leading edge of the obstacle would be.

An important quantity in defining the nature of the boundary layer, the shape factor is ~ 2 for all four humps for Re_t = 47,000 and shows a decreasing trend as h/t is increased. As Re_t is increased, H increases towards that for a laminar boundary layer indicating the dominance curvature effects as h/t is increased. Figure 4.19 shows a similar increasing trend for H as h/t is increased. The values however are in accordance with a turbulent boundary layer.

Table 4.1 Integral quantities, Re_t = 97,000 – laminar boundary layer

	h/t = 3.43	**h/t = 2.86**	**h/t = 2.29**	**h/t = 1.14**
δ (mm)	4.29	1.47	1.63	3.66
δ* (mm)	0.56	0.33	0.33	0.53
θ (mm)	0.45	0.21	0.22	0.40
H	1.25	1.64	1.53	1.32
Re_{δ^*}	1,547.10	861.32	819.63	1,199.49
Re_{θ}	1,258.78	536.67	542.22	908.18

Table 4.2 Integral quantities, Re_t = 97,000 – tripped boundary layer

	h/t = 3.43	**h/t = 2.86**	**h/t = 2.29**	**h/t = 1.14**
δ (mm)	18.26	15.72	19.53	24.61
δ* (mm)	1.22	1.32	1.55	2.08
θ (mm)	0.99	1.11	1.30	1.76
H	1.22	1.20	1.19	1.18
Re_{δ^*}	3,364.27	3,447.48	3,850.44	4,682.70
Re_{θ}	2,740.48	2,890.58	3,225.54	3,946.03

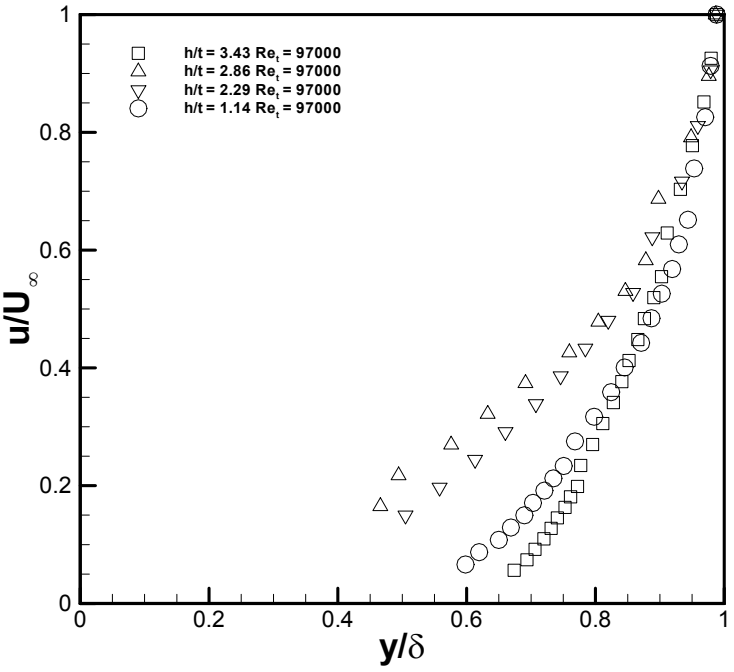

Figure 4.1 Laminar boundary layer profile, Re_t = 97,000

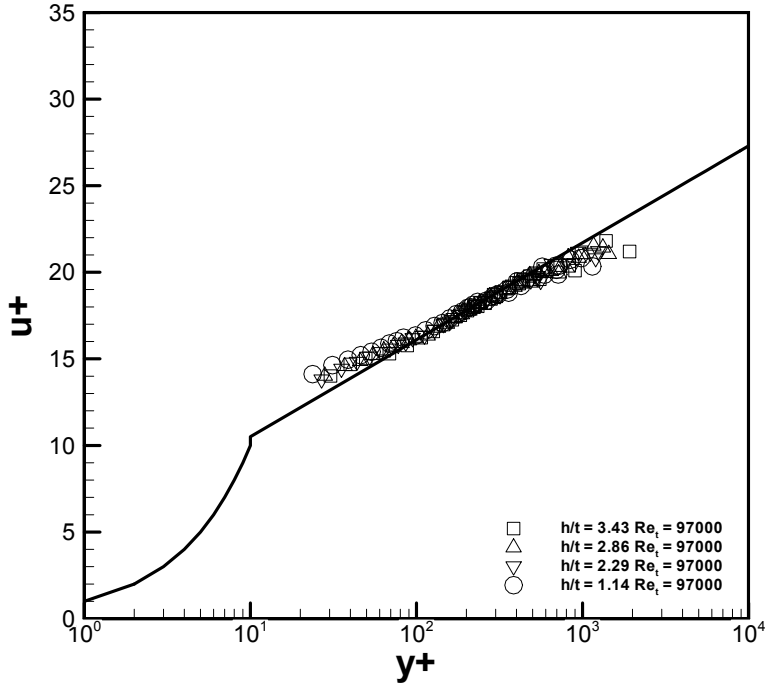

Figure 4.2 Tripped boundary layer profile, Re_t = 97,000

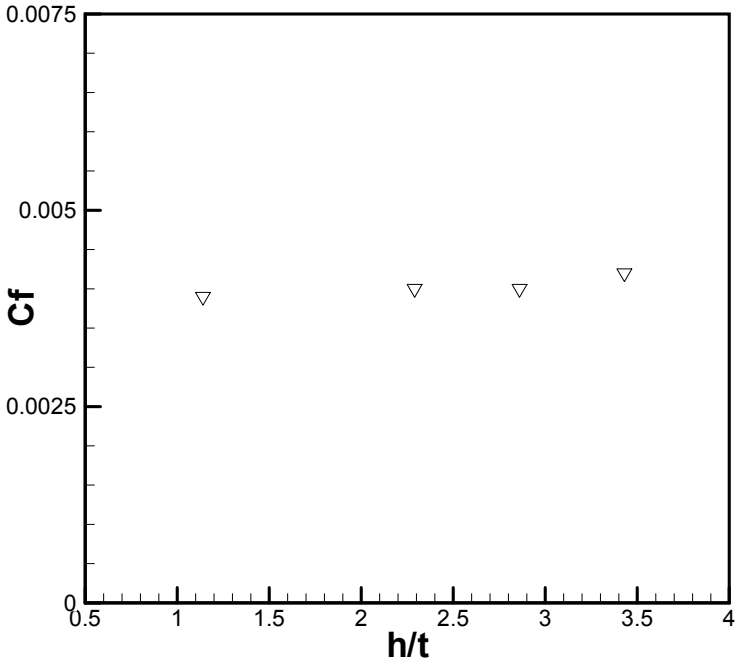

Figure 4.3 Skin friction coefficient, Re_t = 97,000 – tripped boundary layer

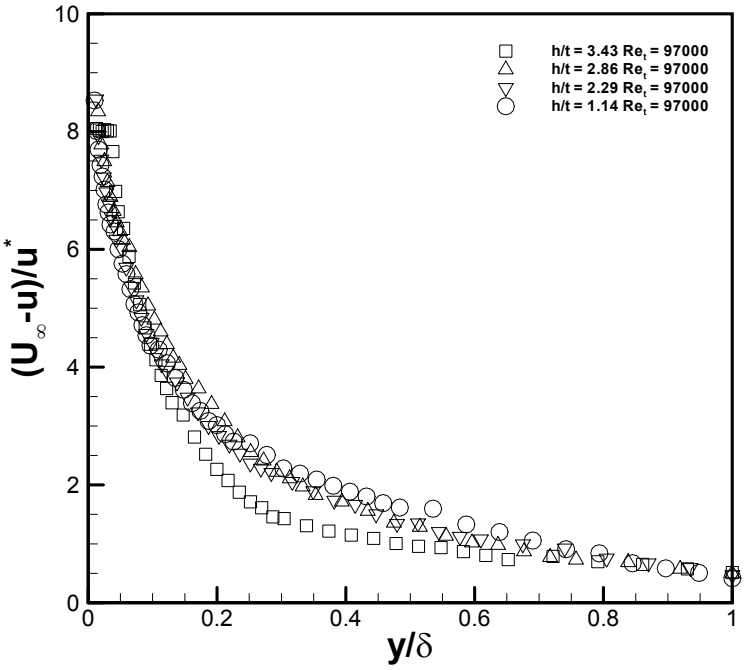

Figure 4.4 Defect profile, Re_t = 97,000 – tripped boundary layer

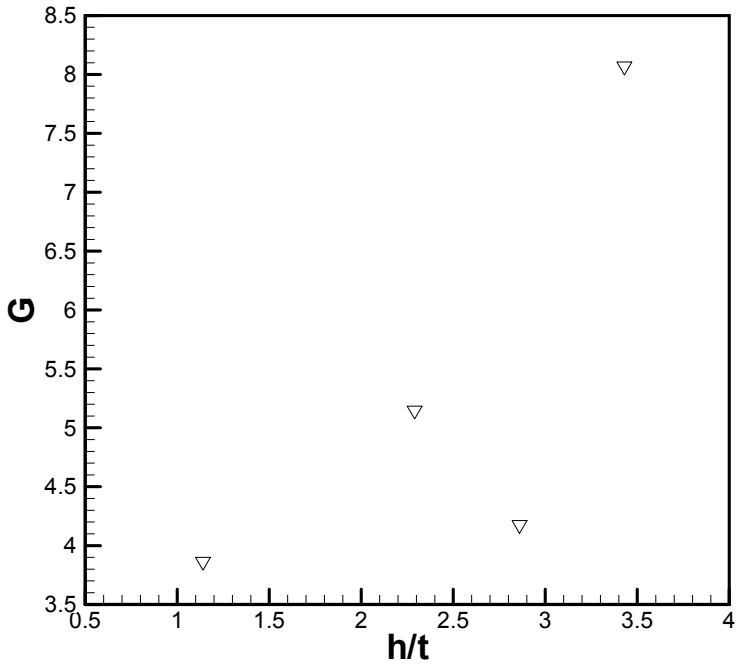

Figure 4.5 Clauser shape factor, Re_t = 97,000 – tripped boundary layer

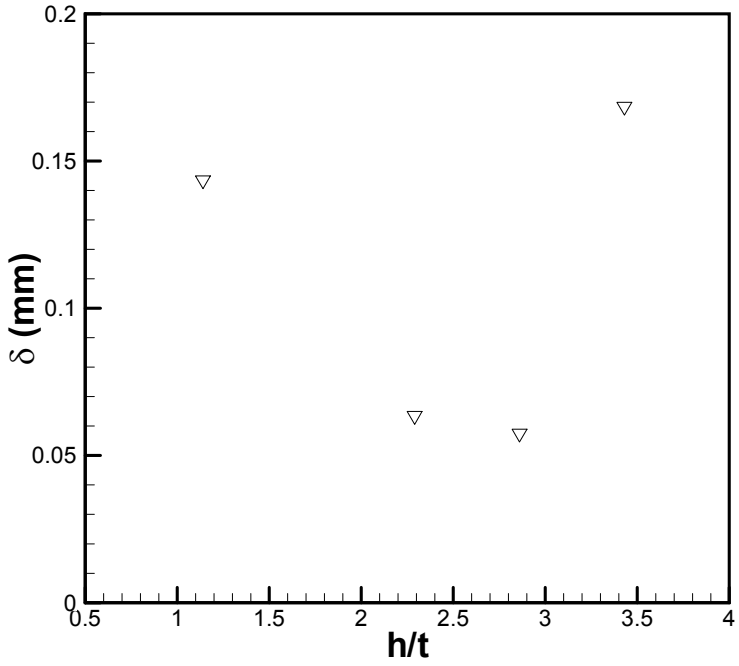

Figure 4.6 Laminar boundary layer thickness, $Re_t = 97{,}000$

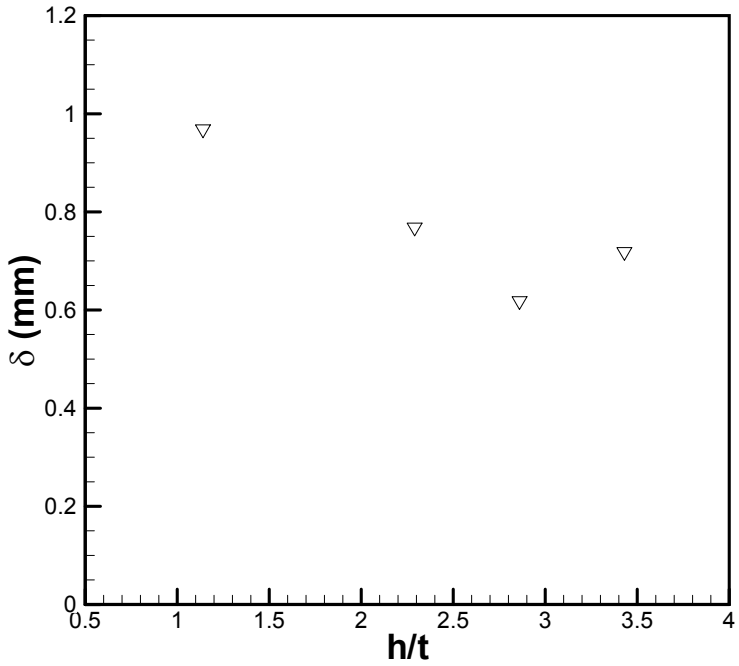

Figure 4.7 Tripped boundary layer thickness, $Re_t = 97{,}000$

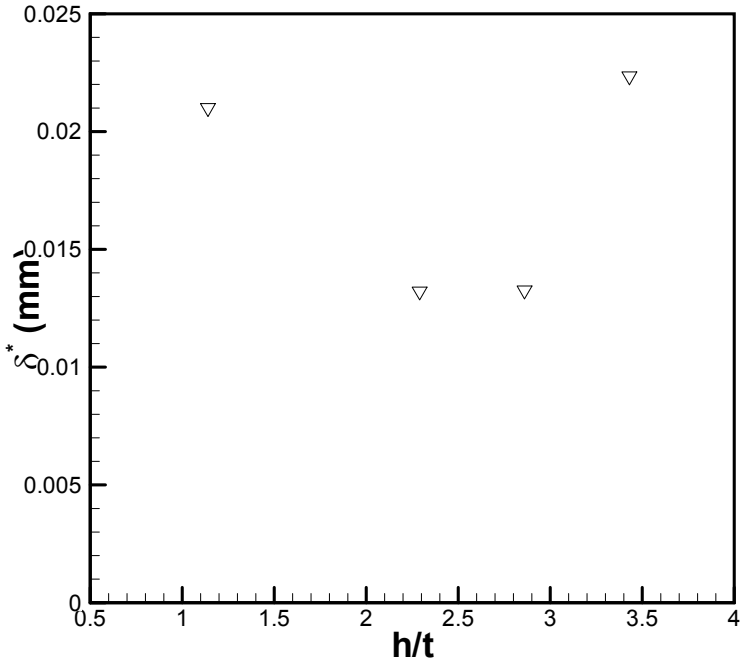

Figure 4.8 Laminar displacement thickness, $Re_t = 97{,}000$

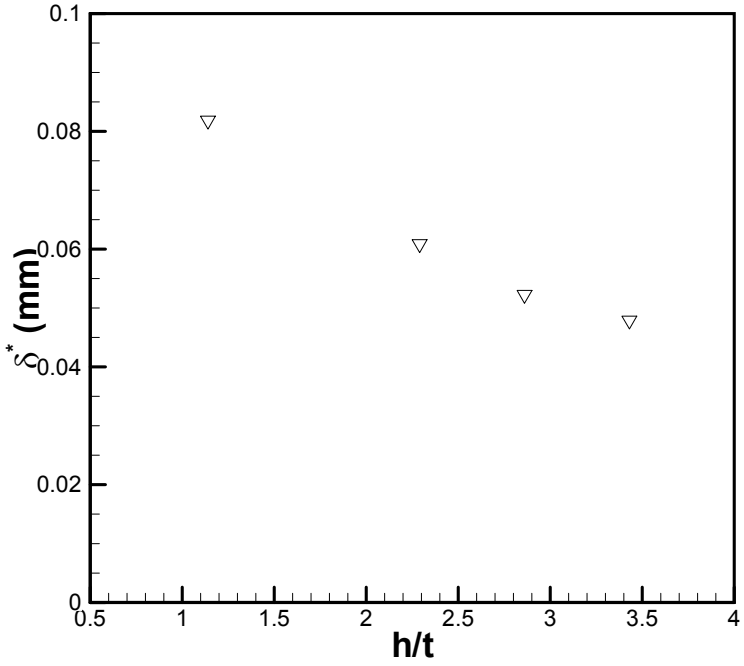

Figure 4.9 Tripped displacement thickness, $Re_t = 97{,}000$

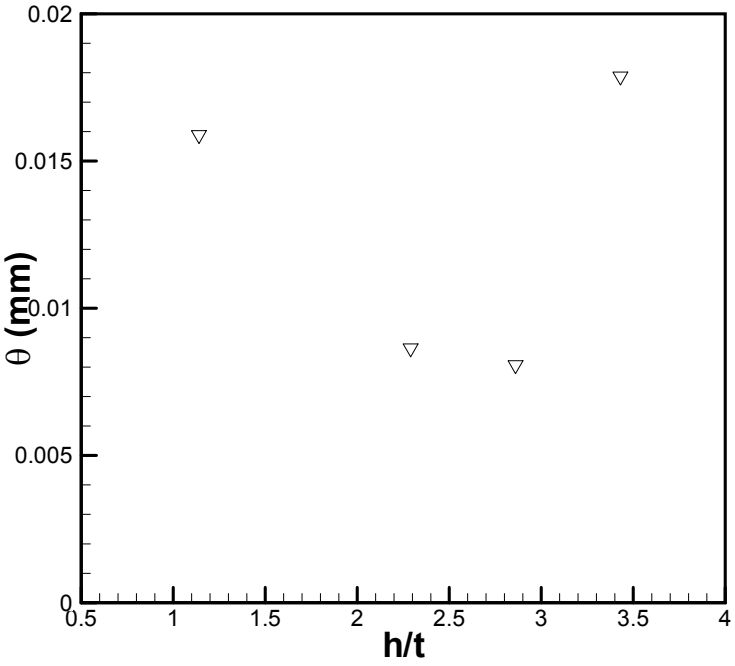

Figure 4.10 Laminar momentum thickness, Re_t = 97,000

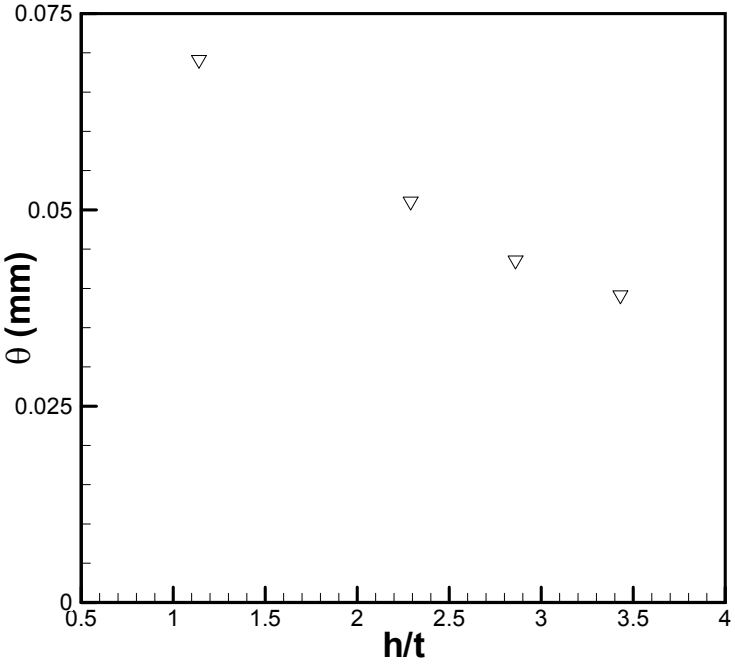

Figure 4.11 Tripped momentum thickness, Re_t = 97,000

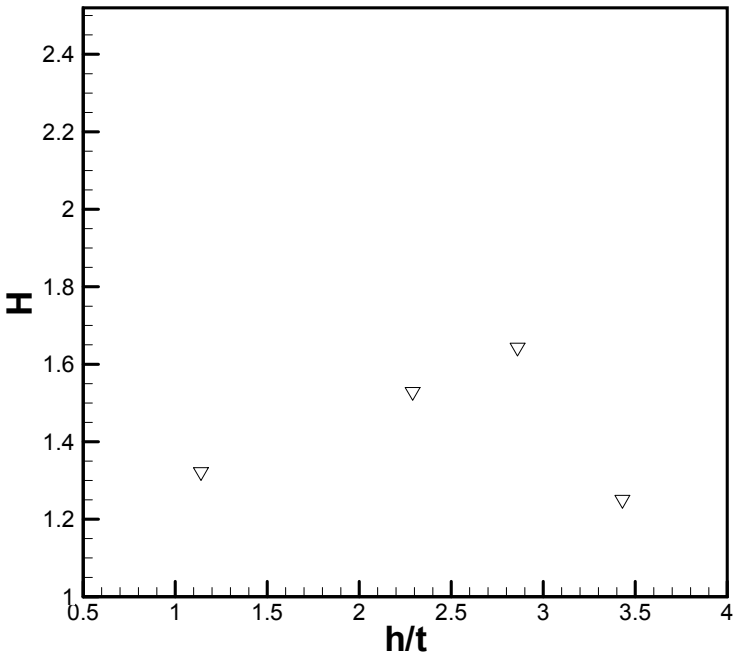

Figure 4.12 Laminar shape factor, $Re_t = 97{,}000$

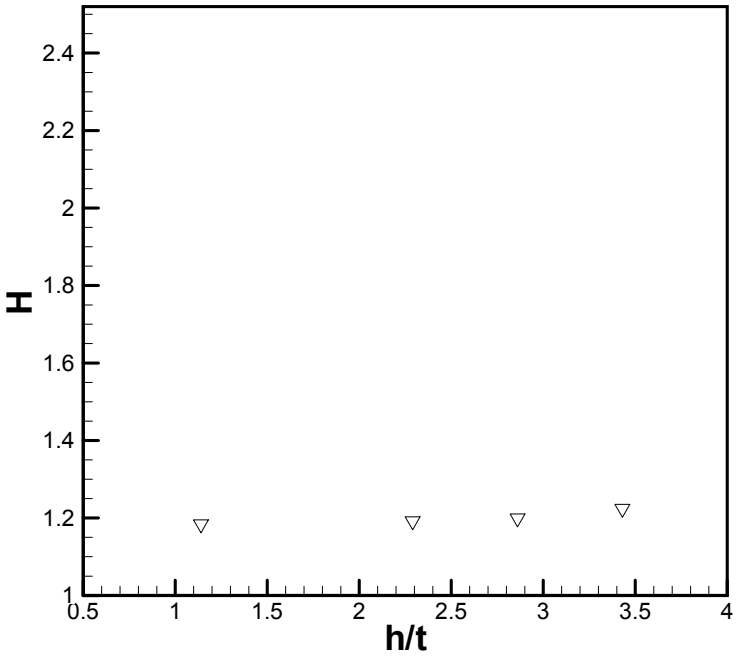

Figure 4.13 Tripped shape factor, $Re_t = 97{,}000$

4.2 Surface Pressure Distribution on Hump

Surface pressure distributions (Figure 4.14-4.15) without the model show the existence of a favorable pressure gradient up to the apex (s/t = -3.00) followed by an adverse pressure gradient downstream. Despite the large favorable pressure gradient for the h/t = 3.43, the increased Clauser shape factor and law of the wall plot would indicate that for tripped juncture flow, the streamline displacement lowers the effectiveness of the favorable pressure gradient in delaying separation. Laminar and tripped profiles are compared in Figure B.20-B.23; the tripped profiles exhibited a slightly lower pressure than laminar profiles. The difference is mostly negligible as static pressure does not change due to either a laminar or tripped boundary layer.

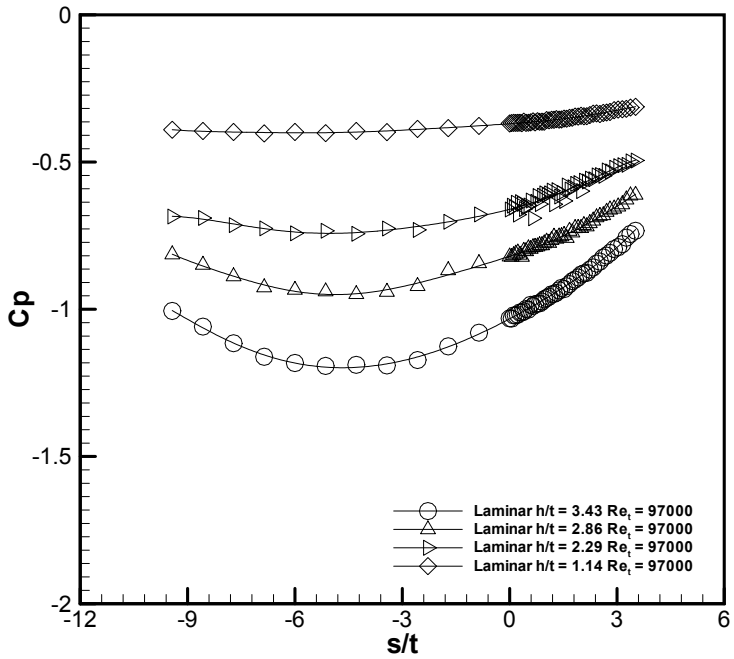

Figure 4.14 Surface pressure distribution, hump only, Re_t = 97,000 – laminar boundary layer

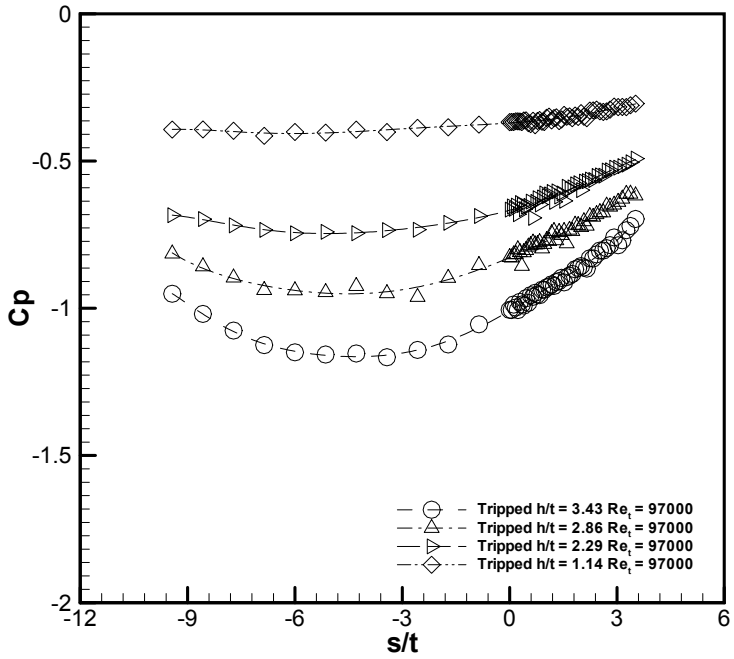

Figure 4.15 Surface pressure distribution, hump only, Re_t = 97,000 – tripped boundary layer

4.3 Flow Visualization

The position of the primary separation point and line were at the leading and trailing edge, respectively, were determined from a kerosene and tempera powder. As *h/t* is increased the primary separation point moves towards the leading edge of the obstacle (Figure 4.16). The difference between the effects between a laminar and tripped boundary layer is seen to decrease as *h/t* is increased. When compared against the results from the laminar juncture vortex, the system is closer to the leading edge in the case of a turbulent juncture vortex. This would imply the primary vortex to be increasingly axially stretched and the system as a whole more compressed for the turbulent system. From Figure 4.17 the general trend shows the difference between the laminar and tripped boundary layer decreasing as *h/t* is increased. Overall the position of the primary separation line from the

centerline of the obstacle showed not much change. The primary separation point is identified in Figure 4.18-4.19. An interesting result is the demarcation of the primary separation line becomes more defined as *h/t* is increased for both laminar and tripped boundary layers indicating a steeper pressure gradient as the flow separates.

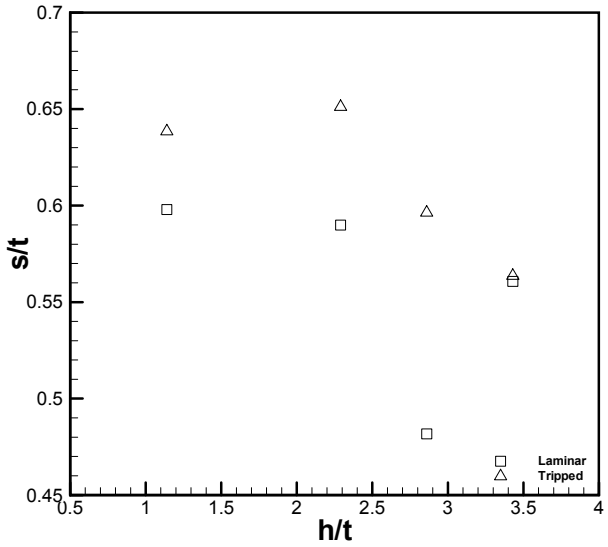

Figure 4.16 Location of primary separation point

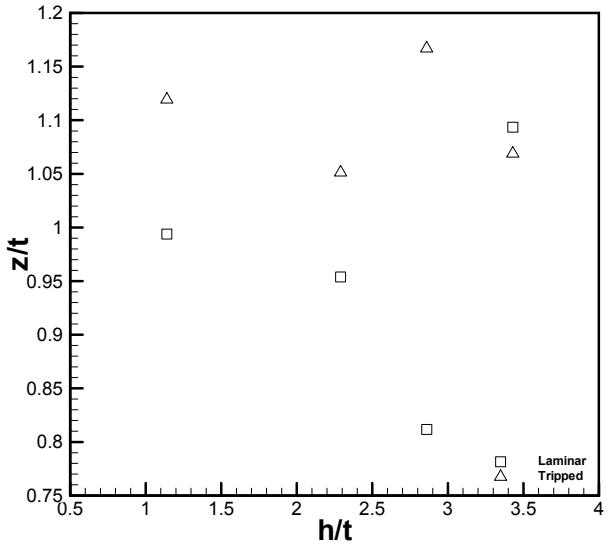

Figure 4.17 Distance from centerline to primary separation line at trailing edge

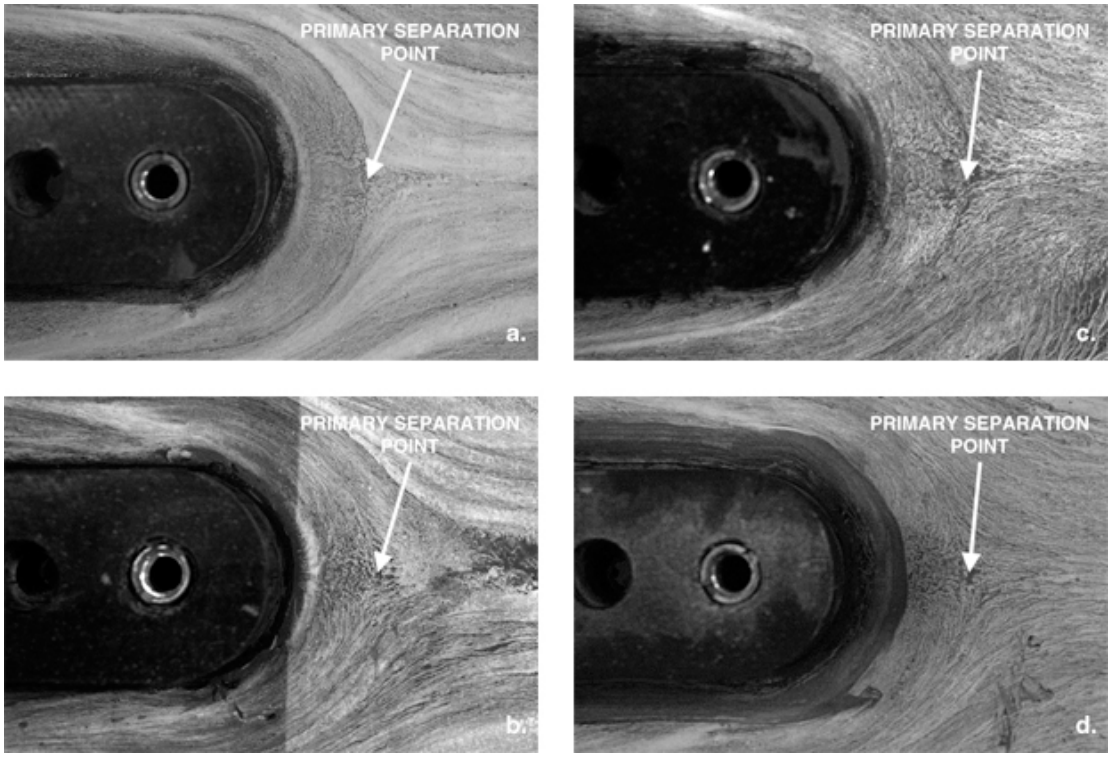

Figure 4.18 Location of primary separation point (a) h/t = 3.43 (b) h/t = 2.86 (c) h/t = 2.29 (d) h/t = 1.14 – laminar boundary layer

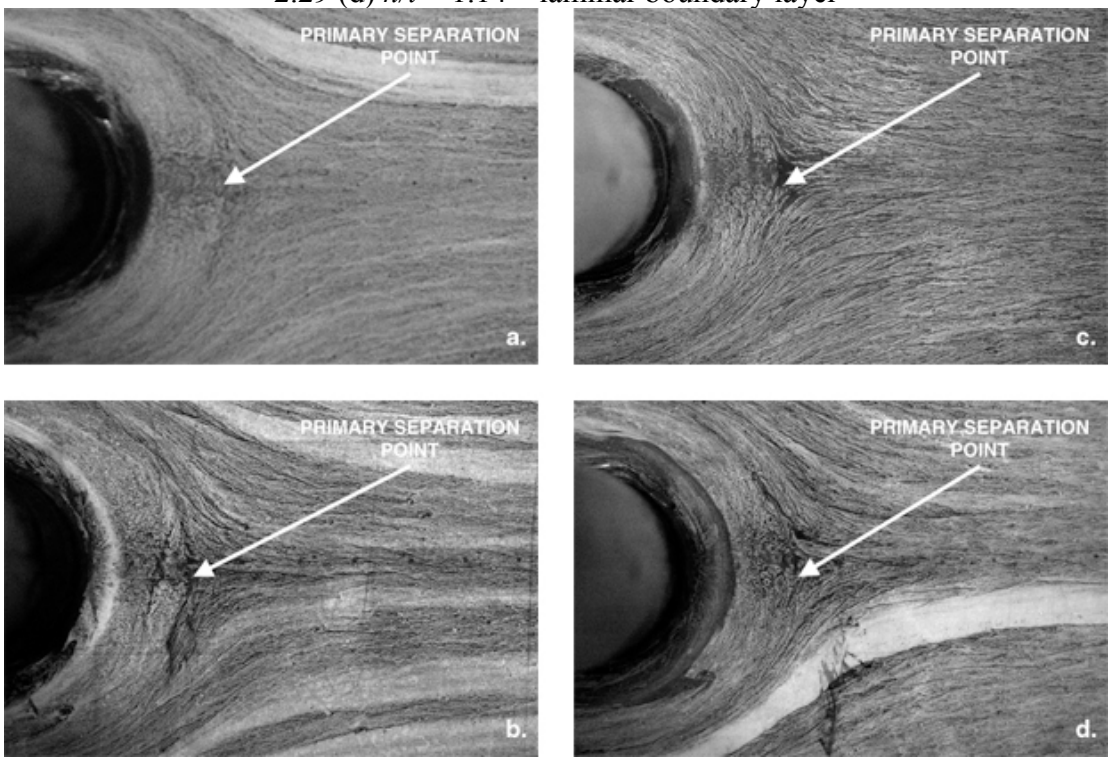

Figure 4.19 Location of primary separation point (a) h/t = 3.43 (b) h/t = 2.86 (c) h/t = 2.29 (d) h/t = 1.14 – tripped boundary layer

4.4 Surface Pressure Distribution on the Hump in the Presence of Obstacle

The pressure experienced at the leading edge of the object is found to be largely unaffected by curvature due to the smaller pressure gradients in this close region. Beyond $s/t \sim 2$ for both laminar and tripped boundary layer, the center-line pressure is largely unaffected by the juncture vortex system and can be seen to closely match the pressure distribution for the hump only (Figure 4.20-4.23). Downstream of $s/t \sim 2$ and the primary separation point, the pressure rises as the boundary layer encounters the adverse pressure gradient due to the obstacle.

Figure 4.24-4.25 shows the tripped centerline pressures for up to $s/t = 3.5$. The location s/t of the local minima corresponding to the location of the vortex is largely unaffected by Re_t and instead moved closer to the leading edge of the obstacle as only h/t is increased. Increasing Re_t widens the gap between the local minima and maxima indicating the increased vortical activity. Whereas the tripped boundary layer shows a smooth transition up to the first plateau or local maxima (shown by Khan et. al. 1995 to be close to the location of the point of attachment), the laminar boundary layer shows this trend to be punctuated by the presence of a 2^{nd} slight plateau which is close to the recorded values of the primary separation point. For $h/t = 3.43$, the recorded Cp is still negative even in the area of the vortex, rising above to positive values downstream of the primary vortex, close to the leading edge. This is an indication of the strength of curvature effects on the system as a whole. Intuition would show the initial steep gradient (Figure 4.25) of $s/t \sim 0.7$ to be the location of the primary separation point.

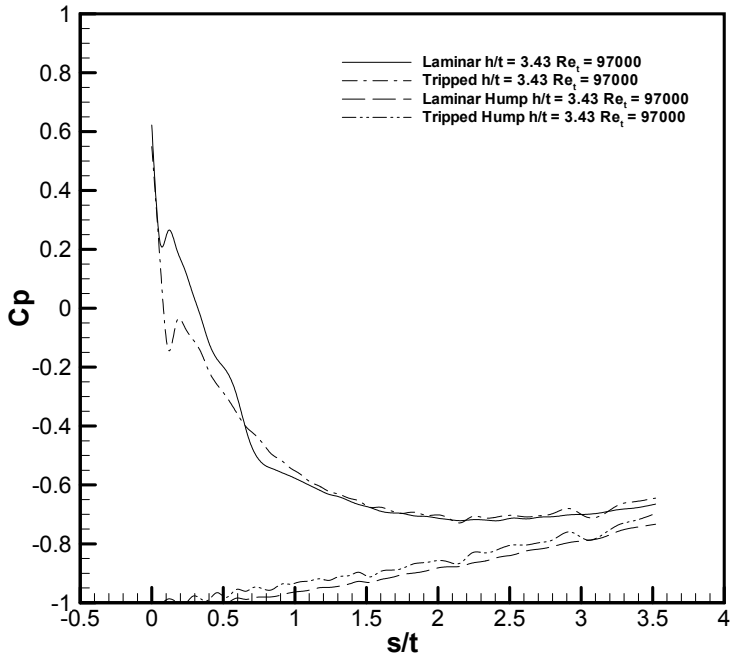

Figure 4.20 Surface pressure distribution, juncture vortex and hump, h/t = 3.43, Re_t = 97,000

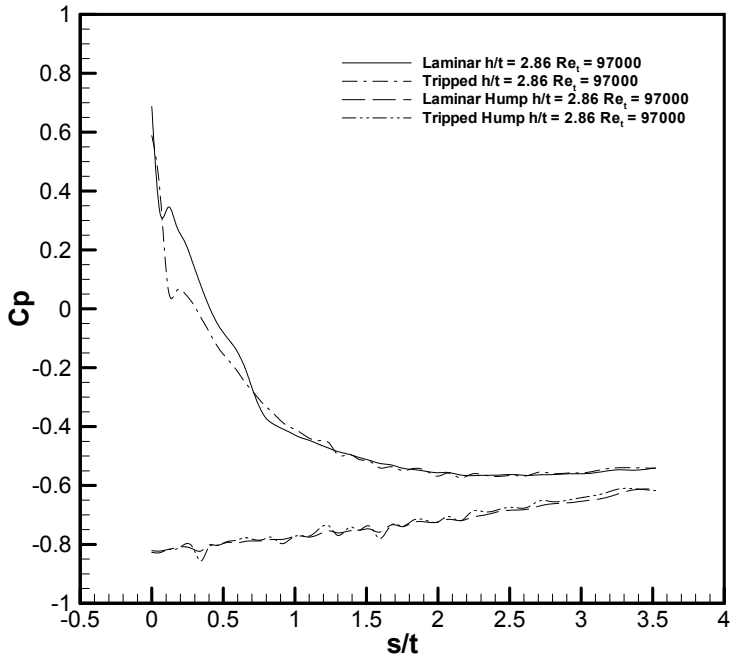

Figure 4.21 Surface pressure distribution, juncture vortex and hump, h/t = 2.86, Re_t = 97,000

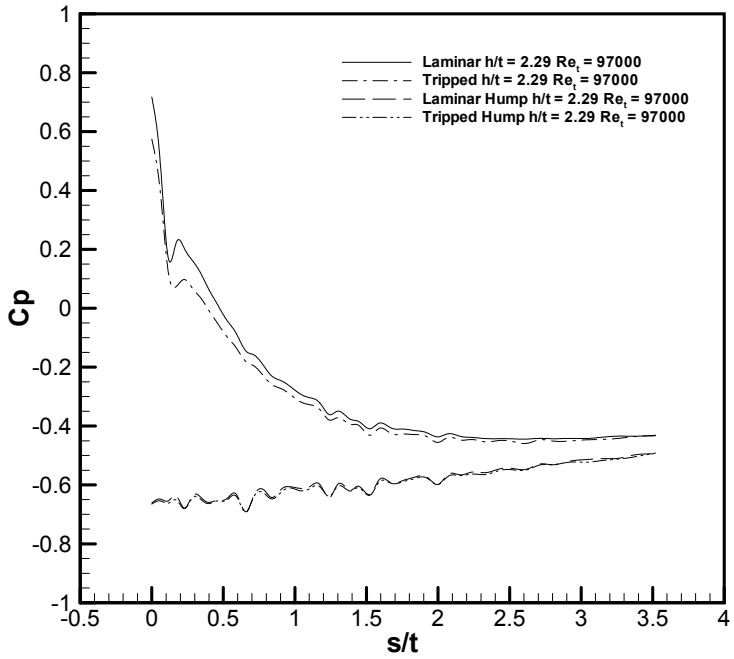

Figure 4.22 Surface pressure distribution, juncture vortex and hump, h/t = 2.29, Re_t = 97,000

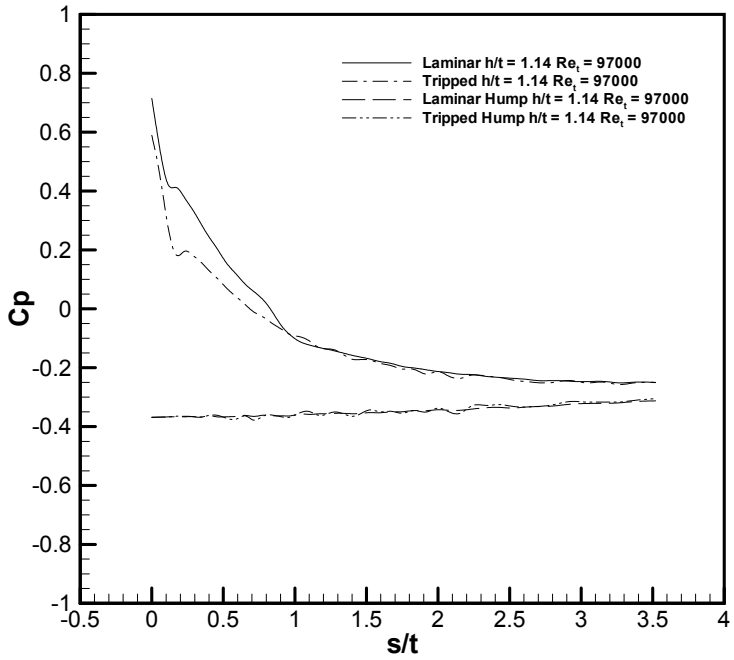

Figure 4.23 Surface pressure distribution, juncture vortex and hump, h/t = 1.14, Re_t = 97,000

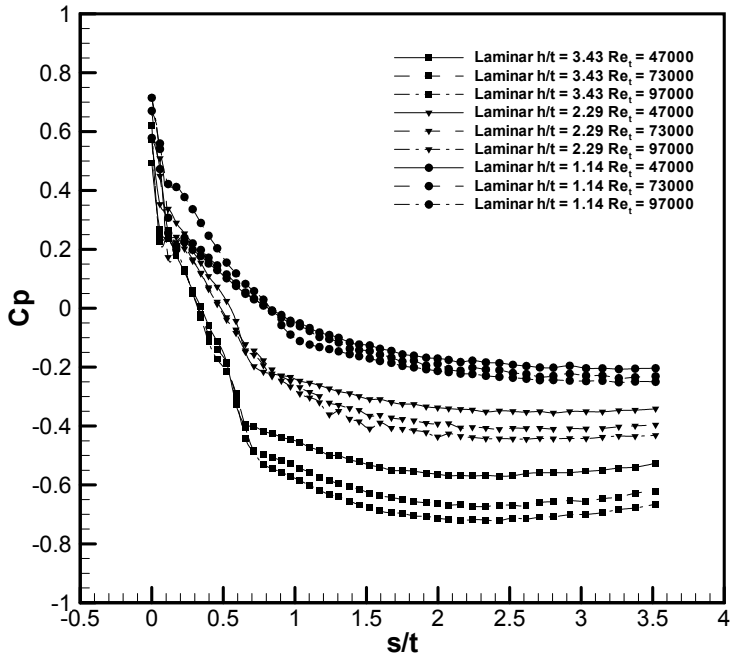

Figure 4.24 Surface pressure distribution, juncture vortex – laminar boundary layer

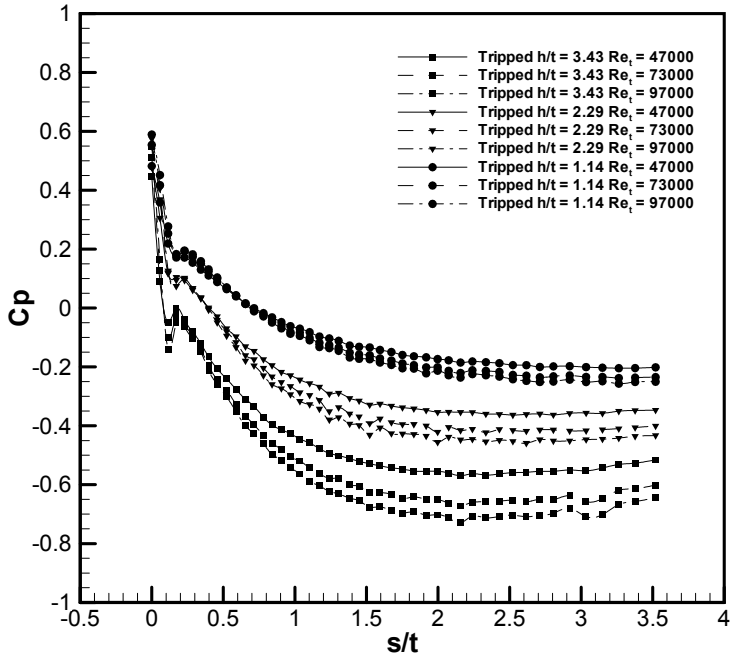

Figure 4.25 Surface pressure distribution, juncture vortex – tripped boundary layer

Figure 4.26 is the pressure jump experienced at the location of the primary vortex. As *h/t* and Re_t are increased, there is a strong linear trend as the juncture vortex grows in strength and causes a pressure rise from the otherwise decreasing pressure distribution (Figure 4.14-4.15). This is analogous to the large gap seen in Figure 4.20-4.23.

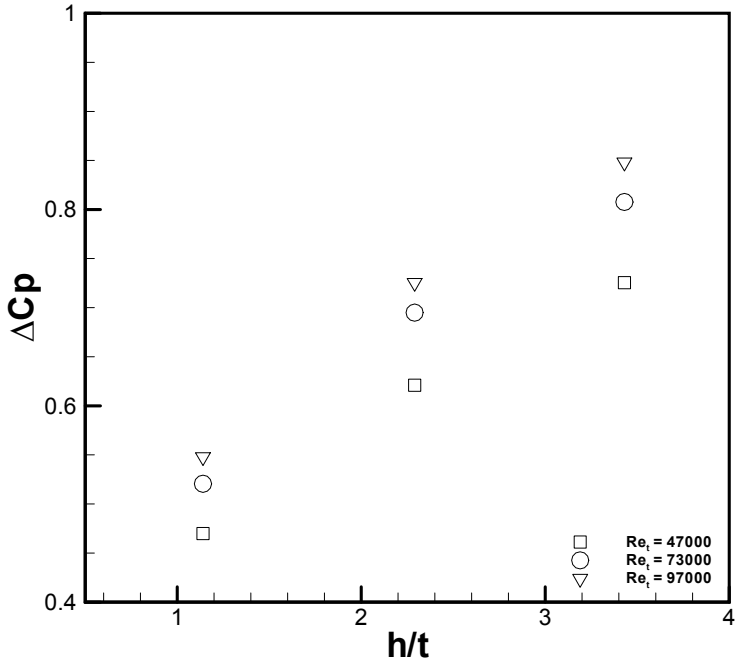

Figure 4.26 Pressure difference at location of primary vortex – tripped boundary layer

Chapter 5

Conclusions

5.1 Conclusions

For both the laminar and turbulent juncture vortex system, the primary singular point of separation was proven to have been moved further downstream. PIV results indicated that the laminar system left a more compact footprint as *h/t* is increased. The bifurcation streamline traveled down the leading edge of the obstacle and the distance between the center of the primary vortex and primary saddle point decreased. The same was inferred for the turbulent juncture vortex system (this compacting of the juncture vortex was accompanied by an increase in the vortical strength and strains as the primary vortex is axially stretched and interacting with its mirror image). As a whole, the juncture vortex system formed closer to the leading edge of the model.

Centerline surface pressure distributions confirmed the presence of the primary vortex and verified the increased vortical activity as Re_t was increased. The position of the vortex did not show dependence on Reynolds number but instead moved closer to the leading edge of the obstacle as *h/t* increased. The attachment and separation points were verified from surface flow visualization for laminar and tripped approaching boundary layers.

The mathematical technique of the Okubo-Weiss criterion was used to define regions where vorticity and or strain dominate. The resulting contours sharply defined the

regions of vortical activity and strain. The primary and secondary vortex were observed along with the foci structure which otherwise could not be resolved by streamlines. It is further concluded that as *h/t* increased, there were more strain dominated regions, which show a tight and compact vortex system.

The objective of the present work was to experimentally determine the effects of a favorable pressure gradient due to a convex hump the laminar and turbulent juncture vortex system. It was assumed that the favorable pressure gradient conveyed to the incoming boundary layer would delay separation and reduce the footprint of the juncture vortex as a whole.

It was found that the arc length to the leading edge of the obstacle was not sufficient for the proper growth of a turbulent boundary layer. The curvature effects were seen to dominate the favorable pressure gradient effects as *h/t* increased resulting in a Clauser shape factor close to that of an equilibrium boundary layer. The defect profiles and centerline pressure distributions confirmed the presence of a favorable pressure gradient.

The range of Reynolds number for the existence of mode 1 and 2 of the laminar system was shown to have been reduced significantly while mode 3 prolonged for the range as reported by earlier investigations. This was due to the near flat variance that mode 3 displayed as *h/t* was increased in regards to the characteristic frequency. This flat variance explained the resistance of the turbulent system to changes in Re_t regarding the location of the primary separation point.

References

1. Khan, M. J. and Ahmed, A. (1994) "Influence of Forward and Back Sweep on Wing-Body Juncture Flow", *Fluid Mechanics Report 01 Department of Aerospace Engineering Texas A&M University*

2. Baker, C. J. (1979) "The Laminar Horseshoe Vortex", *Journal of Fluid Mechanics*. Vol. 95 pp. 347-367

3. Simpson, R. L. (2001) "Junction Flows", *Annual Review of Fluid Mechanics*. Vol. 33 pp. 415-443

4. Devenport, W. J. and Simpson, R. L. (1990) "Time-Dependent and Time-Averaged Turbulence Structure Near the Nose of a Wing-Body Junction", *Journal of Fluid Mechanics*. Vol. 210 pp. 23-55

5. Shabaka, I. M. M. A. and Bradshaw, P. (1981) "Turbulent Flow Measurements in an Idealized Wing/Body Junction", *AIAA Journal*. Vol. 19 No. 2 pp. 131-132

6. Dickinson, S. C. (1988) "Time Dependent Flow Visualization in the Separated Region of an Appendage-Flat Plate Junction", *Experiments in Fluids*. Vol. 6 No. 2 pp. 140-143

7. Simpson, R. L. (1996) "Aspects of Turbulent Boundary Layer Separation", *Progress in Aerospace Sciences.* Vol. 32 No. 5 pp. 457-521

8. Aunapu, N. V., Volino, R. J., and Flack, K. A. (2000) "Surface Flow Visualization of a Scaled-Up Turbine Blade Passage", *Measurement Science and Technology.* Vol. 11 No. 7 pp. 987-991

9. Schwind, R. (1962) "The Three-Dimensional Boundary Layer Near a Strut", *Gas Turbine Laboratory Report MIT*

10. Baker, C. J. (1980) "The Turbulent Horseshoe Vortex", *Journal of Wind Engineering and Industrial Aerodynamics*. Vol. 6 No. 1 pp. 9-23

11. Kawamura, T., Hiwada, M., Hibino, T., Mabuchi, I., and Kumada, M. (1984) "Flow Around a Finite Cylinder on a Flat Plate", *Bulletin of the JSME.* Vol. 27 No. 232 pp. 2142-2151

12. Okamoto, S., and Subabashiri, Y. (1992) "Vortex Shedding from a Circular Cylinder of Finite Length Place on a Ground Plate", *Journal of Fluids Engineering*. Vol. 114 No. 4 pp. 512-521

13. Khan, M. J. and Ahmed, A. (2002) "Influence of Aspect Ratio on the Dynamic Character of End-Wall Flow", *Proceedings of the 1st International Conference on Heat Transfer, Fluid Mechanics and Thermodynamics*. South Africa, April

14. Rifki, R., Ahmed, A., and Khan, M. J. (2007) "Effect of Aspect Ratio on Flow Field of Surface-Mounted Obstacles", *AIAA Journal.* Vol. 45 No. 4 pp. 954-958

15. Mehta R. D. (1984) "Effect on a Wing Nose Shape on the Flow in a Wing/Body Junction", *Aerospace Journal.* Vol. 88 pp. 456-460

16. Rood E. P. (1984) "The Governing Influence of the Nose Radius on the Unsteady Effects of Large Scale Flow Structure in the Turbulent Wing and Plate Junction Flow", *In ASME Forum on Unsteady Flow,* Vol. 15 pp. 7-9

17. Wood D. H. and Westphal R. V. (1992) "Measurements of the Flow around a Lifting-Wing/Body Junction", *AIAA Journal.* Vol. 30 No. 1 pp. 6-12

18. Igarashi, T. (1984) "Characteristics of the Flow around a Square Prism", *Bulletin of JSME*. Vol. 27 No. 231 pp. 1858-1865

19. Shizawa, T., Honami, S., and Yamamoto M. (1996) "Experimental Study of Horseshoe Vortex at Wing/Body Junction with Angle of Attack by Triple Hot-Wire", *AIAA-96-0323.* Presented at AIAA Aerospace Sciences Meeting and Exhibit, 34th, Reno

20. Rood, E.P. and Anthony D. G. (1985) "Tail Profile Effects on Unsteady Large Scale Flow Structure in the Wing and Plate Junction", *In ASME Forum on Unsteady Flow,* Vol. 27 pp. 30-32

21. Herst, D.K. and Gouldin, F. C. (1997) "Turbulent Flow Normal to Triangular Cylinder", *Journal of Fluid Mechanics.* Vol. 331 pp. 107-125

22. Abuomar, M. M. and Martinuzzi, R. J. (2000) "An Experimental Investigation of the Flow Around a Surface-Mounted Pyramid", *Department of Mechanical and Materials Engineering University of Western Ontario.*

23. Khan, M. J. and Ahmed, A. (1995) "Effect of Sweep on Wing-Body Juncture Flow", *AIAA-95-0868.* Presented at AIAA Aerospace Sciences Meeting and Exhibit, 34th, Reno

24. Maughmer, M., Hallman, D., Ruszkowski, R., Chappel, G., and Waitz, I. (1989) "Experimental Investigation of Wing/Fuselage Integration Geometries", *Journal of Aircraft*. Vol. 26 No. 8 pp. 705-711

25. Khan, M. J., Trosper, R. J., and Ahmed, A. (1995) "Dynamics of the Juncture Vortex", *AIAA Journal.* Vol. 33 No. 7 pp. 1273-1278

26. Khan, M. J. and Ahmed, A. (2005) "Topological Model of Flow Regimes in the Plane of Symmetry of a Surface-Mounted Obstacle", *Physics of Fluids.* Vol. 17 045101 pp. 1-8

27. Tobak, M. and Peake, D. J. (1979) "Topology of Two-Dimensional and Three-Dimensional Separated Flows", *AIAA-79-1480.*

28. Baker, C. J. (1991) "The Oscillation of Horseshoe Vortex Systems", *Journal of Fluids Engineering.* Vol. 113 No. 3 pp. 489-495

29. Thomas, A. S. W. (1987) "The Unsteady Characteristics of Laminar Juncture Flow", *Physics of Fluids*. Vol. 30 No. 2 pp. 283-285

30. Muck, K. C., Hoffmann, P. H., and Bradshaw, P. (1985) "The Effect of Convex Surface Curvature on Turbulent Boundary Layers", *Journal of Fluid Mechanics*. Vol. 161 pp. 347-369

31. Baskaran, V., Smits, A. J., and Joubert, P. (1987) A Turbulent Flow over a Curved Hill Part 1. "Growth of an Internal Boundary Layer", *Journal of Fluid Mechanics*. Vol. 182 pp. 47-83

32. Smith, M. C. (1968) "Wake-Induced Effects near the Forward Stagnation Point of a Circular Cylinder", *Physics of Fluids.* Vol. 11 No. 8 pp. 1618-1620

33. Gillis, J. C. and Johnston, J. P. (1983) "Turbulent Boundary-Layer Flow and Structure on a Convex Wall and its Redevelopment on a Flat Wall", *Journal of Fluid Mechanics*. Vol. 35 pp. 123-153

34. Bandyopadhyay, P. R. and Ahmed, A. (1993) "Turbulent Boundary Layers Subjected to Multiple Curvatures and Pressure Gradients", *Journal of Fluid Mechanics*. Vol. 246 pp. 503-527

35. McWilliams, J. (1990) "The Vortices of Two-Dimensional Turbulence", *Journal of Fluid Mechanics.* Vol. 219 pp. 361-385

Appendix A

Water Tunnel Results

A.1 Vector Plots – Laminar Boundary Layer

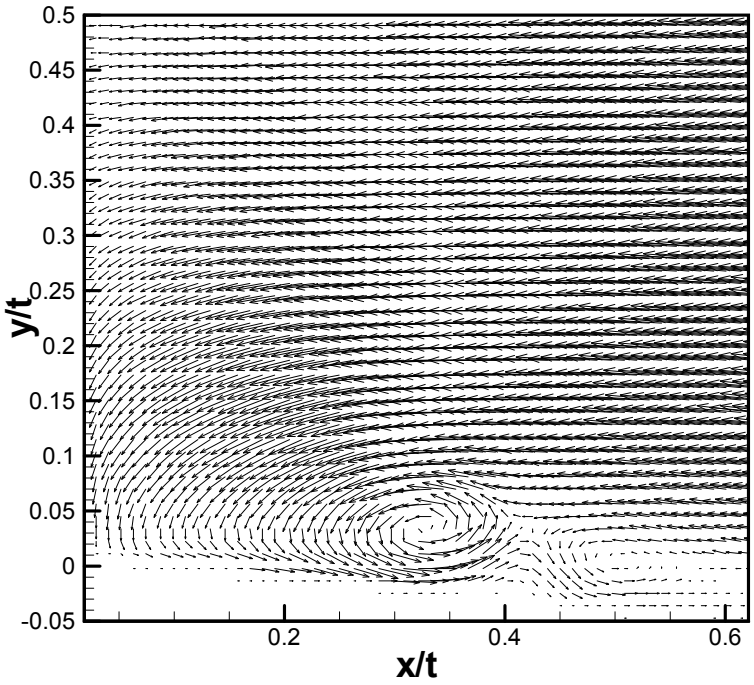

Figure A.1 Vector plot for $h/t = 2.86$ – laminar boundary layer

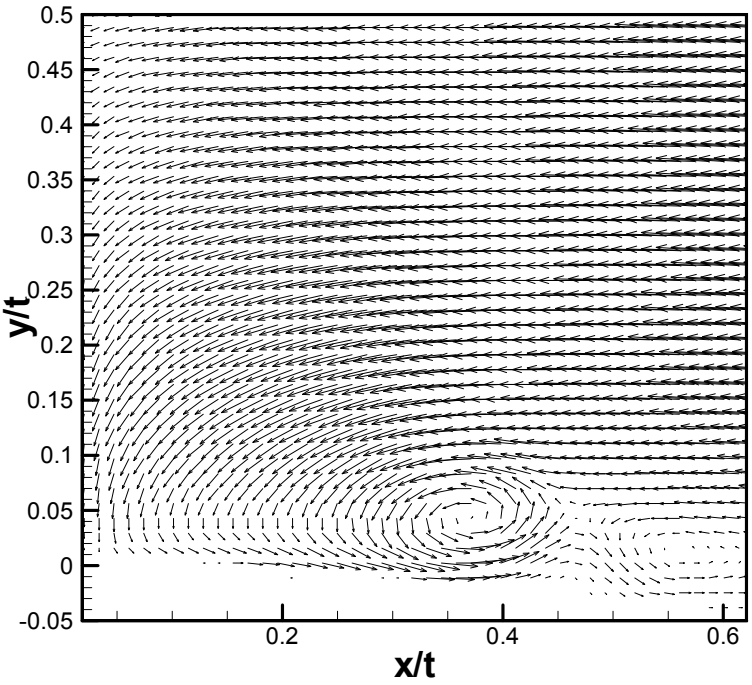

Figure A.2 Vector plot for $h/t = 2.29$ – laminar boundary layer

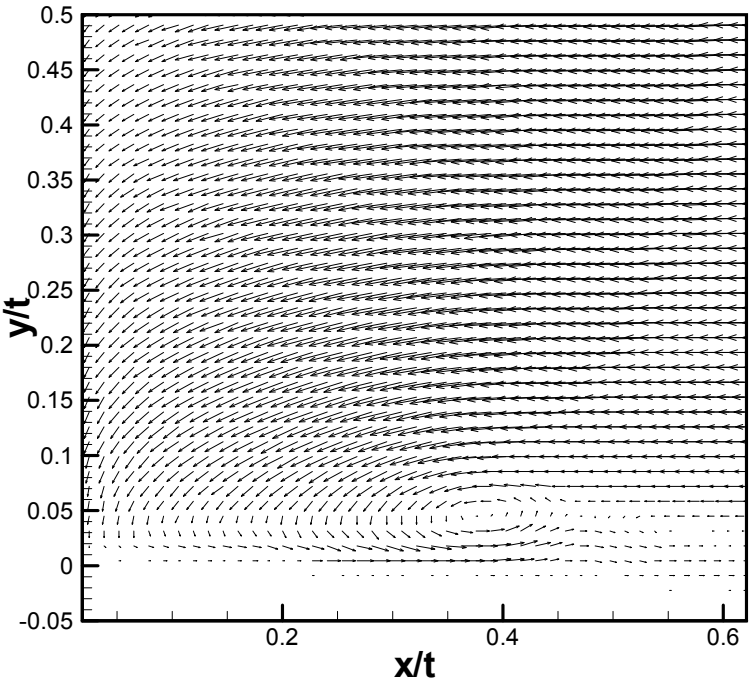

Figure A.3 Vector plot for $h/t = 1.14$ – laminar boundary layer

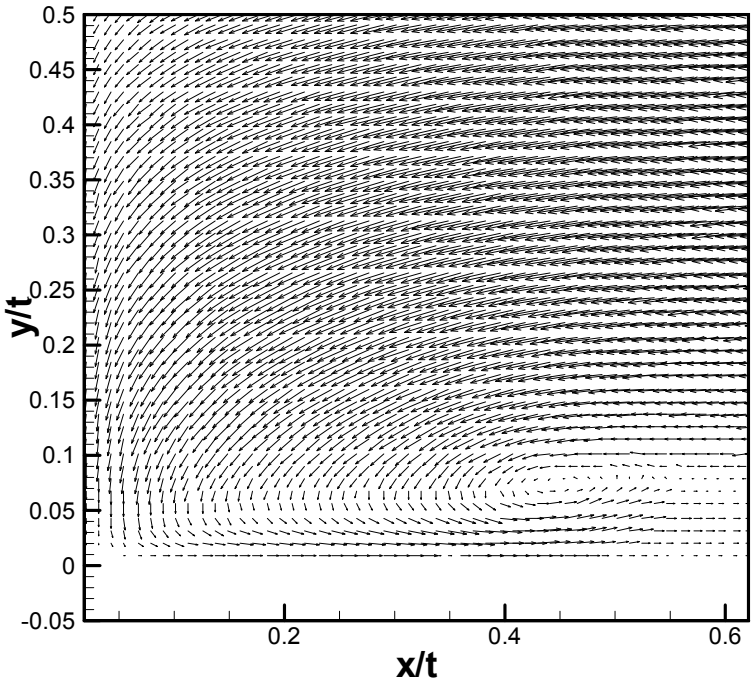

Figure A.4 Vector plot for $h/t = 0.00$ – laminar boundary layer

A.2 Vector Plots – Tripped Boundary Layer

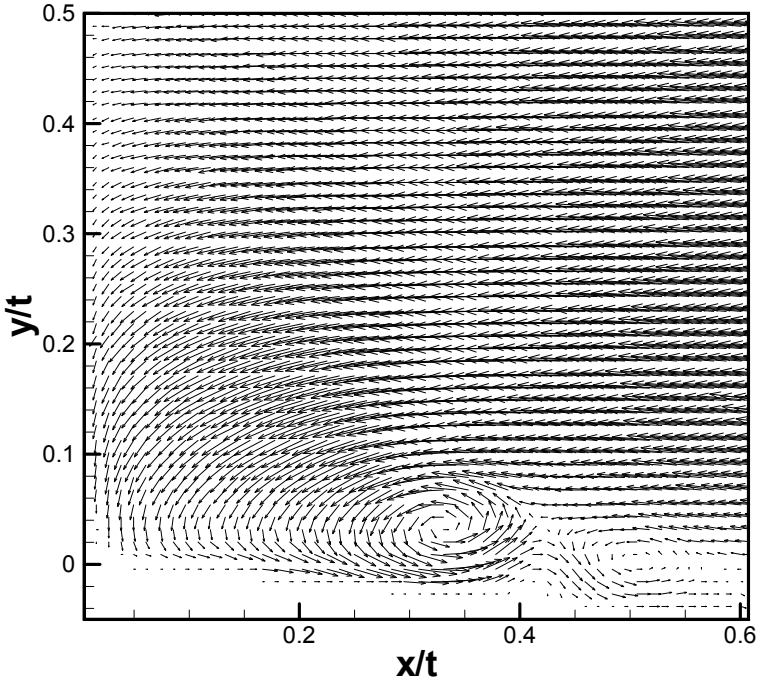

Figure A.5 Vector plot for $h/t = 2.86$ – tripped boundary layer

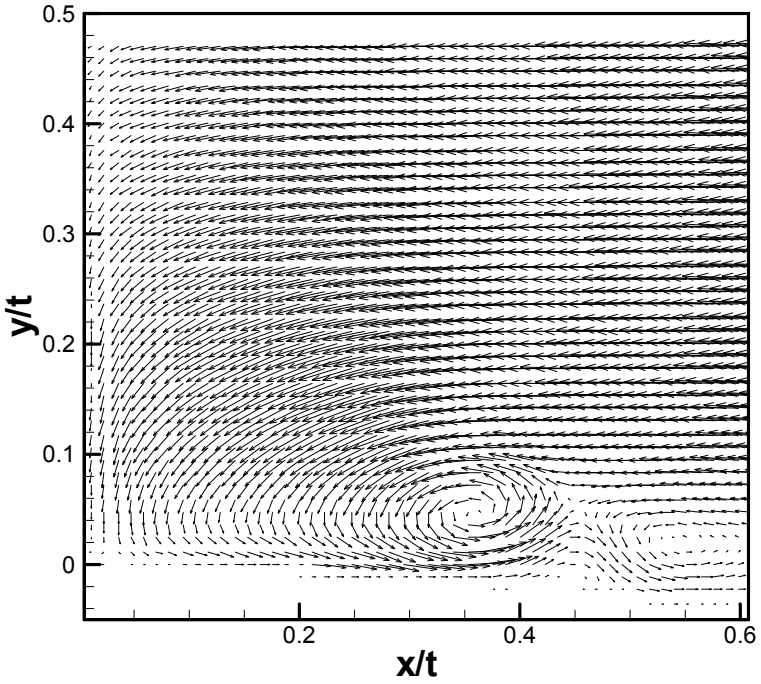

Figure A.6 Vector plot for $h/t = 2.29$ – tripped boundary layer

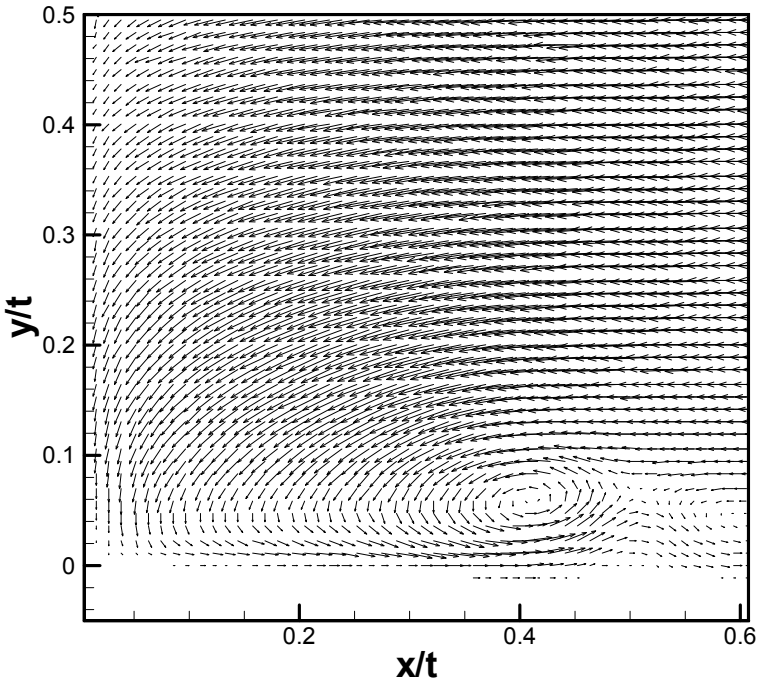

Figure A.7 Vector plot for $h/t = 1.14$ – tripped boundary layer

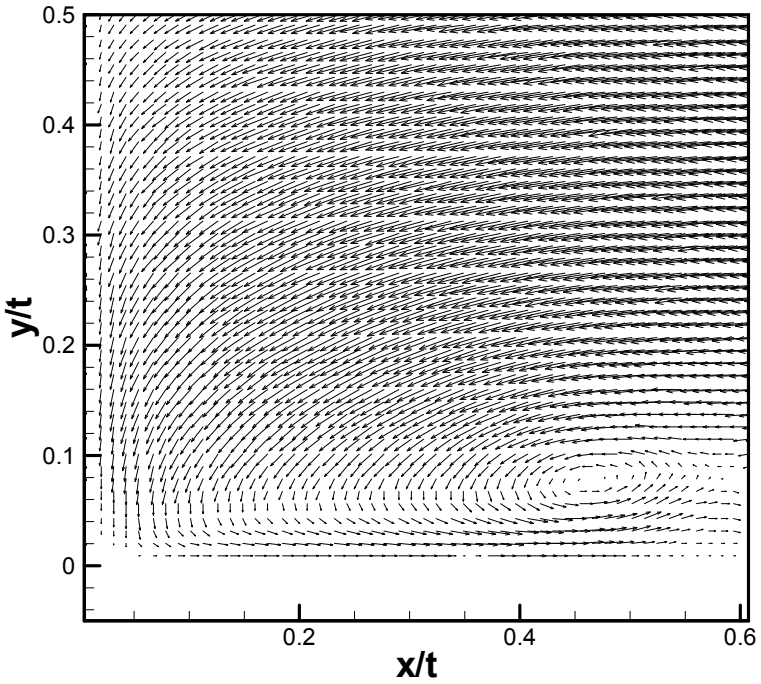

Figure A.8 Vector plot for $h/t = 0.00$ – tripped boundary layer

A.3 Streamlines – Laminar Boundary Layer

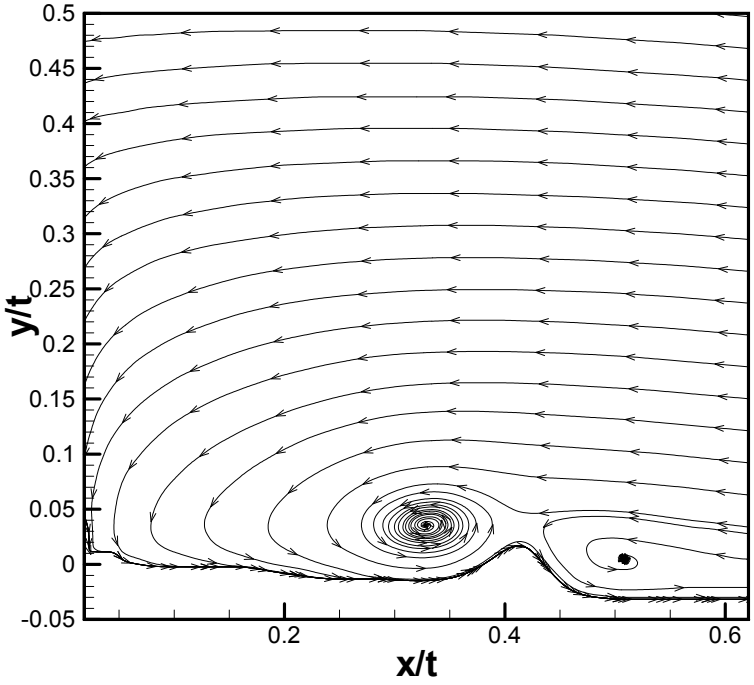

Figure A.9 Streamlines for $h/t = 2.86$ – laminar boundary layer

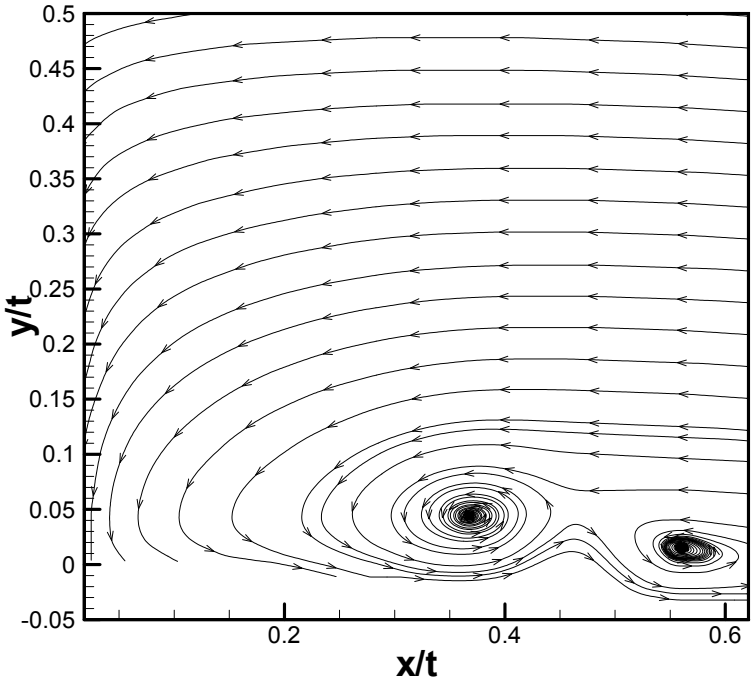

Figure A.10 Streamlines for $h/t = 2.29$ – laminar boundary layer

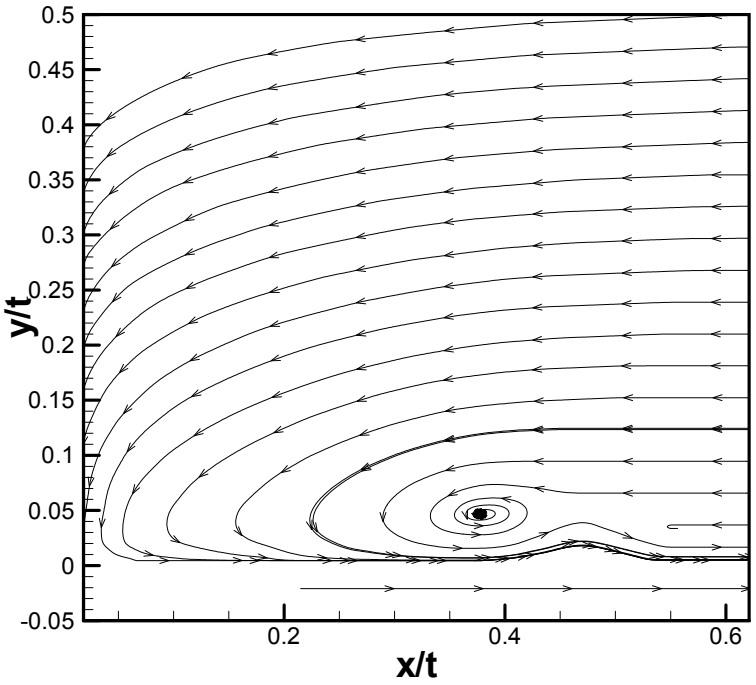

Figure A.11 Streamlines for $h/t = 1.14$ – laminar boundary layer

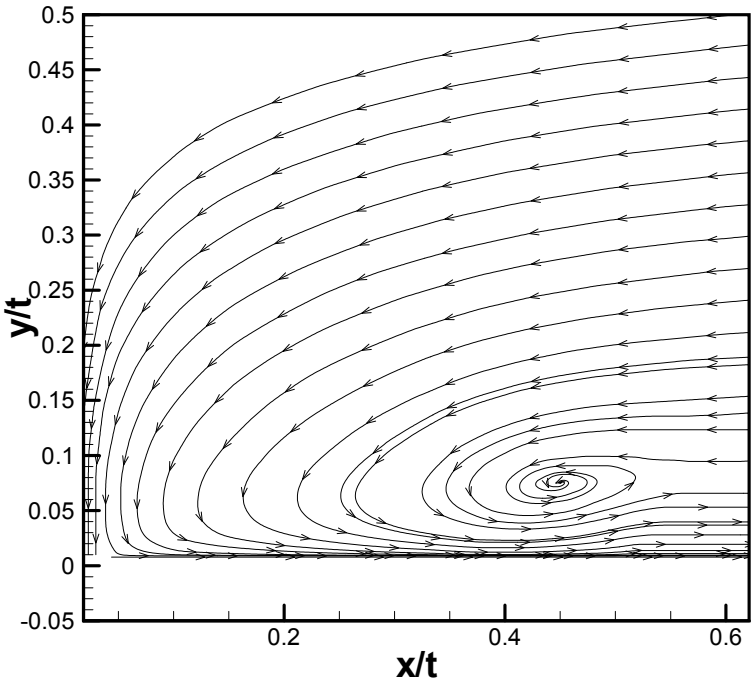

Figure A.12 Streamlines for $h/t = 0.00$ – laminar boundary layer

A.4 Streamlines – Tripped Boundary Layer

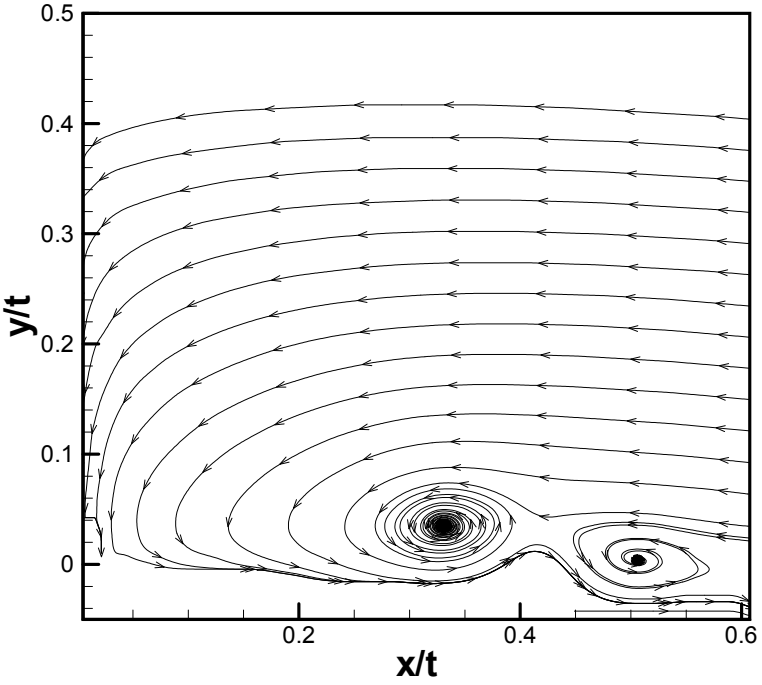

Figure A.13 Streamlines for $h/t = 2.86$ – tripped boundary layer

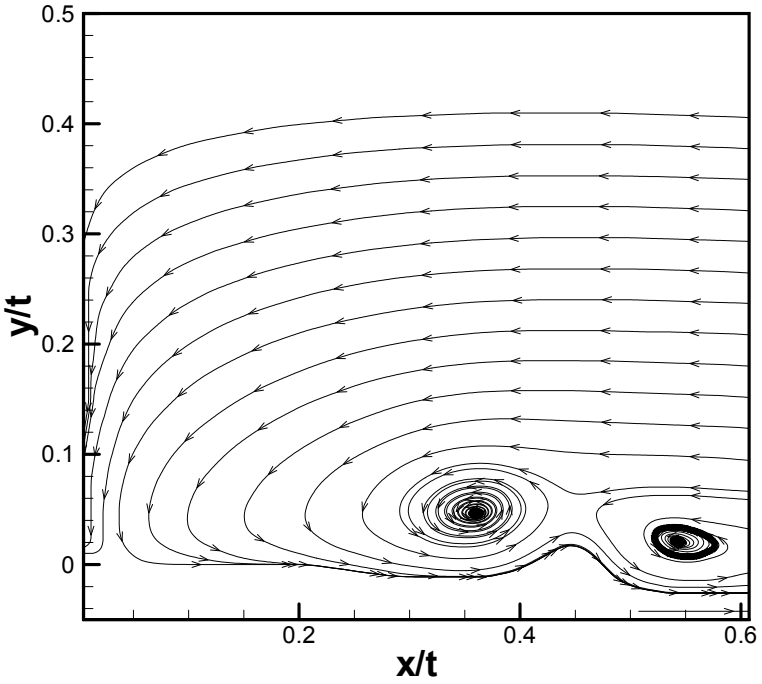

Figure A.14 Streamlines for $h/t = 2.29$ – tripped boundary layer

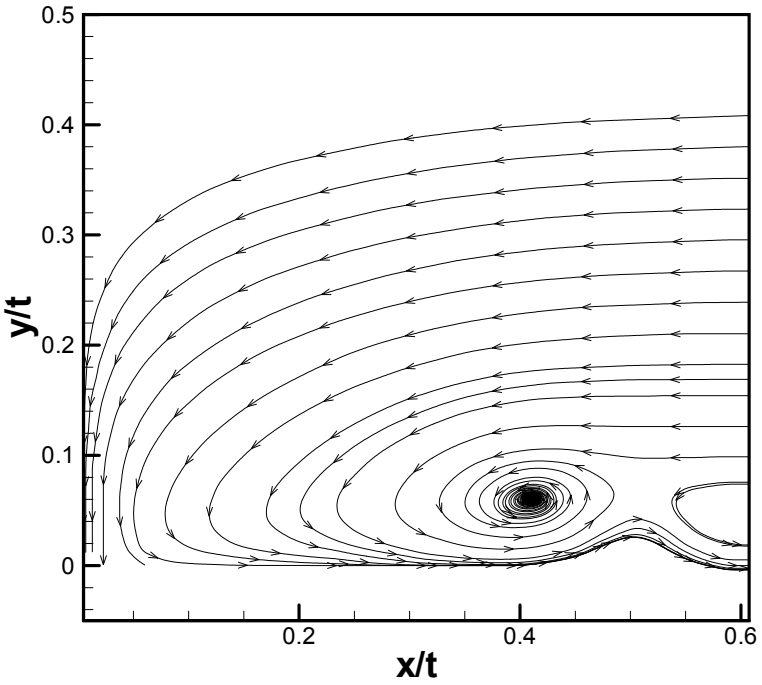

Figure A.15 Streamlines for $h/t = 1.14$ – tripped boundary layer

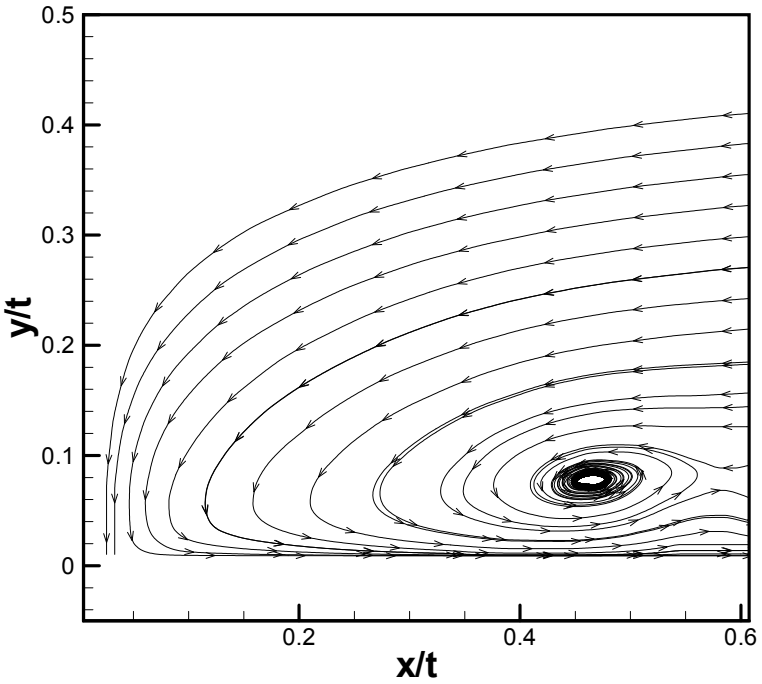

Figure A.16 Streamlines for $h/t = 0.00$ – tripped boundary layer

A.5 Bifurcation Streamline – Laminar Boundary Layer

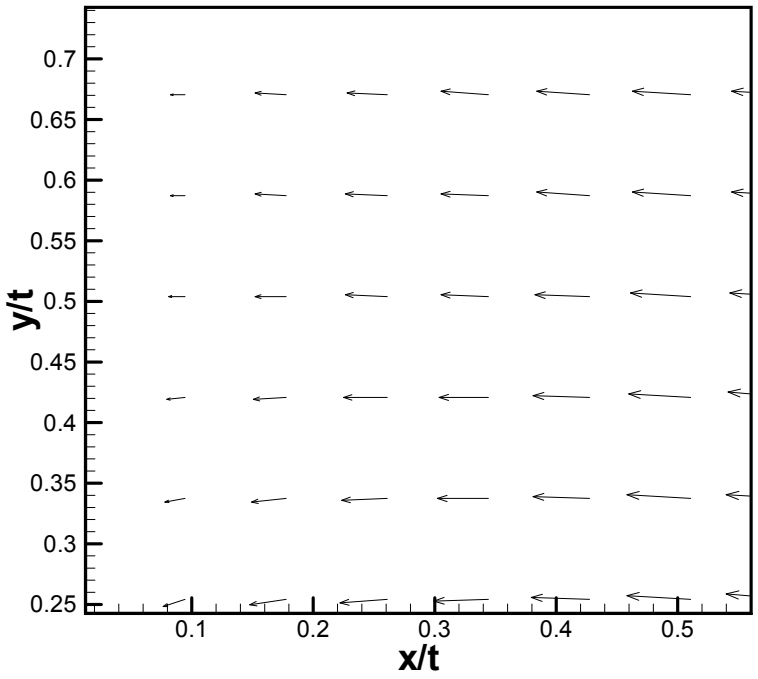

Figure A.17 Bifurcation streamline for $h/t = 2.86$ – laminar boundary layer

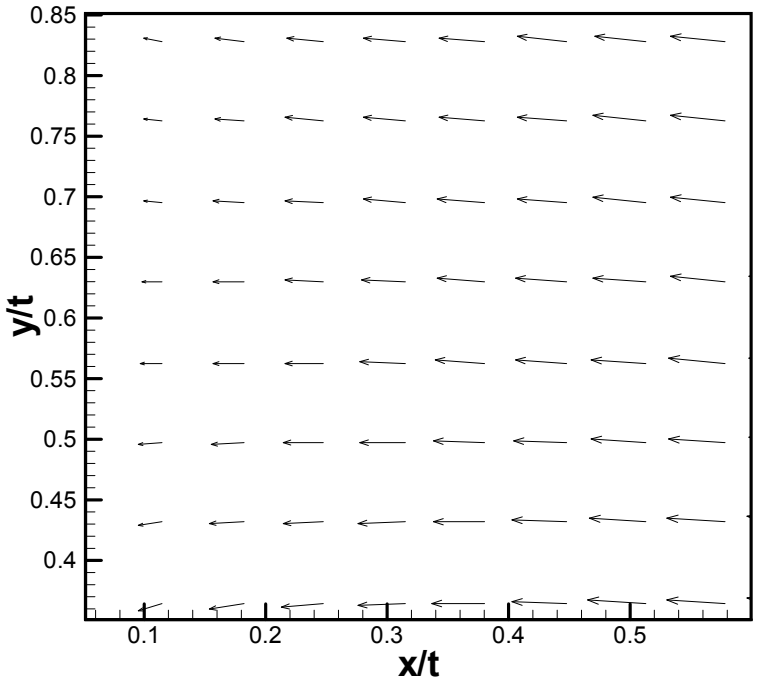

Figure A.18 Bifurcation streamline for $h/t = 2.29$ – laminar boundary layer

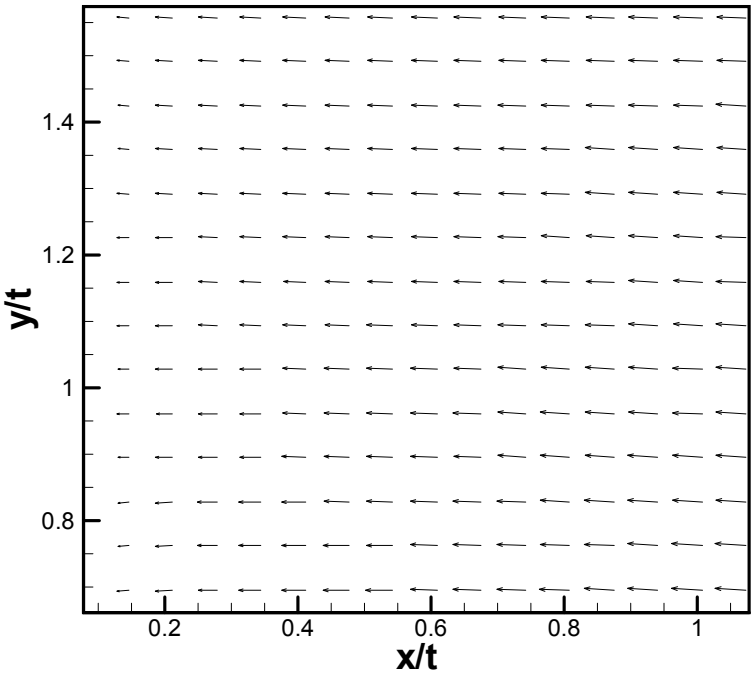

Figure A.19 Bifurcation streamline for $h/t = 1.14$ – laminar boundary layer

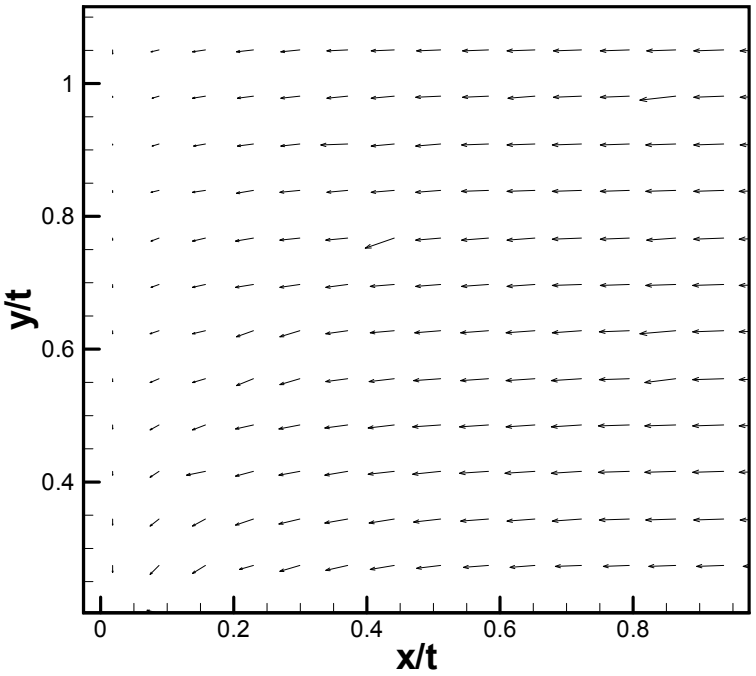

Figure A.20 Bifurcation streamline for $h/t = 0.00$ – laminar boundary layer

A.6 Bifurcation Streamline – Tripped Boundary Layer

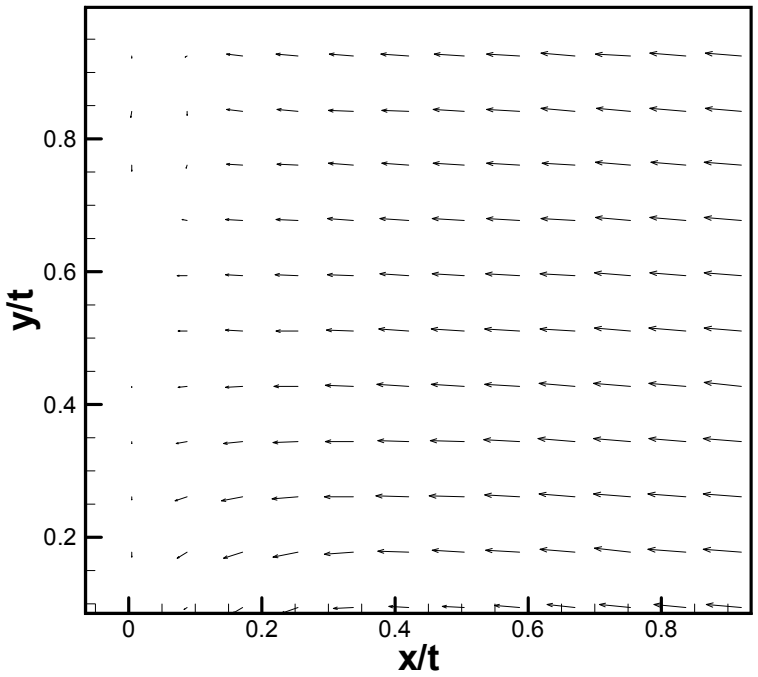

Figure A.21 Bifurcation streamline for $h/t = 2.86$ – tripped boundary layer

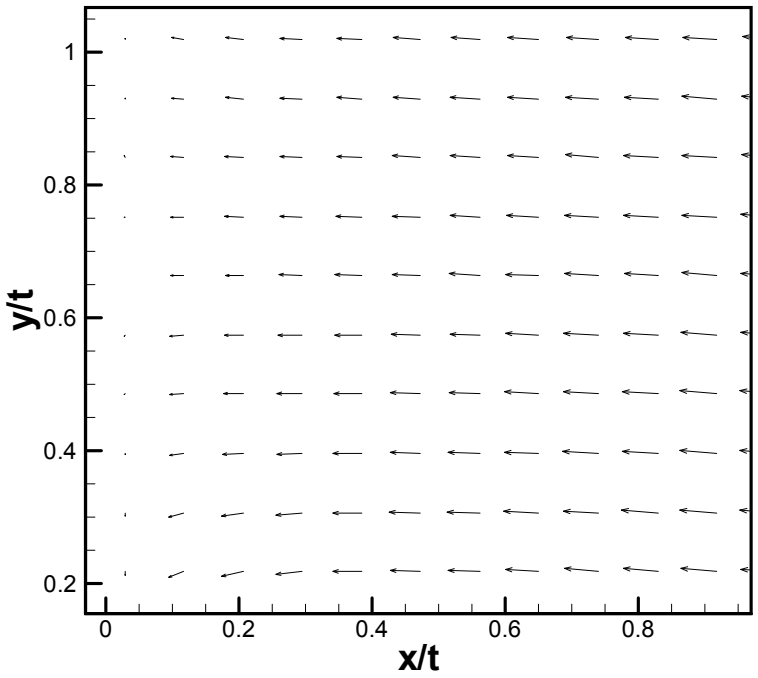

Figure A.22 Bifurcation streamline for $h/t = 2.29$ – tripped boundary layer

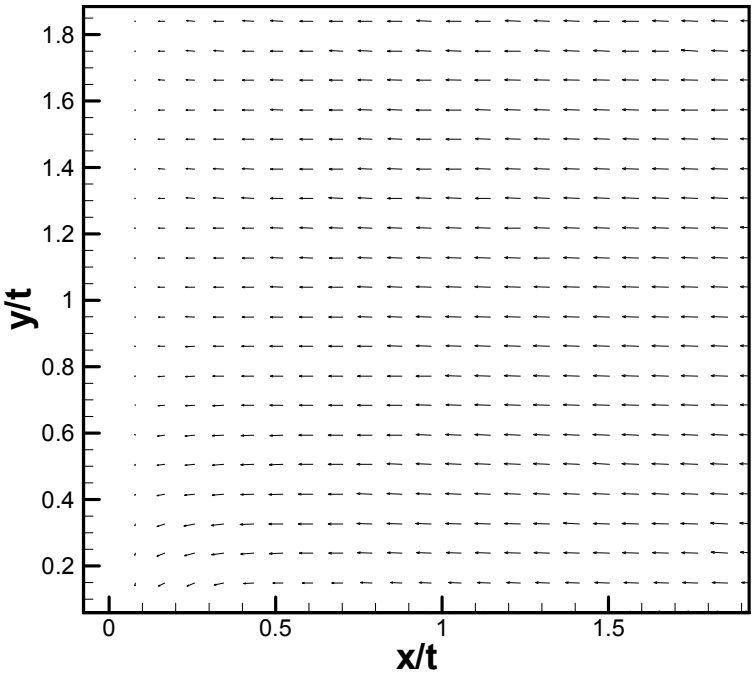

Figure A.23 Bifurcation streamline for h/t = 1.14 – tripped boundary layer

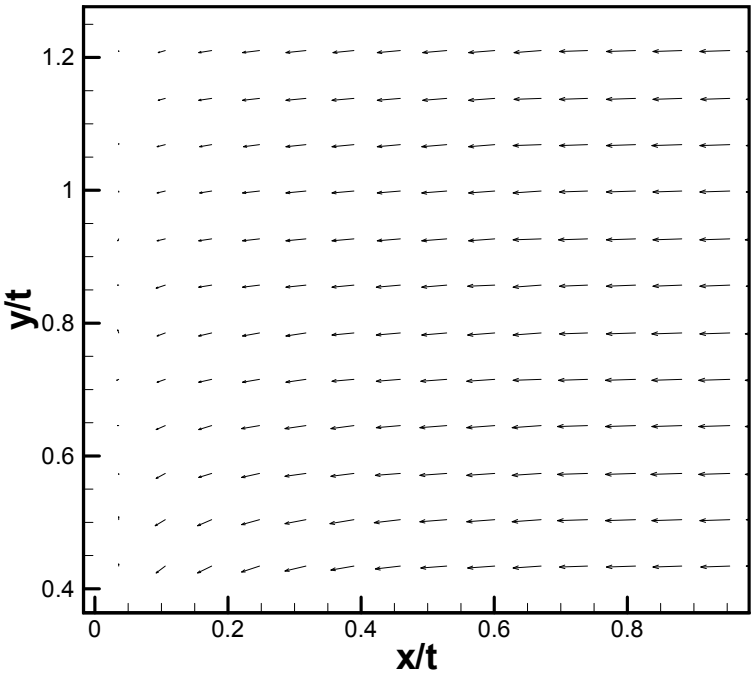

Figure A.24 Bifurcation streamline for h/t = 0.00 – tripped boundary layer

A.7 Vorticity – Laminar Boundary Layer

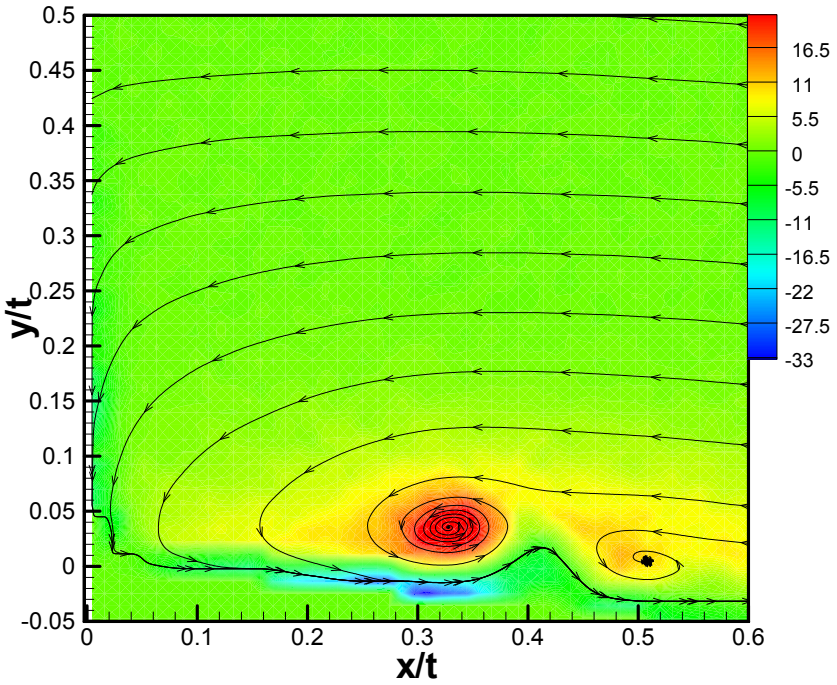

Figure A.25 Vorticity for $h/t = 2.86$ – laminar boundary layer

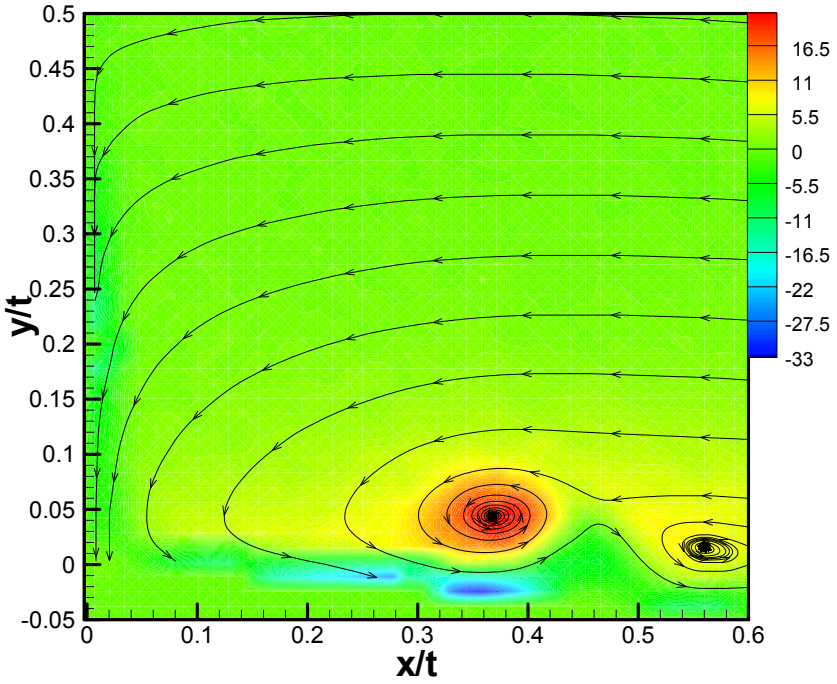

Figure A.26 Vorticity for $h/t = 2.29$ – laminar boundary layer

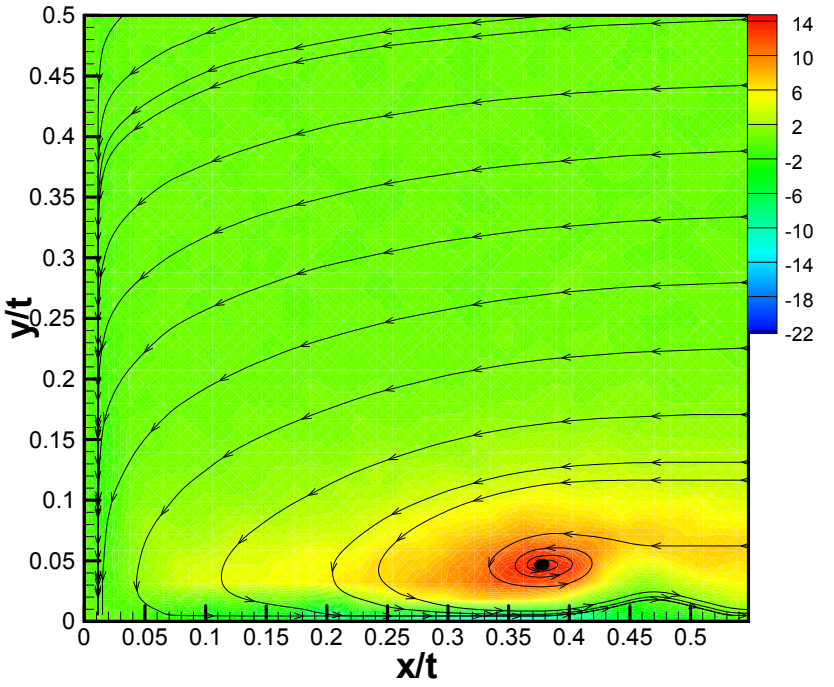

Figure A.27 Vorticity for $h/t = 1.14$ – laminar boundary layer

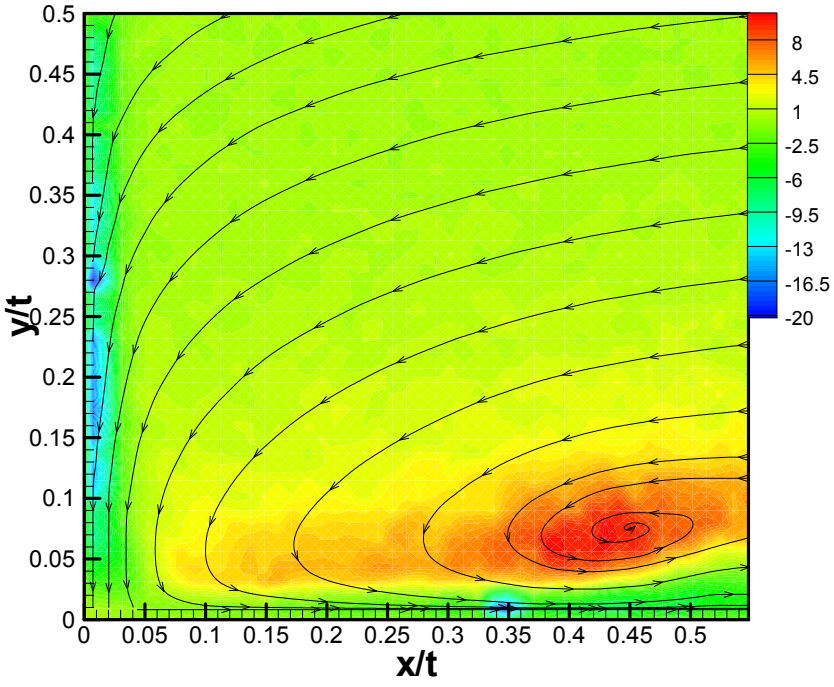

Figure A.28 Vorticity for $h/t = 0.00$ – laminar boundary layer

A.8 Vorticity – Tripped Boundary Layer

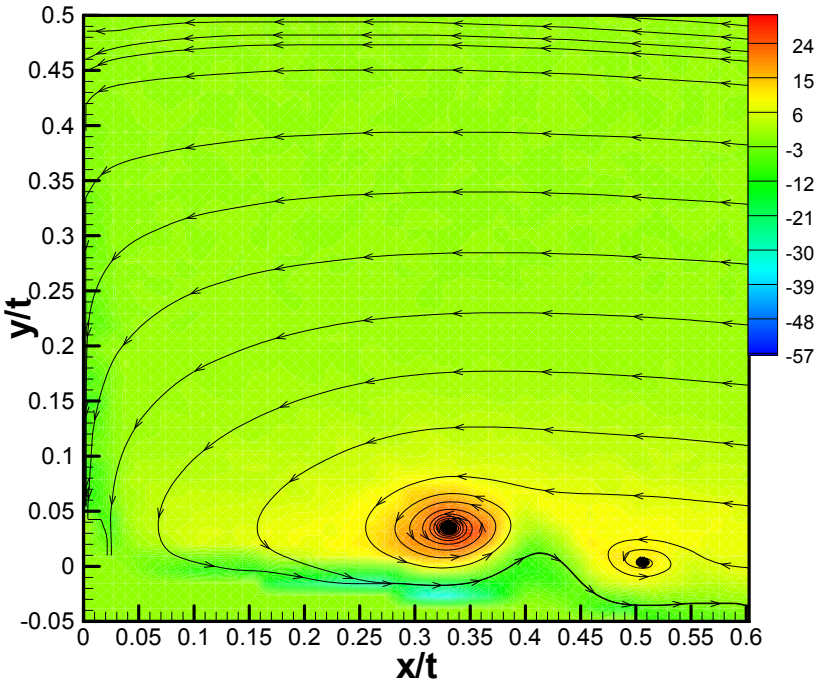

Figure A.29 Vorticity for $h/t = 2.86$ – tripped boundary layer

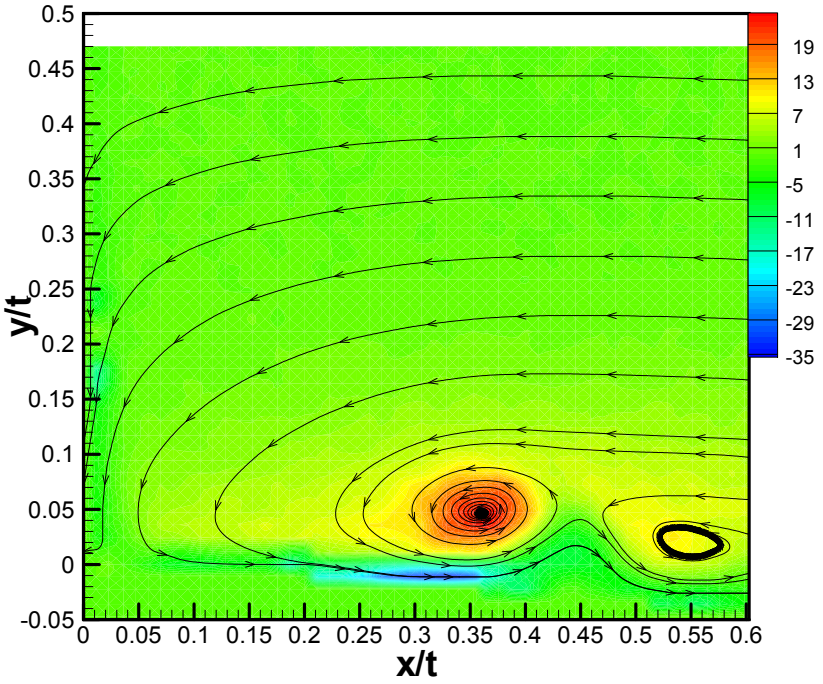

Figure A.30 Vorticity for $h/t = 2.29$ – tripped boundary layer

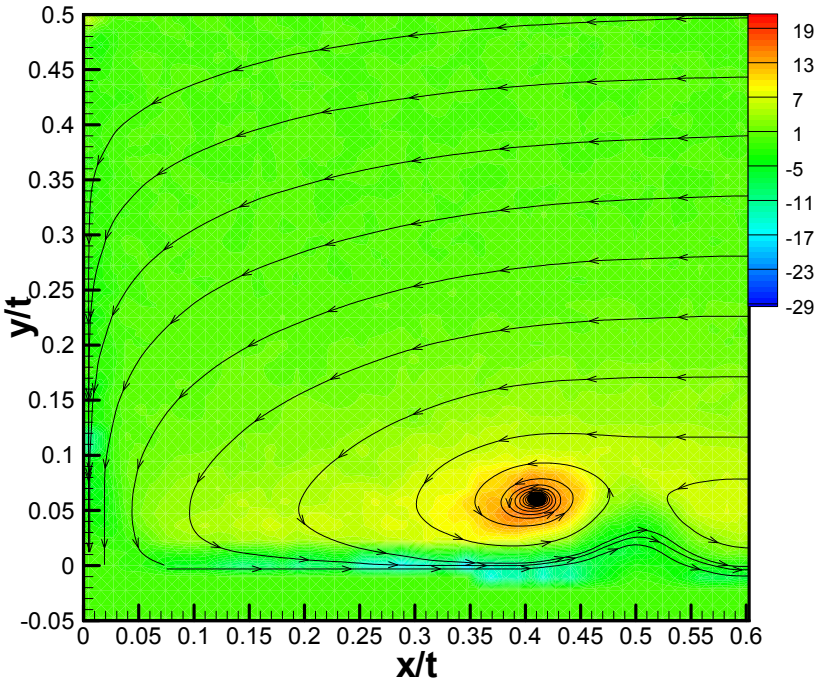

Figure A.31 Vorticity for $h/t = 1.14$ – tripped boundary layer

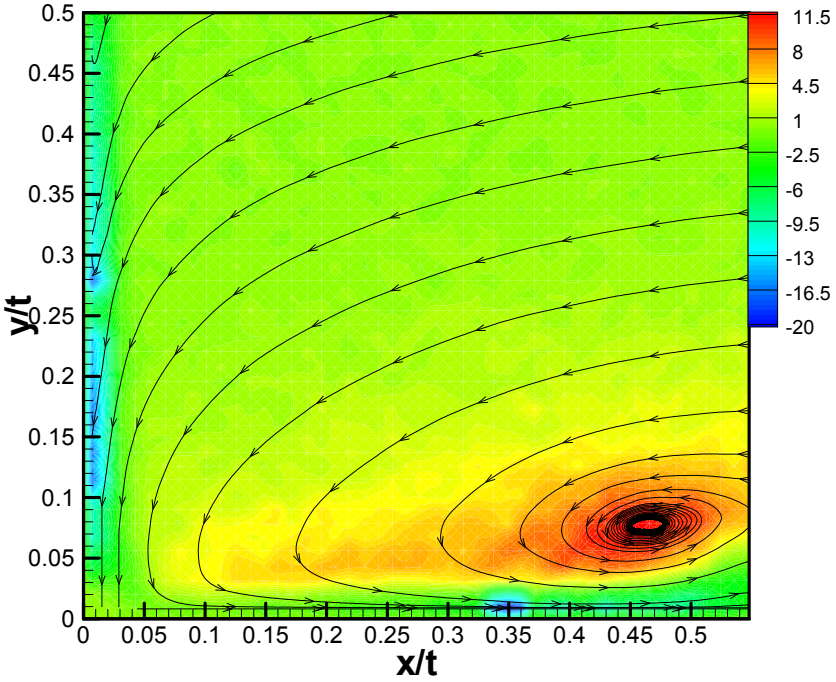

Figure A.32 Vorticity for $h/t = 0.00$ – tripped boundary layer

A.9 Strain – Laminar Boundary Layer

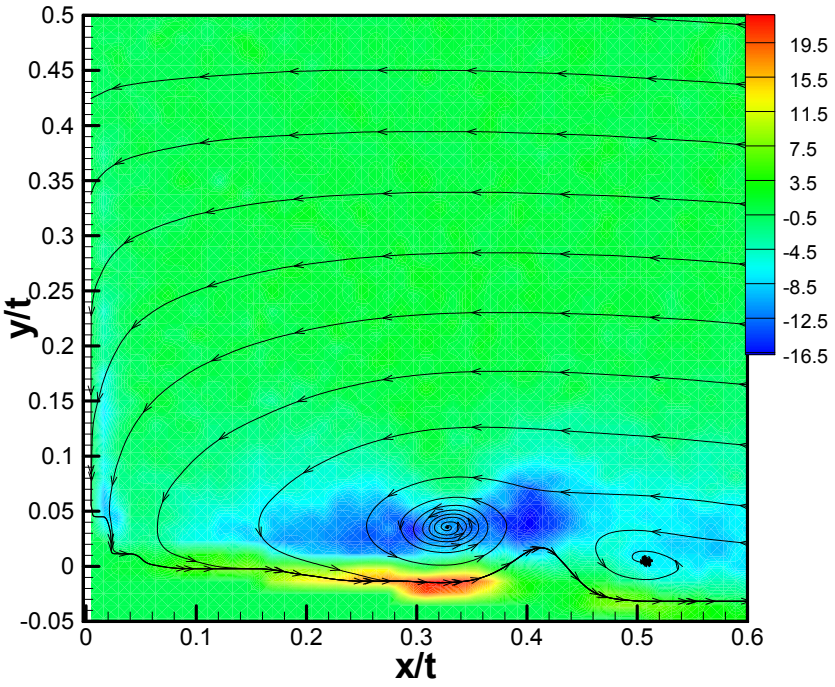

Figure A.33 Strain for $h/t = 2.86$ – laminar boundary layer

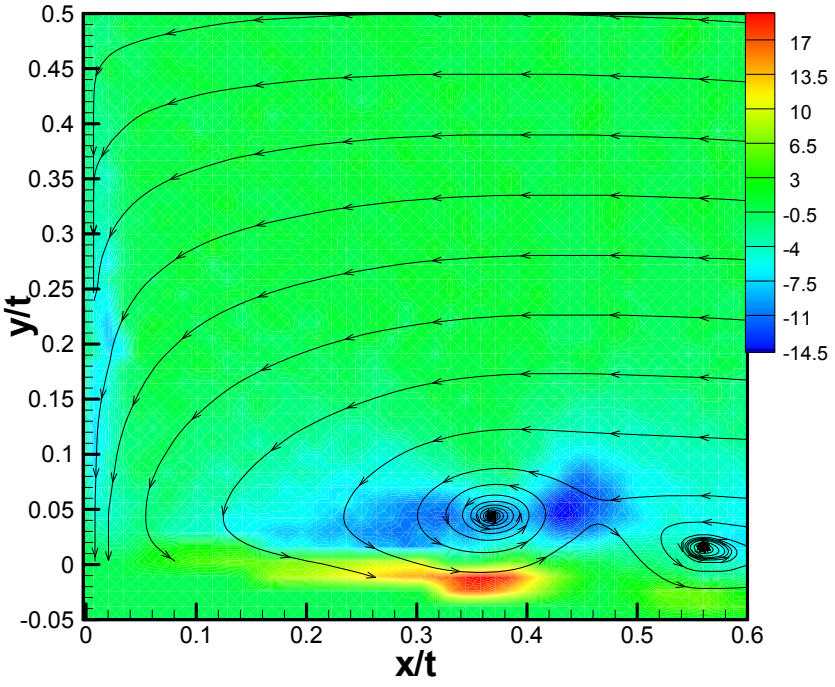

Figure A.34 Strain for $h/t = 2.29$ – laminar boundary layer

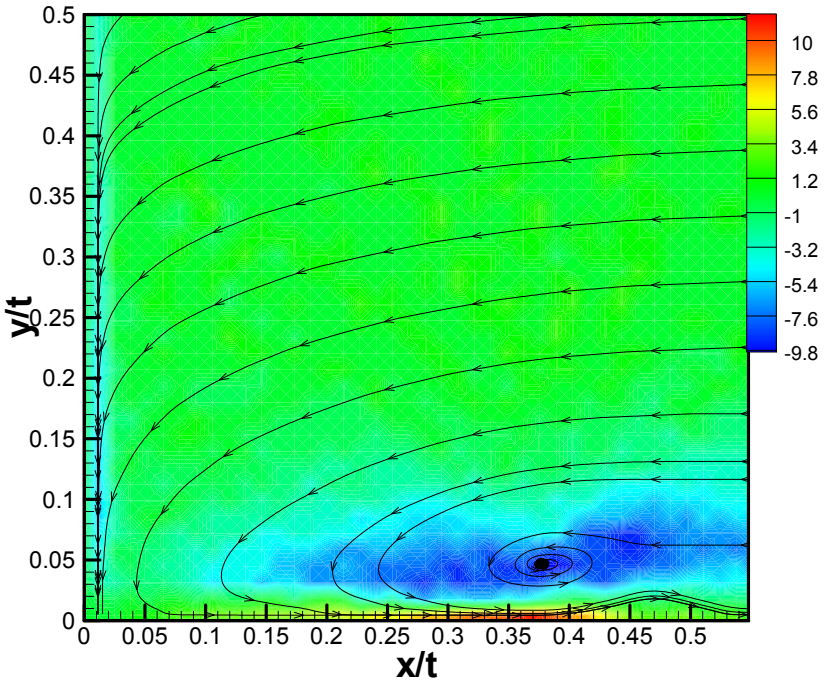

Figure A.35 Strain for $h/t = 1.14$ – laminar boundary layer

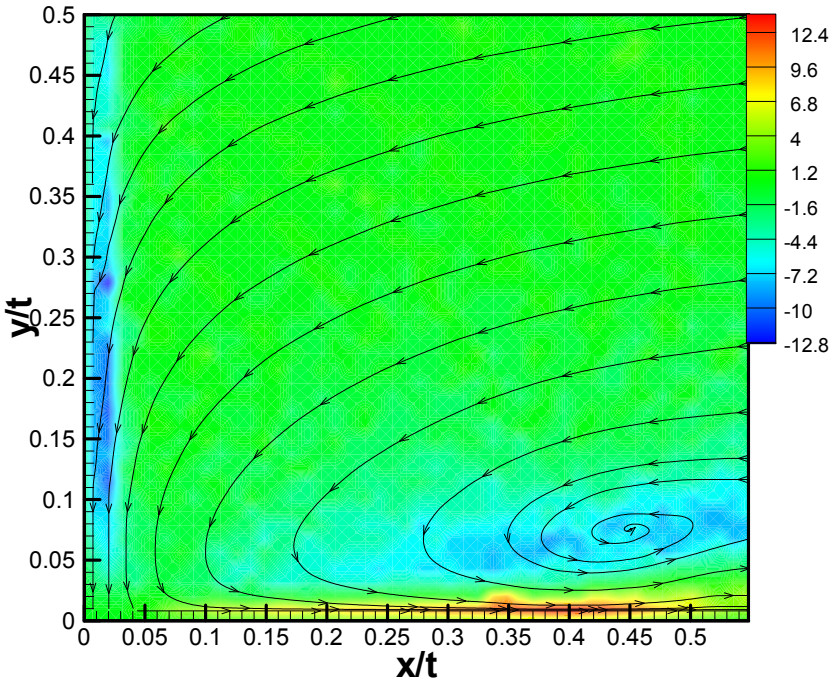

Figure A.36 Strain for $h/t = 0.00$ – laminar boundary layer

A.10 Strain – Tripped Boundary Layer

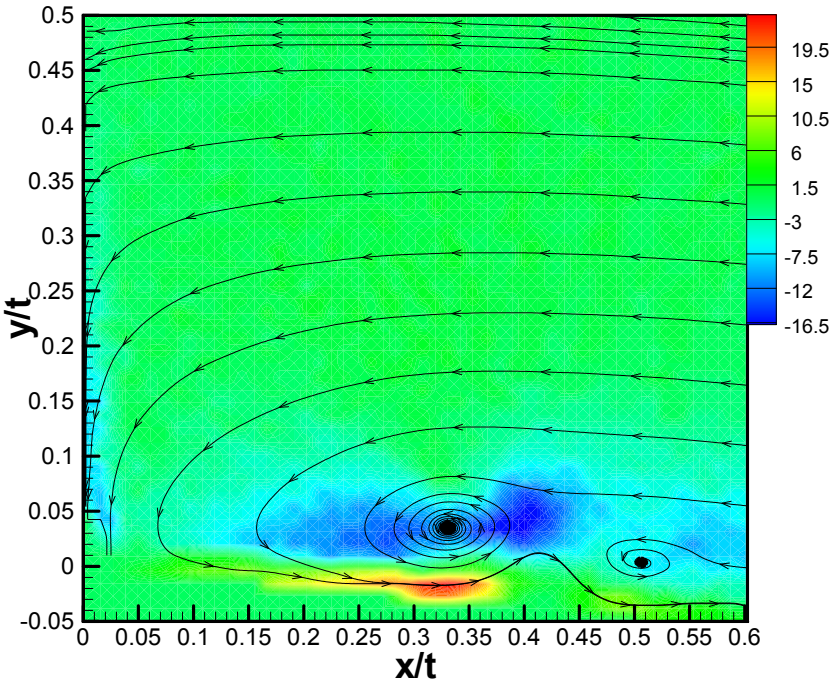

Figure A.37 Strain for h/t = 2.86 – tripped boundary layer

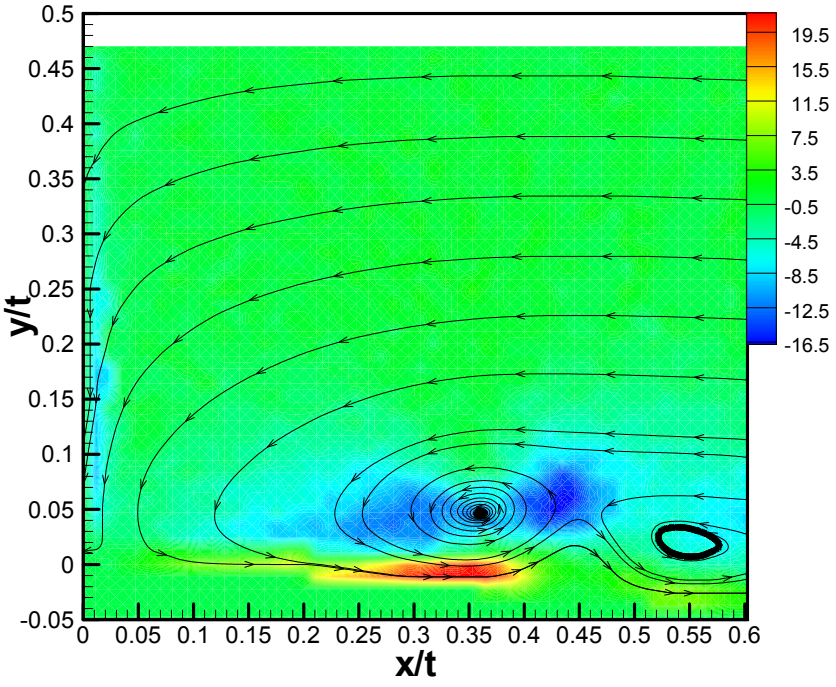

Figure A.38 Strain for h/t = 2.29 – tripped boundary layer

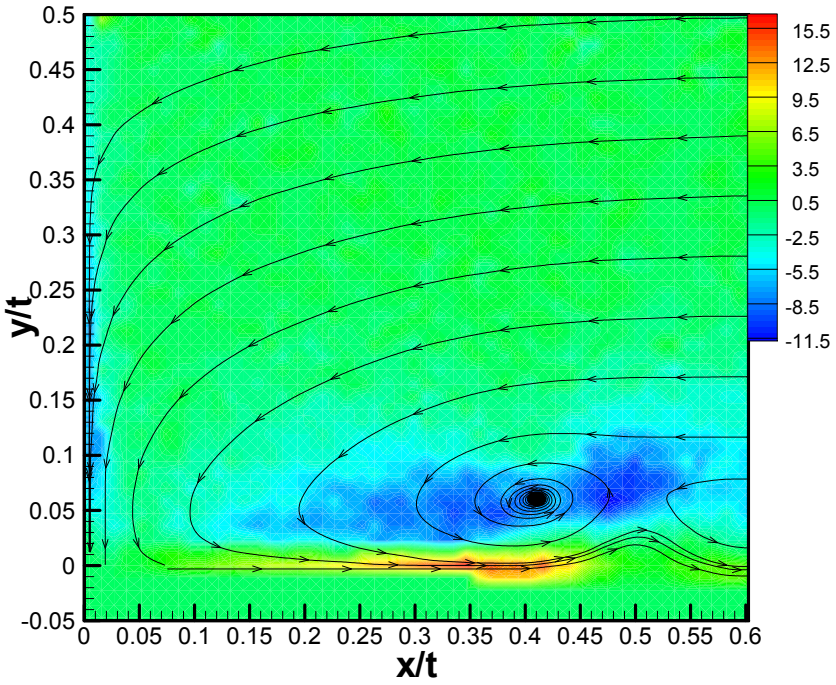

Figure A.39 Strain for h/t = 1.14 – tripped boundary layer

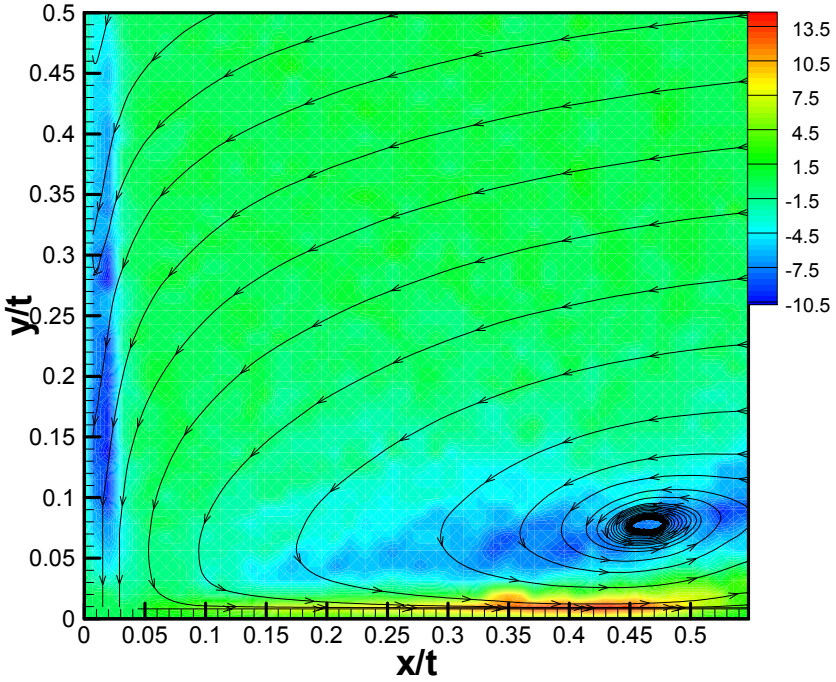

Figure A.40 Strain for h/t = 0.00 – tripped boundary layer

A.11 Vorticity and Strain Relation

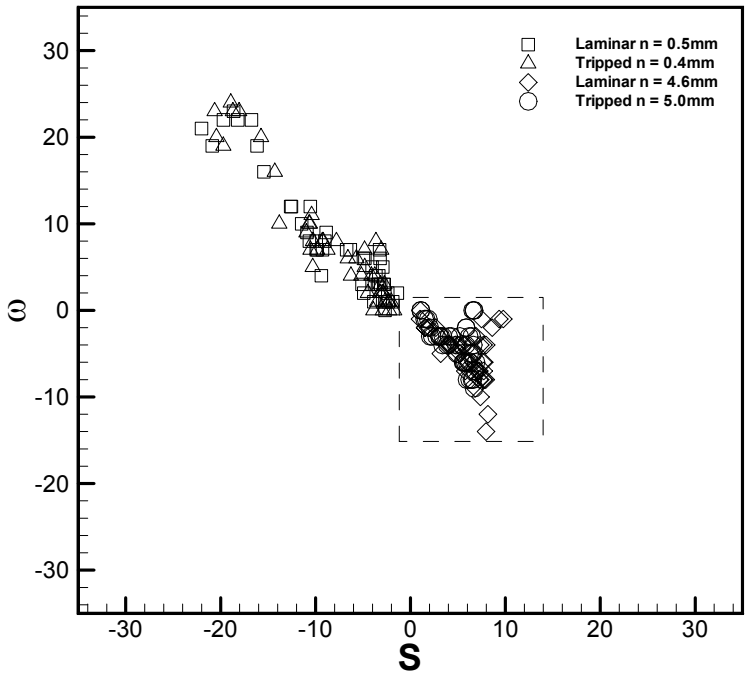

Figure A.41 Vorticity and strain relation for *h/t* = 2.86

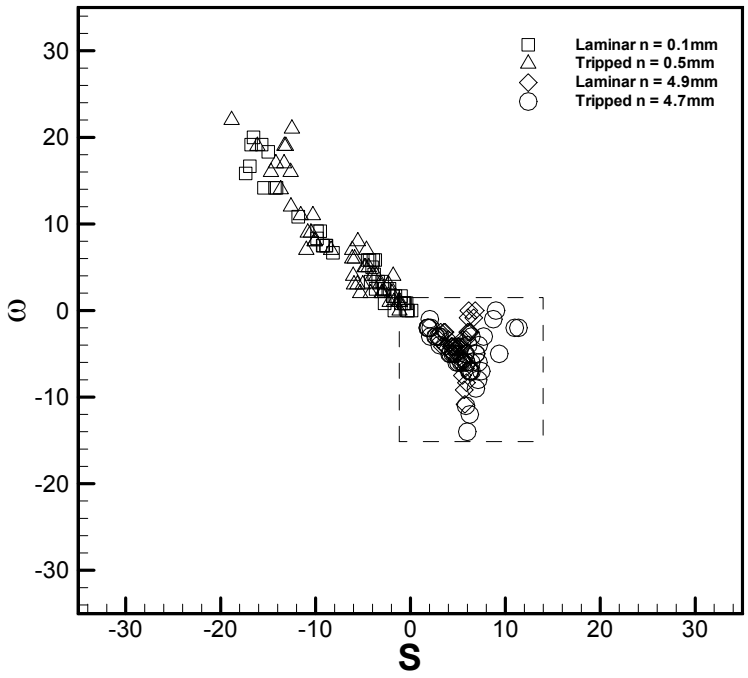

Figure A.42 Vorticity and strain relation for *h/t* = 2.29

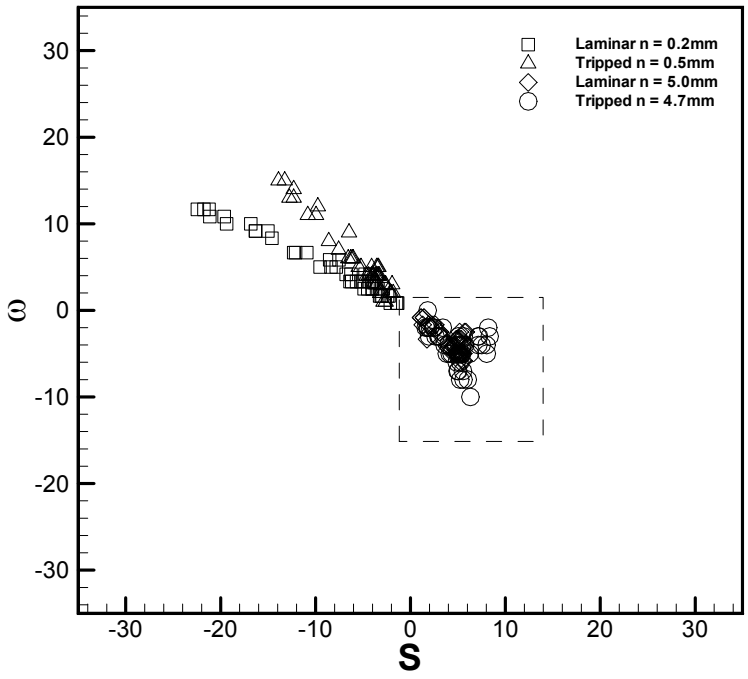

Figure A.43 Vorticity and Strain relation for $h/t = 1.14$

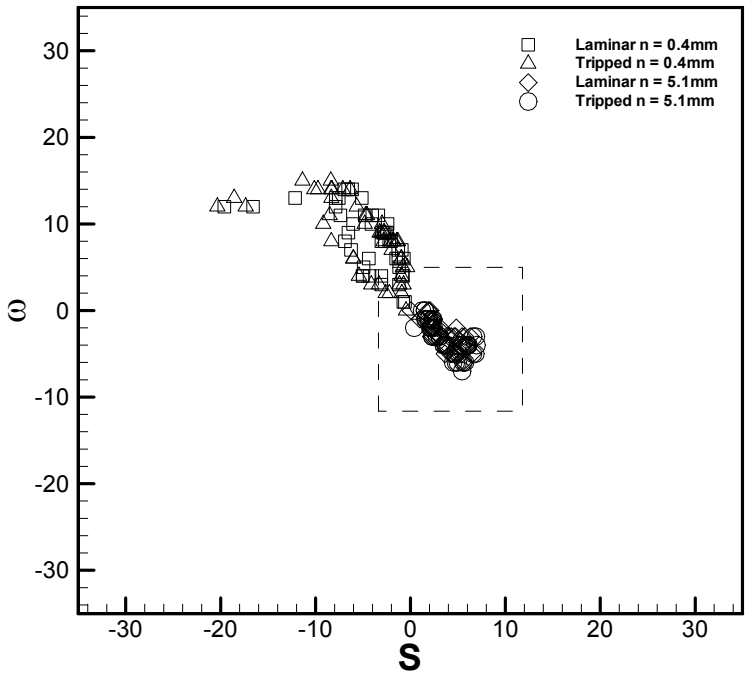

Figure A.44 Vorticity and strain relation for $h/t = 0.00$

A.12 Q Criterion – Laminar Boundary Layer

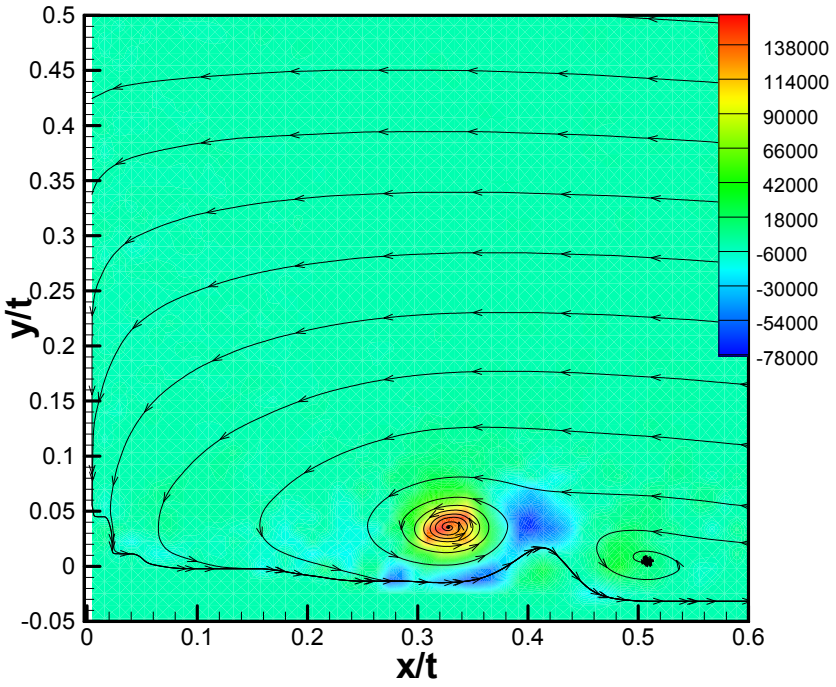

Figure A.45 Q criterion for h/t = 2.86 – laminar boundary layer

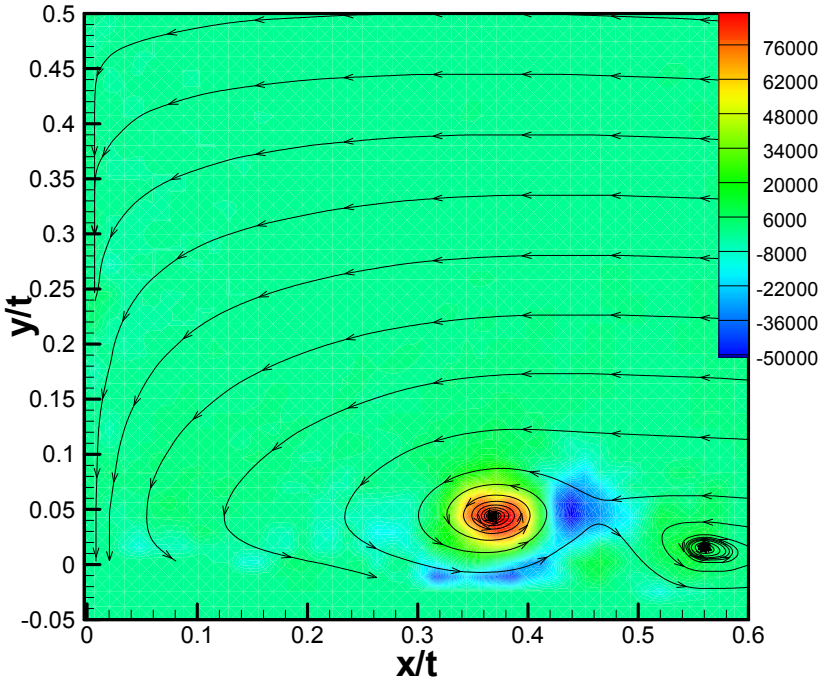

Figure A.46 Q criterion for h/t = 2.29 – laminar boundary layer

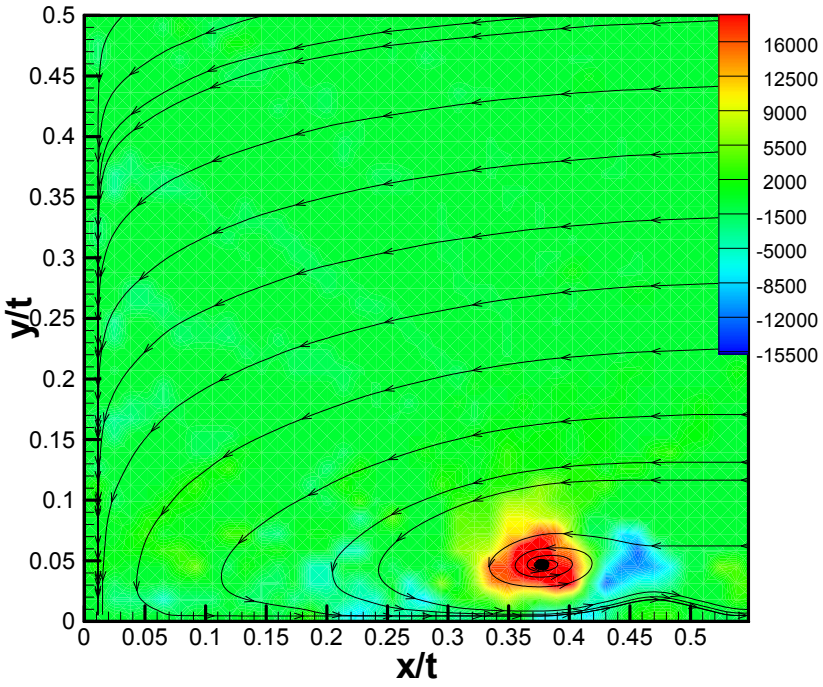

Figure A.47 Q criterion for h/t = 1.14 – laminar boundary layer

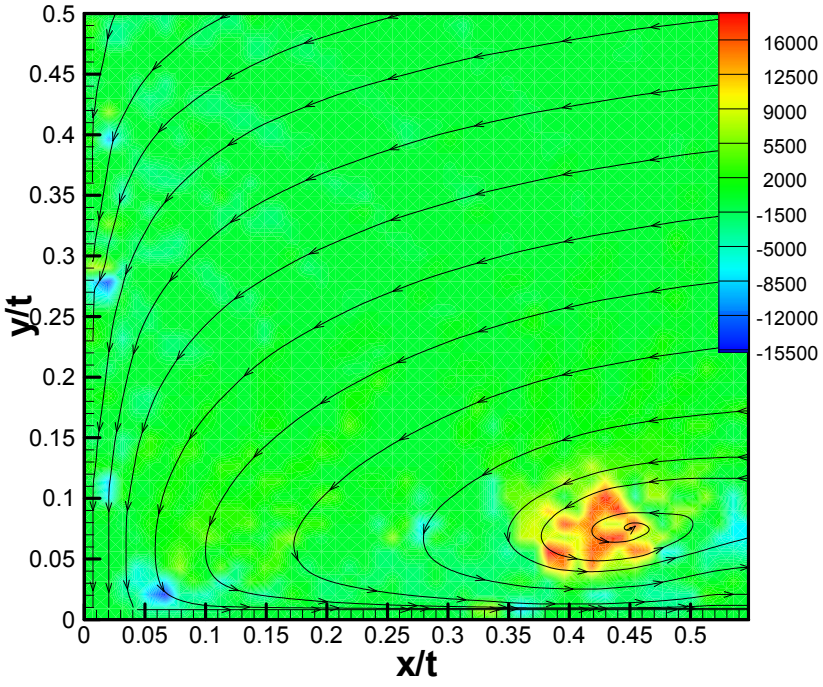

Figure A.48 Q criterion for h/t = 0.00 – laminar boundary layer

A.13 Q Criterion – Tripped Boundary Layer

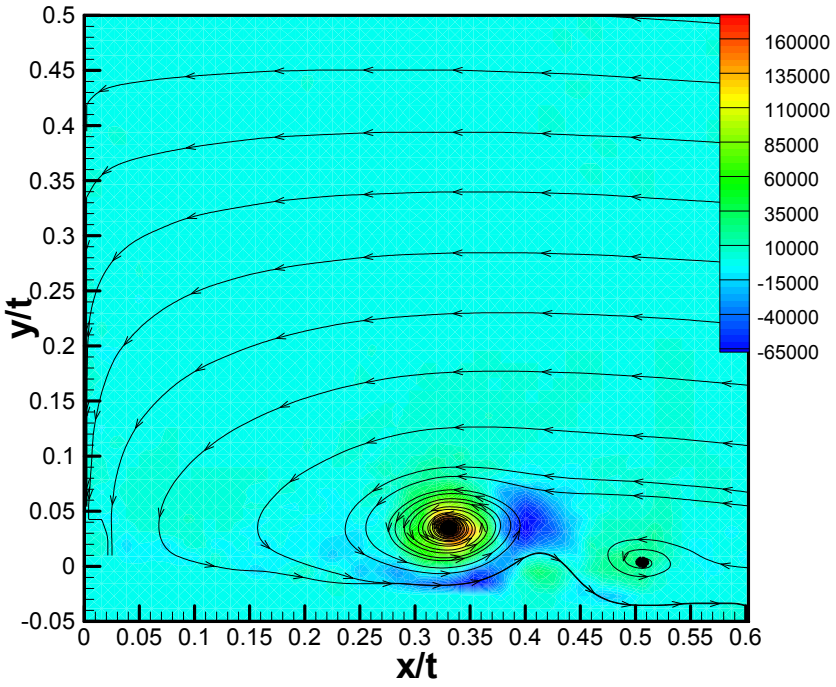

Figure A.49 Q criterion for $h/t = 2.86$ – tripped boundary layer

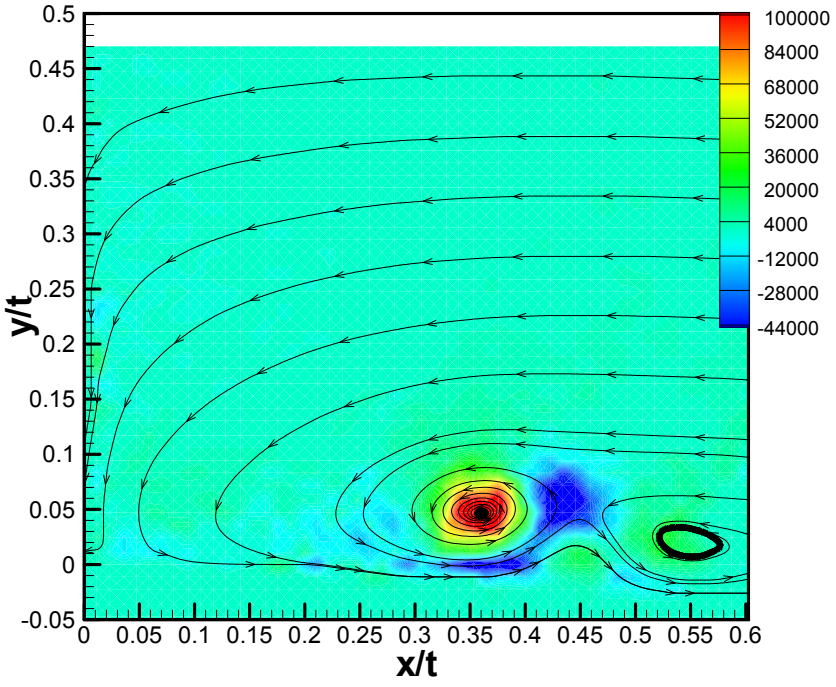

Figure A.50 Q criterion for $h/t = 2.29$ – tripped boundary layer

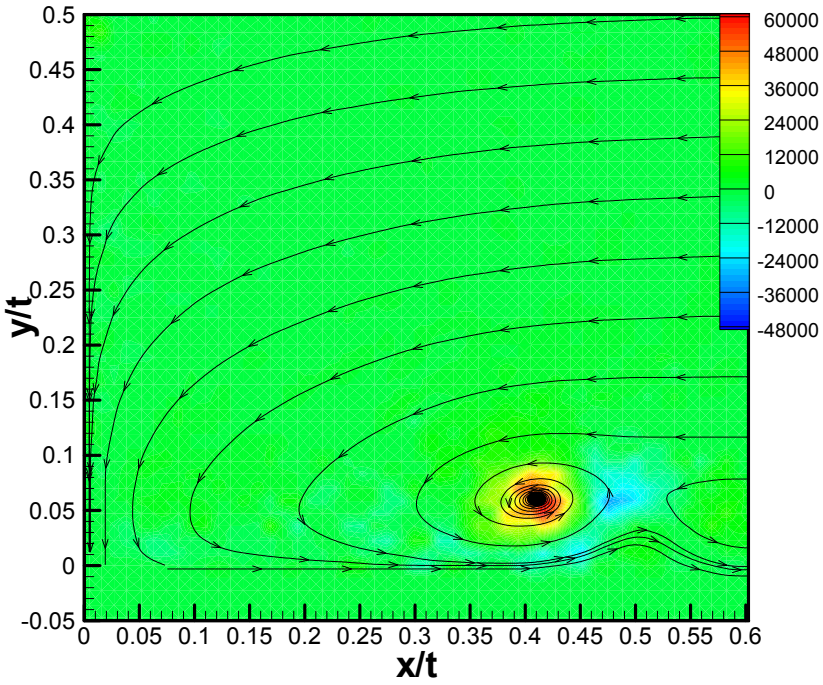

Figure A.51 Q criterion for h/t = 1.14 – tripped boundary layer

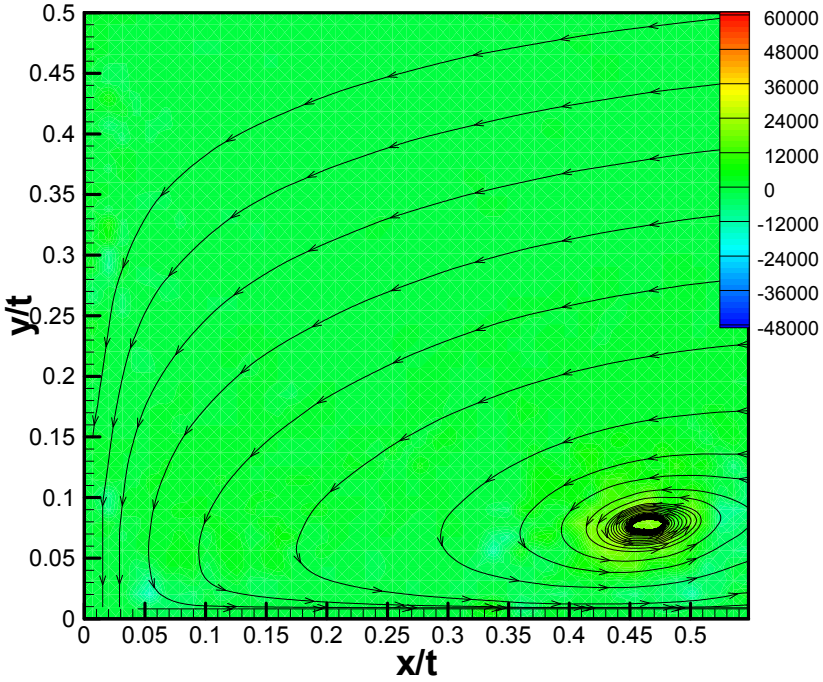

Figure A.52 Q criterion for h/t = 0.00 – tripped boundary layer

Appendix B

Wind Tunnel Results

B.1 Boundary Layer and Integral Values

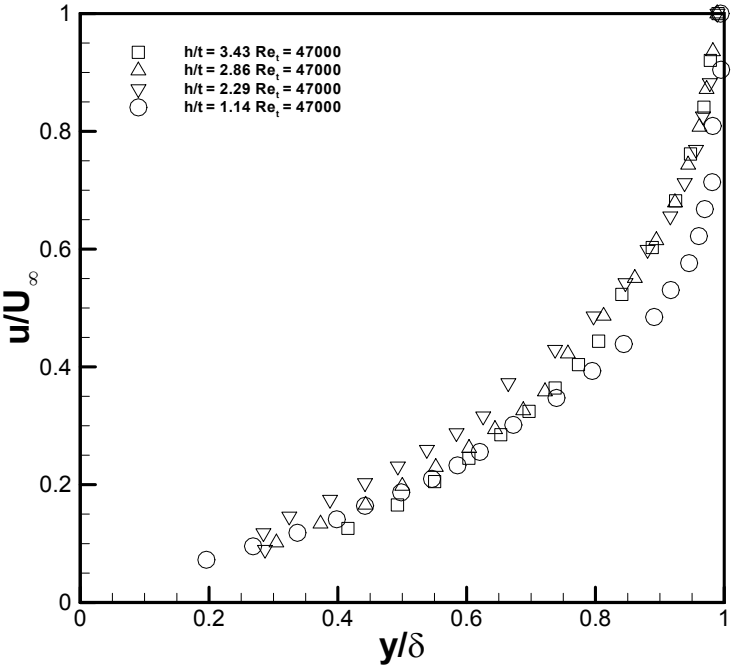

Figure B.1 Laminar boundary layer profile, $Re_t = 47{,}000$

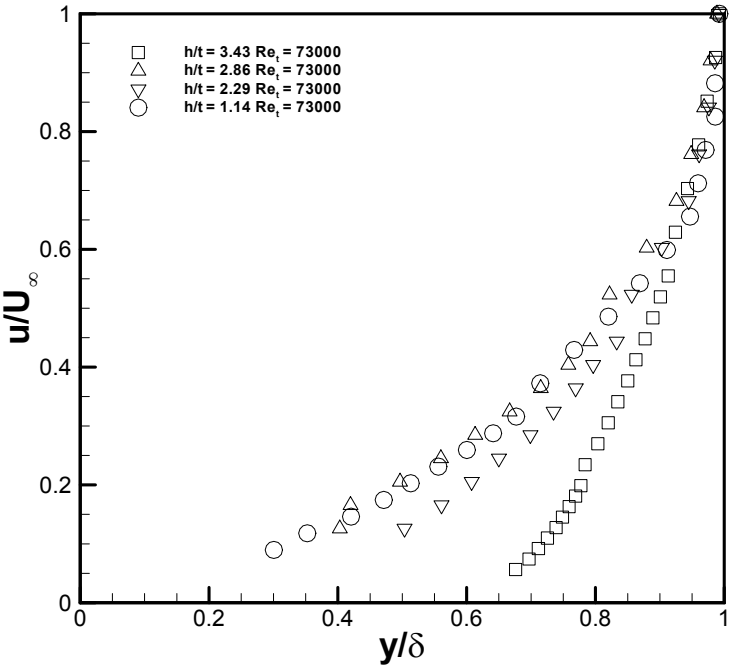

Figure B.2 Laminar boundary layer profile, $Re_t = 73{,}000$

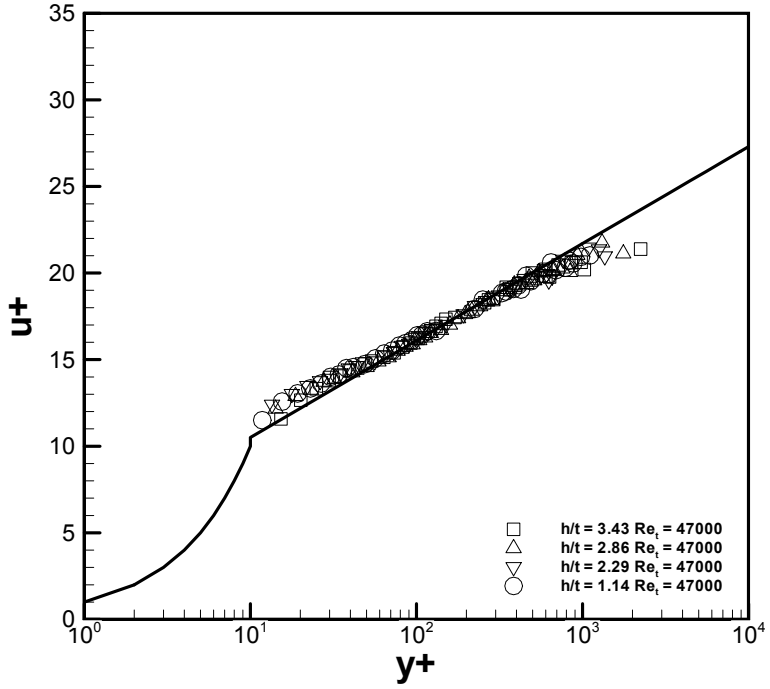

Figure B.3 Tripped boundary layer profile, $Re_t = 47{,}000$

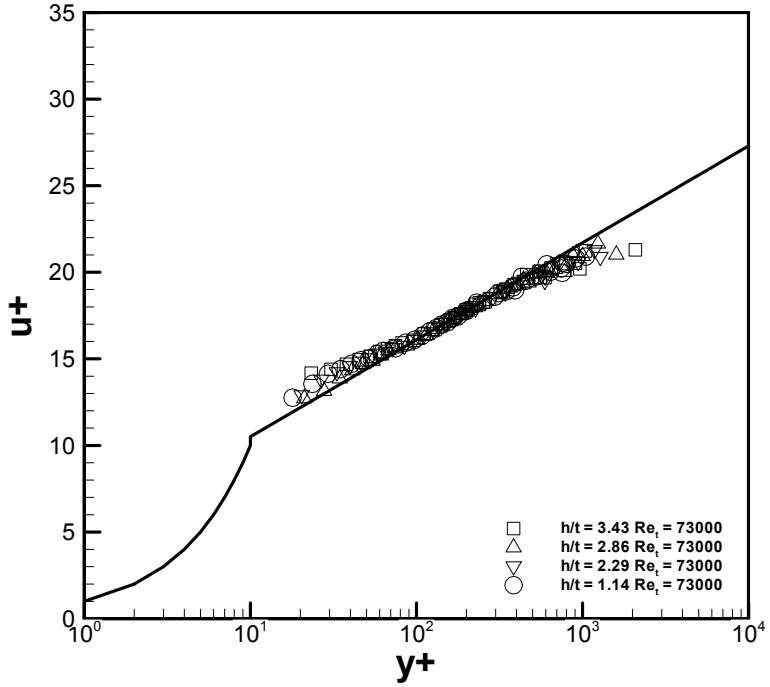

Figure B.4 Tripped boundary layer profile, Re_t = 73,000

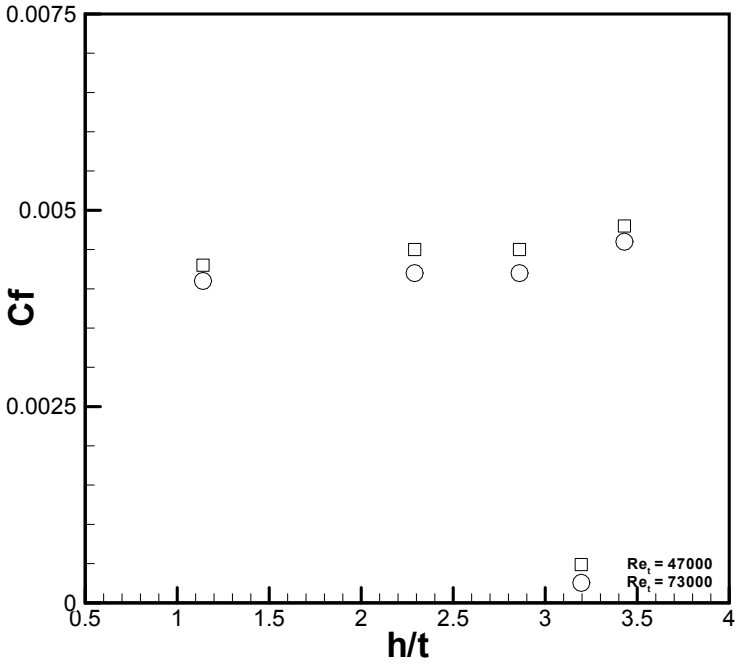

Figure B.5 Skin friction coefficient, Re_t = 47,000, 73,000 – tripped boundary layer

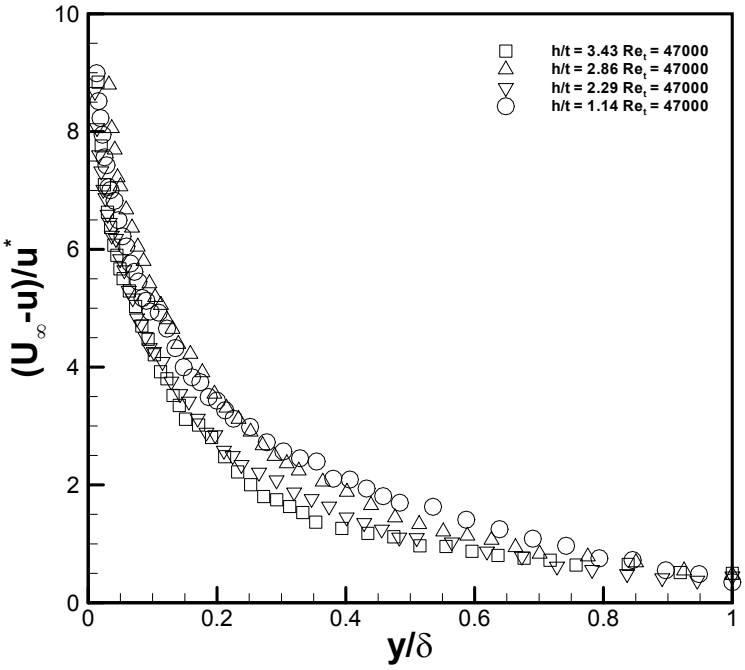

Figure B.6 Defect profile, $Re_t = 47{,}000$ – tripped boundary layer

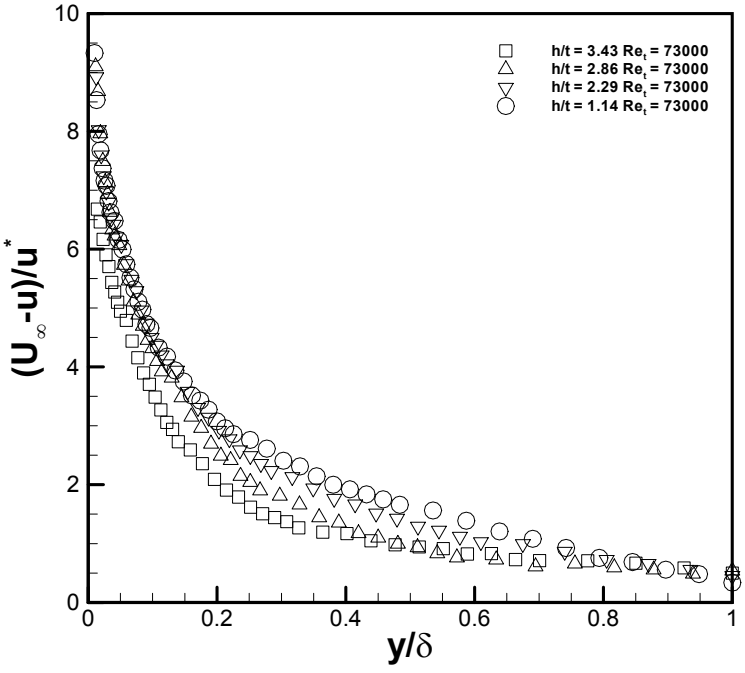

Figure B.7 Defect profile, $Re_t = 73{,}000$ – tripped boundary layer

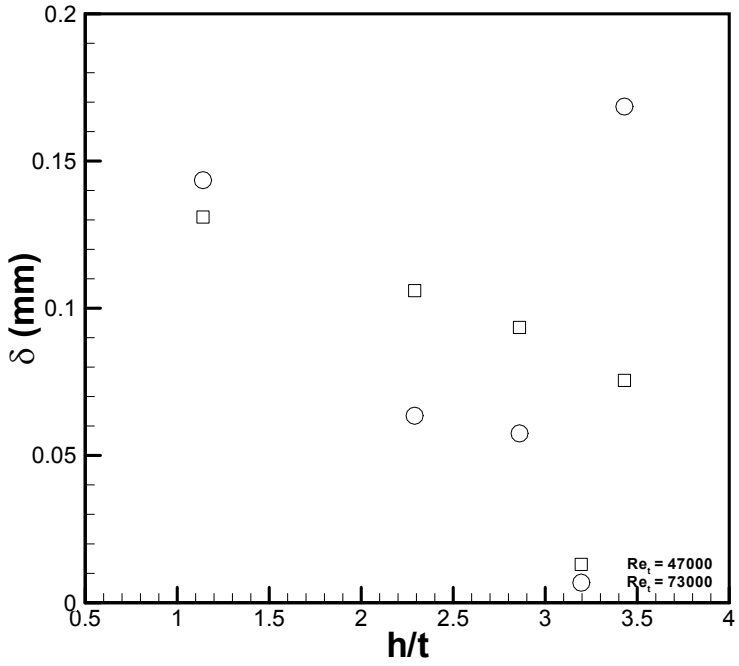

Figure B.8 Laminar boundary layer thickness, Re_t = 47,000, 73,000

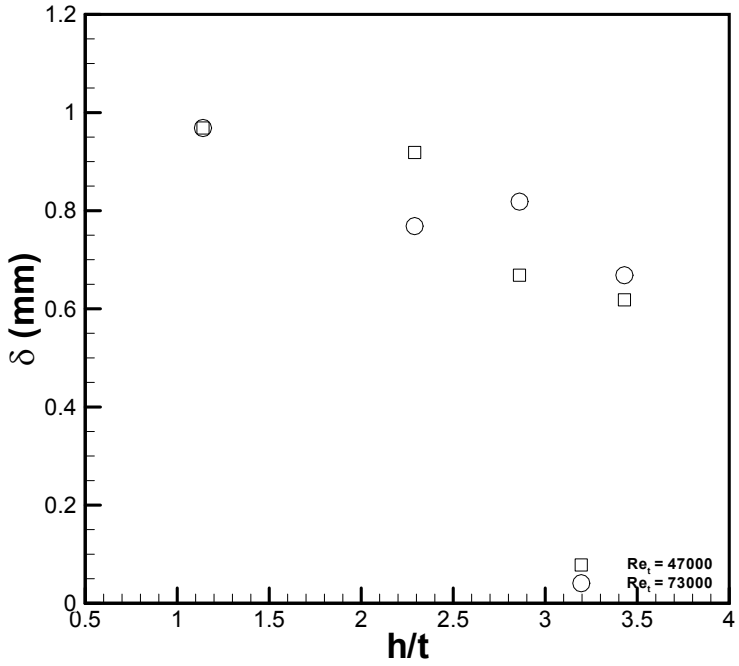

Figure B.9 Tripped boundary layer thickness, Re_t = 47,000, 73,000

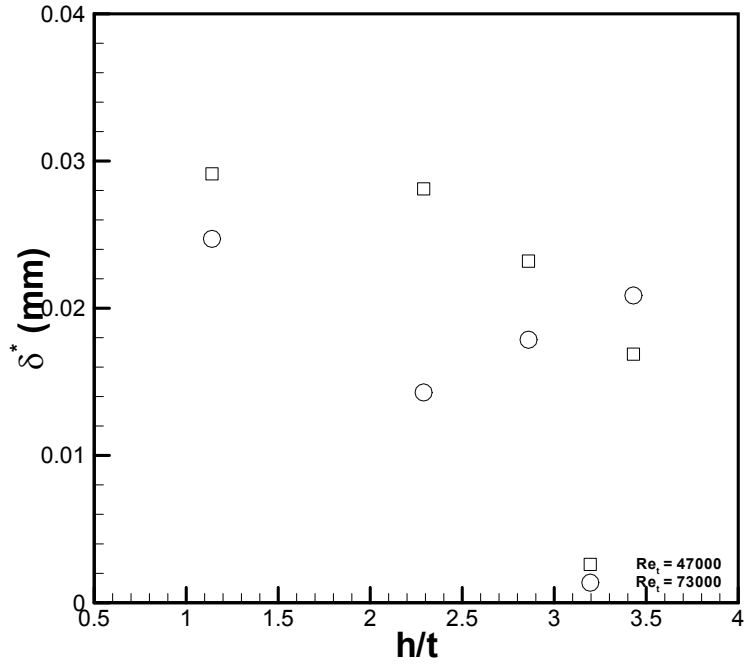

Figure B.10 Laminar displacement thickness, Re_t = 47,000, 73,000

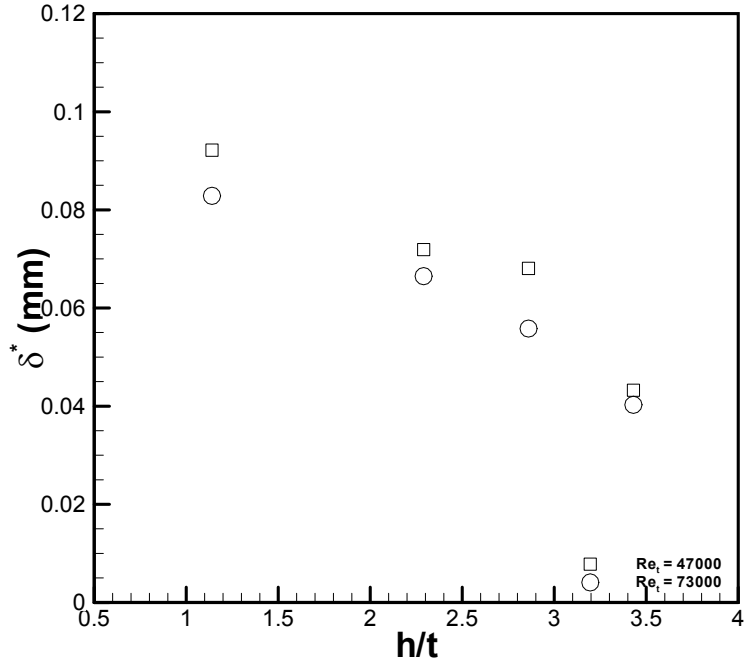

Figure B.11 Tripped displacement thickness, Re_t = 47,000, 73,000

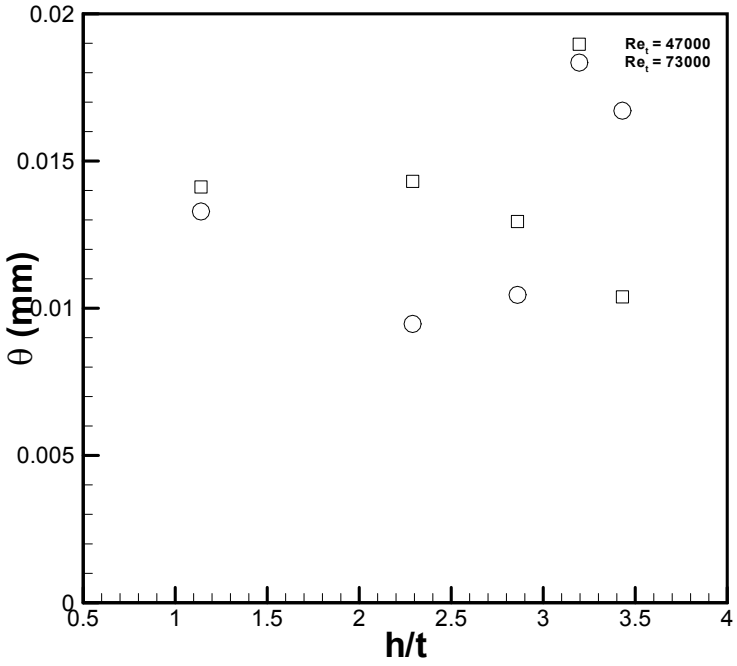

Figure B.12 Laminar momentum thickness, Re_t = 47,000, 73,000

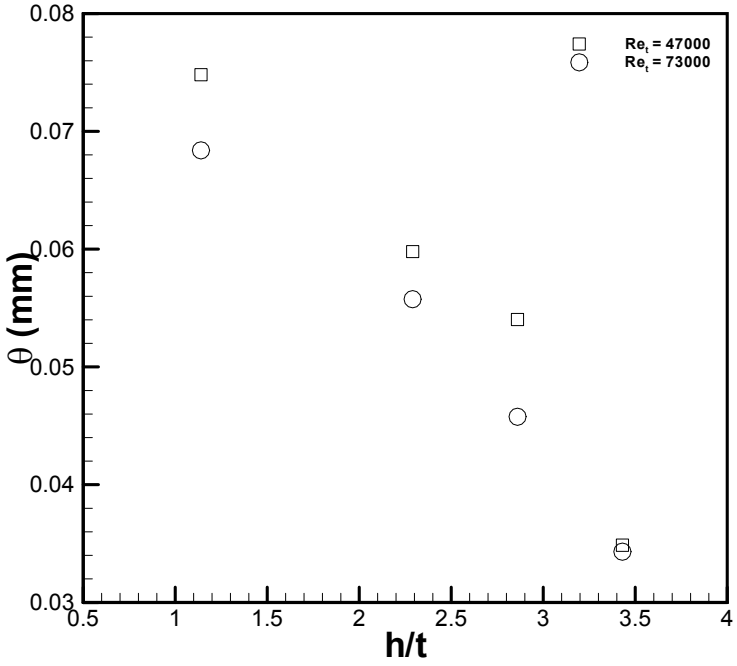

Figure B.13 Tripped momentum thickness, Re_t = 47,000, 73,000

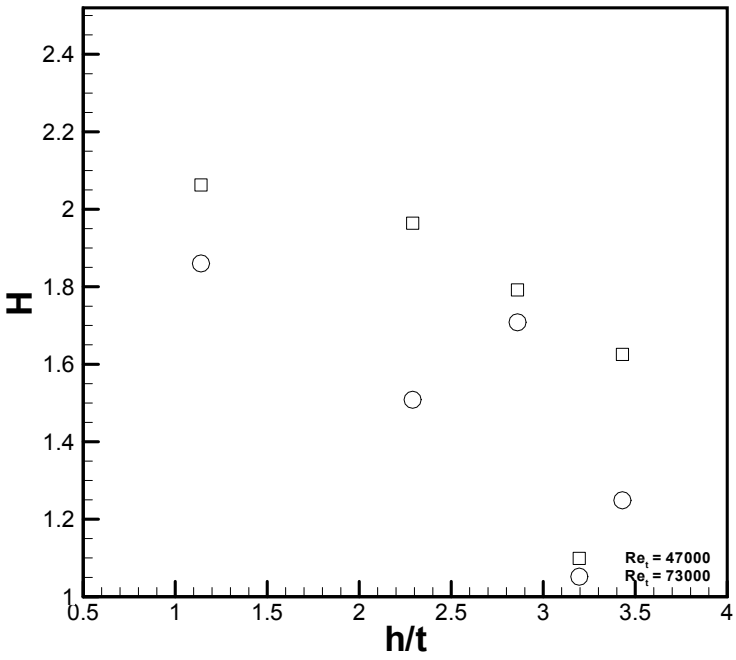

Figure B.14 Laminar shape factor, $Re_t = 47{,}000, 73{,}000$

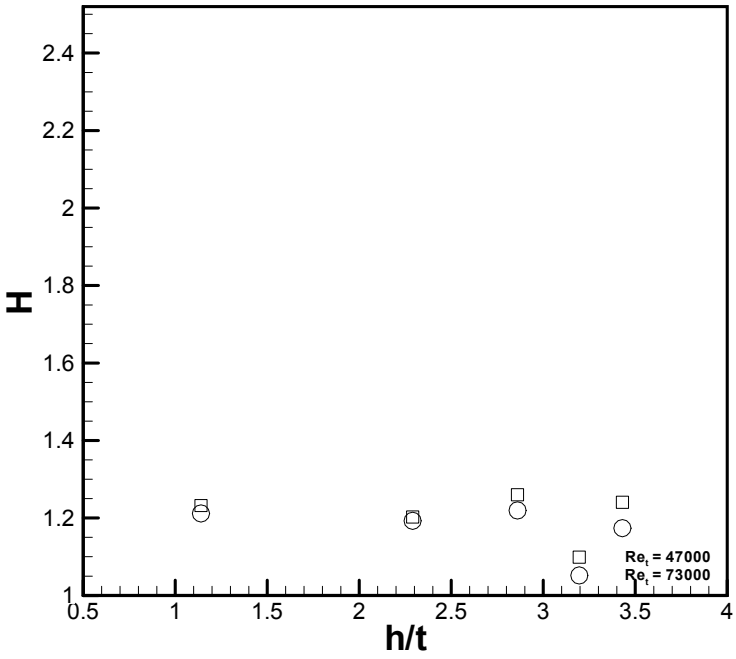

Figure B.15 Tripped shape factor, $Re_t = 47{,}000, 73{,}000$

B.2 Surface Pressure Distribution, Hump Only

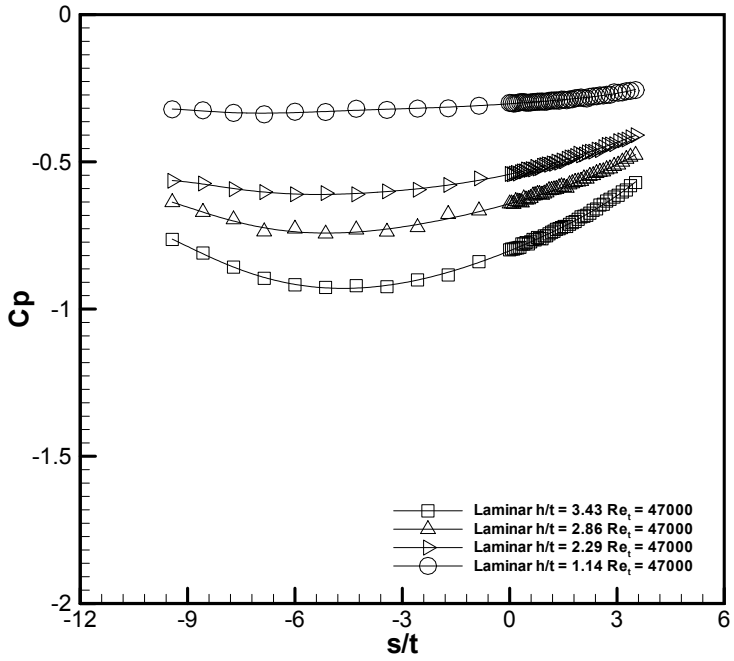

Figure B.16 Surface pressure distribution, hump only, Re_t = 47,000 – laminar boundary layer

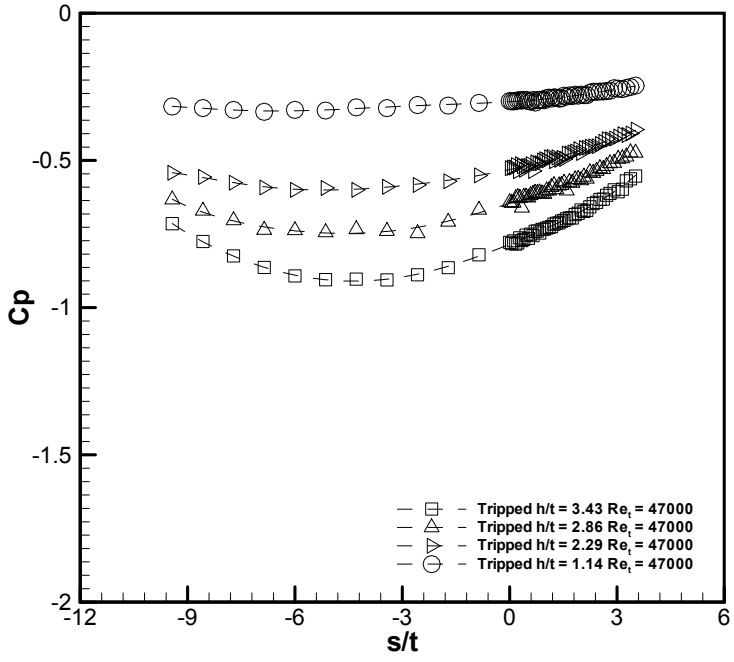

Figure B.17 Surface pressure distribution, hump only, Re_t = 47,000 – tripped boundary layer

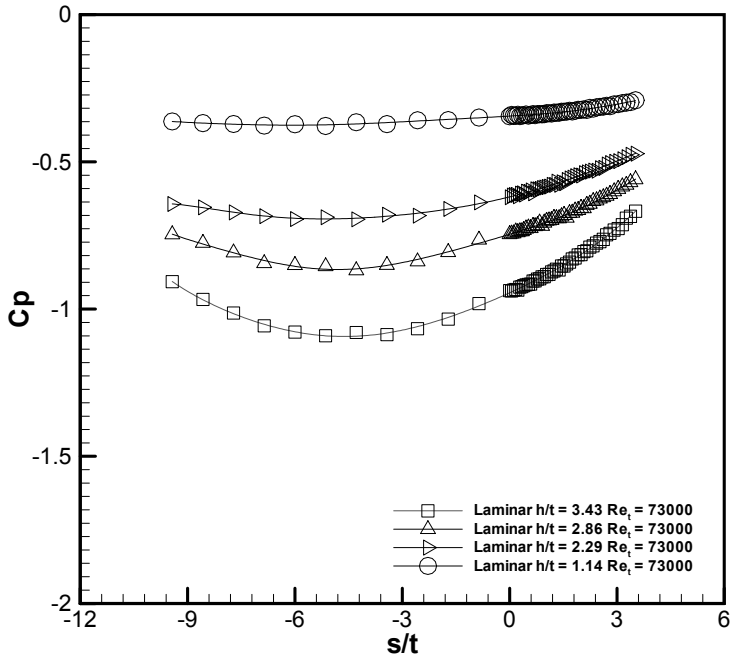

Figure B.18 Surface pressure distribution, hump only, Re_t = 73,000 – laminar boundary layer

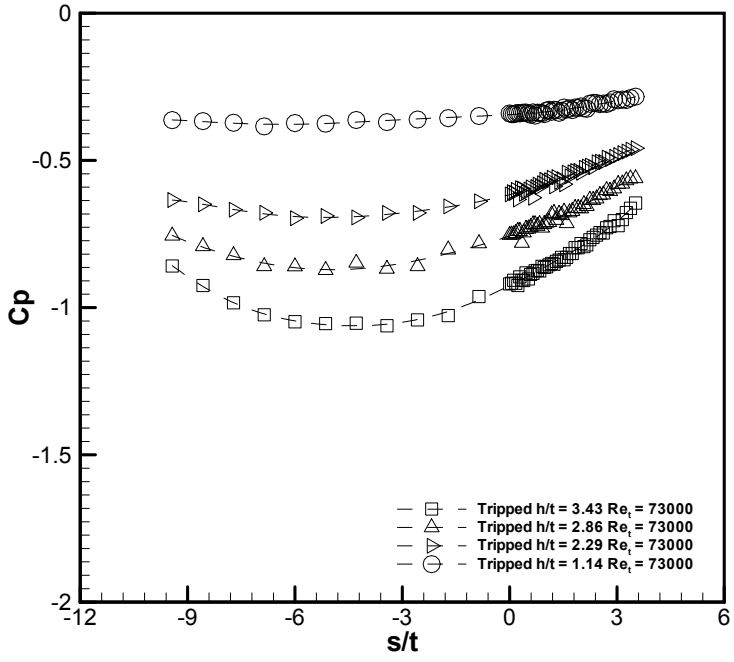

Figure B.19 Surface pressure distribution, hump only, Re_t = 73,000 – tripped boundary layer

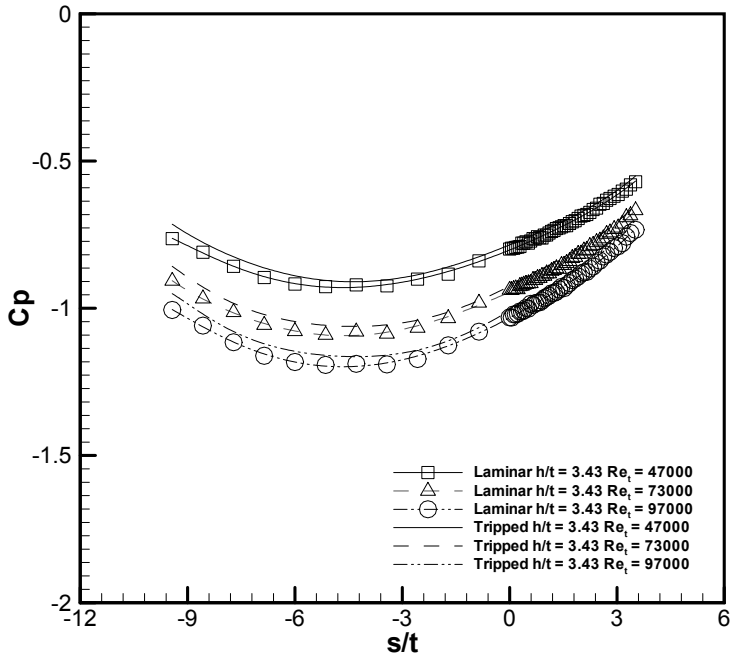

Figure B.20 Surface pressure distribution, hump only, *h/t* = 3.43

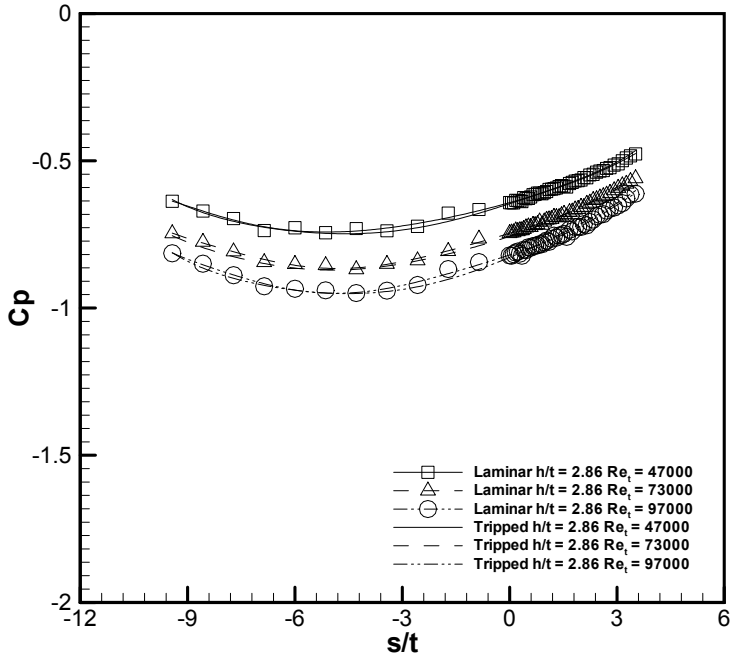

Figure B.21 Surface pressure distribution, hump only, *h/t* = 2.86

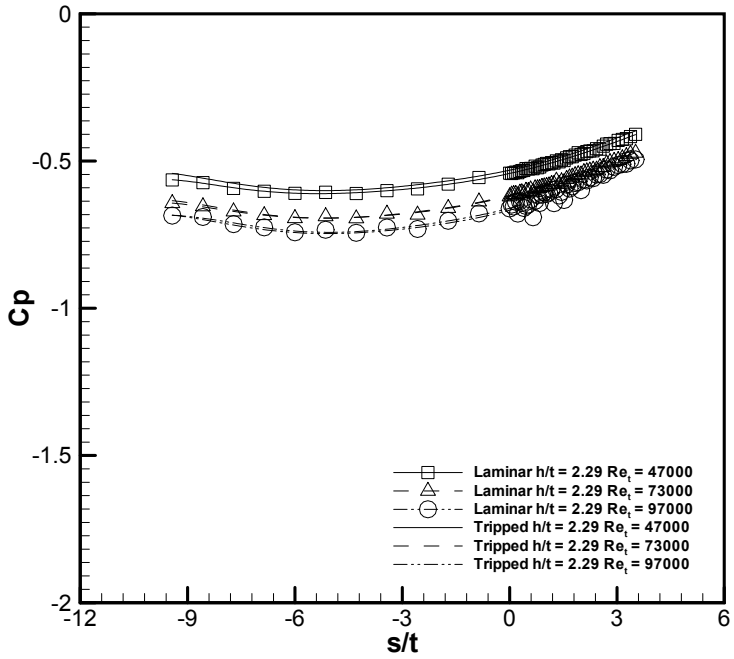

Figure B.22 Surface pressure distribution, hump only, *h/t* = 2.29

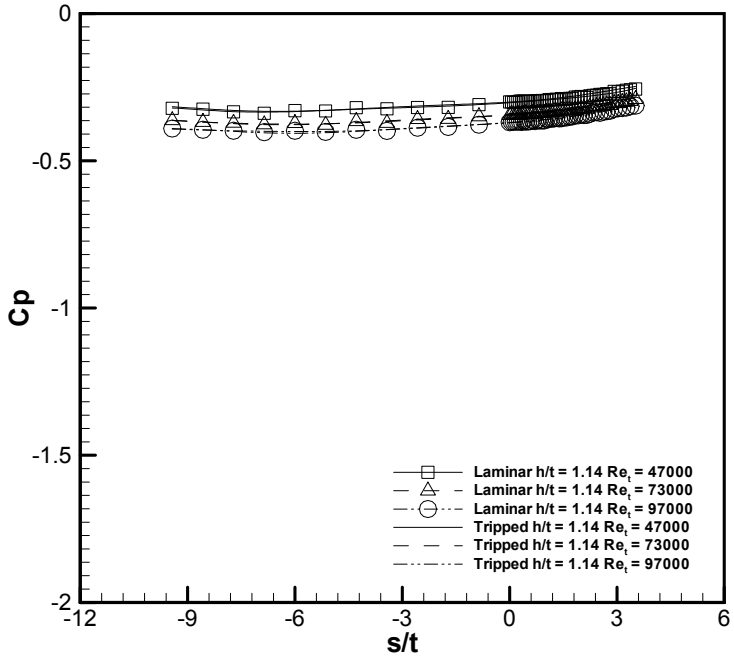

Figure B.23 Surface pressure distribution, hump only, *h/t* = 1.14

B.3 Surface Pressure Distribution, Juncture Vortex and Hump

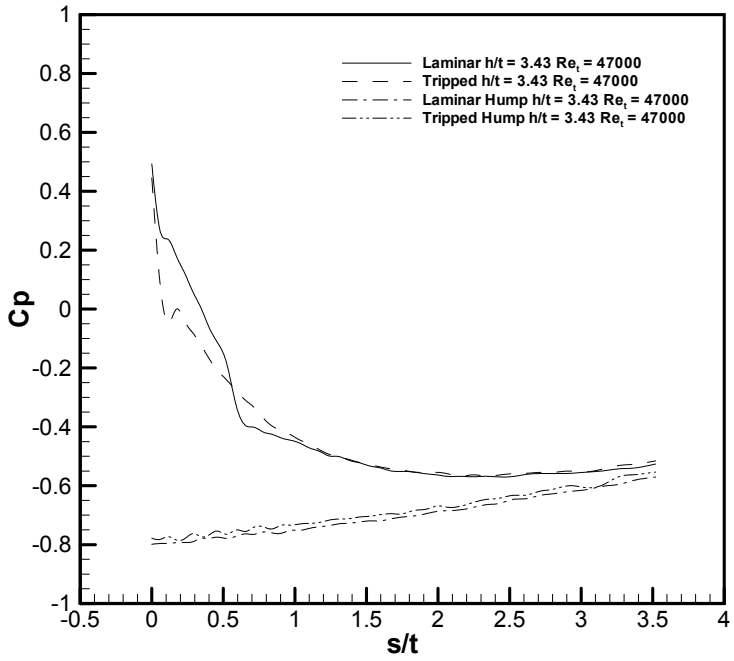

Figure B.24 Surface pressure distribution, juncture vortex and hump, h/t = 3.43, Re_t = 47,000

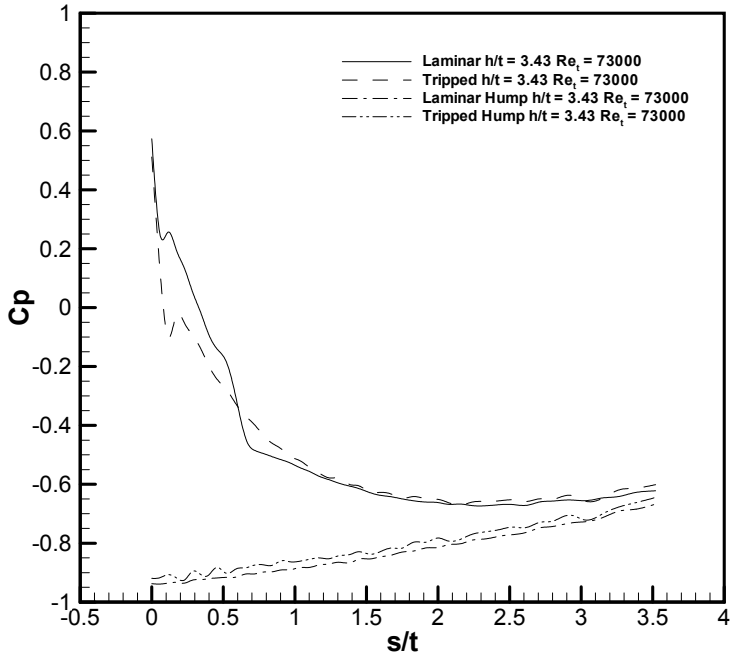

Figure B.25 Surface pressure distribution, juncture vortex and hump, h/t = 3.43 Re_t = 73,000

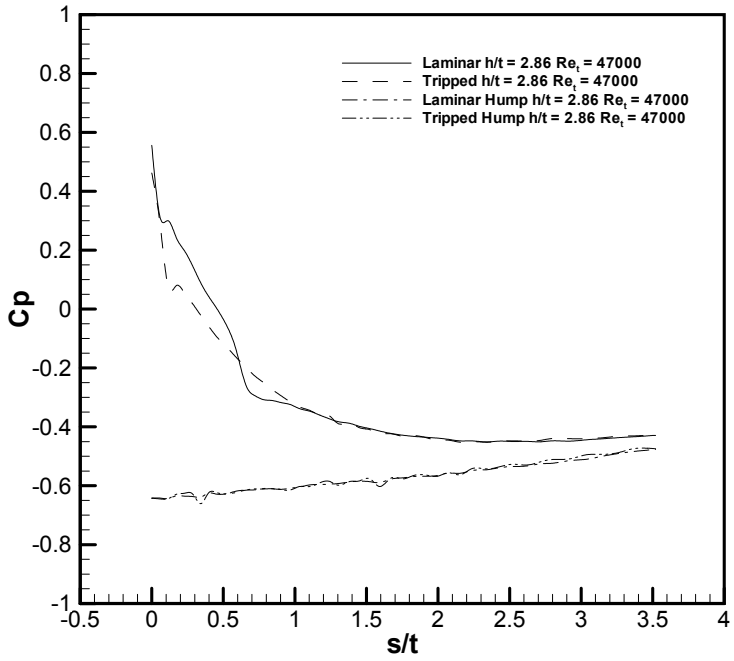

Figure B.26 Surface pressure distribution, juncture vortex and hump, $h/t = 2.86$ $Re_t =$ 47,000

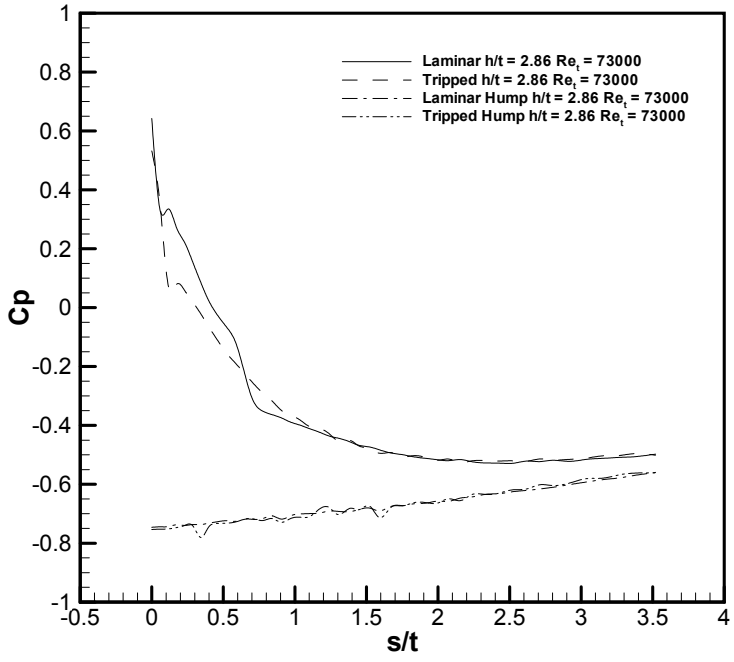

Figure B.27 Surface pressure distribution, juncture vortex and hump, $h/t = 2.86$ $Re_t =$ 73,000

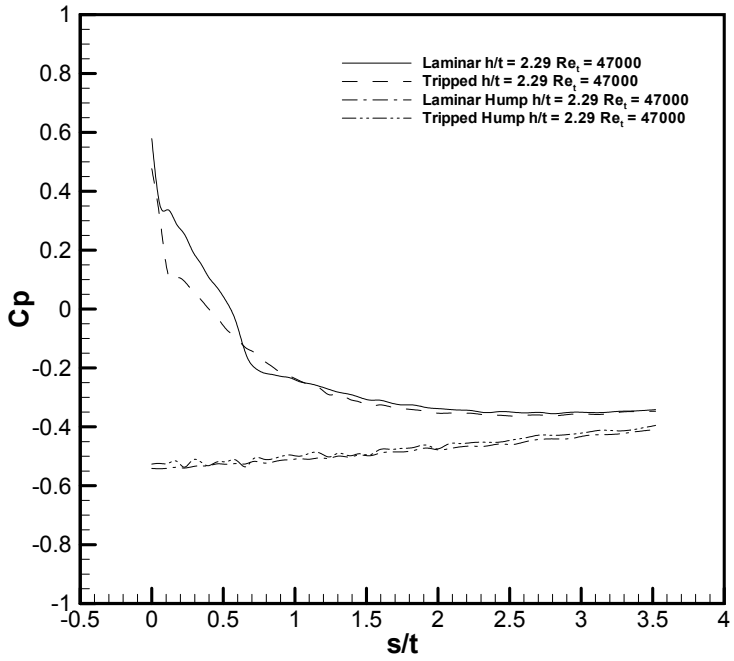

Figure B.28 Surface pressure distribution, juncture vortex and hump, $h/t = 2.29$ $Re_t =$ 47,000

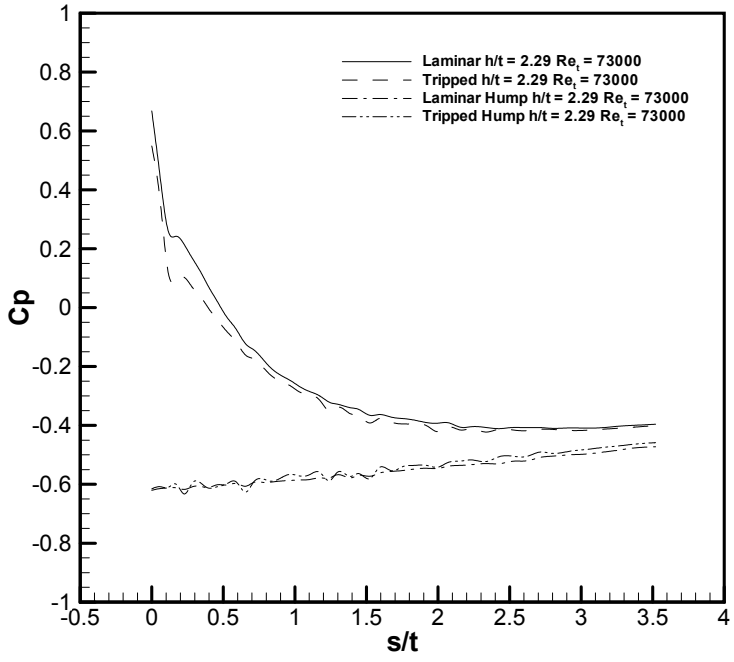

Figure B.29 Surface pressure distribution, juncture vortex and hump, $h/t = 2.29$ $Re_t =$ 73,000

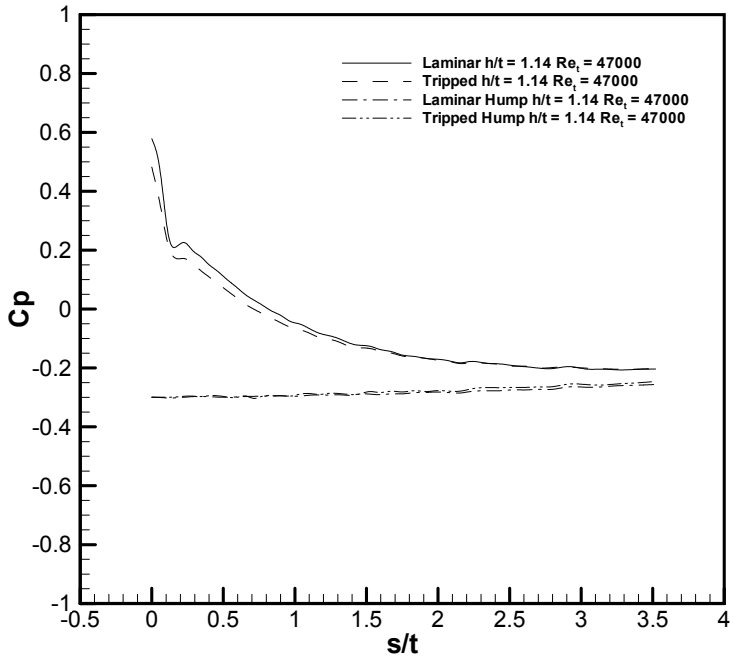

Figure B.30 Surface pressure distribution, juncture vortex and hump, $h/t = 1.14$ $Re_t =$ 47,000

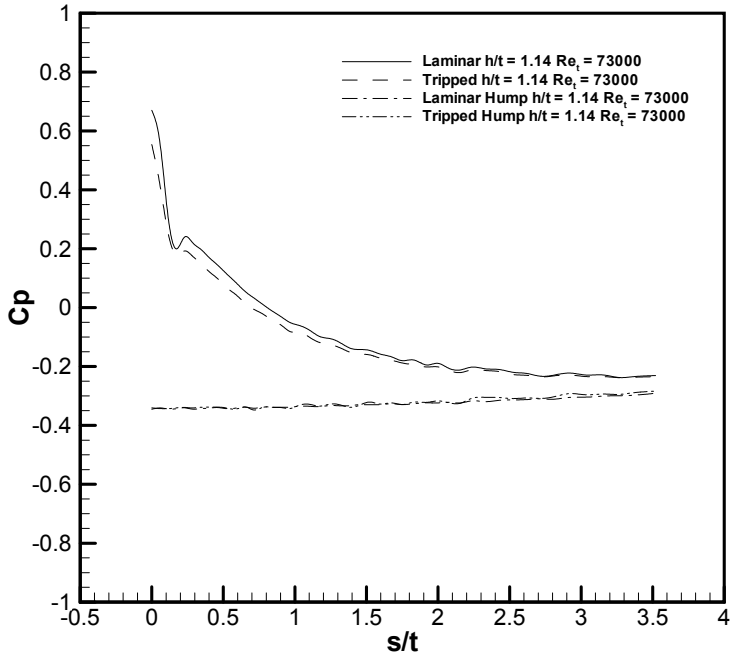

Figure B.31 Surface pressure distribution, juncture vortex and hump, $h/t = 1.14$ $Re_t =$ 73,000

B.4 Surface Pressure Distribution, Juncture Vortex

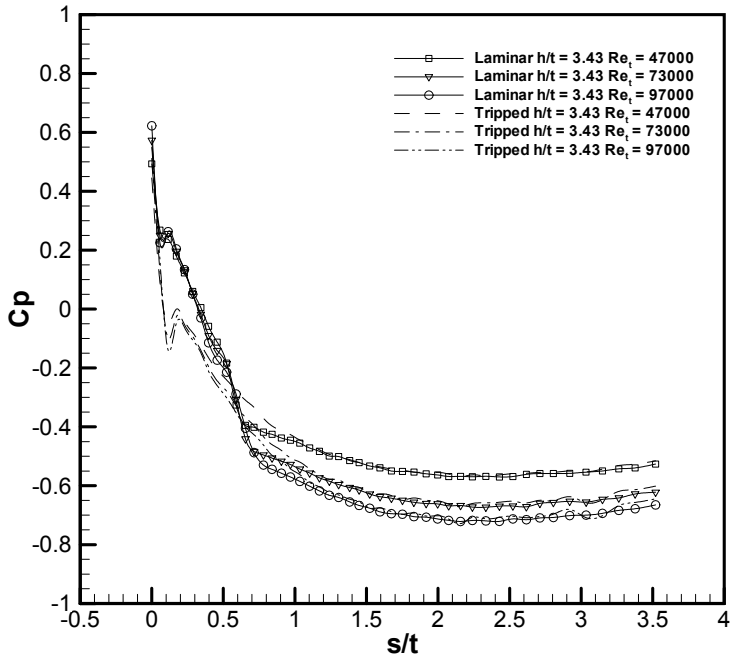

Figure B.32 Surface pressure distribution, juncture vortex, *h/t* = 3.43

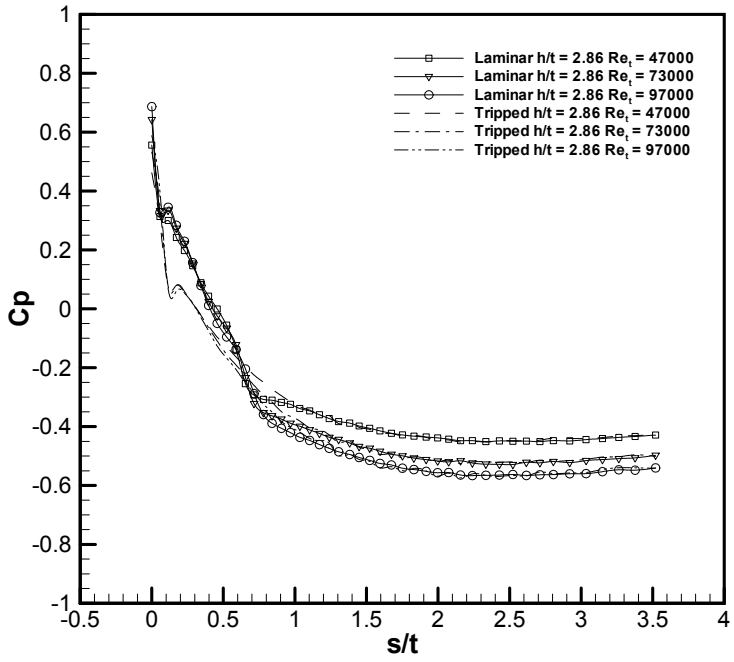

Figure B.33 Surface pressure distribution, juncture vortex, *h/t* = 2.86

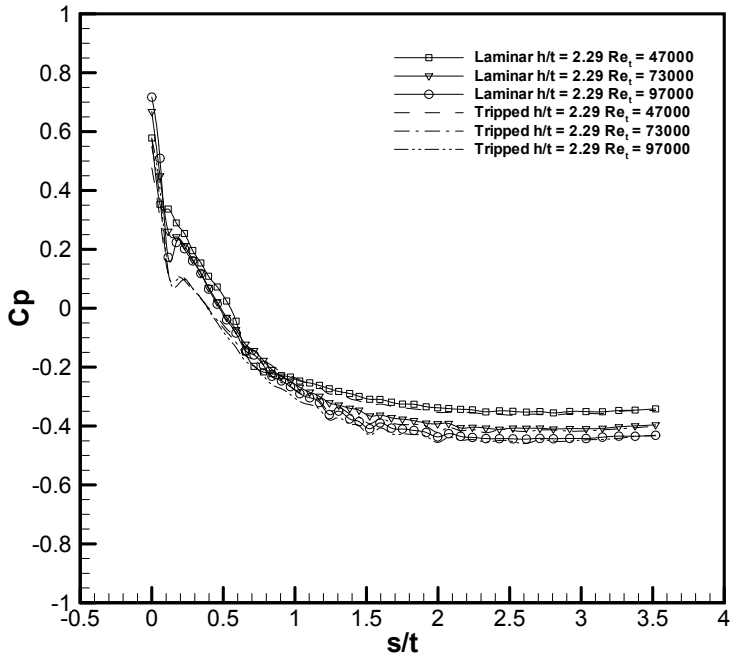

Figure B.34 Surface pressure distribution, juncture vortex, *h/t* = 2.29

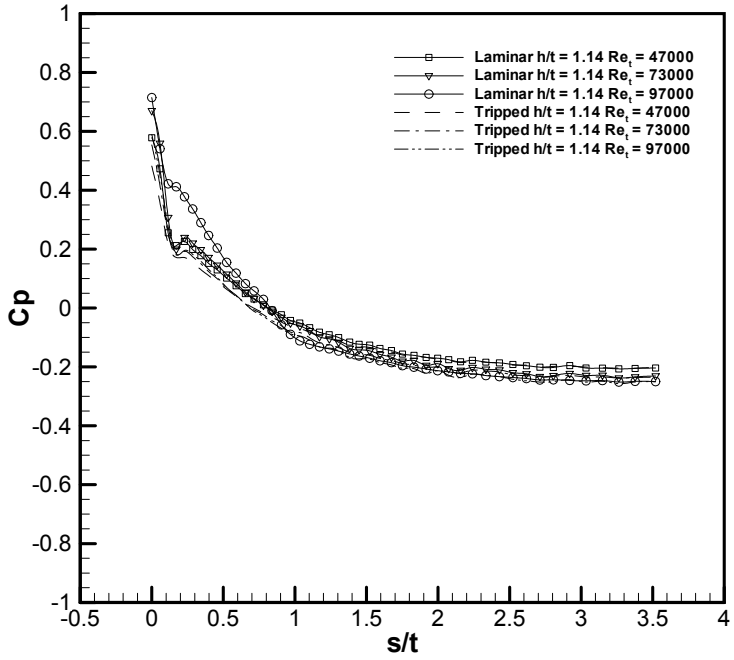

Figure B.35 Surface pressure distribution, juncture vortex, *h/t* = 1.14

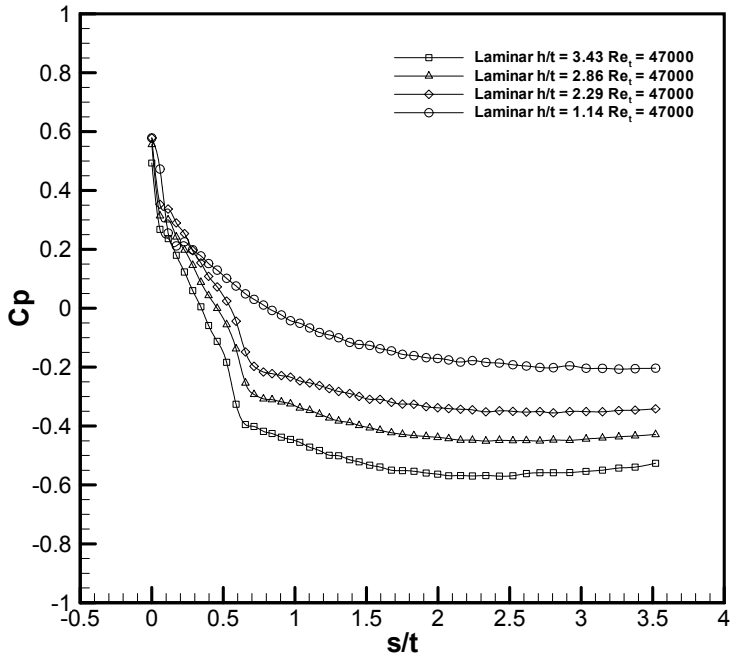

Figure B.36 Surface pressure distribution, juncture vortex, Re_t = 47,000 – laminar boundary layer

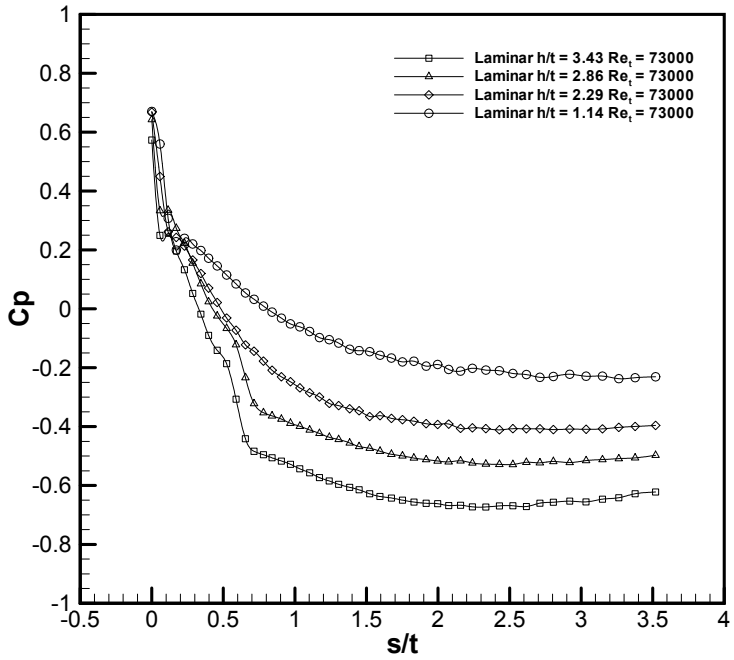

Figure B.37 Surface pressure distribution, juncture vortex, Re_t = 73,000 – laminar boundary layer

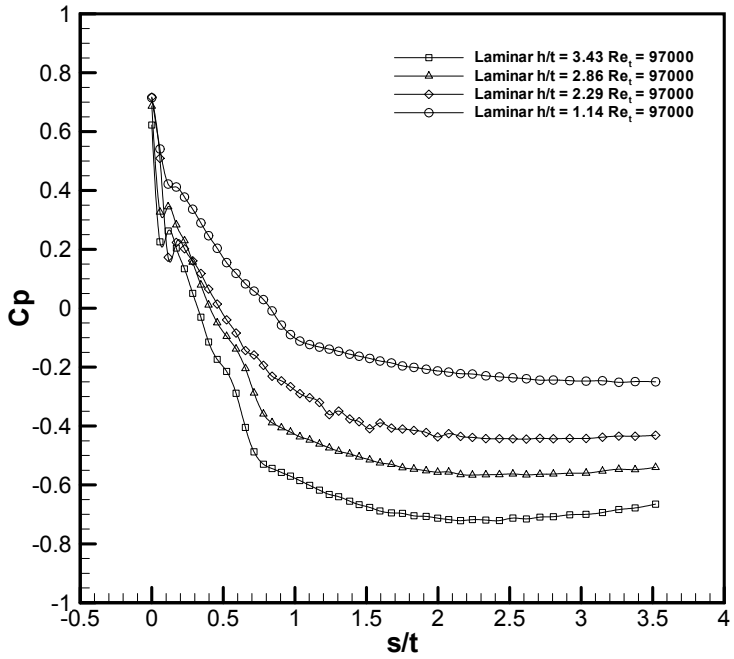

Figure B.38 Surface pressure distribution, juncture vortex, Re_t = 97,000 – laminar boundary layer

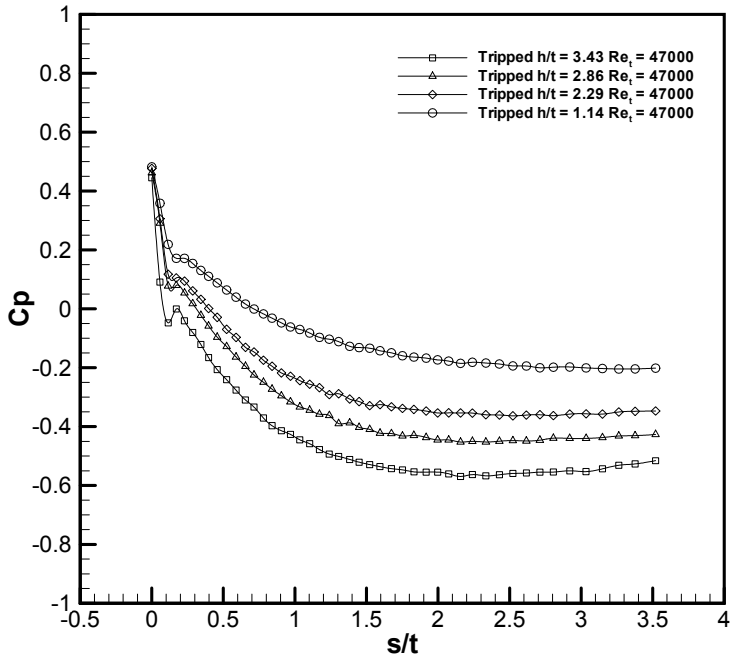

Figure B.39 Surface pressure distribution, juncture vortex, Re_t = 47,000 – tripped boundary layer

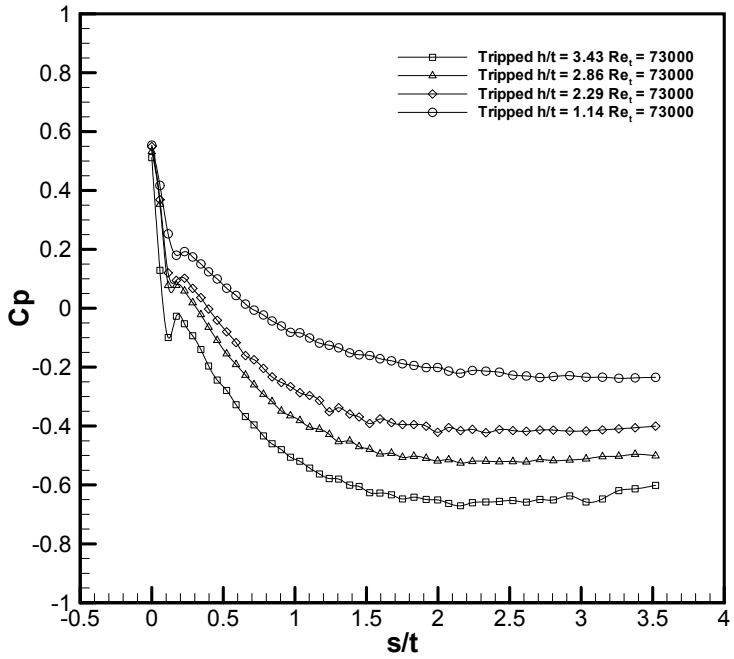

Figure B.40 Surface pressure distribution, juncture vortex, Re_t = 73,000 – tripped boundary layer

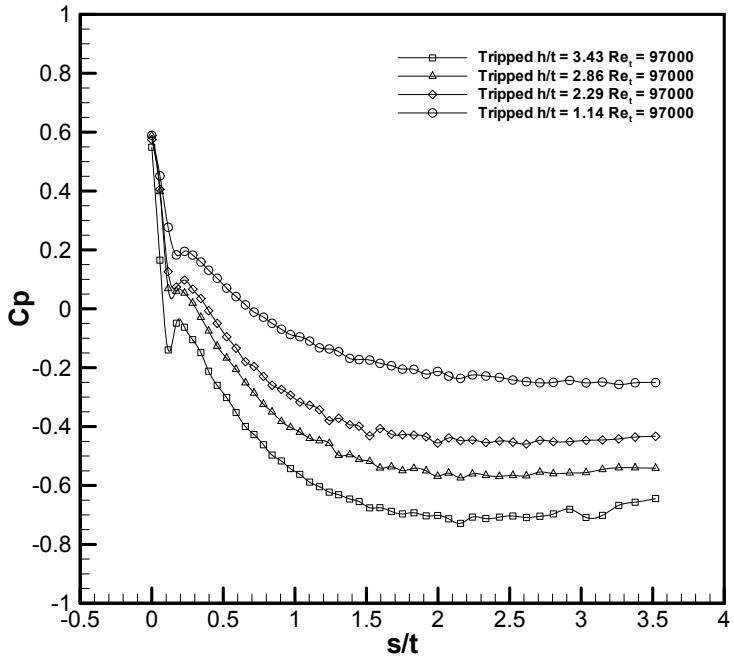

Figure B.41 Surface pressure distribution, juncture vortex, Re_t = 97,000 – tripped boundary layer

Appendix C

Water Tunnel Results

C.1 Laminar Boundary Layer

Table C.1 Laminar boundary layer data for h/t = 3.43, 2.86, 2.29

3.43		**2.86**		**2.29**	
y/δ	**u/U$_\infty$**	**y/δ**	**u/U$_\infty$**	**y/δ**	**u/U$_\infty$**
0.00	0.18	0.00	0.05	0.00	0.02
0.05	0.24	0.05	0.20	0.04	0.09
0.11	0.31	0.10	0.30	0.08	0.23
0.16	0.39	0.15	0.39	0.13	0.31
0.22	0.48	0.20	0.50	0.17	0.39
0.27	0.57	0.25	0.56	0.21	0.46
0.33	0.64	0.29	0.64	0.25	0.55
0.38	0.71	0.34	0.69	0.29	0.61
0.44	0.76	0.39	0.74	0.33	0.66
0.49	0.81	0.44	0.79	0.38	0.71
0.55	0.84	0.49	0.82	0.42	0.75
0.60	0.88	0.54	0.86	0.46	0.79
0.65	0.90	0.59	0.90	0.50	0.82
0.71	0.93	0.64	0.92	0.54	0.86
0.76	0.94	0.69	0.92	0.58	0.87
0.82	0.96	0.74	0.94	0.63	0.89
0.87	0.98	0.79	0.96	0.67	0.91
0.93	0.98	0.83	0.96	0.71	0.93
0.98	0.98	0.88	0.98	0.75	0.95
1.04	1.00	0.93	0.98	0.79	0.95
1.09	1.00	0.98	0.98	0.83	0.95
1.15	1.00	1.03	1.00	0.88	0.97
1.20	1.00	1.08	1.00	0.92	0.98
1.25	1.00	1.13	1.01	0.96	0.98
1.31	1.00	1.18	1.01	1.00	0.99
1.36	1.02	1.23	1.00	1.04	1.00
1.42	1.02	1.28	1.00	1.08	1.01
1.47	1.00	1.33	1.00	1.13	1.00

3.43		2.86		2.29	
y/δ	**u/U_∞**	**y/δ**	**u/U_∞**	**y/δ**	**u/U_∞**
1.53	1.00	1.38	1.00	1.17	1.02
1.58	1.00	1.42	1.00	1.21	1.02
1.64	1.00	1.47	1.01	1.25	1.00
1.69	1.02	1.52	1.01	1.29	1.00
1.74	1.00	1.57	1.00	1.33	1.00
1.80	1.00	1.62	1.00	1.38	1.02
1.85	1.02	1.67	1.00	1.42	1.02
1.91	1.00	1.72	1.00	1.46	1.00
1.96	1.00	1.77	1.00	1.50	1.01
2.02	1.00	1.82	1.00	1.54	1.00
2.07	1.00	1.87	1.00	1.58	1.01
2.13	1.00	1.92	1.01	1.63	1.02
2.18	1.00	1.96	1.01	1.67	1.02
2.24	1.00	2.01	1.00	1.71	1.02
2.29	1.00	2.06	1.00	1.75	1.02
2.34	1.00	2.11	1.01		
2.40	1.00	2.16	1.01		
2.45	1.00	2.21	1.00		
2.51	1.00	2.26	1.00		
2.56	1.00	2.31	1.01		
2.62	0.99	2.36	1.00		
2.67	1.00	2.41	1.00		
2.73	0.99				
2.78	0.99				
2.84	0.99				
2.89	0.99				
2.94	1.00				
3.00	1.00				
3.05	1.00				
3.11	1.00				
3.16	0.99				
3.22	1.00				

Table C.2 Laminar boundary layer data for h/t = 1.14, 0.00

1.14		**0.00**	
y/δ	**u/U$_\infty$**	**y/δ**	**u/U$_\infty$**
0.00	0.03	0.00	0.02
0.03	0.09	0.02	0.04
0.07	0.18	0.05	0.12
0.10	0.24	0.07	0.18
0.14	0.29	0.10	0.23
0.17	0.37	0.12	0.29
0.21	0.43	0.14	0.34
0.24	0.49	0.17	0.38
0.28	0.54	0.19	0.41
0.31	0.60	0.22	0.47
0.34	0.63	0.24	0.51
0.38	0.70	0.26	0.53
0.41	0.73	0.29	0.57
0.45	0.77	0.31	0.61
0.48	0.82	0.34	0.63
0.52	0.83	0.36	0.65
0.55	0.86	0.39	0.69
0.58	0.89	0.41	0.70
0.62	0.91	0.43	0.72
0.65	0.91	0.46	0.75
0.69	0.93	0.48	0.78
0.72	0.94	0.51	0.79
0.76	0.96	0.53	0.81
0.79	0.96	0.55	0.82
0.83	0.96	0.58	0.84
0.86	0.98	0.60	0.85
0.89	0.98	0.63	0.88
0.93	0.98	0.65	0.88
0.96	0.99	0.67	0.88
1.00	0.99	0.70	0.91
1.03	1.00	0.72	0.91
1.07	1.00	0.75	0.94
1.10	1.00	0.77	0.94
1.13	1.00	0.79	0.95
1.17	1.00	0.82	0.95
1.20	1.00	0.84	0.95
1.24	1.00	0.87	0.97
1.27	1.00	0.89	0.97
1.31	1.00	0.92	0.97
1.34	1.00	0.94	0.98
1.38	1.00	0.96	0.98
1.41	1.00	0.99	0.98
1.44	1.01	1.01	1.00

1.14		0.00	
y/δ	**y/δ**	**u/U_∞**	**y/δ**
1.48	1.00	1.04	1.00
1.51	1.00	1.06	1.00
1.55	1.01	1.08	1.00
1.58	1.00	1.11	1.00
1.62	1.00	1.13	1.00
1.65	1.00	1.16	1.00
1.68	1.00	1.18	1.00
1.72	1.00	1.20	1.00
1.75	1.00	1.23	1.00
1.79	1.00	1.25	1.00
1.82	1.00	1.28	1.00
		1.30	1.00
		1.32	1.00
		1.35	1.00
		1.37	1.00
		1.40	1.00
		1.42	1.00
		1.45	1.01

C.2 Tripped Boundary Layer

Table C.3 Tripped boundary layer data for h/t = 3.43, 2.86, 2.29

3.43		2.86		2.29	
u^+	y^+	u^+	y^+	u^+	y^+
2.73	2.80	1.68	1.64	1.78	1.90
4.32	5.07	3.61	4.13	2.80	3.36
5.91	7.80	5.05	6.48	4.07	5.53
7.27	10.89	6.25	8.90	5.34	7.98
8.63	14.20	7.45	11.65	6.86	11.17
9.77	17.50	8.66	14.97	7.88	13.88
10.68	20.69	9.86	18.43	8.90	17.09
11.58	24.50	10.58	21.25	9.66	19.85
12.49	28.25	11.30	24.28	10.68	23.36
12.95	31.18	12.26	28.40	11.44	26.55
13.40	34.24	12.50	30.70	11.95	29.65
13.85	37.84	12.98	33.69	12.71	33.23
14.08	40.53	13.46	36.81	13.22	36.33
14.31	43.29	13.95	40.46	13.47	38.82
14.54	46.11	14.19	43.14	13.73	41.75
14.76	49.43	14.43	45.88	13.98	44.39
14.76	51.60	14.43	47.90	14.24	47.10
14.76	53.77	14.67	51.15	14.24	49.00
14.99	56.80	14.67	53.20	14.49	52.19
14.99	59.44	14.67	55.24	14.49	54.12
14.99	61.64	14.67	57.29	14.74	57.04
14.99	63.84	14.91	60.72	14.74	59.01
14.99	66.04	14.91	62.80	14.74	61.37
14.99	68.68	14.91	64.88	14.74	63.33
14.99	70.88	14.91	66.96	14.74	65.30
14.99	73.09	14.91	69.46	14.74	67.27
14.99	75.29	14.67	70.38	14.74	69.63
14.99	77.93	14.91	73.62	14.74	71.59
14.99	80.13	14.91	75.70	14.74	73.56
14.99	82.33	14.91	78.19	14.74	75.53
14.99	84.53	14.91	80.27	14.74	77.89
14.99	87.17	14.91	82.35	14.74	79.86
14.99	89.38	14.67	83.07	14.74	81.82
14.99	91.58	14.67	85.52	14.74	83.79
14.99	93.78	14.91	89.00	14.74	86.15
14.99	96.42	14.67	89.61	14.74	88.12
14.99	98.62	14.67	91.66	14.74	90.08
14.99	100.82	14.91	95.66	14.74	92.05
14.99	103.02	14.91	97.74	14.74	94.41
14.99	105.67	14.91	99.82	14.74	96.38
14.99	107.87	14.67	100.25	14.74	98.34

3.43		2.86		2.29	
u^+	y^+	u^+	y^+	u^+	y^+
14.99	110.07	14.67	102.71	14.74	100.31
14.99	112.27	14.67	104.76	14.74	102.67
14.99	114.91	14.67	106.80	14.74	104.64
14.99	117.11	14.67	108.85	14.74	106.60
14.99	119.31	14.67	111.30	14.74	108.57
14.76	119.67	14.67	113.35	14.74	110.93
14.76	121.84	14.67	115.39	14.74	112.90
14.76	124.44	14.67	117.44	14.74	114.87
14.76	126.61	14.67	119.49	14.74	116.83
14.76	128.78	14.67	121.94	14.74	118.80
14.76	130.95	14.67	123.99	14.74	121.16
14.76	133.55	14.67	126.03	14.74	123.13
14.76	135.72	14.67	128.08	14.74	125.09
14.76	137.89	14.67	130.53	14.74	127.06
14.76	140.05	14.67	132.58	14.74	129.42
		14.67	134.63	14.74	131.39
		14.67	136.67	14.74	133.35
				14.74	135.32

Table C.4 Tripped boundary layer data for h/t = 1.14, 0.00

1.14		0.00	
u^+	y^+	u^+	y^+
0.95	1.00	1.40	1.27
2.23	2.55	2.44	2.45
3.50	4.36	4.19	4.58
4.46	5.98	5.59	6.62
5.73	8.37	6.98	9.04
6.68	10.43	7.68	10.64
7.64	12.67	9.08	13.40
8.91	15.66	9.78	15.32
9.55	17.91	10.13	16.98
10.18	20.11	10.82	19.14
11.14	23.10	11.17	20.77
11.46	24.89	11.87	23.15
12.09	27.70	11.87	24.45
12.41	29.66	11.87	25.53
12.73	31.68	12.22	27.40
13.05	33.76	12.57	29.33
13.37	36.16	12.92	31.55
13.37	37.48	13.27	33.61
13.68	39.73	13.27	34.82
13.68	41.08	13.62	36.98
14.00	43.69	13.62	38.47
14.32	46.10	13.62	39.71
14.32	47.51	13.97	42.00
14.32	48.93	13.97	43.27
14.64	51.75	14.32	45.92
14.64	53.20	14.32	47.23
14.64	54.64	14.32	48.53
14.96	57.31	14.67	51.05
14.96	59.08	14.67	52.66
14.96	60.56	14.67	53.99
14.96	62.03	14.67	55.33
15.27	64.86	15.02	58.01
15.27	66.67	15.02	59.66
15.27	68.18	15.02	61.02
15.27	69.69	15.02	62.39
15.27	71.20	15.36	65.24
15.27	73.01	15.02	65.40
15.59	76.07	15.36	68.32
15.59	77.61	15.36	69.72
15.59	79.15	15.36	71.12
15.59	80.99	15.36	72.80
15.59	82.53	15.36	74.20
15.59	84.07	15.36	75.60

1.14		0.00	
u^+	y^+	u^+	y^+
15.59	85.61	15.71	78.75
15.91	89.25	15.71	80.47
15.91	90.82	15.71	81.90
15.91	92.39	15.71	83.34
15.91	93.96	15.71	84.77
15.91	95.84	15.71	86.49
15.91	97.42	15.71	87.92
15.91	98.99	16.06	91.34
15.91	100.56	16.06	92.80
15.91	102.13	15.71	92.21
15.91	104.02	15.71	93.93
15.91	105.59	15.71	95.36
15.91	107.16	16.06	98.95
15.91	108.73	16.06	100.41
15.91	110.61	16.06	102.17
15.91	112.19	16.06	103.63
15.91	113.76	15.71	102.81
15.91	115.33	15.71	104.24

C.3 Defect Profile

Table C.5 Defect profile for h/t = 3.43, 2.86, 2.29

3.43		2.86		2.29	
y/δ	**$(U_\infty-u)/u^*$**	**y/δ**	**$(U_\infty-u)/u^*$**	**y/δ**	**$(U_\infty-u)/u^*$**
0.00	12.27	0.00	13.22	0.00	12.96
0.06	10.68	0.06	11.30	0.05	11.95
0.11	9.09	0.10	9.86	0.11	10.68
0.18	7.72	0.15	8.66	0.16	9.41
0.23	6.36	0.20	7.45	0.21	7.88
0.29	5.22	0.25	6.25	0.25	6.86
0.34	4.32	0.30	5.05	0.31	5.85
0.41	3.41	0.34	4.33	0.36	5.08
0.46	2.50	0.39	3.61	0.41	4.07
0.52	2.04	0.45	2.64	0.46	3.30
0.57	1.59	0.49	2.40	0.52	2.80
0.64	1.14	0.54	1.92	0.57	2.03
0.69	0.91	0.59	1.44	0.62	1.53
0.75	0.68	0.64	0.96	0.67	1.27
0.80	0.45	0.69	0.72	0.72	1.02
0.87	0.23	0.74	0.48	0.77	0.76
0.93	0.23	0.78	0.48	0.82	0.51
0.98	0.23	0.84	0.24	0.87	0.51
1.04	0.00	0.89	0.24	0.93	0.25
1.10	0.00	0.93	0.24	0.98	0.25
1.16	0.00	0.98	0.24	1.03	0.00
1.21	0.00	1.03	0.00	1.08	0.00
1.27	0.00	1.08	0.00	1.14	0.00
1.33	0.00	1.13	0.00	1.19	0.00
1.39	0.00	1.17	0.00	1.23	0.00
1.44	0.00	1.23	0.00	1.28	0.00
1.50	0.00	1.28	0.24	1.34	0.00
1.57	0.00	1.32	0.00	1.39	0.00
1.62	0.00	1.37	0.00	1.44	0.00
1.68	0.00	1.43	0.00	1.49	0.00
1.73	0.00	1.47	0.00	1.55	0.00
1.80	0.00	1.52	0.00	1.60	0.00
1.85	0.00	1.57	0.24	1.65	0.00
1.91	0.00	1.62	0.24	1.69	0.00
1.96	0.00	1.67	0.00	1.75	0.00
2.03	0.00	1.72	0.24	1.80	0.00
2.08	0.00	1.76	0.24	1.85	0.00
2.14	0.00	1.82	0.00	1.90	0.00
2.19	0.00	1.86	0.00	1.96	0.00
2.26	0.00	1.91	0.00	2.01	0.00
2.32	0.00	1.96	0.24	2.06	0.00

3.43		2.86		2.29	
y/δ	**$(U_\infty-u)/u^*$**	**y/δ**	**$(U_\infty-u)/u^*$**	**y/δ**	**$(U_\infty-u)/u^*$**
2.37	0.00	2.01	0.24	2.11	0.00
2.43	0.00	2.06	0.24	2.16	0.00
2.49	0.00	2.11	0.24	2.21	0.00
2.55	0.00	2.15	0.24	2.26	0.00
2.60	0.00	2.21	0.24	2.31	0.00
2.66	0.23	2.26	0.24	2.37	0.00
2.71	0.23	2.30	0.24	2.42	0.00
2.78	0.23	2.35	0.24	2.47	0.00
2.83	0.23	2.40	0.24	2.52	0.00
2.89	0.23	2.45	0.24	2.57	0.00
2.94	0.23	2.50	0.24	2.62	0.00
3.01	0.23	2.54	0.24	2.67	0.00
3.07	0.23	2.59	0.24	2.72	0.00
3.12	0.23	2.65	0.24	2.77	0.00
3.18	0.23	2.69	0.24	2.83	0.00

Table C.6 Defect profile for h/t = 1.14, 0.00

1.14		0.00	
y/δ	**$(U_\infty-u)/u^*$**	**y/δ**	**$(U_\infty-u)/u^*$**
0.00	14.96	0.00	14.32
0.02	13.68	0.02	13.27
0.04	12.41	0.04	11.52
0.07	11.46	0.07	10.13
0.09	10.18	0.09	8.73
0.11	9.23	0.12	8.03
0.14	8.27	0.14	6.63
0.16	7.00	0.16	5.94
0.18	6.36	0.19	5.59
0.21	5.73	0.21	4.89
0.23	4.77	0.23	4.54
0.25	4.46	0.25	3.84
0.28	3.82	0.28	3.84
0.30	3.50	0.30	3.84
0.32	3.18	0.32	3.49
0.34	2.86	0.35	3.14
0.37	2.55	0.37	2.79
0.39	2.55	0.40	2.44
0.41	2.23	0.42	2.44
0.43	2.23	0.44	2.10
0.46	1.91	0.47	2.10
0.48	1.59	0.49	2.10
0.50	1.59	0.51	1.75
0.53	1.59	0.53	1.75
0.55	1.27	0.56	1.40
0.57	1.27	0.58	1.40
0.60	1.27	0.60	1.40
0.62	0.95	0.63	1.05
0.64	0.95	0.65	1.05
0.67	0.95	0.68	1.05
0.69	0.95	0.70	1.05
0.71	0.64	0.72	0.70
0.74	0.64	0.75	0.70
0.76	0.64	0.77	0.70
0.78	0.64	0.79	0.70
0.80	0.64	0.81	0.35
0.83	0.64	0.84	0.70
0.85	0.32	0.86	0.35
0.87	0.32	0.88	0.35
0.89	0.32	0.91	0.35
0.92	0.32	0.93	0.35
0.94	0.32	0.96	0.35
0.96	0.32	0.98	0.35

1.14		0.00	
y/δ	**$(U_\infty-u)/u^*$**	**y/δ**	**$(U_\infty-u)/u^*$**
0.99	0.32	1.00	0.00
1.01	0.00	1.03	0.00
1.04	0.00	1.05	0.00
1.06	0.00	1.07	0.00
1.08	0.00	1.09	0.00
1.11	0.00	1.12	0.00
1.13	0.00	1.14	0.00
1.15	0.00	1.16	-0.35
1.17	0.00	1.19	-0.35
1.19	0.00	1.21	0.00
1.22	0.00	1.24	0.00
1.24	0.00	1.26	0.00
1.26	0.00	1.28	-0.35

Appendix D

Wind Tunnel Results

D.1 Integral Quantities

Table D.1 Integral quantities - laminar boundary layer

	Re_t	h/t = 3.43	h/t = 2.86	h/t = 2.29	h/t = 1.14
δ (mm)	47,000	1.93	2.39	2.69	3.33
	73,000	4.29	1.93	1.93	2.69
δ* (mm)	47,000	0.43	0.58	0.71	0.74
	73,000	0.53	0.46	0.36	0.64
θ (mm)	47,000	0.26	0.33	0.36	0.36
	73,000	0.42	0.27	0.24	0.34
H	47,000	1.63	1.79	1.96	2.06
	73,000	1.25	1.71	1.51	1.86
Re_{δ^*}	47,000	586.30	747.84	859.42	809.50
	73,000	1,101.29	888.34	657.77	1,068.14
Re_{θ}	47,000	358.68	419.44	438.92	393.58
	73,000	875.79	518.20	446.34	568.25

Table D.2 Integral quantities – tripped boundary layer

	Re_t	h/t = 3.43	h/t = 2.86	h/t = 2.29	h/t = 1.14
δ (mm)	47,000	15.72	16.99	23.34	24.61
	73,000	16.99	20.80	19.53	24.61
δ* (mm)	47,000	1.09	1.73	1.83	2.34
	73,000	1.02	1.42	1.68	2.11
θ (mm)	47,000	0.89	1.37	1.52	1.90
	73,000	0.87	1.16	1.41	1.74
H	47,000	1.24	1.26	1.20	1.23
	73,000	1.17	1.22	1.19	1.21
Re_{δ^*}	47,000	1,475.72	2,200.54	2,217.74	2,564.72
	73,000	2,093.43	2,763.53	3,105.08	3,539.27
Re_{θ}	47,000	1,197.74	1,747.49	1,841.95	2,085.23
	73,000	1,795.12	2,260.17	2,620.50	2,916.70

D.2 Laminar Boundary Layer

Table D.3 Laminar boundary layer data for $h/t = 3.43$

Re_t = 47,000		Re_t = 73,000		Re_t = 97,000	
y/δ	**u/U$_\infty$**	**y/δ**	**u/U$_\infty$**	**y/δ**	**u/U$_\infty$**
0.00	0.00	0.00	0.00	0.00	0.00
0.13	0.42	0.06	0.68	0.06	0.67
0.17	0.49	0.07	0.70	0.07	0.69
0.21	0.55	0.09	0.71	0.09	0.71
0.25	0.60	0.11	0.73	0.11	0.72
0.28	0.65	0.13	0.74	0.13	0.73
0.32	0.70	0.15	0.75	0.15	0.74
0.36	0.74	0.16	0.76	0.16	0.75
0.40	0.77	0.18	0.77	0.18	0.76
0.44	0.80	0.20	0.78	0.20	0.77
0.52	0.84	0.23	0.78	0.23	0.78
0.60	0.89	0.27	0.80	0.27	0.80
0.68	0.92	0.31	0.82	0.31	0.81
0.76	0.95	0.34	0.83	0.34	0.83
0.84	0.97	0.38	0.85	0.38	0.84
0.92	0.98	0.41	0.86	0.41	0.85
1.00	0.99	0.45	0.88	0.45	0.87
1.08	0.99	0.48	0.89	0.48	0.88
1.16	0.99	0.52	0.90	0.52	0.89
1.24	1.00	0.55	0.91	0.55	0.90
1.40	1.00	0.63	0.92	0.63	0.91
1.57	1.00	0.70	0.94	0.70	0.93
1.74	1.00	0.78	0.96	0.78	0.95
1.90	1.00	0.85	0.97	0.85	0.97
2.07	1.00	0.93	0.99	0.93	0.98
2.23	1.00	1.00	0.99	1.00	0.99

Table D.4 Laminar boundary layer data for h/t = 2.86

Re_t = 47,000		Re_t = 73,000		Re_t = 97,000	
y/δ	**u/U$_\infty$**	**y/δ**	**u/U$_\infty$**	**y/δ**	**u/U$_\infty$**
0.00	0.00	0.00	0.00	0.00	0.00
0.10	0.30	0.13	0.40	0.17	0.47
0.13	0.37	0.17	0.42	0.22	0.49
0.17	0.44	0.21	0.50	0.27	0.58
0.20	0.50	0.25	0.56	0.32	0.63
0.23	0.55	0.28	0.61	0.37	0.69
0.26	0.60	0.32	0.67	0.43	0.76
0.29	0.64	0.36	0.71	0.48	0.80
0.33	0.69	0.40	0.76	0.53	0.85
0.36	0.72	0.44	0.79	0.58	0.88
0.42	0.76	0.52	0.82	0.69	0.90
0.49	0.81	0.60	0.88	0.79	0.95
0.55	0.86	0.68	0.93	0.90	0.98
0.61	0.89	0.76	0.95	1.00	0.99
0.68	0.92	0.84	0.97	1.10	0.99
0.74	0.94	0.92	0.98	1.21	1.00
0.81	0.96	1.00	0.99	1.31	1.00
0.87	0.97	1.08	0.99	1.42	1.00
0.94	0.98	1.16	0.99	1.52	1.00
1.00	0.99	1.24	1.00	1.63	1.00

Table D.5 Laminar boundary layer data for h/t = 2.29

Re_t = 47,000		Re_t = 73,000		Re_t = 97,000	
y/δ	**u/U$_\infty$**	**y/δ**	**u/U$_\infty$**	**y/δ**	**u/U$_\infty$**
0	0	0	0	0	0
0.29	0.09	0.13	0.50	0.15	0.51
0.28	0.12	0.17	0.56	0.20	0.56
0.32	0.15	0.21	0.61	0.24	0.61
0.39	0.17	0.25	0.65	0.29	0.66
0.44	0.20	0.28	0.70	0.34	0.71
0.49	0.23	0.32	0.73	0.39	0.75
0.54	0.26	0.36	0.77	0.43	0.78
0.58	0.29	0.40	0.80	0.48	0.82
0.63	0.32	0.44	0.83	0.53	0.86
0.66	0.37	0.52	0.86	0.62	0.89
0.74	0.43	0.60	0.90	0.72	0.93
0.80	0.49	0.68	0.94	0.81	0.96
0.85	0.54	0.76	0.96	0.91	0.98
0.88	0.60	0.84	0.98	1.00	0.99
0.92	0.66	0.92	0.99	1.09	0.99
0.94	0.71	1.00	0.99	1.19	1.00
0.96	0.77	1.08	1.00	1.28	1.00
0.97	0.83	1.16	1.00	1.38	1.00
0.98	0.88	1.24	1.00	1.47	1.00
0.99	1.00	1.40	1.00	1.67	1.00

Table D.6 Laminar boundary layer data for h/t = 1.14

Re_t = 47,000		Re_t = 73,000		Re_t = 97,000	
y/δ	**u/U$_\infty$**	**y/δ**	**u/U$_\infty$**	**y/δ**	**u/U$_\infty$**
0.00	0.00	0.00	0.00	0.00	0.00
0.07	0.20	0.09	0.30	0.07	0.60
0.10	0.27	0.12	0.35	0.09	0.62
0.12	0.34	0.15	0.42	0.11	0.65
0.14	0.40	0.17	0.47	0.13	0.67
0.16	0.44	0.20	0.51	0.15	0.69
0.19	0.50	0.23	0.56	0.17	0.70
0.21	0.55	0.26	0.60	0.19	0.72
0.23	0.59	0.29	0.64	0.21	0.73
0.26	0.62	0.32	0.68	0.23	0.75
0.30	0.67	0.37	0.71	0.28	0.77
0.35	0.74	0.43	0.77	0.32	0.80
0.39	0.79	0.49	0.82	0.36	0.82
0.44	0.84	0.54	0.87	0.40	0.85
0.48	0.89	0.60	0.91	0.44	0.87
0.53	0.92	0.66	0.95	0.48	0.89
0.58	0.95	0.71	0.96	0.53	0.90
0.62	0.96	0.77	0.97	0.57	0.92
0.67	0.97	0.83	0.99	0.61	0.93
0.71	0.98	0.88	0.99	0.65	0.94
0.81	0.98	1.00	0.99	0.74	0.95
0.90	0.99	1.12	1.00	0.83	0.97
1.00	0.99	1.24	1.00	0.91	0.98
1.10	1.00	1.35	1.00	1.00	0.99

D.3 Tripped Boundary Layer

Table D.7 Tripped boundary layer data for $h/t = 3.43$

Re_t = 47,000		Re_t = 73,000		Re_t = 97,000	
u^+	y^+	u^+	y^+	u^+	y^+
0	0	0	0	0	0
11.58	15.28	14.18	23.23	13.77	29.99
12.66	20.11	14.39	30.56	13.80	39.46
13.32	24.94	14.69	37.90	13.83	48.93
13.79	29.76	14.95	45.24	13.79	58.40
14.05	34.59	15.16	52.57	13.81	67.87
14.35	39.42	15.42	59.91	13.82	77.34
14.52	44.24	15.59	67.24	14.17	86.81
14.75	49.07	15.76	74.58	14.85	96.28
14.92	53.90	15.92	81.91	15.20	105.75
15.13	63.55	16.07	96.58	15.48	124.69
15.40	73.20	16.43	111.25	15.96	143.63
15.73	82.86	16.71	125.93	16.41	162.57
15.96	92.51	16.98	140.60	16.78	181.51
16.23	102.16	17.17	155.27	17.18	200.45
16.52	111.81	17.39	169.94	17.46	219.39
16.64	121.47	17.61	184.61	17.72	238.33
16.92	131.12	17.82	199.28	17.99	257.27
17.09	140.77	17.95	213.95	18.22	276.21
17.33	150.43	18.16	228.62	18.46	295.15
17.43	170.54	18.30	259.19	18.68	334.61
17.65	190.65	18.54	289.75	19.06	374.07
17.98	210.76	18.81	320.31	19.35	413.53
18.25	230.87	19.00	350.88	19.62	452.99
18.47	250.98	19.12	381.44	19.81	492.44
18.68	271.09	19.30	412.01	20.02	531.90
18.74	291.20	19.42	442.57	20.19	571.36
18.86	311.31	19.49	473.14	20.29	610.82
18.97	331.42	19.57	503.70	20.45	650.28
19.13	351.53	19.68	534.27	20.49	689.74
19.25	391.75	19.76	595.39	20.62	768.66
19.34	431.97	19.79	656.52	20.72	847.57
19.41	472.19	19.93	717.65	20.80	926.49
19.58	512.41	20.01	778.78	20.87	1,005.41
19.60	552.64	20.05	839.91	20.97	1,084.33
19.69	592.86	20.09	901.04	21.03	1,163.24
19.77	633.08	20.20	962.17	21.06	1,242.16
19.83	673.30	20.20	1,023.30	21.14	1,321.08
19.88	713.52	20.31	1,084.43	21.22	1,400.00
19.97	753.74	20.34	1,145.55	21.30	1,478.91
19.98	834.18	20.37	1,267.81	21.27	1,636.75
20.14	914.62	20.43	1,390.07	21.38	1,794.58

Table D.8 Tripped boundary layer data for $h/t = 2.86$

Re_t = 47,000		Re_t = 73,000		Re_t = 97,000	
u^+	y^+	u^+	y^+	u^+	y^+
0.00	0.00	0.00	0.00	0.00	0.00
11.03	14.05	12.72	21.13	14.02	28.10
10.93	18.48	13.14	27.80	14.58	36.97
10.93	22.92	13.86	34.47	14.87	45.84
11.05	27.35	14.33	41.14	15.22	54.71
12.29	31.79	14.69	47.81	15.48	63.58
13.03	36.22	14.89	54.48	15.72	72.46
13.40	40.66	15.20	61.16	15.91	81.33
13.87	45.09	15.50	67.83	16.06	90.20
14.02	49.53	15.60	74.50	16.21	99.07
14.42	58.40	15.77	87.84	16.34	116.82
14.73	67.27	16.10	101.18	16.80	134.56
15.05	76.14	16.37	114.53	17.03	152.31
15.30	85.01	16.73	127.87	17.33	170.05
15.68	93.88	16.95	141.21	17.58	187.79
15.91	102.76	17.15	154.56	17.78	205.54
16.05	111.63	17.39	167.90	18.00	223.28
16.30	120.50	17.53	181.24	18.23	241.03
16.46	129.37	17.75	194.59	18.35	258.77
16.72	138.24	17.93	207.93	18.59	276.52
16.89	156.72	18.04	235.73	18.76	313.48
17.21	175.20	18.38	263.52	19.03	350.45
17.58	193.68	18.71	291.32	19.33	387.42
17.82	212.16	18.91	319.12	19.60	424.39
18.01	230.65	19.18	346.92	19.86	461.35
18.23	249.13	19.39	374.72	20.01	498.32
18.47	267.61	19.47	402.51	20.20	535.29
18.66	286.09	19.74	430.31	20.32	572.26
18.78	304.57	19.85	458.11	20.46	609.22
18.91	323.05	20.00	485.91	20.61	646.19
19.11	360.01	20.10	541.50	20.73	720.13
19.29	396.98	20.26	597.10	20.90	794.06
19.53	433.94	20.48	652.69	21.11	868.00
19.75	470.90	20.58	708.29	21.19	941.93
19.87	507.86	20.77	763.89	21.35	1,015.87
20.00	544.83	20.86	819.48	21.48	1,089.80
20.08	581.79	20.97	875.08	21.53	1,163.74
20.16	618.75	21.04	930.67	21.65	1,237.67
20.30	655.71	21.15	986.27	21.76	1,311.60
20.42	692.68	21.23	1,041.87	21.81	1,385.54
20.48	766.60	21.29	1,153.06	21.87	1,533.41
20.60	840.53	21.42	1,264.25	22.01	1,681.28
20.76	914.45	21.39	1,375.44	22.10	1,829.15
20.85	988.38	21.48	1,486.63	22.18	1,977.02
20.94	1,062.30	21.53	1,597.82	22.25	2,124.89
21.00	1,136.23	21.62	1,709.02	22.30	2,272.76

Table D.9 Tripped boundary layer data for $h/t = 2.29$

Re_t = 47,000		Re_t = 73,000		Re_t = 97,000	
u^+	y^+	u^+	y^+	u^+	y^+
0.00	0.00	0.00	0.00	0.00	0.00
12.41	13.49	12.90	20.32	13.81	26.85
13.02	17.76	13.80	26.74	14.44	35.33
13.48	22.02	14.23	33.16	14.84	43.81
13.76	26.28	14.59	39.58	15.14	52.29
14.07	30.54	14.85	46.00	15.39	60.77
14.22	34.80	15.03	52.42	15.60	69.25
14.50	39.06	15.30	58.84	15.81	77.74
14.64	43.32	15.41	65.25	15.95	86.22
14.85	47.59	15.63	71.67	16.20	94.70
14.91	56.11	15.76	84.51	16.34	111.66
15.26	64.63	16.09	97.35	16.68	128.62
15.45	73.15	16.35	110.18	17.01	145.58
15.80	81.68	16.55	123.02	17.24	162.54
15.93	90.20	16.88	135.86	17.54	179.50
16.27	98.72	17.10	148.69	17.81	196.46
16.37	107.25	17.35	161.53	17.96	213.42
16.59	115.77	17.48	174.37	18.14	230.38
16.78	124.29	17.65	187.20	18.33	247.34
16.85	132.81	17.80	200.04	18.44	264.30
17.02	150.57	17.91	226.78	18.65	299.63
17.35	168.33	18.27	253.53	18.91	334.97
17.57	186.08	18.55	280.27	19.16	370.30
17.70	203.84	18.72	307.01	19.40	405.64
17.99	221.59	18.95	333.76	19.57	440.97
18.23	239.35	19.09	360.50	19.72	476.30
18.28	257.11	19.29	387.24	19.88	511.64
18.55	274.86	19.39	413.99	20.05	546.97
18.64	292.62	19.52	440.73	20.14	582.31
18.80	310.37	19.65	467.47	20.22	617.64
18.94	345.89	19.76	520.96	20.38	688.31
19.07	381.40	19.96	574.44	20.54	758.98
19.29	416.91	20.14	627.93	20.71	829.65
19.41	452.42	20.24	681.42	20.79	900.31
19.54	487.93	20.41	734.90	20.96	970.98
19.73	523.45	20.50	788.39	21.13	1,041.65
19.84	558.96	20.65	841.88	21.13	1,112.32
19.95	594.47	20.72	895.36	21.28	1,182.99
20.10	629.98	20.83	948.85	21.37	1,253.66
20.11	665.49	20.93	1,002.34	21.42	1,324.32
20.20	736.52	20.98	1,109.31	21.52	1,465.66
20.37	807.54	21.13	1,216.28	21.61	1,607.00
20.47	878.57	21.28	1,323.25	21.80	1,748.33
20.66	949.59	21.36	1,430.23	21.89	1,889.67
20.73	1,020.61	21.48	1,537.20	21.99	2,031.01
20.82	1,091.64	21.60	1,644.17	22.13	2,172.34

Table D.10 Tripped boundary layer data for h/t = 1.14

Re_t = 47,000		Re_t = 73,000		Re_t = 97,000	
u^+	y^+	u^+	y^+	u^+	y^+
0.00	0.00	0.00	0.00	0.00	0.00
11.50	11.80	12.76	17.96	14.12	23.71
12.58	15.52	13.56	23.63	14.64	31.20
13.05	19.25	14.14	29.30	14.95	38.68
13.34	22.97	14.41	34.97	15.21	46.17
13.62	26.70	14.72	40.64	15.41	53.66
14.01	30.42	14.93	46.31	15.64	61.15
14.14	34.15	15.01	51.98	15.89	68.63
14.51	37.87	15.27	57.65	16.02	76.12
14.56	41.60	15.46	63.32	16.23	83.61
14.74	49.05	15.61	74.66	16.35	98.58
15.08	56.50	15.93	86.00	16.65	113.56
15.35	63.95	16.10	97.35	16.89	128.53
15.52	71.40	16.35	108.69	17.07	143.51
15.81	78.85	16.58	120.03	17.33	158.48
15.96	86.30	16.78	131.37	17.58	173.46
16.12	93.74	16.99	142.71	17.73	188.43
16.40	101.19	17.12	154.05	17.94	203.41
16.45	108.64	17.37	165.39	18.11	218.38
16.63	116.09	17.44	176.73	18.29	233.35
16.65	131.62	17.77	200.36	18.36	264.55
16.93	147.14	17.93	223.99	18.59	295.75
17.26	162.66	18.16	247.62	18.85	326.95
17.59	178.18	18.35	271.24	19.05	358.14
17.76	193.70	18.59	294.87	19.28	389.34
17.84	209.22	18.68	318.50	19.41	420.54
18.10	224.74	18.84	342.13	19.58	451.73
18.16	240.26	19.04	365.75	19.66	482.93
18.33	255.78	19.16	389.38	19.81	514.13
18.47	271.30	19.26	413.01	19.94	545.33
18.61	302.34	19.36	460.26	19.97	607.72
18.88	333.38	19.51	507.52	20.17	670.11
19.04	364.43	19.72	554.77	20.41	732.51
19.16	395.47	19.82	602.03	20.50	794.90
19.21	426.51	19.99	649.28	20.60	857.30
19.51	457.55	20.14	696.54	20.71	919.69
19.53	488.59	20.22	743.79	20.82	982.09
19.68	519.63	20.31	791.05	20.90	1,044.48
19.82	550.67	20.40	838.30	21.02	1,106.87
19.93	581.72	20.49	885.56	21.10	1,169.27
20.01	643.80	20.60	980.07	21.12	1,294.06
20.24	705.88	20.78	1,074.58	21.40	1,418.85
20.41	767.96	20.97	1,169.09	21.54	1,543.63
20.57	830.05	21.10	1,263.60	21.69	1,668.42
20.70	892.13	21.27	1,358.10	21.85	1,793.21
20.92	954.21	21.44	1,452.61	21.92	1,918.00

D.4 Defect Profile

Table D.11 Defect profile for $h/t = 3.43$

Re_t = 47,000		Re_t = 73,000		Re_t = 97,000	
y/δ	$(U_\infty\text{-u})/u^*$	y/δ	$(U_\infty\text{-u})/u^*$	y/δ	$(U_\infty\text{-u})/u^*$
0.00	20.41	0.00	20.85	0.00	21.82
0.02	8.84	0.01	6.68	0.01	8.05
0.02	7.76	0.02	6.46	0.02	8.02
0.03	7.10	0.02	6.17	0.02	8.00
0.03	6.63	0.03	5.90	0.03	8.03
0.03	6.37	0.03	5.70	0.03	8.01
0.04	6.07	0.04	5.44	0.03	8.01
0.04	5.90	0.04	5.27	0.04	7.66
0.05	5.67	0.05	5.10	0.04	6.98
0.05	5.50	0.05	4.95	0.05	6.64
0.06	5.29	0.06	4.79	0.05	6.36
0.07	5.03	0.07	4.44	0.06	5.88
0.08	4.70	0.08	4.16	0.07	5.43
0.09	4.47	0.09	3.90	0.08	5.06
0.10	4.21	0.09	3.70	0.09	4.67
0.11	3.92	0.10	3.49	0.10	4.39
0.12	3.80	0.11	3.27	0.11	4.13
0.13	3.52	0.12	3.06	0.11	3.86
0.14	3.35	0.13	2.94	0.12	3.64
0.15	3.12	0.14	2.73	0.13	3.40
0.17	3.02	0.16	2.59	0.15	3.19
0.19	2.80	0.18	2.36	0.16	2.81
0.21	2.48	0.20	2.09	0.18	2.52
0.23	2.22	0.21	1.91	0.20	2.26
0.25	2.00	0.23	1.79	0.22	2.08
0.27	1.80	0.25	1.62	0.23	1.87
0.29	1.75	0.27	1.51	0.25	1.71
0.31	1.63	0.29	1.44	0.27	1.61
0.33	1.53	0.31	1.37	0.29	1.46
0.35	1.37	0.33	1.27	0.30	1.43
0.39	1.26	0.36	1.19	0.34	1.31
0.43	1.18	0.40	1.17	0.37	1.22
0.47	1.12	0.44	1.05	0.41	1.15
0.51	0.97	0.48	0.98	0.44	1.09
0.56	0.95	0.51	0.94	0.48	1.01
0.60	0.87	0.55	0.91	0.51	0.96
0.64	0.80	0.59	0.82	0.55	0.94
0.68	0.76	0.63	0.83	0.58	0.87
0.72	0.72	0.66	0.73	0.62	0.80
0.76	0.64	0.70	0.71	0.65	0.73
0.84	0.65	0.78	0.71	0.72	0.79
0.92	0.51	0.85	0.67	0.79	0.70

Table D.12 Defect profile for h/t = 2.86

Re_t = 47,000		Re_t = 73,000		Re_t = 97,000	
y/δ	$(U_\infty-u)/u^*$	y/δ	$(U_\infty-u)/u^*$	y/δ	$(U_\infty-u)/u^*$
0.00	21.08	0.00	21.82	0.00	22.36
0.01	10.05	0.01	9.10	0.02	8.34
0.02	10.15	0.02	8.68	0.02	7.78
0.02	10.16	0.02	7.96	0.03	7.50
0.03	10.04	0.02	7.49	0.03	7.14
0.03	8.80	0.03	7.14	0.03	6.89
0.04	8.06	0.03	6.94	0.04	6.65
0.04	7.69	0.03	6.63	0.04	6.46
0.05	7.22	0.04	6.33	0.05	6.31
0.05	7.07	0.04	6.23	0.05	6.16
0.06	6.68	0.05	6.06	0.06	6.04
0.07	6.37	0.06	5.73	0.07	5.58
0.08	6.04	0.06	5.46	0.08	5.35
0.09	5.80	0.07	5.11	0.09	5.04
0.09	5.42	0.08	4.89	0.10	4.81
0.10	5.19	0.08	4.69	0.11	4.60
0.11	5.06	0.09	4.46	0.12	4.39
0.12	4.81	0.10	4.32	0.13	4.16
0.13	4.65	0.11	4.10	0.14	4.04
0.14	4.39	0.11	3.92	0.15	3.80
0.16	4.22	0.13	3.81	0.17	3.64
0.18	3.91	0.14	3.48	0.19	3.37
0.20	3.55	0.16	3.15	0.21	3.08
0.21	3.31	0.18	2.96	0.23	2.81
0.23	3.12	0.19	2.69	0.25	2.56
0.25	2.90	0.21	2.49	0.27	2.41
0.27	2.67	0.22	2.42	0.29	2.22
0.29	2.49	0.24	2.15	0.31	2.11
0.31	2.37	0.25	2.05	0.33	1.97
0.33	2.24	0.27	1.90	0.35	1.83
0.36	2.05	0.30	1.81	0.39	1.71
0.40	1.88	0.33	1.66	0.43	1.56
0.44	1.66	0.36	1.44	0.47	1.36
0.48	1.45	0.39	1.35	0.51	1.29
0.51	1.33	0.42	1.17	0.56	1.14
0.55	1.21	0.45	1.10	0.60	1.02
0.59	1.14	0.48	0.99	0.64	0.98
0.63	1.07	0.51	0.94	0.68	0.87
0.66	0.94	0.54	0.83	0.72	0.77
0.70	0.83	0.57	0.76	0.76	0.73
0.78	0.78	0.63	0.73	0.84	0.69
0.85	0.68	0.69	0.61	0.92	0.57
0.93	0.55	0.76	0.66	1.00	0.50
1.00	0.47	0.82	0.59	1.08	0.43
1.07	0.40	0.88	0.56	1.16	0.39
1.15	0.37	0.94	0.49	1.24	0.36

Table D.13 Defect profile for $h/t = 2.29$

Re_t = 47,000		Re_t = 73,000		Re_t = 97,000	
y/δ	**$(U_\infty-u)/u^*$**	**y/δ**	**$(U_\infty-u)/u^*$**	**y/δ**	**$(U_\infty-u)/u^*$**
0.00	21.08	0.00	21.82	0.00	22.36
0.01	8.68	0.01	8.92	0.01	8.55
0.01	8.06	0.02	8.02	0.02	7.93
0.02	7.60	0.02	7.59	0.02	7.53
0.02	7.33	0.02	7.24	0.02	7.22
0.02	7.01	0.03	6.98	0.03	6.97
0.03	6.87	0.03	6.79	0.03	6.77
0.03	6.59	0.04	6.52	0.04	6.55
0.03	6.45	0.04	6.42	0.04	6.42
0.04	6.24	0.04	6.20	0.04	6.17
0.04	6.18	0.05	6.07	0.05	6.03
0.05	5.83	0.06	5.75	0.06	5.69
0.06	5.65	0.07	5.48	0.07	5.37
0.06	5.30	0.07	5.29	0.07	5.14
0.07	5.17	0.08	4.96	0.08	4.84
0.08	4.83	0.09	4.74	0.09	4.57
0.08	4.72	0.10	4.49	0.10	4.42
0.09	4.52	0.11	4.36	0.11	4.24
0.10	4.33	0.11	4.20	0.11	4.05
0.10	4.26	0.12	4.05	0.12	3.94
0.12	4.09	0.14	3.94	0.14	3.74
0.13	3.76	0.15	3.58	0.15	3.49
0.14	3.54	0.17	3.31	0.17	3.23
0.16	3.42	0.19	3.14	0.19	3.00
0.17	3.13	0.20	2.92	0.20	2.83
0.18	2.89	0.22	2.77	0.22	2.68
0.20	2.85	0.24	2.58	0.24	2.53
0.21	2.58	0.25	2.49	0.25	2.36
0.22	2.49	0.27	2.35	0.27	2.28
0.24	2.34	0.28	2.23	0.28	2.20
0.27	2.21	0.32	2.13	0.32	2.05
0.29	2.08	0.35	1.94	0.35	1.90
0.32	1.88	0.38	1.76	0.38	1.73
0.35	1.76	0.41	1.67	0.41	1.66
0.37	1.64	0.45	1.51	0.45	1.50
0.40	1.45	0.48	1.42	0.48	1.34
0.43	1.35	0.51	1.29	0.51	1.35
0.46	1.24	0.54	1.22	0.54	1.20
0.48	1.11	0.58	1.12	0.58	1.12
0.51	1.10	0.61	1.03	0.61	1.08
0.56	1.03	0.67	0.99	0.67	0.99
0.62	0.87	0.74	0.86	0.74	0.92
0.67	0.78	0.80	0.73	0.80	0.75
0.73	0.61	0.87	0.66	0.87	0.67
0.78	0.56	0.93	0.56	0.93	0.59
0.84	0.49	1.00	0.45	1.00	0.47

Table D.14 Defect profile for h/t = 1.14

Re_t = 47,000		Re_t = 73,000		Re_t = 97,000	
y/δ	$(U_\infty-u)/u^*$	y/δ	$(U_\infty-u)/u^*$	y/δ	$(U_\infty-u)/u^*$
0.00	21.57	0.00	22.09	0.00	22.65
0.01	10.07	0.01	9.33	0.01	8.53
0.01	8.99	0.01	8.53	0.01	8.01
0.02	8.52	0.02	7.95	0.02	7.69
0.02	8.23	0.02	7.68	0.02	7.43
0.02	7.95	0.02	7.37	0.02	7.24
0.03	7.56	0.03	7.16	0.03	7.01
0.03	7.43	0.03	7.08	0.03	6.76
0.03	7.06	0.03	6.82	0.03	6.63
0.03	7.01	0.03	6.63	0.03	6.42
0.04	6.83	0.04	6.48	0.04	6.30
0.05	6.50	0.05	6.16	0.05	6.00
0.05	6.22	0.05	5.99	0.05	5.76
0.06	6.05	0.06	5.74	0.06	5.58
0.07	5.76	0.07	5.51	0.07	5.32
0.07	5.62	0.07	5.32	0.07	5.07
0.08	5.45	0.08	5.11	0.08	4.93
0.08	5.17	0.08	4.97	0.08	4.71
0.09	5.13	0.09	4.73	0.09	4.54
0.10	4.95	0.10	4.66	0.10	4.37
0.11	4.93	0.11	4.33	0.11	4.30
0.12	4.66	0.12	4.17	0.12	4.07
0.14	4.32	0.14	3.94	0.14	3.82
0.15	4.00	0.15	3.75	0.15	3.62
0.16	3.83	0.16	3.52	0.16	3.39
0.17	3.74	0.17	3.43	0.17	3.26
0.19	3.49	0.19	3.27	0.19	3.09
0.20	3.43	0.20	3.08	0.20	3.02
0.21	3.27	0.21	2.96	0.21	2.86
0.23	3.12	0.23	2.86	0.23	2.74
0.25	2.99	0.25	2.76	0.25	2.71
0.28	2.73	0.28	2.61	0.28	2.51
0.30	2.57	0.30	2.41	0.30	2.28
0.33	2.45	0.33	2.31	0.33	2.19
0.35	2.40	0.35	2.14	0.35	2.09
0.38	2.11	0.38	2.00	0.38	1.99
0.41	2.09	0.41	1.92	0.41	1.89
0.43	1.94	0.43	1.84	0.43	1.80
0.46	1.81	0.46	1.75	0.46	1.69
0.48	1.70	0.48	1.66	0.48	1.61
0.54	1.63	0.54	1.56	0.54	1.60
0.59	1.41	0.59	1.39	0.59	1.33
0.64	1.25	0.64	1.21	0.64	1.20
0.69	1.09	0.69	1.08	0.69	1.06
0.74	0.97	0.74	0.93	0.74	0.91
0.79	0.75	0.79	0.76	0.79	0.84

D.5 Surface Pressure Distribution, Hump Only – Laminar Boundary Layer

Table D.15 Surface pressure distribution, hump only for $h/t = 3.43$, $Re_t = 47{,}000$ – laminar boundary layer

s/t	Cp	s/t	Cp
-10.29	-0.66	1.03	-0.75
-9.43	-0.76	1.10	-0.74
-8.57	-0.81	1.17	-0.74
-7.71	-0.86	1.24	-0.74
-6.86	-0.90	1.31	-0.73
-6.00	-0.92	1.38	-0.73
-5.14	-0.93	1.45	-0.72
-4.29	-0.92	1.52	-0.72
-3.43	-0.92	1.59	-0.72
-2.57	-0.90	1.67	-0.71
-1.71	-0.88	1.75	-0.71
-0.86	-0.84	1.83	-0.70
0.00	-0.80	1.92	-0.69
0.06	-0.80	2.00	-0.69
0.11	-0.80	2.07	-0.68
0.17	-0.79	2.16	-0.68
0.23	-0.79	2.24	-0.67
0.29	-0.79	2.33	-0.66
0.34	-0.78	2.43	-0.66
0.40	-0.78	2.52	-0.65
0.46	-0.77	2.62	-0.64
0.52	-0.78	2.71	-0.63
0.59	-0.77	2.81	-0.63
0.65	-0.76	2.92	-0.62
0.71	-0.77	3.03	-0.61
0.78	-0.76	3.15	-0.60
0.84	-0.76	3.26	-0.60
0.91	-0.76	3.38	-0.58
0.97	-0.75	3.52	-0.57

Table D.16 Surface pressure distribution, hump only for h/t = 3.43, Re_t = 73,000 – laminar boundary layer

s/t	Cp	s/t	Cp
-10.29	-0.80	1.03	-0.88
-9.43	-0.91	1.10	-0.88
-8.57	-0.97	1.17	-0.87
-7.71	-1.01	1.24	-0.87
-6.86	-1.06	1.31	-0.86
-6.00	-1.08	1.38	-0.87
-5.14	-1.09	1.45	-0.85
-4.29	-1.08	1.52	-0.85
-3.43	-1.09	1.59	-0.85
-2.57	-1.07	1.67	-0.84
-1.71	-1.03	1.75	-0.83
-0.86	-0.98	1.83	-0.83
0.00	-0.94	1.92	-0.82
0.06	-0.94	2.00	-0.81
0.11	-0.94	2.07	-0.80
0.17	-0.93	2.16	-0.80
0.23	-0.94	2.24	-0.79
0.29	-0.93	2.33	-0.79
0.34	-0.92	2.43	-0.78
0.40	-0.92	2.52	-0.77
0.46	-0.92	2.62	-0.76
0.52	-0.92	2.71	-0.75
0.59	-0.92	2.81	-0.74
0.65	-0.90	2.92	-0.73
0.71	-0.90	3.03	-0.73
0.78	-0.90	3.15	-0.71
0.84	-0.90	3.26	-0.69
0.91	-0.89	3.38	-0.68
0.97	-0.89	3.52	-0.67

Table D.17 Surface pressure distribution, hump only for $h/t = 3.43$, $Re_t = 97{,}000$ – laminar boundary layer

s/t	Cp	s/t	Cp
-10.29	-0.88	1.03	-0.96
-9.43	-1.01	1.10	-0.96
-8.57	-1.06	1.17	-0.95
-7.71	-1.12	1.24	-0.95
-6.86	-1.16	1.31	-0.94
-6.00	-1.18	1.38	-0.94
-5.14	-1.19	1.45	-0.93
-4.29	-1.19	1.52	-0.93
-3.43	-1.19	1.59	-0.92
-2.57	-1.17	1.67	-0.91
-1.71	-1.13	1.75	-0.90
-0.86	-1.08	1.83	-0.90
0.00	-1.03	1.92	-0.89
0.06	-1.03	2.00	-0.88
0.11	-1.02	2.07	-0.88
0.17	-1.02	2.16	-0.88
0.23	-1.02	2.24	-0.87
0.29	-1.01	2.33	-0.86
0.34	-1.01	2.43	-0.84
0.40	-1.01	2.52	-0.84
0.46	-1.00	2.62	-0.82
0.52	-1.00	2.71	-0.82
0.59	-0.98	2.81	-0.81
0.65	-0.99	2.92	-0.80
0.71	-0.98	3.03	-0.79
0.78	-0.98	3.15	-0.78
0.84	-0.98	3.26	-0.76
0.91	-0.97	3.38	-0.74
0.97	-0.97	3.52	-0.73

Table D.18 Surface pressure distribution, hump only for $h/t = 2.86$, $Re_t = 47{,}000$ – laminar boundary layer

s/t	Cp	s/t	Cp
-10.29	-0.58	1.03	-0.60
-9.43	-0.64	1.10	-0.60
-8.57	-0.67	1.17	-0.60
-7.71	-0.70	1.24	-0.59
-6.86	-0.74	1.31	-0.59
-6.00	-0.73	1.38	-0.59
-5.14	-0.74	1.45	-0.58
-4.29	-0.73	1.52	-0.59
-3.43	-0.74	1.59	-0.59
-2.57	-0.72	1.67	-0.58
-1.71	-0.68	1.75	-0.57
-0.86	-0.67	1.83	-0.57
0.00	-0.64	1.92	-0.57
0.06	-0.64	2.00	-0.57
0.11	-0.64	2.07	-0.56
0.17	-0.63	2.16	-0.56
0.23	-0.64	2.24	-0.55
0.29	-0.64	2.33	-0.55
0.34	-0.64	2.43	-0.54
0.40	-0.62	2.52	-0.53
0.46	-0.63	2.62	-0.53
0.52	-0.63	2.71	-0.53
0.59	-0.62	2.81	-0.52
0.65	-0.62	2.92	-0.51
0.71	-0.61	3.03	-0.51
0.78	-0.61	3.15	-0.50
0.84	-0.61	3.26	-0.49
0.91	-0.61	3.38	-0.48
0.97	-0.61	3.52	-0.48

Table D.19 Surface pressure distribution, hump only for h/t = 2.86, Re_t = 73,000 – laminar boundary layer

s/t	Cp	s/t	Cp
-10.29	-0.69	1.03	-0.70
-9.43	-0.75	1.10	-0.70
-8.57	-0.78	1.17	-0.70
-7.71	-0.81	1.24	-0.69
-6.86	-0.84	1.31	-0.69
-6.00	-0.85	1.38	-0.69
-5.14	-0.85	1.45	-0.69
-4.29	-0.87	1.52	-0.68
-3.43	-0.85	1.59	-0.69
-2.57	-0.84	1.67	-0.67
-1.71	-0.81	1.75	-0.67
-0.86	-0.76	1.83	-0.67
0.00	-0.75	1.92	-0.66
0.06	-0.74	2.00	-0.66
0.11	-0.74	2.07	-0.66
0.17	-0.74	2.16	-0.65
0.23	-0.74	2.24	-0.64
0.29	-0.74	2.33	-0.63
0.34	-0.74	2.43	-0.63
0.40	-0.73	2.52	-0.63
0.46	-0.73	2.62	-0.62
0.52	-0.72	2.71	-0.62
0.59	-0.73	2.81	-0.61
0.65	-0.72	2.92	-0.60
0.71	-0.72	3.03	-0.59
0.78	-0.72	3.15	-0.58
0.84	-0.71	3.26	-0.58
0.91	-0.72	3.38	-0.57
0.97	-0.71	3.52	-0.56

Table D.20 Surface pressure distribution, hump only for $h/t = 2.86$, $Re_t = 97{,}000$ – laminar boundary layer

s/t	Cp	s/t	Cp
-10.29	-0.75	1.03	-0.77
-9.43	-0.81	1.10	-0.78
-8.57	-0.85	1.17	-0.76
-7.71	-0.89	1.24	-0.75
-6.86	-0.93	1.31	-0.76
-6.00	-0.93	1.38	-0.75
-5.14	-0.94	1.45	-0.75
-4.29	-0.95	1.52	-0.75
-3.43	-0.94	1.59	-0.76
-2.57	-0.92	1.67	-0.73
-1.71	-0.87	1.75	-0.74
-0.86	-0.84	1.83	-0.72
0.00	-0.82	1.92	-0.72
0.06	-0.82	2.00	-0.72
0.11	-0.82	2.07	-0.71
0.17	-0.81	2.16	-0.72
0.23	-0.81	2.24	-0.71
0.29	-0.82	2.33	-0.70
0.34	-0.82	2.43	-0.69
0.40	-0.80	2.52	-0.68
0.46	-0.80	2.62	-0.68
0.52	-0.79	2.71	-0.67
0.59	-0.80	2.81	-0.66
0.65	-0.79	2.92	-0.66
0.71	-0.79	3.03	-0.65
0.78	-0.79	3.15	-0.64
0.84	-0.78	3.26	-0.63
0.91	-0.78	3.38	-0.61
0.97	-0.78	3.52	-0.61

Table D.21 Surface pressure distribution, hump only for $h/t = 2.29$, $Re_t = 47{,}000$ – laminar boundary layer

s/t	Cp	s/t	Cp
-10.29	-0.52	1.03	-0.51
-9.43	-0.56	1.10	-0.51
-8.57	-0.57	1.17	-0.51
-7.71	-0.59	1.24	-0.51
-6.86	-0.60	1.31	-0.50
-6.00	-0.61	1.38	-0.50
-5.14	-0.61	1.45	-0.50
-4.29	-0.61	1.52	-0.50
-3.43	-0.60	1.59	-0.49
-2.57	-0.59	1.67	-0.49
-1.71	-0.58	1.75	-0.49
-0.86	-0.56	1.83	-0.48
0.00	-0.54	1.92	-0.47
0.06	-0.54	2.00	-0.48
0.11	-0.54	2.07	-0.47
0.17	-0.54	2.16	-0.47
0.23	-0.54	2.24	-0.47
0.29	-0.54	2.33	-0.47
0.34	-0.53	2.43	-0.46
0.40	-0.53	2.52	-0.46
0.46	-0.53	2.62	-0.45
0.52	-0.53	2.71	-0.44
0.59	-0.52	2.81	-0.44
0.65	-0.53	2.92	-0.44
0.71	-0.52	3.03	-0.43
0.78	-0.52	3.15	-0.43
0.84	-0.52	3.26	-0.42
0.91	-0.51	3.38	-0.42
0.97	-0.51	3.52	-0.41

Table D.22 Surface pressure distribution, hump only for $h/t = 2.29$, $Re_t = 73{,}000$ – laminar boundary layer

s/t	Cp	s/t	Cp
-10.29	-0.60	1.03	-0.59
-9.43	-0.64	1.10	-0.58
-8.57	-0.65	1.17	-0.58
-7.71	-0.67	1.24	-0.58
-6.86	-0.68	1.31	-0.57
-6.00	-0.69	1.38	-0.58
-5.14	-0.69	1.45	-0.57
-4.29	-0.70	1.52	-0.57
-3.43	-0.68	1.59	-0.56
-2.57	-0.68	1.67	-0.56
-1.71	-0.66	1.75	-0.55
-0.86	-0.64	1.83	-0.55
0.00	-0.62	1.92	-0.55
0.06	-0.61	2.00	-0.55
0.11	-0.61	2.07	-0.54
0.17	-0.61	2.16	-0.54
0.23	-0.62	2.24	-0.53
0.29	-0.61	2.33	-0.53
0.34	-0.61	2.43	-0.53
0.40	-0.61	2.52	-0.52
0.46	-0.60	2.62	-0.52
0.52	-0.60	2.71	-0.51
0.59	-0.60	2.81	-0.50
0.65	-0.61	2.92	-0.50
0.71	-0.59	3.03	-0.50
0.78	-0.59	3.15	-0.49
0.84	-0.59	3.26	-0.48
0.91	-0.59	3.38	-0.48
0.97	-0.59	3.52	-0.47

Table D.23 Surface pressure distribution, hump only for $h/t = 2.29$, $Re_t = 97{,}000$ – laminar boundary layer

s/t	Cp	s/t	Cp
-10.29	-0.63	1.03	-0.61
-9.43	-0.69	1.10	-0.61
-8.57	-0.69	1.17	-0.60
-7.71	-0.71	1.24	-0.64
-6.86	-0.73	1.31	-0.60
-6.00	-0.74	1.38	-0.62
-5.14	-0.73	1.45	-0.60
-4.29	-0.74	1.52	-0.63
-3.43	-0.73	1.59	-0.58
-2.57	-0.73	1.67	-0.59
-1.71	-0.70	1.75	-0.59
-0.86	-0.68	1.83	-0.57
0.00	-0.66	1.92	-0.57
0.06	-0.65	2.00	-0.60
0.11	-0.65	2.07	-0.56
0.17	-0.64	2.16	-0.57
0.23	-0.68	2.24	-0.56
0.29	-0.64	2.33	-0.56
0.34	-0.64	2.43	-0.55
0.40	-0.66	2.52	-0.54
0.46	-0.65	2.62	-0.55
0.52	-0.65	2.71	-0.53
0.59	-0.63	2.81	-0.53
0.65	-0.69	2.92	-0.52
0.71	-0.64	3.03	-0.51
0.78	-0.62	3.15	-0.51
0.84	-0.64	3.26	-0.51
0.91	-0.61	3.38	-0.50
0.97	-0.61	3.52	-0.49

Table D.24 Surface pressure distribution, hump only for $h/t = 1.14$, $Re_t = 47{,}000$ – laminar boundary layer

s/t	Cp	s/t	Cp
-10.29	-0.30	1.03	-0.30
-9.43	-0.32	1.10	-0.29
-8.57	-0.32	1.17	-0.29
-7.71	-0.33	1.24	-0.29
-6.86	-0.34	1.31	-0.29
-6.00	-0.33	1.38	-0.29
-5.14	-0.33	1.45	-0.29
-4.29	-0.32	1.52	-0.29
-3.43	-0.32	1.59	-0.29
-2.57	-0.32	1.67	-0.29
-1.71	-0.32	1.75	-0.29
-0.86	-0.31	1.83	-0.28
0.00	-0.30	1.92	-0.28
0.06	-0.30	2.00	-0.28
0.11	-0.30	2.07	-0.28
0.17	-0.30	2.16	-0.28
0.23	-0.30	2.24	-0.28
0.29	-0.30	2.33	-0.28
0.34	-0.30	2.43	-0.28
0.40	-0.30	2.52	-0.27
0.46	-0.30	2.62	-0.27
0.52	-0.30	2.71	-0.27
0.59	-0.30	2.81	-0.27
0.65	-0.30	2.92	-0.26
0.71	-0.30	3.03	-0.27
0.78	-0.30	3.15	-0.26
0.84	-0.30	3.26	-0.26
0.91	-0.29	3.38	-0.26
0.97	-0.30	3.52	-0.26

Table D.25 Surface pressure distribution, hump only for h/t = 1.14, Re_t = 73,000 – laminar boundary layer

s/t	Cp	s/t	Cp
-10.29	-0.34	1.03	-0.33
-9.43	-0.36	1.10	-0.34
-8.57	-0.37	1.17	-0.34
-7.71	-0.37	1.24	-0.33
-6.86	-0.38	1.31	-0.33
-6.00	-0.37	1.38	-0.33
-5.14	-0.38	1.45	-0.33
-4.29	-0.37	1.52	-0.33
-3.43	-0.37	1.59	-0.33
-2.57	-0.36	1.67	-0.33
-1.71	-0.36	1.75	-0.33
-0.86	-0.35	1.83	-0.33
0.00	-0.35	1.92	-0.32
0.06	-0.34	2.00	-0.32
0.11	-0.34	2.07	-0.32
0.17	-0.34	2.16	-0.32
0.23	-0.34	2.24	-0.32
0.29	-0.34	2.33	-0.32
0.34	-0.34	2.43	-0.31
0.40	-0.34	2.52	-0.31
0.46	-0.34	2.62	-0.31
0.52	-0.34	2.71	-0.31
0.59	-0.34	2.81	-0.31
0.65	-0.34	2.92	-0.30
0.71	-0.34	3.03	-0.30
0.78	-0.34	3.15	-0.30
0.84	-0.34	3.26	-0.30
0.91	-0.34	3.38	-0.30
0.97	-0.34	3.52	-0.29

Table D.26 Surface pressure distribution, hump only for $h/t = 1.14$, $Re_t = 97{,}000$ – laminar boundary layer

s/t	Cp	s/t	Cp
-10.29	-0.37	1.03	-0.36
-9.43	-0.39	1.10	-0.36
-8.57	-0.39	1.17	-0.36
-7.71	-0.40	1.24	-0.36
-6.86	-0.40	1.31	-0.35
-6.00	-0.40	1.38	-0.36
-5.14	-0.40	1.45	-0.36
-4.29	-0.39	1.52	-0.35
-3.43	-0.40	1.59	-0.35
-2.57	-0.39	1.67	-0.35
-1.71	-0.38	1.75	-0.35
-0.86	-0.38	1.83	-0.35
0.00	-0.37	1.92	-0.35
0.06	-0.37	2.00	-0.34
0.11	-0.37	2.07	-0.34
0.17	-0.37	2.16	-0.34
0.23	-0.37	2.24	-0.34
0.29	-0.37	2.33	-0.34
0.34	-0.37	2.43	-0.33
0.40	-0.36	2.52	-0.34
0.46	-0.37	2.62	-0.33
0.52	-0.37	2.71	-0.33
0.59	-0.37	2.81	-0.33
0.65	-0.36	2.92	-0.32
0.71	-0.37	3.03	-0.32
0.78	-0.36	3.15	-0.32
0.84	-0.36	3.26	-0.32
0.91	-0.36	3.38	-0.31
0.97	-0.36	3.52	-0.31

D.6 Surface Pressure Distribution, Hump – Tripped Boundary Layer

Table D.27 Surface pressure distribution, hump only for $h/t = 3.43$, $Re_t = 47{,}000$ – tripped boundary layer

s/t	Cp	s/t	Cp
-10.29	-0.62	1.03	-0.73
-9.43	-0.71	1.10	-0.73
-8.57	-0.78	1.17	-0.72
-7.71	-0.82	1.24	-0.72
-6.86	-0.86	1.31	-0.71
-6.00	-0.89	1.38	-0.71
-5.14	-0.91	1.45	-0.71
-4.29	-0.90	1.52	-0.70
-3.43	-0.91	1.59	-0.70
-2.57	-0.89	1.67	-0.70
-1.71	-0.86	1.75	-0.70
-0.86	-0.82	1.83	-0.68
0.00	-0.78	1.92	-0.68
0.06	-0.78	2.00	-0.67
0.11	-0.77	2.07	-0.67
0.17	-0.78	2.16	-0.67
0.23	-0.78	2.24	-0.66
0.29	-0.76	2.33	-0.65
0.34	-0.77	2.43	-0.64
0.40	-0.77	2.52	-0.63
0.46	-0.75	2.62	-0.63
0.52	-0.76	2.71	-0.62
0.59	-0.75	2.81	-0.61
0.65	-0.76	2.92	-0.60
0.71	-0.74	3.03	-0.61
0.78	-0.74	3.15	-0.60
0.84	-0.75	3.26	-0.57
0.91	-0.73	3.38	-0.56
0.97	-0.73	3.52	-0.55

Table D.28 Surface pressure distribution, hump only for $h/t = 3.43$, $Re_t = 73{,}000$ – tripped boundary layer

s/t	Cp	s/t	Cp
-10.29	-0.75	1.03	-0.86
-9.43	-0.86	1.10	-0.85
-8.57	-0.93	1.17	-0.85
-7.71	-0.98	1.24	-0.85
-6.86	-1.02	1.31	-0.84
-6.00	-1.05	1.38	-0.84
-5.14	-1.05	1.45	-0.83
-4.29	-1.05	1.52	-0.84
-3.43	-1.06	1.59	-0.83
-2.57	-1.04	1.67	-0.82
-1.71	-1.03	1.75	-0.82
-0.86	-0.96	1.83	-0.80
0.00	-0.92	1.92	-0.80
0.06	-0.92	2.00	-0.78
0.11	-0.91	2.07	-0.79
0.17	-0.92	2.16	-0.79
0.23	-0.93	2.24	-0.77
0.29	-0.90	2.33	-0.76
0.34	-0.91	2.43	-0.75
0.40	-0.91	2.52	-0.75
0.46	-0.88	2.62	-0.75
0.52	-0.90	2.71	-0.73
0.59	-0.89	2.81	-0.72
0.65	-0.88	2.92	-0.70
0.71	-0.87	3.03	-0.72
0.78	-0.87	3.15	-0.70
0.84	-0.88	3.26	-0.68
0.91	-0.86	3.38	-0.66
0.97	-0.86	3.52	-0.64

Table D.29 Surface pressure distribution, hump only for $h/t = 3.43$, $Re_t = 97{,}000$ – tripped boundary layer

s/t	Cp	s/t	Cp
-10.29	-0.83	1.03	-0.93
-9.43	-0.95	1.10	-0.93
-8.57	-1.02	1.17	-0.92
-7.71	-1.08	1.24	-0.92
-6.86	-1.12	1.31	-0.91
-6.00	-1.15	1.38	-0.91
-5.14	-1.16	1.45	-0.90
-4.29	-1.15	1.52	-0.91
-3.43	-1.17	1.59	-0.89
-2.57	-1.14	1.67	-0.89
-1.71	-1.12	1.75	-0.88
-0.86	-1.05	1.83	-0.87
0.00	-1.01	1.92	-0.86
0.06	-1.01	2.00	-0.86
0.11	-0.99	2.07	-0.86
0.17	-1.00	2.16	-0.87
0.23	-1.01	2.24	-0.83
0.29	-0.98	2.33	-0.83
0.34	-0.99	2.43	-0.82
0.40	-0.99	2.52	-0.80
0.46	-0.97	2.62	-0.80
0.52	-0.98	2.71	-0.80
0.59	-0.96	2.81	-0.79
0.65	-0.96	2.92	-0.76
0.71	-0.95	3.03	-0.79
0.78	-0.95	3.15	-0.77
0.84	-0.96	3.26	-0.74
0.91	-0.94	3.38	-0.72
0.97	-0.94	3.52	-0.70

Table D.30 Surface pressure distribution, hump only for $h/t = 2.86$, $Re_t = 47{,}000$ – tripped boundary layer

s/t	Cp	s/t	Cp
-10.29	-0.58	1.03	-0.60
-9.43	-0.63	1.10	-0.60
-8.57	-0.67	1.17	-0.59
-7.71	-0.70	1.24	-0.58
-6.86	-0.74	1.31	-0.60
-6.00	-0.74	1.38	-0.59
-5.14	-0.74	1.45	-0.58
-4.29	-0.73	1.52	-0.58
-3.43	-0.74	1.59	-0.60
-2.57	-0.75	1.67	-0.57
-1.71	-0.71	1.75	-0.58
-0.86	-0.67	1.83	-0.56
0.00	-0.64	1.92	-0.56
0.06	-0.64	2.00	-0.57
0.11	-0.64	2.07	-0.56
0.17	-0.63	2.16	-0.56
0.23	-0.63	2.24	-0.54
0.29	-0.63	2.33	-0.54
0.34	-0.66	2.43	-0.54
0.40	-0.62	2.52	-0.53
0.46	-0.62	2.62	-0.53
0.52	-0.63	2.71	-0.52
0.59	-0.62	2.81	-0.51
0.65	-0.61	2.92	-0.51
0.71	-0.61	3.03	-0.49
0.78	-0.61	3.15	-0.49
0.84	-0.61	3.26	-0.49
0.91	-0.61	3.38	-0.47
0.97	-0.61	3.52	-0.47

Table D.31 Surface pressure distribution, hump only for $h/t = 2.86$, $Re_t = 73{,}000$ – tripped boundary layer

s/t	Cp	s/t	Cp
-10.29	-0.70	1.03	-0.71
-9.43	-0.76	1.10	-0.71
-8.57	-0.79	1.17	-0.68
-7.71	-0.82	1.24	-0.68
-6.86	-0.86	1.31	-0.70
-6.00	-0.86	1.38	-0.68
-5.14	-0.87	1.45	-0.69
-4.29	-0.85	1.52	-0.67
-3.43	-0.87	1.59	-0.71
-2.57	-0.86	1.67	-0.68
-1.71	-0.80	1.75	-0.67
-0.86	-0.78	1.83	-0.66
0.00	-0.75	1.92	-0.66
0.06	-0.75	2.00	-0.66
0.11	-0.75	2.07	-0.65
0.17	-0.75	2.16	-0.66
0.23	-0.74	2.24	-0.63
0.29	-0.74	2.33	-0.63
0.34	-0.78	2.43	-0.63
0.40	-0.75	2.52	-0.62
0.46	-0.73	2.62	-0.62
0.52	-0.73	2.71	-0.60
0.59	-0.73	2.81	-0.60
0.65	-0.72	2.92	-0.60
0.71	-0.72	3.03	-0.58
0.78	-0.72	3.15	-0.58
0.84	-0.72	3.26	-0.57
0.91	-0.73	3.38	-0.56
0.97	-0.72	3.52	-0.56

Table D.32 Surface pressure distribution, hump only for $h/t = 2.86$, $Re_t = 97{,}000$ – tripped boundary layer

s/t	Cp	s/t	Cp
-10.29	-0.76	1.03	-0.77
-9.43	-0.81	1.10	-0.77
-8.57	-0.86	1.17	-0.75
-7.71	-0.90	1.24	-0.74
-6.86	-0.94	1.31	-0.77
-6.00	-0.94	1.38	-0.74
-5.14	-0.95	1.45	-0.75
-4.29	-0.92	1.52	-0.74
-3.43	-0.95	1.59	-0.78
-2.57	-0.96	1.67	-0.73
-1.71	-0.90	1.75	-0.74
-0.86	-0.85	1.83	-0.72
0.00	-0.83	1.92	-0.72
0.06	-0.83	2.00	-0.72
0.11	-0.82	2.07	-0.71
0.17	-0.82	2.16	-0.72
0.23	-0.80	2.24	-0.69
0.29	-0.81	2.33	-0.69
0.34	-0.86	2.43	-0.68
0.40	-0.81	2.52	-0.67
0.46	-0.80	2.62	-0.68
0.52	-0.79	2.71	-0.65
0.59	-0.79	2.81	-0.66
0.65	-0.78	2.92	-0.65
0.71	-0.78	3.03	-0.64
0.78	-0.78	3.15	-0.63
0.84	-0.78	3.26	-0.61
0.91	-0.80	3.38	-0.61
0.97	-0.78	3.52	-0.62

Table D.33 Surface pressure distribution, hump only for $h/t = 2.29$, $Re_t = 47{,}000$ – tripped boundary layer

s/t	Cp	s/t	Cp
-10.29	-0.51	1.03	-0.50
-9.43	-0.54	1.10	-0.49
-8.57	-0.56	1.17	-0.49
-7.71	-0.58	1.24	-0.50
-6.86	-0.59	1.31	-0.49
-6.00	-0.60	1.38	-0.50
-5.14	-0.59	1.45	-0.49
-4.29	-0.60	1.52	-0.50
-3.43	-0.59	1.59	-0.48
-2.57	-0.58	1.67	-0.48
-1.71	-0.57	1.75	-0.47
-0.86	-0.55	1.83	-0.47
0.00	-0.53	1.92	-0.46
0.06	-0.52	2.00	-0.47
0.11	-0.52	2.07	-0.46
0.17	-0.52	2.16	-0.46
0.23	-0.54	2.24	-0.45
0.29	-0.51	2.33	-0.45
0.34	-0.52	2.43	-0.45
0.40	-0.53	2.52	-0.44
0.46	-0.52	2.62	-0.44
0.52	-0.52	2.71	-0.43
0.59	-0.51	2.81	-0.43
0.65	-0.54	2.92	-0.43
0.71	-0.51	3.03	-0.42
0.78	-0.51	3.15	-0.41
0.84	-0.51	3.26	-0.41
0.91	-0.50	3.38	-0.41
0.97	-0.50	3.52	-0.40

Table D.34 Surface pressure distribution, hump only for $h/t = 2.29$, $Re_t = 73{,}000$ – tripped boundary layer

s/t	Cp	s/t	Cp
-10.29	-0.59	1.03	-0.57
-9.43	-0.63	1.10	-0.57
-8.57	-0.65	1.17	-0.56
-7.71	-0.67	1.24	-0.59
-6.86	-0.68	1.31	-0.56
-6.00	-0.70	1.38	-0.57
-5.14	-0.69	1.45	-0.56
-4.29	-0.69	1.52	-0.58
-3.43	-0.68	1.59	-0.54
-2.57	-0.68	1.67	-0.55
-1.71	-0.66	1.75	-0.54
-0.86	-0.64	1.83	-0.54
0.00	-0.62	1.92	-0.54
0.06	-0.61	2.00	-0.54
0.11	-0.61	2.07	-0.53
0.17	-0.60	2.16	-0.52
0.23	-0.63	2.24	-0.52
0.29	-0.59	2.33	-0.52
0.34	-0.60	2.43	-0.51
0.40	-0.61	2.52	-0.50
0.46	-0.61	2.62	-0.51
0.52	-0.60	2.71	-0.49
0.59	-0.59	2.81	-0.50
0.65	-0.63	2.92	-0.49
0.71	-0.59	3.03	-0.48
0.78	-0.58	3.15	-0.48
0.84	-0.59	3.26	-0.47
0.91	-0.58	3.38	-0.46
0.97	-0.57	3.52	-0.46

Table D.35 Surface pressure distribution, hump only for $h/t = 2.29$, $Re_t = 97{,}000$ – tripped boundary layer

s/t	Cp	s/t	Cp
-10.29	-0.64	1.03	-0.62
-9.43	-0.68	1.10	-0.61
-8.57	-0.70	1.17	-0.60
-7.71	-0.72	1.24	-0.64
-6.86	-0.73	1.31	-0.60
-6.00	-0.75	1.38	-0.62
-5.14	-0.74	1.45	-0.61
-4.29	-0.74	1.52	-0.64
-3.43	-0.73	1.59	-0.59
-2.57	-0.73	1.67	-0.59
-1.71	-0.71	1.75	-0.59
-0.86	-0.69	1.83	-0.58
0.00	-0.66	1.92	-0.58
0.06	-0.65	2.00	-0.60
0.11	-0.66	2.07	-0.57
0.17	-0.65	2.16	-0.57
0.23	-0.68	2.24	-0.56
0.29	-0.64	2.33	-0.56
0.34	-0.65	2.43	-0.55
0.40	-0.66	2.52	-0.55
0.46	-0.65	2.62	-0.55
0.52	-0.65	2.71	-0.53
0.59	-0.64	2.81	-0.53
0.65	-0.69	2.92	-0.52
0.71	-0.64	3.03	-0.52
0.78	-0.63	3.15	-0.52
0.84	-0.65	3.26	-0.51
0.91	-0.62	3.38	-0.50
0.97	-0.61	3.52	-0.49

Table D.36 Surface pressure distribution, hump only for h/t = 1.14, Re_t = 47,000 – tripped boundary layer

s/t	Cp	s/t	Cp
-10.29	-0.29	1.03	-0.29
-9.43	-0.32	1.10	-0.29
-8.57	-0.32	1.17	-0.29
-7.71	-0.33	1.24	-0.29
-6.86	-0.33	1.31	-0.29
-6.00	-0.33	1.38	-0.29
-5.14	-0.33	1.45	-0.29
-4.29	-0.32	1.52	-0.28
-3.43	-0.32	1.59	-0.28
-2.57	-0.31	1.67	-0.28
-1.71	-0.31	1.75	-0.28
-0.86	-0.30	1.83	-0.28
0.00	-0.30	1.92	-0.28
0.06	-0.30	2.00	-0.28
0.11	-0.30	2.07	-0.28
0.17	-0.30	2.16	-0.28
0.23	-0.30	2.24	-0.27
0.29	-0.30	2.33	-0.27
0.34	-0.30	2.43	-0.27
0.40	-0.29	2.52	-0.27
0.46	-0.29	2.62	-0.27
0.52	-0.30	2.71	-0.26
0.59	-0.30	2.81	-0.26
0.65	-0.29	2.92	-0.25
0.71	-0.30	3.03	-0.26
0.78	-0.29	3.15	-0.26
0.84	-0.29	3.26	-0.25
0.91	-0.29	3.38	-0.25
0.97	-0.30	3.52	-0.25

Table D.37 Surface pressure distribution, hump only for h/t = 1.14, Re_t = 73,000 – tripped boundary layer

s/t	Cp	s/t	Cp
-10.29	-0.34	1.03	-0.33
-9.43	-0.36	1.10	-0.33
-8.57	-0.37	1.17	-0.33
-7.71	-0.37	1.24	-0.33
-6.86	-0.38	1.31	-0.33
-6.00	-0.37	1.38	-0.34
-5.14	-0.38	1.45	-0.33
-4.29	-0.36	1.52	-0.32
-3.43	-0.37	1.59	-0.33
-2.57	-0.36	1.67	-0.32
-1.71	-0.36	1.75	-0.33
-0.86	-0.35	1.83	-0.32
0.00	-0.34	1.92	-0.32
0.06	-0.34	2.00	-0.32
0.11	-0.34	2.07	-0.32
0.17	-0.34	2.16	-0.32
0.23	-0.34	2.24	-0.31
0.29	-0.34	2.33	-0.30
0.34	-0.34	2.43	-0.31
0.40	-0.34	2.52	-0.31
0.46	-0.34	2.62	-0.31
0.52	-0.34	2.71	-0.31
0.59	-0.34	2.81	-0.30
0.65	-0.34	2.92	-0.29
0.71	-0.35	3.03	-0.30
0.78	-0.34	3.15	-0.29
0.84	-0.34	3.26	-0.29
0.91	-0.34	3.38	-0.29
0.97	-0.34	3.52	-0.28

Table D.38 Surface pressure distribution, hump only for $h/t = 1.14$, $Re_t = 97{,}000$ – tripped boundary layer

s/t	Cp	s/t	Cp
-10.29	-0.37	1.03	-0.35
-9.43	-0.39	1.10	-0.35
-8.57	-0.39	1.17	-0.36
-7.71	-0.40	1.24	-0.35
-6.86	-0.41	1.31	-0.35
-6.00	-0.40	1.38	-0.36
-5.14	-0.40	1.45	-0.36
-4.29	-0.39	1.52	-0.34
-3.43	-0.40	1.59	-0.35
-2.57	-0.39	1.67	-0.35
-1.71	-0.39	1.75	-0.35
-0.86	-0.38	1.83	-0.35
0.00	-0.37	1.92	-0.35
0.06	-0.37	2.00	-0.34
0.11	-0.37	2.07	-0.35
0.17	-0.36	2.16	-0.35
0.23	-0.37	2.24	-0.33
0.29	-0.37	2.33	-0.33
0.34	-0.37	2.43	-0.33
0.40	-0.36	2.52	-0.33
0.46	-0.36	2.62	-0.33
0.52	-0.37	2.71	-0.33
0.59	-0.37	2.81	-0.33
0.65	-0.36	2.92	-0.31
0.71	-0.38	3.03	-0.32
0.78	-0.36	3.15	-0.32
0.84	-0.36	3.26	-0.32
0.91	-0.37	3.38	-0.31
0.97	-0.37	3.52	-0.31

D.7 Surface Pressure Distribution, Juncture Vortex and Hump – Laminar Boundary Layer

Table D.39 Surface pressure distribution, juncture vortex and hump for $h/t = 3.43$, $Re_t =$ 47,000 – laminar boundary layer

s/t	Cp	s/t	Cp
0.00	0.49	1.45	-0.52
0.06	0.27	1.52	-0.53
0.11	0.24	1.59	-0.54
0.17	0.18	1.67	-0.55
0.23	0.12	1.75	-0.55
0.29	0.06	1.83	-0.55
0.34	0.00	1.92	-0.56
0.40	-0.06	2.00	-0.56
0.46	-0.11	2.07	-0.57
0.52	-0.18	2.16	-0.57
0.59	-0.33	2.24	-0.57
0.65	-0.40	2.33	-0.57
0.71	-0.40	2.43	-0.57
0.78	-0.42	2.52	-0.57
0.84	-0.43	2.62	-0.56
0.91	-0.44	2.71	-0.56
0.97	-0.45	2.81	-0.56
1.03	-0.46	2.92	-0.56
1.10	-0.47	3.03	-0.55
1.17	-0.48	3.15	-0.55
1.24	-0.50	3.26	-0.54
1.31	-0.50	3.38	-0.54
1.38	-0.51	3.52	-0.53

Table D.40 Surface pressure distribution, juncture vortex and hump for h/t = 3.43, Re_t = 73,000 – laminar boundary layer

s/t	Cp	s/t	Cp
0.00	0.57	1.45	-0.61
0.06	0.25	1.52	-0.63
0.11	0.26	1.59	-0.64
0.17	0.20	1.67	-0.64
0.23	0.13	1.75	-0.65
0.29	0.05	1.83	-0.66
0.34	-0.02	1.92	-0.66
0.40	-0.09	2.00	-0.66
0.46	-0.14	2.07	-0.67
0.52	-0.19	2.16	-0.67
0.59	-0.31	2.24	-0.67
0.65	-0.44	2.33	-0.67
0.71	-0.48	2.43	-0.67
0.78	-0.50	2.52	-0.67
0.84	-0.51	2.62	-0.67
0.91	-0.52	2.71	-0.66
0.97	-0.53	2.81	-0.66
1.03	-0.54	2.92	-0.65
1.10	-0.56	3.03	-0.66
1.17	-0.57	3.15	-0.65
1.24	-0.58	3.26	-0.64
1.31	-0.60	3.38	-0.63
1.38	-0.61	3.52	-0.62

Table D.41 Surface pressure distribution, juncture vortex and hump for $h/t = 3.43$, $Re_t =$ 97,000 – laminar boundary layer

s/t	Cp	s/t	Cp
0.00	0.62	1.45	-0.67
0.06	0.23	1.52	-0.68
0.11	0.26	1.59	-0.69
0.17	0.20	1.67	-0.69
0.23	0.13	1.75	-0.70
0.29	0.05	1.83	-0.70
0.34	-0.03	1.92	-0.71
0.40	-0.11	2.00	-0.71
0.46	-0.17	2.07	-0.72
0.52	-0.21	2.16	-0.72
0.59	-0.29	2.24	-0.72
0.65	-0.40	2.33	-0.72
0.71	-0.49	2.43	-0.72
0.78	-0.53	2.52	-0.71
0.84	-0.54	2.62	-0.72
0.91	-0.56	2.71	-0.71
0.97	-0.57	2.81	-0.71
1.03	-0.59	2.92	-0.70
1.10	-0.60	3.03	-0.70
1.17	-0.62	3.15	-0.69
1.24	-0.63	3.26	-0.68
1.31	-0.64	3.38	-0.68
1.38	-0.66	3.52	-0.67

Table D.42 Surface pressure distribution, juncture vortex and hump for h/t = 2.86, Re_t = 47,000 – laminar boundary layer

s/t	Cp	s/t	Cp
0.00	0.56	1.45	-0.40
0.06	0.31	1.52	-0.41
0.11	0.30	1.59	-0.41
0.17	0.24	1.67	-0.42
0.23	0.20	1.75	-0.43
0.29	0.15	1.83	-0.43
0.34	0.09	1.92	-0.44
0.40	0.04	2.00	-0.44
0.46	0.00	2.07	-0.44
0.52	-0.06	2.16	-0.45
0.59	-0.14	2.24	-0.45
0.65	-0.25	2.33	-0.45
0.71	-0.29	2.43	-0.45
0.78	-0.31	2.52	-0.45
0.84	-0.31	2.62	-0.45
0.91	-0.32	2.71	-0.45
0.97	-0.32	2.81	-0.45
1.03	-0.34	2.92	-0.45
1.10	-0.35	3.03	-0.44
1.17	-0.36	3.15	-0.44
1.24	-0.37	3.26	-0.44
1.31	-0.38	3.38	-0.43
1.38	-0.39	3.52	-0.43

Table D.43 Surface pressure distribution, juncture vortex and hump for h/t = 2.86, Re_t = 73,000 – laminar boundary layer

s/t	Cp	s/t	Cp
0.00	0.64	1.45	-0.47
0.06	0.33	1.52	-0.47
0.11	0.34	1.59	-0.48
0.17	0.27	1.67	-0.49
0.23	0.22	1.75	-0.50
0.29	0.16	1.83	-0.51
0.34	0.09	1.92	-0.51
0.40	0.02	2.00	-0.52
0.46	-0.02	2.07	-0.52
0.52	-0.07	2.16	-0.52
0.59	-0.12	2.24	-0.52
0.65	-0.23	2.33	-0.53
0.71	-0.32	2.43	-0.53
0.78	-0.35	2.52	-0.53
0.84	-0.36	2.62	-0.52
0.91	-0.37	2.71	-0.52
0.97	-0.39	2.81	-0.52
1.03	-0.40	2.92	-0.52
1.10	-0.41	3.03	-0.52
1.17	-0.42	3.15	-0.51
1.24	-0.44	3.26	-0.51
1.31	-0.44	3.38	-0.51
1.38	-0.46	3.52	-0.50

Table D.44 Surface pressure distribution, juncture vortex and hump for h/t = 2.86, Re_t = 97,000 – laminar boundary layer

s/t	Cp	s/t	Cp
0.00	0.69	1.45	-0.50
0.06	0.33	1.52	-0.51
0.11	0.34	1.59	-0.53
0.17	0.28	1.67	-0.53
0.23	0.23	1.75	-0.54
0.29	0.16	1.83	-0.55
0.34	0.08	1.92	-0.55
0.40	0.01	2.00	-0.56
0.46	-0.05	2.07	-0.56
0.52	-0.10	2.16	-0.56
0.59	-0.14	2.24	-0.57
0.65	-0.20	2.33	-0.57
0.71	-0.29	2.43	-0.56
0.78	-0.36	2.52	-0.56
0.84	-0.39	2.62	-0.57
0.91	-0.41	2.71	-0.56
0.97	-0.42	2.81	-0.56
1.03	-0.44	2.92	-0.56
1.10	-0.45	3.03	-0.56
1.17	-0.46	3.15	-0.55
1.24	-0.47	3.26	-0.55
1.31	-0.49	3.38	-0.55
1.38	-0.49	3.52	-0.54

Table D.45 Surface pressure distribution, juncture vortex and hump for $h/t = 2.29$, $Re_t =$ 47,000 – laminar boundary layer

s/t	Cp	s/t	Cp
0.00	0.58	1.45	-0.30
0.06	0.35	1.52	-0.31
0.11	0.34	1.59	-0.31
0.17	0.29	1.67	-0.32
0.23	0.25	1.75	-0.33
0.29	0.20	1.83	-0.33
0.34	0.15	1.92	-0.33
0.40	0.11	2.00	-0.34
0.46	0.07	2.07	-0.34
0.52	0.02	2.16	-0.34
0.59	-0.04	2.24	-0.35
0.65	-0.15	2.33	-0.35
0.71	-0.20	2.43	-0.35
0.78	-0.22	2.52	-0.35
0.84	-0.22	2.62	-0.35
0.91	-0.23	2.71	-0.35
0.97	-0.23	2.81	-0.36
1.03	-0.25	2.92	-0.35
1.10	-0.25	3.03	-0.35
1.17	-0.26	3.15	-0.35
1.24	-0.27	3.26	-0.35
1.31	-0.28	3.38	-0.35
1.38	-0.29	3.52	-0.34

Table D.46 Surface pressure distribution, juncture vortex and hump for $h/t = 2.29$, $Re_t =$ 73,000 – laminar boundary layer

s/t	Cp	s/t	Cp
0.00	0.67	1.45	-0.35
0.06	0.45	1.52	-0.37
0.11	0.26	1.59	-0.36
0.17	0.24	1.67	-0.37
0.23	0.21	1.75	-0.38
0.29	0.17	1.83	-0.38
0.34	0.12	1.92	-0.39
0.40	0.07	2.00	-0.39
0.46	0.02	2.07	-0.39
0.52	-0.03	2.16	-0.41
0.59	-0.07	2.24	-0.40
0.65	-0.12	2.33	-0.41
0.71	-0.14	2.43	-0.41
0.78	-0.18	2.52	-0.41
0.84	-0.21	2.62	-0.41
0.91	-0.23	2.71	-0.41
0.97	-0.25	2.81	-0.41
1.03	-0.27	2.92	-0.41
1.10	-0.28	3.03	-0.41
1.17	-0.30	3.15	-0.41
1.24	-0.32	3.26	-0.40
1.31	-0.33	3.38	-0.40
1.38	-0.34	3.52	-0.40

Table D.47 Surface pressure distribution, juncture vortex and hump for $h/t = 2.29$, $Re_t =$ 97,000 – laminar boundary layer

s/t	Cp	s/t	Cp
0.00	0.72	1.45	-0.39
0.06	0.51	1.52	-0.41
0.11	0.17	1.59	-0.39
0.17	0.22	1.67	-0.41
0.23	0.20	1.75	-0.41
0.29	0.16	1.83	-0.41
0.34	0.12	1.92	-0.42
0.40	0.07	2.00	-0.44
0.46	0.01	2.07	-0.43
0.52	-0.04	2.16	-0.44
0.59	-0.08	2.24	-0.44
0.65	-0.14	2.33	-0.44
0.71	-0.16	2.43	-0.44
0.78	-0.19	2.52	-0.44
0.84	-0.23	2.62	-0.44
0.91	-0.25	2.71	-0.44
0.97	-0.27	2.81	-0.44
1.03	-0.29	2.92	-0.44
1.10	-0.30	3.03	-0.44
1.17	-0.32	3.15	-0.44
1.24	-0.36	3.26	-0.43
1.31	-0.35	3.38	-0.43
1.38	-0.38	3.52	-0.43

Table D.48 Surface pressure distribution, juncture vortex and hump for h/t = 1.14, Re_t = 47,000 – laminar boundary layer

s/t	Cp	s/t	Cp
0.00	0.58	1.45	-0.12
0.06	0.47	1.52	-0.13
0.11	0.26	1.59	-0.14
0.17	0.21	1.67	-0.14
0.23	0.23	1.75	-0.16
0.29	0.20	1.83	-0.16
0.34	0.18	1.92	-0.17
0.40	0.15	2.00	-0.17
0.46	0.13	2.07	-0.18
0.52	0.10	2.16	-0.18
0.59	0.08	2.24	-0.18
0.65	0.05	2.33	-0.18
0.71	0.03	2.43	-0.19
0.78	0.01	2.52	-0.19
0.84	-0.01	2.62	-0.20
0.91	-0.02	2.71	-0.20
0.97	-0.04	2.81	-0.20
1.03	-0.05	2.92	-0.20
1.10	-0.07	3.03	-0.20
1.17	-0.08	3.15	-0.20
1.24	-0.09	3.26	-0.21
1.31	-0.10	3.38	-0.21
1.38	-0.12	3.52	-0.20

Table D.49 Surface pressure distribution, juncture vortex and hump for h/t = 1.14, Re_t = 73,000 – laminar boundary layer

s/t	Cp	s/t	Cp
0.00	0.67	1.45	-0.14
0.06	0.56	1.52	-0.15
0.11	0.31	1.59	-0.16
0.17	0.20	1.67	-0.17
0.23	0.24	1.75	-0.18
0.29	0.22	1.83	-0.18
0.34	0.20	1.92	-0.19
0.40	0.17	2.00	-0.19
0.46	0.15	2.07	-0.21
0.52	0.11	2.16	-0.21
0.59	0.08	2.24	-0.20
0.65	0.05	2.33	-0.21
0.71	0.03	2.43	-0.21
0.78	0.01	2.52	-0.22
0.84	-0.01	2.62	-0.22
0.91	-0.03	2.71	-0.23
0.97	-0.05	2.81	-0.23
1.03	-0.06	2.92	-0.22
1.10	-0.08	3.03	-0.23
1.17	-0.10	3.15	-0.23
1.24	-0.10	3.26	-0.24
1.31	-0.12	3.38	-0.23
1.38	-0.14	3.52	-0.23

Table D.50 Surface pressure distribution, juncture vortex and hump for h/t = 1.14, Re_t = 97,000 – laminar boundary layer

s/t	Cp	s/t	Cp
0.00	0.71	1.45	-0.16
0.06	0.54	1.52	-0.17
0.11	0.42	1.59	-0.18
0.17	0.41	1.67	-0.19
0.23	0.38	1.75	-0.20
0.29	0.34	1.83	-0.20
0.34	0.29	1.92	-0.21
0.40	0.25	2.00	-0.21
0.46	0.20	2.07	-0.22
0.52	0.16	2.16	-0.22
0.59	0.12	2.24	-0.22
0.65	0.08	2.33	-0.23
0.71	0.06	2.43	-0.23
0.78	0.03	2.52	-0.24
0.84	-0.01	2.62	-0.24
0.91	-0.06	2.71	-0.24
0.97	-0.09	2.81	-0.24
1.03	-0.11	2.92	-0.25
1.10	-0.12	3.03	-0.25
1.17	-0.13	3.15	-0.25
1.24	-0.14	3.26	-0.25
1.31	-0.15	3.38	-0.25
1.38	-0.16	3.52	-0.25

D.8 Surface Pressure Distribution, Juncture Vortex and Hump – Tripped Boundary Layer

Table D.51 Surface pressure distribution, juncture vortex and hump for $h/t = 3.43$, $Re_t =$ 47,000 – tripped boundary layer

s/t	Cp	s/t	Cp
0.00	0.44	1.45	-0.52
0.06	0.09	1.52	-0.53
0.11	-0.05	1.59	-0.54
0.17	0.00	1.67	-0.54
0.23	-0.04	1.75	-0.55
0.29	-0.08	1.83	-0.55
0.34	-0.12	1.92	-0.55
0.40	-0.17	2.00	-0.55
0.46	-0.21	2.07	-0.56
0.52	-0.24	2.16	-0.57
0.59	-0.28	2.24	-0.56
0.65	-0.31	2.33	-0.57
0.71	-0.33	2.43	-0.56
0.78	-0.37	2.52	-0.56
0.84	-0.40	2.62	-0.56
0.91	-0.41	2.71	-0.55
0.97	-0.43	2.81	-0.55
1.03	-0.44	2.92	-0.55
1.10	-0.46	3.03	-0.55
1.17	-0.48	3.15	-0.54
1.24	-0.49	3.26	-0.53
1.31	-0.50	3.38	-0.53
1.38	-0.51	3.52	-0.52

Table D.52 Surface pressure distribution, juncture vortex and hump for h/t = 3.43, Re_t = 73,000 – tripped boundary layer

s/t	Cp	s/t	Cp
0.00	0.51	1.45	-0.61
0.06	0.13	1.52	-0.63
0.11	-0.10	1.59	-0.63
0.17	-0.03	1.67	-0.63
0.23	-0.05	1.75	-0.65
0.29	-0.09	1.83	-0.64
0.34	-0.14	1.92	-0.65
0.40	-0.20	2.00	-0.65
0.46	-0.24	2.07	-0.66
0.52	-0.28	2.16	-0.67
0.59	-0.33	2.24	-0.66
0.65	-0.37	2.33	-0.66
0.71	-0.40	2.43	-0.66
0.78	-0.43	2.52	-0.65
0.84	-0.46	2.62	-0.66
0.91	-0.48	2.71	-0.65
0.97	-0.51	2.81	-0.65
1.03	-0.52	2.92	-0.64
1.10	-0.54	3.03	-0.66
1.17	-0.56	3.15	-0.65
1.24	-0.58	3.26	-0.62
1.31	-0.58	3.38	-0.61
1.38	-0.60	3.52	-0.60

Table D.53 Surface pressure distribution, juncture vortex and hump for h/t = 3.43, Re_t = 97,000 – tripped boundary layer

s/t	Cp	s/t	Cp
0.00	0.55	1.45	-0.65
0.06	0.17	1.52	-0.68
0.11	-0.14	1.59	-0.68
0.17	-0.05	1.67	-0.69
0.23	-0.06	1.75	-0.70
0.29	-0.10	1.83	-0.69
0.34	-0.15	1.92	-0.70
0.40	-0.21	2.00	-0.70
0.46	-0.26	2.07	-0.71
0.52	-0.30	2.16	-0.73
0.59	-0.35	2.24	-0.71
0.65	-0.40	2.33	-0.71
0.71	-0.43	2.43	-0.71
0.78	-0.46	2.52	-0.70
0.84	-0.50	2.62	-0.71
0.91	-0.52	2.71	-0.70
0.97	-0.54	2.81	-0.70
1.03	-0.56	2.92	-0.68
1.10	-0.59	3.03	-0.71
1.17	-0.60	3.15	-0.70
1.24	-0.62	3.26	-0.67
1.31	-0.63	3.38	-0.66
1.38	-0.65	3.52	-0.64

Table D.54 Surface pressure distribution, juncture vortex and hump for h/t = 2.86, Re_t = 47,000 – tripped boundary layer

s/t	Cp	s/t	Cp
0.00	0.46	1.45	-0.40
0.06	0.29	1.52	-0.41
0.11	0.08	1.59	-0.42
0.17	0.08	1.67	-0.42
0.23	0.05	1.75	-0.43
0.29	0.02	1.83	-0.43
0.34	-0.02	1.92	-0.44
0.40	-0.06	2.00	-0.45
0.46	-0.10	2.07	-0.45
0.52	-0.13	2.16	-0.45
0.59	-0.16	2.24	-0.45
0.65	-0.20	2.33	-0.45
0.71	-0.22	2.43	-0.45
0.78	-0.25	2.52	-0.45
0.84	-0.27	2.62	-0.45
0.91	-0.30	2.71	-0.45
0.97	-0.32	2.81	-0.44
1.03	-0.33	2.92	-0.44
1.10	-0.34	3.03	-0.44
1.17	-0.36	3.15	-0.44
1.24	-0.36	3.26	-0.43
1.31	-0.39	3.38	-0.43
1.38	-0.39	3.52	-0.43

Table D.55 Surface pressure distribution, juncture vortex and hump for h/t = 2.86, Re_t = 73,000 – tripped boundary layer

s/t	Cp	s/t	Cp
0.00	0.53	1.45	-0.47
0.06	0.35	1.52	-0.48
0.11	0.08	1.59	-0.49
0.17	0.08	1.67	-0.49
0.23	0.06	1.75	-0.51
0.29	0.02	1.83	-0.50
0.34	-0.02	1.92	-0.51
0.40	-0.06	2.00	-0.52
0.46	-0.11	2.07	-0.51
0.52	-0.15	2.16	-0.53
0.59	-0.19	2.24	-0.52
0.65	-0.23	2.33	-0.52
0.71	-0.26	2.43	-0.52
0.78	-0.29	2.52	-0.52
0.84	-0.32	2.62	-0.52
0.91	-0.35	2.71	-0.51
0.97	-0.36	2.81	-0.52
1.03	-0.38	2.92	-0.52
1.10	-0.40	3.03	-0.51
1.17	-0.41	3.15	-0.50
1.24	-0.43	3.26	-0.50
1.31	-0.45	3.38	-0.50
1.38	-0.45	3.52	-0.50

Table D.56 Surface pressure distribution, juncture vortex and hump for h/t = 2.86, Re_t = 97,000 – tripped boundary layer

s/t	Cp	s/t	Cp
0.00	0.59	1.45	-0.51
0.06	0.40	1.52	-0.52
0.11	0.07	1.59	-0.54
0.17	0.06	1.67	-0.54
0.23	0.05	1.75	-0.55
0.29	0.02	1.83	-0.54
0.34	-0.03	1.92	-0.55
0.40	-0.08	2.00	-0.57
0.46	-0.13	2.07	-0.56
0.52	-0.17	2.16	-0.57
0.59	-0.21	2.24	-0.56
0.65	-0.25	2.33	-0.57
0.71	-0.29	2.43	-0.57
0.78	-0.32	2.52	-0.57
0.84	-0.35	2.62	-0.57
0.91	-0.38	2.71	-0.55
0.97	-0.40	2.81	-0.56
1.03	-0.42	2.92	-0.56
1.10	-0.44	3.03	-0.56
1.17	-0.45	3.15	-0.55
1.24	-0.46	3.26	-0.54
1.31	-0.50	3.38	-0.54
1.38	-0.50	3.52	-0.54

Table D.57 Surface pressure distribution, juncture vortex and hump for h/t = 2.29, Re_t = 47,000 – tripped boundary layer

s/t	Cp	s/t	Cp
0.00	0.48	1.45	-0.31
0.06	0.31	1.52	-0.33
0.11	0.12	1.59	-0.33
0.17	0.10	1.67	-0.33
0.23	0.09	1.75	-0.34
0.29	0.06	1.83	-0.34
0.34	0.03	1.92	-0.35
0.40	0.00	2.00	-0.35
0.46	-0.03	2.07	-0.35
0.52	-0.07	2.16	-0.35
0.59	-0.10	2.24	-0.35
0.65	-0.13	2.33	-0.36
0.71	-0.15	2.43	-0.36
0.78	-0.17	2.52	-0.36
0.84	-0.19	2.62	-0.36
0.91	-0.22	2.71	-0.36
0.97	-0.23	2.81	-0.36
1.03	-0.24	2.92	-0.36
1.10	-0.26	3.03	-0.36
1.17	-0.27	3.15	-0.36
1.24	-0.29	3.26	-0.35
1.31	-0.29	3.38	-0.35
1.38	-0.31	3.52	-0.35

Table D.58 Surface pressure distribution, juncture vortex and hump for h/t = 2.29, Re_t = 73,000 – tripped boundary layer

s/t	Cp	s/t	Cp
0.00	0.55	1.45	-0.37
0.06	0.37	1.52	-0.39
0.11	0.12	1.59	-0.38
0.17	0.09	1.67	-0.39
0.23	0.10	1.75	-0.39
0.29	0.07	1.83	-0.39
0.34	0.04	1.92	-0.40
0.40	0.00	2.00	-0.42
0.46	-0.04	2.07	-0.41
0.52	-0.08	2.16	-0.42
0.59	-0.12	2.24	-0.41
0.65	-0.16	2.33	-0.42
0.71	-0.17	2.43	-0.41
0.78	-0.20	2.52	-0.42
0.84	-0.23	2.62	-0.42
0.91	-0.25	2.71	-0.41
0.97	-0.27	2.81	-0.41
1.03	-0.29	2.92	-0.42
1.10	-0.30	3.03	-0.42
1.17	-0.31	3.15	-0.41
1.24	-0.35	3.26	-0.41
1.31	-0.34	3.38	-0.41
1.38	-0.36	3.52	-0.40

Table D.59 Surface pressure distribution, juncture vortex and hump for h/t = 2.29, Re_t = 97,000 – tripped boundary layer

s/t	Cp	s/t	Cp
0.00	0.57	1.45	-0.40
0.06	0.41	1.52	-0.43
0.11	0.13	1.59	-0.41
0.17	0.07	1.67	-0.43
0.23	0.10	1.75	-0.43
0.29	0.07	1.83	-0.43
0.34	0.03	1.92	-0.43
0.40	-0.01	2.00	-0.46
0.46	-0.05	2.07	-0.44
0.52	-0.09	2.16	-0.45
0.59	-0.13	2.24	-0.45
0.65	-0.18	2.33	-0.45
0.71	-0.20	2.43	-0.45
0.78	-0.23	2.52	-0.45
0.84	-0.26	2.62	-0.46
0.91	-0.27	2.71	-0.45
0.97	-0.29	2.81	-0.45
1.03	-0.32	2.92	-0.45
1.10	-0.33	3.03	-0.45
1.17	-0.34	3.15	-0.45
1.24	-0.38	3.26	-0.44
1.31	-0.37	3.38	-0.44
1.38	-0.39	3.52	-0.43

Table D.60 Surface pressure distribution, juncture vortex and hump for h/t = 1.14, Re_t = 47,000 – tripped boundary layer

s/t	Cp	s/t	Cp
0.00	0.48	1.45	-0.13
0.06	0.36	1.52	-0.13
0.11	0.22	1.59	-0.14
0.17	0.17	1.67	-0.15
0.23	0.17	1.75	-0.16
0.29	0.15	1.83	-0.16
0.34	0.13	1.92	-0.17
0.40	0.11	2.00	-0.17
0.46	0.09	2.07	-0.18
0.52	0.06	2.16	-0.19
0.59	0.04	2.24	-0.18
0.65	0.02	2.33	-0.18
0.71	0.00	2.43	-0.19
0.78	-0.02	2.52	-0.19
0.84	-0.03	2.62	-0.19
0.91	-0.05	2.71	-0.20
0.97	-0.06	2.81	-0.20
1.03	-0.07	2.92	-0.20
1.10	-0.08	3.03	-0.20
1.17	-0.10	3.15	-0.20
1.24	-0.10	3.26	-0.20
1.31	-0.11	3.38	-0.20
1.38	-0.13	3.52	-0.20

Table D.61 Surface pressure distribution, juncture vortex and hump for h/t = 1.14, Re_t = 73,000 – tripped boundary layer

s/t	Cp	s/t	Cp
0.00	0.55	1.45	-0.16
0.06	0.42	1.52	-0.16
0.11	0.25	1.59	-0.17
0.17	0.18	1.67	-0.18
0.23	0.19	1.75	-0.19
0.29	0.17	1.83	-0.19
0.34	0.15	1.92	-0.20
0.40	0.12	2.00	-0.20
0.46	0.10	2.07	-0.21
0.52	0.07	2.16	-0.22
0.59	0.04	2.24	-0.21
0.65	0.01	2.33	-0.21
0.71	-0.01	2.43	-0.22
0.78	-0.02	2.52	-0.23
0.84	-0.04	2.62	-0.23
0.91	-0.06	2.71	-0.24
0.97	-0.08	2.81	-0.23
1.03	-0.08	2.92	-0.23
1.10	-0.10	3.03	-0.23
1.17	-0.12	3.15	-0.23
1.24	-0.13	3.26	-0.24
1.31	-0.13	3.38	-0.24
1.38	-0.15	3.52	-0.23

Table D.62 Surface pressure distribution, juncture vortex and hump for h/t = 1.14, Re_t = 97,000 – tripped boundary layer

s/t	Cp	s/t	Cp
0.00	0.59	1.45	-0.17
0.06	0.45	1.52	-0.17
0.11	0.28	1.59	-0.19
0.17	0.18	1.67	-0.19
0.23	0.20	1.75	-0.20
0.29	0.18	1.83	-0.21
0.34	0.16	1.92	-0.22
0.40	0.13	2.00	-0.21
0.46	0.10	2.07	-0.23
0.52	0.07	2.16	-0.24
0.59	0.04	2.24	-0.22
0.65	0.01	2.33	-0.23
0.71	-0.01	2.43	-0.23
0.78	-0.03	2.52	-0.24
0.84	-0.05	2.62	-0.25
0.91	-0.07	2.71	-0.25
0.97	-0.09	2.81	-0.25
1.03	-0.09	2.92	-0.24
1.10	-0.11	3.03	-0.25
1.17	-0.13	3.15	-0.25
1.24	-0.14	3.26	-0.26
1.31	-0.15	3.38	-0.25
1.38	-0.17	3.52	-0.25